A mechanistic study of Photochemical Internalisation and enhanced drug delivery in cancer cells

Derick Kofi Adigbli

Division of Surgery and Interventional Science,
Faculty of Medical Sciences, UCL.

A Thesis Submitted in Fulfillment of the degree of Doctor of Philosophy (Ph.D.)

Statement of Originality

I, Derick Kofi Adigbli, certify that the work presented in this thesis is my own. Where information has been derived from other sources, I confirm that this has been indicated in the thesis.

Abstract

Inefficient intracellular drug delivery is a significant limiting factor to success in cancer therapeutics. Photochemical internalisation (PCI) utilises the fundamental principles of photodynamic therapy (PDT): photosensitiser plus light and oxygen, at sub-lethal level to facilitate targeted intracellular drug delivery. This effect is mediated by reactive oxygen species (ROS). This thesis investigates the mechanisms underpinning sulfonated meso-tetraphenylporphine ($TPPS_{2a}$) mediated PCI to enhance the delivery of two cytotoxins, saporin or mitoxantrone, and a novel Small Molecule Carrier (SMoC) *in vitro*. PCI of saporin was also assessed in a 3D-tumour model.

In vitro experiments using 4T1 murine breast adenocarcinoma cells were performed to investigate which factors determined the likelihood of PDT versus PCI predominant cytotoxicity. The role of the intracellular REDOX environment in PDT/PCI was assessed using a free radical potentiator and quenchers. The results suggested that the localisation and total amount of ROS produced exerts the greatest influence in determining the likelihood of PDT versus PCI induced cell kill. In addition, PCI further enhanced SMoC-aided delivery of siRNA in MCF7 human breast cancer cells.

A compressed collagen scaffold, embedded with 4T1 cells, was used to investigate $TPPS_{2a}$-mediated PCI of saporin in a 3D tumour model. The results indicated that a 3D-model is potentially a useful tool for pre-clinical assessment of PCI.

Bioluminescent PDT studies were also carried out on MCF7 cells transduced with luciferase and the 4T1-luc2 cell line, which is stably transfected with luciferase. These studies demonstrated that bioluminescence can be used to activate a photosensitiser for a cytotoxic effect (PDT).

Overall, this thesis demonstrated that by further understanding the mechanisms that underpin PCI it is possible to further enhance its facilitative effects for drug

delivery. The ongoing phase II clinical trials into PCI show its translational potential as a means to improve the therapeutic effectiveness of anti-cancer drugs.

Table of Contents

List of Figures

List of Tables

List of Abbreviations

ACM	Artificial cancer mass
AIDS	Acquired immune deficiency syndrome
ALA	5-aminolevulinate
ALL	Acute lymphoblastic leukaemia
$AlPcS_{2a}$	Disulfonated aluminium phthalocyanine
AML	Acute myeloid leukaemia
ARE	Antioxidant response element
ASPA	Animals (scientific procedures) Act
ATCC (CRL-2535™)	Murine breast adenocarcinoma cell line
B/M	Buthionine sulfoximine + mitoxantrone
BRET	Bioluminescence resonance energy transfer
B/S	Buthionine sulfoximine + saporin
B/S/M	Buthionine sulfoximine + saporin + mitoxantrone
BSO	Buthionine sulfoximine
Ca^{2+}	Calcium ion
Coele.	Coelenterazine
CSF	Colony stimulating factor
CYP450	Cytochrome p450 enzymes
dH_2O	Deionised water
D-Luc	*D*-Luciferin
DMEM F-12	Dulbecco's modified Eagle's medium + Ham F-12
DNA	Deoxyribonucleic acid
DU-145	Prostate cancer cell line
ECM	Extracellular matrix
EDTA	Ethylenediaminetetraacetic acid
EGF	Epidermal growth factor
EGFR	Epidermal growth factor receptor
FACS	Fluorescence-activated cell sorting
Fig.	Figure
FITC	Fluorescein
FLuc	Firefly luciferase

FRET	Fluorecence resonance energy transfer
GFP	Green fluorescent protein
GLuc	Gaussia luciferase
GSH	Glutathione
$GSHP_x$	Glutathione peroxidase
HCT-116	Colorectal carcinoma cell line
HeLa	Cervical carcinoma cell line
HHE	4-hydroxy-2-hexenal
HNE	4-hydroxy-2-neonal
HPD	Haematoporphyrin-derivative
HYP	Hypericin
H_2O	Water
H_2O_2	Hydrogen peroxide
i.p	Intraperitoneal
kDa	Kilodalton
LA	Light after
LB	Light before
LH	L-Histidine
$LOO^{\cdot}$	Lipid peroxyl radical
LOOH	Hydroperoxide
LRP	Lipoprotein receptor-related protein
LYG	Lysotracker Green®
mBCl	Monochlorobimane
MCF7	Human breast cancer cell line
MCF7-FLuc	Human breast cancer cell line expressing Firefly luciferase
MCF7-GLuc	Human breast cancer cell line expressing Gaussia luciferase
MCF7/R	Human breast cancer cell line (resistant)
MDR	Multi-drug resistance
MEM	Minimum essential Eagle's medium
mg kg^{-1} or mg/kg	Milligrams per kilogram
mg ml^{-1} or mg/ml	Milligrams per millilitre
Mg^{2+}	Magnesium ion
MGUH1/R	Bladder cancer cell line (resistant)

min	Minute(s)
ml	Millilitre
ml^{-1}	per millilitre
mm	Millimetre
mM	Millimolar
MMP	Matrix metalloproteinase
µM	Micromolar
µm	Micrometre
mTHPC	*Meso*-tetraphenyl chlorin
MTT	3- [4,5-dimethylthiazolyl]-2,5-diphenyltetrazolium bromide
MTX	Mitoxantrone
NA	Numerical aperture
NaOH	Sodium hydroxide
NFE2L2 or Nrf2	Nuclear factor (erythroid-derived 2)-like 2
nm	Nanometre
nM	Nanomolar
$OH^{\cdot}$	Hydroxyl radical
$^1O_2$	Singlet oxygen
O_2^{-}	Superoxide
pK_a	Acid dissociation constant
pM	Picomolar
NuTu-19	Rat ovarian carcinoma
PAP	Pokeweed antiviral protein
PBS	Phosphate buffered saline
PCI	Photochemical internalisation
PDT	Photodynamic therapy
PEG	Polyethylene glycol
Pgp	P-glycoprotein
PS	Photosensitiser
PUFA	Polyunsaturated fatty acid
QD	Quantom dot
REDOX	Reduction-Oxidation
RIP	Ribosome inactivating protein

RNA	Ribonucleic acid
rRNA	Ribosomal ribonucleic acid
$RO^{\cdot}$	Alkoxyl radical
$ROO^{\cdot}$	Peroxyl radical
ROS	Reactive oxygen species
RPMI-1640	Roswell Park Memorial Institute-1640 media
SAP	Saporin
siRNA	Silencing ribonucleic acid
SMoC	Small molecule carrier
S/M	Saporin + mitoxantron
SOD	Superoxide dismutase
TBR or TBR-123	Tetrabromorhodamine-123
$TPCS_{2a}$	Amphinex®
$TPPS_{2a}$ or TP	Disulfonated tetraphenylprophin
U2OS	Osteosarcoma cell line
UV	Ultraviolet
VEGF	Vascular endothelial growth factor
WiDr	Colorectal adenocarcinoma cell line
2D	Two-dimensional
2-MeOE	Methoxyestradiol
3D	Three-dimensional
4G-SMoC	4G-BfSMoC-COOH, 2

Acknowledgements

The work in this thesis was primarily conducted at the National Medical Laser Centre, Division of Surgery and Interventional Science, UCL. I would like to extend my sincere thanks to all the staff and students who have assisted me with completing the experiments and supported me during the write-up. Particular thanks go to my two supervisors Professor A.J. MacRobert and Dr M. Loizidou. Professor MacRobert has always provided me with invaluable guidance and support in ensuring that the work performed was of the standard expected within the Division. Dr Loizidou is quite simply the most complete academic that I have had the pleasure to work with. Her determination, enthusiasm and scientific knowledge humble me.

I would also like to acknowledge the specific contributions made by Dr M. Bovis, Dr J. Woodhams, Dr E. Yaghini, Dr J. Seebaluck, Miss A. Martinez De Pinillos Bayona, Dr A. Jathoul, Dr M. Pule and Professor D. Selwood.

During the write up of this thesis, some dear friends have kindly helped with proof reading so I would like to mention a special thank you to Mrs. E. Tweed and Miss A. Burn-Murdoch.

The work in this thesis has been made possible by funding from the UCL Grand Challenges and associated partners to whom I extend my warmest thanks.

My wife Dr T. Bishop has been a pillar of support and even tolerated me writing part of this thesis on our honeymoon and I thank her sincerely. Alongside her, my family: Moses and Diana (parents), Delali, George, Claude and Claudia (siblings) have made significant sacrifices to facilitate my ongoing education and research. I am forever indebted to you all.

Finally, I would like to thank Mr L. Hamilton and Sir A. Ferguson for inspiring me to strive for excellence.

Chapter 1: Introduction to Photodynamic Therapy and Photochemical Internalisation

1.1 HISTORY OF PHOTOSENSITISERS AND PHOTODYNAMIC THERAPY.

Photodynamic therapy (PDT) is a cytotoxic treatment modality, which is dependent on the presence of a photosensitiser, molecular oxygen and light. Under such conditions reactive oxygen species are generated(1), which in a time and distance dependent manner can cause localised damage to cellular organelles resulting in irreparable damage and cell death(2).

The medicinal use of photosensitive compounds can trace their origins back to ancient Egyptian and Indian civilizations for the treatment of simple dermatological complaints. The turn of the century saw the pioneering work performed by Niels Finsen on the use of red-light and UV exposure for the treatment of smallpox pustules(3) and cutaneous tuberculosis(4), respectively. Finsen's work ushered in the era of modern light therapy, and, in 1903, his work on the 'therapeutic use of concentrated light' was awarded the Nobel Prize for Physiology or Medicine. Subsequently, the discovery of the toxic effects of photosensitising dyes, such as eosin, by Raab and von Tappeiner led to a clinical trial using 1% eosin (topical) +/- light on 6 patients with skin carcinoma. 4 patients showed evidence of tumour resolution at 12 months(5). In 1907, following work by von Tappeiner and Jodlbauer the term 'photodynamic action' was first coined.

The discovery of the photosensitising properties of the porphyrin-based compounds marked an important step in the development of modern day photosensitisers and PDT. In 1911, W. Hausmann described the photosensitive and phototoxic effects of haematoporphyrin on the skin of mice following exposure to light(6). Porphyrins are the main precursors of haem, which is a vital component of naturally occurring structural and enzymatic proteins including haemoglobin, myoglobin, catalase and the P450 liver cytochromes. Clinically, the disordered synthesis/metabolism of haemoglobin can result in porphyria, a group of diseases that can affect multiple organ systems including liver, heart and skin. Interestingly, acute attacks of porphyria can be triggered by excessive exposure to sunlight.

Porphyrins comprise a porphine tetrapyrrolic structure based on four pyrrole rings connected in most cases by one-carbon bridges in a cyclical configuration(4), and often with central metal coordination such as iron in haem. In 1913, Friedrich Mayer-Betz applied haematoporphyrin, topically, on his own skin(7). Following light exposure he observed swelling and pain. This work also demonstrated the selective properties of PDT, as the photo-induced dermatological reactions were restricted to light-exposed areas.

In 1955, crude haematoporphyrin was purified by Schwartz et al. (8) into a form named 'haematoporphyrin-derivative' (HpD). Richard Lipson and colleagues, based at the Mayo Clinic, used HpD in a range of studies that heralded the modern era of PDT, for example the use of HpD to image tumours(9). Independent *in vivo* studies by Dougherty and Kelly in 1975 showed the translational potential of PDT by demonstrating the antitumor efficacy of HpD plus red-light(10, 11). Kelly and colleagues would subsequently commence clinical trials in humans using HpD-based PDT to treat bladder cancer(12). Further development and purification of HpD resulted in the synthesis of Photofrin® (Porfimer sodium), which, in 1993, was approved for treatment of bladder cancer in Canada(2). This followed decades of research into the use of PDT to treat, often advanced-stage, cancers including oesophageal(13) and gastric (14) carcinomas. Despite its approval for use in humans, Photofrin® was found to have a number of limitations that have stifled its use. Firstly, being a mixture of monomers, dimers and oligomers(15) it is difficult to synthesize identical batches of Photofrin®. In addition, the relatively low extinction coefficient (ε) at the red end of the spectrum, which limits tissue penetration(16), and prolonged photosensitivity have further limited its clinical application(2). However, the potential benefits of PDT within the clinical sphere, for example, the potential for repeated exposure to non-ionising light confers a theoretically protective effect on tissue surrounding a lesion compared to radiotherapy(17).

Nevertheless, the need for more suitable agents for clinical application resulted in the development of the so-called second-generation photosensitisers based

on porphyrin/chlorophyll analogues such as chlorins, bacteriochlorins and phthalocyanines within the basic structure. The second-generation agents were designed to exhibit greater absorbance in the red-spectrum for example *meso*-tetrahydroxyphenyl chlorin (652 nm) and sulfonated aluminium phthalocyanine (675 nm)(2), enhanced tumour selectivity, reduced skin photosensitivity and increased chemical purity. The development of these agents has been the catalyst for the increased investigation into PDT within the last twenty years.

Both the first and second generation photosensitisers have representation, albeit limited, within the clinical arena. Despite the highlighted limitations of Photofrin®, it is currently licensed in Canada, Japan and the USA for the treatment of both premalignant (Barrett's oesophagus) and malignant (bladder and lung cancer) lesions.

Visudyne® (benzoporphyrin derivative monoacid/verteporfin) is a newer porphyrin-based photosensitiser that is licensed for the treatment of wet macular degeneration (a not uncommon cause of significant visual impairment in the elderly population) in the USA, Canada, European Union (2000) and Japan (2003). Verteporfin benefits from a red-shifted absorption peak at 689 nm wavelength(18) enabling better tissue penetration of the photosensitiser-activating laser. It has been found to cause selective damage to neovascular endothelial cells found in choroidal vessels. This results in thrombosis and the occlusion of subfoveal lesions patients with age-related macular degeneration. This example is particular important as it demonstrates the versatility of PDT as a treatment modality for non-malignant lesion.

m-THPC (Foscan®) is a chlorin based photosensitiser that is licensed within the European Union for the palliative treatment of Head & Neck Squamous cell carcinoma(19). Foscan is given by intravenous injection prior to laser treatment (652 nm)(2) and was licensed due to its beneficial effects on patient morbidity (28 (22%) of 128 patients assessed in a study found that treatment with foscan significantly improved their most troubling symptom in addition to approximately 1 in 5 patients experiencing a reduction in tumour size)(19).

Sulfonated Aluminium Phthalocyanine ($AlPcS_{2a}$) is currently licensed in Russia (2001) for the treatment of various malignant tumours (Photosense®)(2). Despite demonstrating good red-shifted light absorption at 670 nm wavelength, the use of this photosensitiser has mainly been limited to preclinical studies(20). In addition, owing to a the large number of isomers formed during its synthesis $AlPcS_{2a}$ has an unfortunate relatively high level of batch to batch variation(21, 22), which has contributed to stifling its use beyond pre-clinical applications.

The development of new photosensitisers over the past 20 years has resulted in the development of a range of amphiphilic compounds, which owing to the presence of 1-2 carboxyl groups on the side of the compound enable it to retain enough hydrophobicity to facilitate penetration of the cell membrane(20, 23). This confers three advantages as described by Berg et al. (2011)(20):

1. Sufficient solubility in biocompatible solutions.
2. Good cell membrane penetrability secondary to the relatively high pK_a values generated by the carboxyl groups.
3. Intercalation within phospholipid membranes where the life-time and cytotoxicity of singlet oxygen is enhanced, compared to aqueous solution.

Another strategy that is of particular importance to PCI is the substitution of carboxyl groups with sulfonate groups. This reduces the penetrating potential of photosensitisers across a cell membrane, particularly when 2 sulfonate groups are present(24); and the associated low pK_a of the sulfonate groups prevents protonation of the compounds even in acidic environments such as lysosomes(20). Consequently, disulfonated photosensitisers including $AlPcS_{2a}$ and disulfonated tetraphenylprophin ($TPPS_{2a}$) the latter is the main photosensitiser used in this thesis, are taken up by adsorptive endocytosis and reside within the inner leaflet of endocytic vesicles making them potentially suitable for photochemical internalisation (PCI)(20). Other chemical modifications have been made to photosensitisers to enhance their suitability for clinical application. For example, the development of nanoformulations, which has been particularly useful with verteporfin that is complexed with liposomes to improve cellular uptake.

1.2 CHALLENGES ASSOCIATED WITH DRUG DELIVERY

The bulk of conventional chemotherapeutic agents, such as taxanes and alkylating agents, exert their cytotoxic effects by gaining access to DNA in a replication-selective manner and this requires access to the cytosol(25). Endocytosis is a cellular uptake process whereby mammalian cells can internalise hydrophilic molecules larger than 1 kDa (fig. 1.1a)(26). Endocytosis initiates with interaction, including cell surface receptors, between the cell membrane and the molecule to be internalised. Consequently, there is invagination of the phospholipid membrane of the cell and subsequent formation of endocytic vesicles(27). In order for a therapeutic cytotoxin to reach its final intracellular target, it must 'escape' from these vesicles and any others that may have formed via fusion, such as lysosomes. Photochemical internalisation (PCI) spawned from PDT and utilises the fundamental mechanisms of photoactivation and production of reactive oxygen species (ROS) to facilitate the release of endocytosed molecules into the cytosol (fig 1.1)(26). As a result of this PCI acts as an enabling mechanism to enhance the delivery of therapeutic agents to their site of action. In doing so PCI can be considered as a novel intracellular delivery tool for macromolecules.

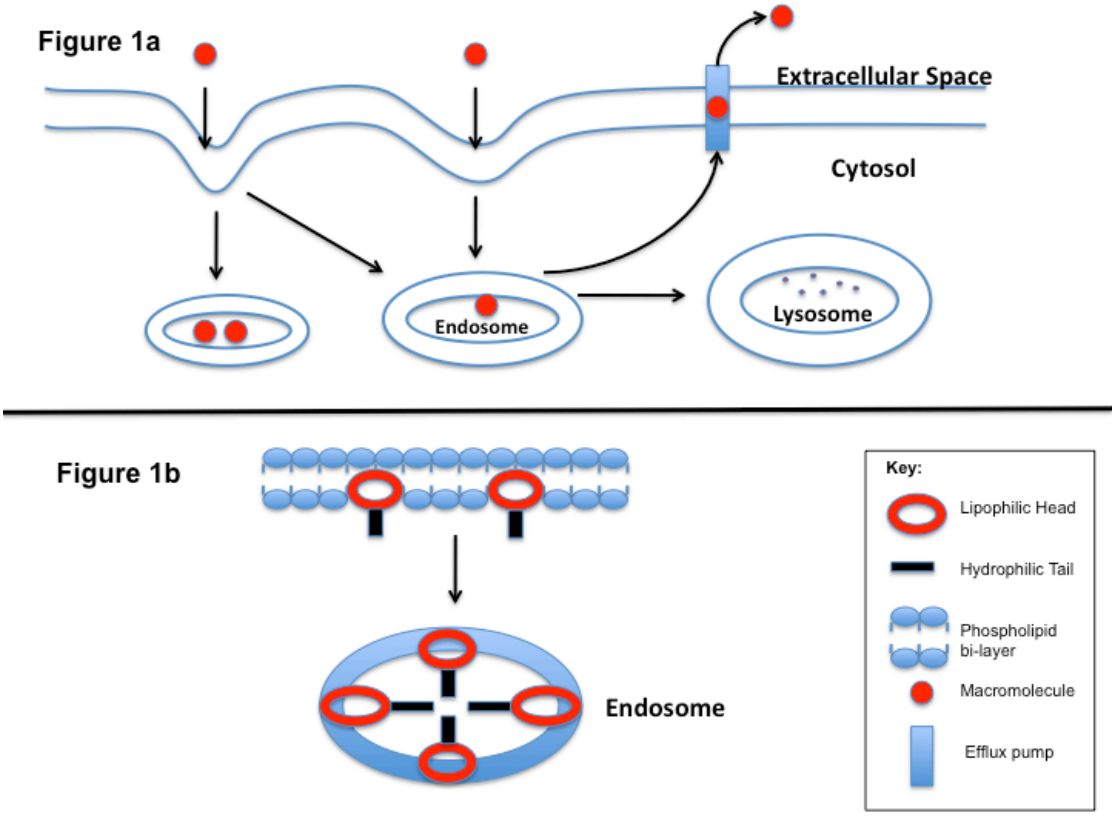

Figure 1.1 - Endocytic mechanism of drug uptake and destruction/efflux.
(a) Depicts the uptake of a macromolecule by endocytosis, packaging within endosomes and subsequent enzymatic degradation within lysosomes or efflux from the cell via cell membrane pumps. Such a mechanism may be up-regulated in the multidrug resistance phenotype expressed by many cancers. **(b)** Illustrates the incorporation of amphiphilic photosensitisers within the phospholipid bi-layer. Following the formation of endo/lysosomes, the photosensitiser is retained within the membrane of the organelle. (Image and legend first published in Adigbli DK et al., 2012)(26).

1.3 MECHANISMS OF PCI

PCI employs the basic mechanisms that underpin PDT but at a sub-cellular level with the aim to enhance the intracellular delivery of endocytosed, biologically active macromolecules, including cytotoxic chemotherapeutic agents(25, 28, 29). In PDT the ROS produced, principally singlet oxygen ($^1O_2$), but also superoxide (O_2^-) to induce non-site specific cytotoxic damage with the ultimate aim of inducing cell death. In slight contrast, PCI utilises ROS production that is localized to the membranes of vesicles that enclose the endocytosed molecule (drug). This localized effect is made possible via the selective localisation of a photosensitiser to the phospholipid membrane. Compounds with amphiphilic properties are able interact with hydrophilic (water-loving) and hydrophobic (water-intolerant) environments. If one end of the molecule is more

hydrophobic the molecule can then partition to phospholipid membranes without fully crossing into the cytosol(30). The hydrophobic end interacts with the lipid bilayer of the membrane whereas the hydrophilic end interacts with the ionized surface of the lipid bilayer. Therefore, any molecule that is subsequently endocytosed will reside in vesicles (endosomes and lysosomes), where the photosensitiser is localized preferentially within their phospholipid membranes instead of the central aqueous compartment. This localised distribution of the photosensitiser coupled with the short-range and survival of ROS such as singlet oxygen, results in restricted phototoxic damage to and consequent rupture of endo-lysosomal membranes. The attenuated and restricted nature of this process negates the direct photo/ROS-mediated cytotoxicity(31-33) (see fig. 1.1b). This relatively 'controlled' production of ROS is essential for 'true' PCI as the technique aims to enhance the delivery therapeutic molecules without damaging/modifying the co-delivered bioactive agent within the central aqueous compartment or lethally damaging the cell. This may be particularly relevant when delivering non-stable and primarily non-toxic molecules such as siRNA and other genetic material. The principal protocol for PCI involves activating the photosensitiser after pre-incubating cells with photosensitiser and the molecule to be internalised, however, a second protocol exists whereby the cells are photochemically treated prior to delivery of the molecule of choice(34). The latter mechanism is postulated to involve the fusion of newly formed endosomes with previously ruptured (PCI) endocytic membranes(30).

1.4 *IN VITRO* PCI

The body of evidence to support PCI-induced cell death *in vitro* is already well established. The two main classes of photosensitiser used for PCI are the amphiphilic disulfonated porphyrin(20, 35) and phthalocyanine(30) photosensitisers, which can be activated using red light. The benefit of this is that red light can penetrate tissues to greater depths than green and blue light(36), thus are likely to be more relevant to potential clinical applications. However, other photosensitisers such as hypericin have also been demonstrated to be effective(25). PCI has been used to enhance/facilitate the intracellular

delivery of a variety of different compounds including; cytotoxic chemotherapeutics(20, 25), immunotoxins(37-39), immune therapies(39) and genes(20). The diversity of compounds utilised demonstrates the versatility of PCI as a delivery tool. The type II topoisomerase inhibitor (mitoxantrone, MTX) is used for the treatment cancer including haematological (Acute Myeloid Leukemia (AML) and refractory Acute Lymphoblastic Leukaemia (ALL)), and metastatic solid tumours (breast and prostate). The success of MTX is limited by the multidrug resistant phenotype (MDR), which attenuates the efficacy of many other chemotherapeutic agents. In addition to MDR, narrow therapeutic indices and intolerable systemic toxicity e.g. myelosuppression are also factors that significantly reduce the success rates of conventional anticancer cytotoxins. *In vitro,* MDR expressing breast and bladder cancer cell lines (MCF7/R and MGHU1/R, respectively) are known to express dose dependent resistance to mitoxantrone, amongst other chemotherapeutics(25). Following endocytic uptake of a drug, the MDR phenotype can manifest in multiple mechanisms including the fusion of endosomes with enzymatic lysosomes and/or efflux of the drug via cell membrane pumps e.g. P-glycoprotein pumps (PgP). PCI, using the St John's Wort extract hypericin as a photosensitiser, was shown to reverse this MDR phenotype in both cancer cell lines with up to 38 % increased killing ($p<0.05$)(25).

Although hypericin has membrane-localising properties, newer amphiphilic porphyrin based photosensitisers such as meso-tetraphenyl chlorin disulfonate ($TPCS_{2a}$,) have been designed to selectively target endosomal and lysosomal membranes(20). Such drugs are consequently optimised for PCI as opposed to PDT. In the latter, non-selective sub-cellular localisation may be advantageous in order to maximise cell kill(37). Disulfonated meso-tetraphenyl porphine ($TPPS_{2a}$) has been used to facilitate the delivery of an endothelial growth factor (EGF)-saporin chimera into an EGF resistant EGFR-positive rat epithelial ovarian cancer cell line (NuTu-19)(40). Saporin is a Type I ribosome-inactivating protein (RIP) that exerts its cytotoxicity by disrupting protein synthesis. However, unlike type II RIPs, such as ricin, saporin has relatively poor cytotoxicity since it lacks the necessary cell-binding domain and is not efficiently taken up/retained

by the cell following endocytosis. Consequently, saporin is a good candidate molecule for PCI potentiated delivery(41).

EGFR positivity is not an uncommon occurrence in carcinomas, therefore such a receptor is a good target for selective cancer chemotherapy. A previous study demonstrated that following exposure to light; the viability of NuTu-19 cells treated with both $TPPS_{2a}$ and the EGF-saporin chimera was reduced by 50 %; this is consistent with PCI(40). Furthermore, the LD_{96} required to achieve approximately a 50 % reduction in cell viability was ~10 nM for PCI of saporin alone, compared to ~10 pM for PCI of the EGF-saporin chimera. This indicates that by targeting PCI, it is possible to attain even greater selectivity and consequently widen the therapeutic index of a drug. These findings were supported by Yip et al. who used PCI to deliver cetuximab-saporin chimera into colorectal (HCT-116); prostate (DU-145) and epidermal (A-431) carcinoma cell lines(41). $TPCS_{2a}$ has been used to mediate the PCI of gelonin (Type I RIP) in WiDr (human colorectal adenocarcinoma cell line)(20). The same group went on to demonstrate the versatility of PCI by using it to increase the transfection efficiency of enhanced green fluorescence protein (EGFP)-encoding plasmid and also induce gene silencing using siRNA. Other groups have also reported success in photochemically internalising silencing RNA and also showed that delayed PCI on cells previously transfected with siRNA significantly prolonged the knockdown of the target protein when siRNA was carried by nanogels(42). These findings demonstrate the use of PCI as a versatile delivery tool for macromolecules. Although not currently established as anti-cancer therapies, both gene silencing and gene transfection may play a significant role in future cancer therapy and PCI may provide a means of enhancing selective delivery of such compounds into cancer cells.

1.5 *IN VIVO* PCI

The development of *in vivo* PCI models has aided the acquisition of further understanding of the technique, its strengths and weaknesses, including significant direct cytotoxicity in whole organisms(43). An additional effect, which could not be modeled using current *in vitro* techniques, is vascular starvation(44). In addition, an immune mediated component has been postulated (Norum O.J. and Berg K., unpublished data). Given the important roles that angiogenesis and the immune system play in carcinogenesis, any potential beneficial effects of PCI on these factors is promising. Nevertheless, far more work is required to truly understand these findings as paradoxically, vascular damage may blunt the delivery of therapeutic molecules to a tumour bed, thus there may be implications for repeated therapies. *In vivo* work has included both local injection of drugs directly into a tumour mass and systemic administration with positive observations(26). Subcutaneous human adenocarcinoma (WiDr) tumours have been grown in athymic nude mice. The mice were treated with the photosensitiser aluminium phthalocyanine disulfonate ($AlPcS_{2a}$), via intraperitoneal (i.p.) injection, 48h prior to illumination. The cytotoxin, gelonin, was given intratumorally 6h before light therapy. The group observed complete remission in 6 of 9 treated mice(43). Significantly, tumour growth was unaffected by treatment with $AlPcS_{2a}$, gelonin or a combination of the two compounds in the absence of light, indicating that photoactivation and ROS generation are likely to play important roles in PCI. Furthermore, PDT alone was not as effective as PCI in opposing tumour growth. The study also managed to demonstrate PCI induced re-localisation of $AlPcS_{2a}$ from a granular pattern (indicating endosomal targeting) prior to light, to a diffuse pattern in the cytoplasm following light treatment. Such a finding is important when considering the potential mechanisms the underpin PCI, thus the release of endocytosed molecules from cytosolic vesicles would be consistent with a change in distribution from granular (vesicular) to diffuse (cytosolic). This is supported by *in vitro* studies that report re-localisation of both photosensitiser and cytotoxin following PCI(25).

$AlPcS_{2a}$ has also been used to sensitise the effect of bleomycin on orthotopically implanted HT1080 fibrosarcoma cells(44). This was one of the first studies to look at the effect of PCI on deep-lying tumours *in vivo*. The tumours were grown in the gastrocnemius (calf) muscle of nude mice. Treatment was initiated with i.p. administration of $AlPcS_{2a}$ (10 mg kg^{-1}) once tumours were 80-150 mm^3 in volume. 48 h following injection with $AlPcS_{2a}$ bleomycin (1500 IU) was given i.p. prior to illumination with a 670 nm diode laser, 30 minutes later. Tumour size was subsequently measured five times per week. The study found that PDT ($AlPcS_{2a}$) alone delayed tumour growth by 5 days, which was more effective than light or bleomycin alone. However, PCI treated tumours had a mean growth delay of 21 days compared to control and 15 days compared to PDT alone ($p<0.001$). Histological examination of the tumours demonstrated that 7-days post treatment with PDT alone there was evidence of central necrosis with a relatively spared tumour periphery whereas PCI showed more extensive central necrosis with only a thin layer of spared periphery in the deep layer. This study not only demonstrated that PCI of bleomycin increased the selective toxicity of the chemotherapeutic agent *in vivo* but also that it was superior to PDT in delaying tumour regrowth, with enhanced tumour damage at the periphery. Bleomycin has also been used in combination with $TPCS_{2a}$ for *in vivo* PCI in athymic mice, subcutaneously inoculated with CT26.CL25 cells (metastatic colorectal cancer) (20). In this study, Berg et al. reported that bleomycin-$TPCS_{2a}$ PCI was superior to PDT with the photosensitiser *meso*-tetraphenyl chlorin (mTHPC) in inhibiting tumour growth.

Although still at a relatively early stage of technical development and refinement, the *in vivo* findings highlighted above do indicate the potential use of PCI in live multicellular organisms and are an important step in the development of protocols that could lead to clinical application. Work by Woodhams et al. (45) provided further evidence of the mechanisms that underpin PCI mediated cytotoxicity, *in vivo*. Using $AlPcS_{2a}$ in a normal rat liver model, the group demonstrated *in vivo* that gelonin, following endocytosis, is trapped in lysosomes but can be released into the cytosol following PCI treatment. Furthermore, they also observed that the depth of necrosis post PCI

was greater than that achieved with PDT alone in keeping with the reports from other groups(44).

1.6 POTENTIAL LIMITATIONS OF PCI

Despite the promising results of PCI in both *in vitro* and *in vivo* studies there are limitations. The first is the issue of tissue light penetration. The benefit of selective cell killing, concentrated to areas exposed to light and drugs, forms the basis of one of PCI's drawbacks. Given that non-ionising light will only penetrate superficial tissue layers the photodynamic component of PCI will only be utilised in superficial lesions on skin or the apical surface of luminal or tubular organs. This hurdle has already been encountered in clinically applied PDT; where the use of novel light sources including fiber optics has enabled access to deeper lesions. Linked to this would be the limited access in disseminated/metastatic disease. Another problem encountered in PCI studies is the time taken to determine the optimal doses of photosensitiser, which may vary significantly in different cell/tumour types. However, as PCI continues to be developed, the library of available amphiphilic photosensitisers continues to grow. $TPCS_{2a}$ is an example of this, being an optimised variant of $AlPcS_{2a}$ specifically designed for clinical application.

1.7 UK BASED CLINICAL TRIAL FOR PCI

A clinical trial, evaluating the use of $TPCS_{2a}$-bleomycin PCI in head and neck cancers is currently taking place at University College London Hospital, London, UK. Following promising results from a Phase I study(46), Phase II trials are now in progress. This pioneering trial is vital for the development of PCI into a safe and economically viable treatment modality in oncology.

1.8 INTRODUCTION TO SMALL-MOLECULE CARRIERS (SMOCS)

Small molecule carriers are a class of transporter that can ferry biomolecules across phospholipid bilayers into and within the cell. They are based on the third helix of drosophila PTD Antennapedia homeodomain(47). These SMoCs essentially mimic the amphipathic helix of PTDs(48) enabling them to readily interact with both hydrophobic and hydrophilic regions of the cell membrane.

SMoCs present an interesting tool for enhanced cellular drug and therapeutic delivery. Of particular interest are the variable routes of uptake, including endocytosis, which opens up the possibility of combining SMoCs and photochemical internalisation (PCI) with possible additive effects.

1.9 INTRODUCTION TO 3D-TUMOROID CANCER MODEL

In vitro studies form a fundamental part of investigations into cancer biology and therapeutics. 2-D cell models have many benefits, including cost effectiveness, reproducibility, various options for assaying treatment response, reducing the demand for *in vivo* studies and general efficiency of time. However, the need for *in vivo* studies and the role of *in vitro* investigations primarily as pilot pre-clinical data indicates that limitations do exist, particularly those related to mimicking the chaotic, heterogeneous and dynamic tumour stromal environment, and the impact of host-related factors on the progression phase of carcinogenesis(49).

Recent work by Nyga et al. (2013)(50) demonstrated how partial plastic compression could be used to develop a 3-D colorectal cancer model that also comprised stromal cells (fibroblast +/- endothelial). The important findings from the group include: reduced rate of cell growth compared to 2-D culture, the formation of spheroids preferentially in the periphery of the cancer compartment within the construct away from the hypoxic core and the production of VEGF at the invasive edge. In this way the Nyga model does appear to be a far better mimic of *in vivo* conditions compared to the much tested 2-D cell cultures.

1.10 INTRODUCTION TO BIOLUMINESCENT PDT

The ability of certain biological systems to emit light from an organic source is of much interest to biomedical research(51). Bioluminescence is naturally occurring process whereby visible light is emitted as a by-product of a chemical reaction taking place within living organisms(51). This natural phenomenon happens in various types of organisms including bacteria, marine organisms (including plants) and insects(52-54). *Photinus pyralis* (American firefly) is one

of the best-studied organisms found across the different species of bioluminescent insects(51, 55). Most bioluminescent systems involve the energy dependent oxidation of the heterocyclic carboxylic acid, Luciferin (LH_2) or Luciferin-like substrate. The best studied is the firefly Luciferin-Luciferase (Luc) system(51) which occurs as follows:

Stage 1: Luc mediated conversion of firefly Luciferin (*D-Luciferin)* to a luciferyl adenylate (reaction requires ATP and Mg^{2+} as co-factor)

$Luc + LH_2 + ATP\ (Mg^{2+}) \rightleftharpoons Luc \cdot LH_2\text{-}AMP + PP_i$

Stage 2: Oxidation of reactive luciferyl adenylate at active site of Luciferase, resulting in production of an excited by-product (oxyluciferin)

$Luc \cdot LH_2\text{-}AMP + O_2 \rightarrow Luc \cdot AMP \cdot Oxyluciferin^{\cdot} + CO_2$

Stage 3: Return of excited oxyluciferin to ground state associated with emission of a photon of visible light

$Luc \cdot AMP \cdot Oxyluciferin^{\cdot} \rightarrow Luc + Oxyluciferin + AMP + h\nu\ (\approx 600\ nm)$

Equations adapted from Branchini et al.(55)

The versatility and emission profiles of the different luciferases make them an intriguing and exciting prospect for PDT and potentially PCI. The benefits would include a greater level of accessibility to deep lying tumours and/or metastases allied to a suitable level of tissue penetration giving the red-shifted emission peaks of Fluc. A benefit may also be seen in irregularly shaped tumours that are often difficult to illuminate in a uniform manner.

1.11 SUMMARY OF OBJECTIVES:

Chapter 3 – The Role of Reduction and Oxidation in Photochemical Internalisation.

The studies performed in this chapter investigated the role of the intracellular REDOX environment in PCI-enhanced delivery of both saporin and mitoxantrone. Furthermore, it reports on the factors that influenced the balance between PDT and PCI induced cytotoxicity. These experiments were carried out in 4T1-luc2 murine breast adenocarcinoma cells.

Chapter 4 – Photochemical Internalisation and Small Molecule Carriers.

This chapter aimed to investigate the effect that SMoCs had on the delivery of fluorescently labeled siRNA into 4T1-luc2 and MCF7 (human breast cancer cells). It went on to assess the impact of PCI on SMoC-enhanced deliver of fluorescently labeled siRNA.

Chapter 5 – Photochemical Internalisation in a £D Tumour Model.

In this chapter the novel compressed collagen artificial cancer mass model was used to assess the potency of PCI in a 3D structure. The aims of the studies were to first assess if 4T1 cells could be grown into 3D tumoroids and subsequently determine if PCI could be used to enhance saporin cytotoxicity in a 3D model.

Chapter 6 – Bioluminescent Photodynamic Therapy.

In this chapter Gaussia (MCF7-GLuc) and firefly (4T1-luc2) luciferase expressing cancer cells were used to investigate if bioluminescence could be used to trigger PDT induced cytotoxicity. Two photosensitisers were assessed: tetrabromorhodamine-123 and hypericin.

Chapter 2: Materials and Methodology

CELL LINES

2.1 4T1-luc2 cell line

The 4T1-luc2 (initial passage number = 7, all experiments carried out within 20 passages) murine mammary adenocarcinoma cell line (Caliper Life Sciences, Hopkinton, MA, USA) expresses a stably transfected firefly luciferase gene (Luc2). This was the main cell line used throughout the PhD study to investigate Photodynamic Therapy (PDT), Photochemical Internalisation (PCI), Bioluminescence-mediated PDT and the work on Small Molecule Carries (SMoCs). The parental cell line is the ATCC (CRL – 2539™) cell line. Gene transfer was performed using a pGL4 luc2 Lentivirus. *In vitro* bioluminescence produces approximately 6500 photons/sec/cell depending on imaging and culturing conditions. Thus this enables *in vivo* bioluminescent imaging for growing tumours and is therefore suitable for extrapolating this investigation to *in vivo* preclinical model (Nu/nu) mice in the future(56, 57).

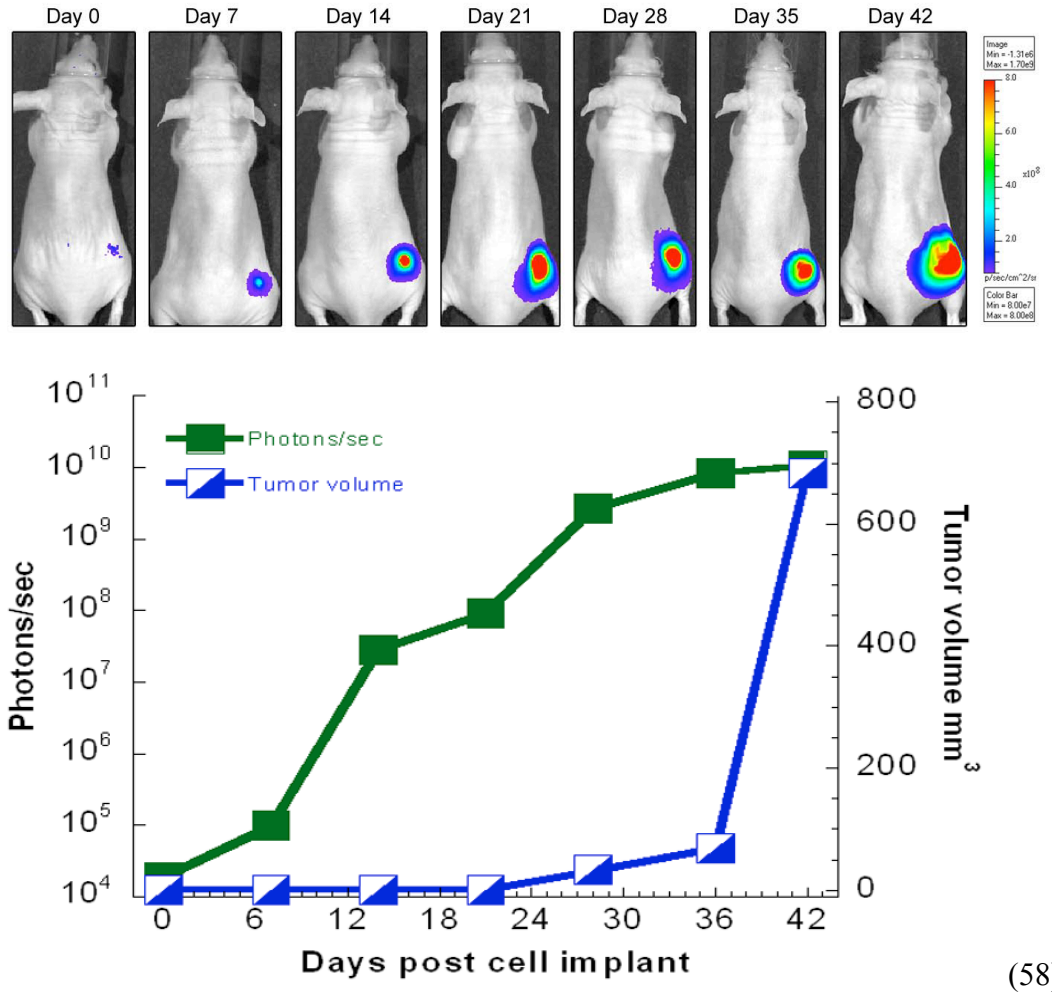

(58)

Figure 2.1– 4T1 *in vivo* bioluminescence (subcutaneous implantation model). 4T1-luc2 cells (five) were subcutaneously injected into dorsal aspect near the thigh in female nu/nu mouse. Imaging was undertaken 10 minutes after intraperitoneal (i.p.) injection of Luciferin (150 mg/kg). Detection of the bioluminescent signal (measured by IVIS spectrum) significantly preceded caliper measurement. (Adapted from Caliper Lifesciences, UK)(58).

2.2 MCF7 cell line

The MCF7 (initial passage number = 26, all experiments carried out with 12 passages), human breast adenocarcinoma cell line (European Collection of Animal Cell Cultures, Porton Down, UK), was previously bought and was available in the laboratory at UCL.

2.3 MCF7 Firefly and Gaussia Luciferase

The native MCF7 cells were transduced to produce two luciferase expressing cell lines: MCF7-FLuc and MCF7-GLuc.

2.4 CELL CULTURE PREPARATION AND REAGENTS

The 4T1 cells were routinely cultured in Roswell Park Memorial Institute medium (RPMI 1640, Sigma-Aldrich®, Poole (Dorset), UK) supplemented with 10% (v/v) fetal bovine serum (FBS, Gibco® Life Technologies, Paisley, UK) in a humidified atmosphere of 5% CO_2/air, 37°C. MCF7 cells were grown in Dulbecco's Modified Eagle's Medium/Nutrient F-12 Ham (DMEM F-12, Sigma-Aldrich) .

Cells were split via standard technique. Confluent cells were washed twice in phosphate buffered saline (1X without Ca^{2+} or Mg^{2+}), prior to trypsinisation (3 minutes – 4T1, 2 minutes – MCF7) (1.0 mg ml^{-1} in 0.2% phosphate-buffered saline (PBS)/EDTA), centrifuged (×2, 400g, 5 min). Once the supernatant was discarded, cells were re-suspended in media and used for routine passage or further experimental work. For plating (experimental) into 96-well plates (Nunc, Roskilde, Denmark) (100 µL $well^{-1}$) cells were re-suspended at 10,000 cells/100 µL.

2.5 CHEMICALS AND DRUGS

All chemicals were purchased from Sigma-Aldrich, unless otherwise indicated in the text.

2.6 Photosensitisers

$TPPS_{2a}$ (disulfonated meso-tetraphenylporphyrin, PCI Biotech, Oslo, Norway) dissolved in dimethyl sulfoxide (DMSO) to a stock concentration of 350 µg/ml and subsequently divided in to aliquots and stored (as solution) at −40°C,
in the dark, until use. Serial dilutions were subsequently dissolved into PBS and appropriate media. The final dissolved concentration of DMSO about <1% and was well below cytotoxic levels.

Hypericin (HYP) was prepared in DMSO and was diluted in PBS to a stock solution of 1.0 mM in aliquots and stored at -20°C. Serial dilutions were subsequently dissolved into PBS and appropriate media.

Tetrabromorhodamine-123 (TBR, Biotium®, Cambridge Bioscience®, Cambridge, UK) was dissolved in DMSO to a stock solution of 100 μM and stored in the dark at 4°C. Serial dilutions were subsequently dissolved into PBS and appropriate media.

2.7 Cytotoxins

Saporin (SAP, lyophilized protein), a type 1 Ribosome inactivating protein (cytotoxin) was initially dissolved in sterile water and then PBS to a stock solution of 1 μM and stored at 4°C. Serial dilutions were made up in appropriate media.

The anthracenedione Mitoxantrone (MTX) was dissolved in DMSO to a stock solution of 250 μg/ml and stored at 4^0C.

2.8 Reduction-Oxidation reagents

Powdered L-histidine (LH)) was dissolved in heated (37.5°C) PBS to a stock solution of 50 mM.

Buthionine Sulfoximine (BSO) a glutathione-depleting agent was dissolved in PBS to a stock concentration of 100 μg/ml and subsequently stored at 4^0C.

Bovine superoxide dismutase (SOD), a reducing enzyme that quenches intracellular superoxide free radical load (fig. 2.2). SOD was dissolved sterile water and subsequently PBS to a stock solution of 5 KU in aliquots and stored at -20°C.

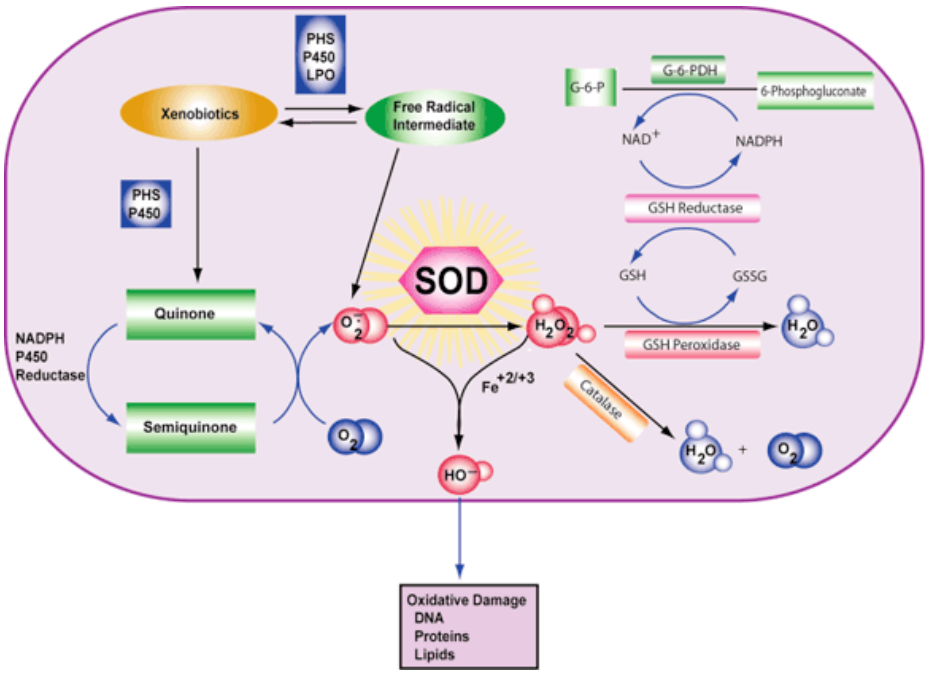

Figure 2.2 – Influence of superoxide dismutase (SOD) on the intracellular REDOX environment.
SOD plays an important role in maintaining superoxide and, in conjunction with catalase, hydroxyl radical homeostasis. Therefore, it may play an important role in quenching the excess of reactive oxygen species produced following activation of a photosensitiser. (Taken from Sigma Aldrich® website)(59)

2.9 Luciferases

Coelenterazine (Coele., Life Technologies® , Paisley, UK) is a substrate for Gaussia Luciferase, which was expressed within MCF7-GLuc cells. Due to its poor solubility coelenterazine was dissolved in methanol to a stock solution of 100 µg/ml. Serial dilutions were made up in PBS. Due to its poor oxidative stability and lack of equipment to create an oxygen free environment, Coele. was not kept frozen. This along with the issues encountered with its residual toxicity at higher doses resulted in the MCF7-GLuc-Coele. model for bioluminescence being abandoned in favour of the 4T1-luc2-Luciferin model.

D-Luciferin (D-Luc, Life Technologies) is a substrate for firefly luciferase, which was expressed in both the MCF7-FLuc and 4T1-luc2 cell lines. The sodium salt preparation of D-Luc was readily dissolvable in PBS into aliquots (100 µg/ml) and stored at -20°C.

2.10 Alexa-488 labeled saporin

PROTEIN BUFFER EXCHANGE:

5 mg of Saporin lyophilized protein (Molecular Weight : 30000) was made up in 1.5 ml de-ionised water (dH_20) to a concentration of 3.33 mg/ml, which is equal to 111 µM. Carbonate buffer; (9 ml 0.1 M $NaHCO_3$ + 1 ml 0.1 M Na_2CO_3) was made up and pH buffered to make a final solution (pH = 9.24). This was subsequently sterile filtered through a 0.45 µm syringe filter.

A PD10 column (GE Healthcare, Little Chalfont (Bucks), UK) was equilibrated 3 times with carbonate buffer (pH 9.24) using a spin protocol (1000g / 2 min) to elute. Sample was then transferred to a clean falcon tube with 1.5 ml protein solution added to the top, followed by adding 1ml stacking buffer (carbonate, pH 9.24) before further spinning to elute protein in new buffer.

2 ml was removed out of the column. It was assumed no loss of protein therefore protein concentration 2.5 mg/ml or 83.3 µM in carbonate (pH 9.24).

CONJUGATION REACTION:

1 mg of Alexa Fluor 488 carboxylic acid, succinimidyl ester (Molecular Weight: 643.41, Life Technologies), was dissolved in 233 µL DMSO to a concentration of 4.29 mg/ml; this equals 6.668 mM. This solution was vortexed to mix and 222 µL was immediately added to the 2 ml protein solution above. This new mixture was vortexed again to mix, covered in foil and placed on overhead rotation to mix at 12 rpm for 1 hour at room temperature.

Final volume = 2222 µL
Final Saporin = 75 µM
Final Alexa Dye = 666.2 µM
Molar dye to protein ratio = 9 to 1
Final DMSO = 10%

CLEAN UP/BUFFER EXCHANGE:

A PD10 column (GE Healthcare) was equilibrated 3 times with PBS using a spin protocol (1000g / 2 min) to elute. This was transferred to a clean falcon with

2.222 ml of conjugate solution added to the top. Subsequently, 278 µL of stacking buffer (PBS) was added and the mixture spun to elute the conjugated protein in new buffer. This was then sterile filtered through a 0.45 µm syringe filter. 2.5 ml of filtered solution was recovered out of column. Again assuming no loss, the protein was now at 2 mg/ml or 67 µM in PBS. This was then stored in the dark at 4°C.

QUANTIFICATION

Quantification was calculated using the following equations:

$$\text{Protein Concentration (M)} = \frac{[A_{280} - (A_{495} \times 0.11)] \times \textit{dilution factor}}{23380}$$

where 23380 cm^{-1} M^{-1} is the molar extinction coefficient of saporin and 0.11 is a correction factor to account for absorption of the dye at 280 nm.

$$\text{Moles dye per mole protein} = \frac{A_{495} \times \textit{dilution factor}}{71000 \times \textit{protein concentration (M)}}.$$

where 71000 cm^{-1} M^{-1} is the approximate molar extinction coefficient of Alexa Fluor®488 at 495 nm.

Absorbance = Abs

MW saporin = 28501, Abs max ε280 = 23380 $cm^{-1}m^{-1}$
MW dye = 643.41, Abs max ε495 = 71000 $cm^{-1}m^{-1}$.
Correction factor for dye → 0.11 = A280/A495 (fig. 2.3)

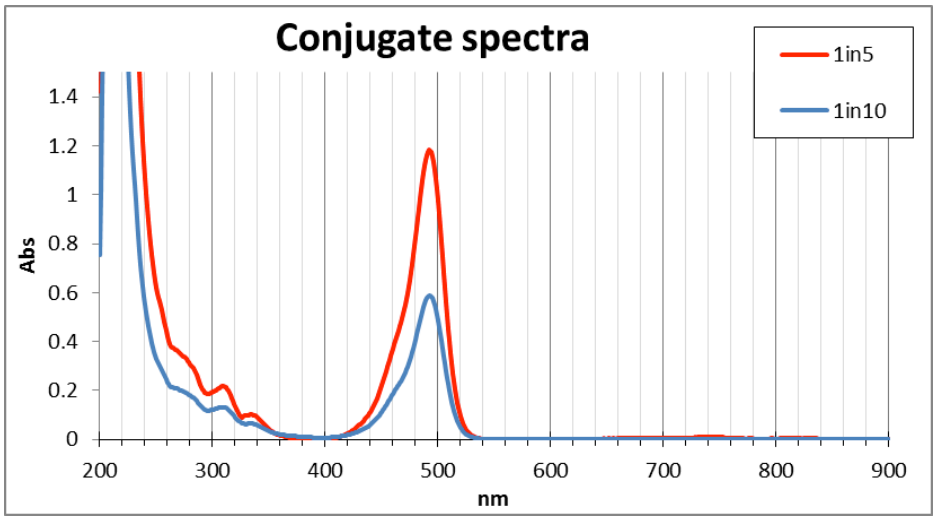

Figure 2.3 – Absorption spectroscopy for SAP – Alexa-488 conjugate.
Two samples: (1) Red line - diluted 1 in 5 in PBS, (2) Blue line - diluted 1 in 10 in PBS. Data was normalised to 900 nm. For the 1 in 5 dilution the ABS = 1 therefore cannot use reliably.

A

1 in 10	**Wavelength (nm)**	**Absorption (A BS)**
Dye	495	0.58
Protein	280	0.18

B

	Molecular weight	**Extinction Coefficient @ 280 nm (ε280)**	**Extinction Coefficient @ 495 nm (ε495)**
Dye	643.41	7810	71000
Protein	28501	23380	-

C

	Molar	**µM**	**µg/ml**
Dye	8.12×10^{-6}	81.76	0.052
Protein	4.94×10^{-6}	49.428	1.409

Table 1 - Calculation of conjugation ratio and SAP stock concentration.
A = ε x C where A = absorption, C = molar concentration, ε = extinction coefficient. **M = B/R** where M = molar concentration, B = mg/ml, R = molecular weight

Based on Table 1 (above) the following calculations can be made:
Molar Dye (A495) = 8.12×10^{-6}
At this **M** the abs for the dye @ 280 = 0.06
Based on A280 for dye, the A280 for protein = 0.12
Therefore **Molar Protein (A280)** = 4.94×10^{-6}
This translates into a protein concentration (SAP) of 49 µM with a dye-loading ratio of 2 per molecule of SAP.

2.11 SMoCs

The SMoCs used in this thesis were kindly synthesised and donated by Professor David Selwood, Wolfson Institute, UCL.

2.12 SMoC – siRNA-Alexa-555 conjugation

In order to monitor the facilitative SMoC effect on the uptake of siRNA a fluorescently labelled siRNA oligomer was used. Alexa Fluor® Red Fluorescent oligonucleotide (Invitrogen, LifeTechnologies, Poole (Dorset), UK) supplied as a 20 µM stock of Alexa Fluor® 555-labeled, double stranded RNA oligomer in 100 mM KOAc, 30 mM HEPES-KOH, pH 7.4, and 2 mM MgOAc (annealing buffer). Confocal microscopy was used to determine the intracellular localisation. Lipofectamine® RNAiMAX (Invitrogen) was chosen as a positive control for 'gold standard' siRNA transfection. The oligonucleotide was diluted in PBS to a final concentration of 1 µM either alone or in combination with 10 µM 4G-

BfSMoC- COOH, 2. The oligonucleotide/4G-BfSMoC-COOH, 2 was given 15 minutes to complex at room temperature. Final dilutions were made in the appropriate cell medium (4T1 – RPMI, MCF7 – DMEM F-12). Both cell lines were treated with media (alone), oligonucleotide (alone), 4G-BfSMoC-COOH, 2 (alone) or oligonucleotide/4G-BfSMoC-COOH, 2 for 24 hours at 37°C. Lipofectamine controls were transfected according to manufacturers' instructions to a final concentration of 3.75 µL/mL + oligonucleotide. Cells were washed twice with PBS and treated with phenol-red-free media (Sigma-Aldrich®) prior to confocal imaging.

2.13 3- [4, 5-dimethylthiazolyl]-2, 5-diphenyltetrazolium bromide (MTT) Assay

The primary cell viability assay utilised for the *in vitro* studies in this thesis was the 3- [4,5-dimethylthiazolyl]-2,5-diphenyltetrazolium bromide (MTT, Sigma-Aldrich®) assay. Reduction of the hydrophilic tetrazonium salt by mitochondrial dehydrogenases results in purple insoluble formazan derivative. Therefore, metabolic activity was taken as a measure of viability. At experimental end points, medium was aspirated and washed (PBS), followed by a 2 hour incubation with 100 µl MTT (1 µg/ml in RPMI) at 37°C, 5% CO_2. MTT was replaced with Dimethyl Sulfoxide (DMSO, 100 µL/well) to solubilise formazan crystals. The absorbance of the formazan derivative was quantified using a micro plate reader (ELx800 Biotek 4, Bedfordshire, UK). This protocol is well described in the literature(25, 37).

2.14 AlamarBlue®

AlamarBlue® was used as an alternative to MTT for the 3D-tumour model, mainly due to the benefit of it being a non-toxic metabolic assay. As with the MTT assay, it is commonly used to assess cell viability. The assay comprises a fluorometric/colorimetric growth indicator, which is proportional to the metabolic activity of the cells. It specifically incorporates an oxidation-reduction (REDOX) indicator, which both fluoresces and undergoes a shift in colour in response to reduction of the growth medium resulting from cell growth(60).

AlamarBlue® was added to cell seeded collagen gels and was performed on day

7 by adding 2 ml of 1:10 AlamarBlue® to the existing media surrounding the collagen gels. The samples were then incubated for 4h before transferring 100 µL (x6) samples of the media into a clear flat-bottom 96-well plate. Subsequently, fluorescence was scanned for each treatment group (Ex 560 nm/ Em 590 nm).

2.15 LUCIFERASE TRANSDUCTION

Transduction of human MCF7 cells with firefly and Gaussia luciferase was required in order to perform prospective bioluminescence studies. The materials required for gene transduction (lentiviral vector, luciferase genes and polybrene) were kindly supplied by Dr Martin Pulé (Cancer Institute, UCL) with experimental guidance provided by Dr Amit Jathoul (Cancer Institute, UCL).

Procedure

24 hours prior to transduction:

MCF7 cells were split into a 6-well tissue culture plate at $3.0x10^5$ per well in DMEM F-12 supplemented 10% FBS.

The cells were then incubated at 37°C for 24h to enable growth to a desired confluence of 40-60%, which is necessary for optimal transduction.

Transduction:

Cells were checked under a light microscope in order to assess health and confirm that they had reached the right confluence.

The media was aspirated and replaced with 1.5 ml of new media in each well. 150 µL of viral supernatant per well for 1x concentration was added to each appropriate well. In addition to this a linker molecule (polybrene) was added directly to media to achieve a final concentration of 8 µg/ml. The plates were gently rocked on a plate shaker to facilitate the even distribution of both virus and linkers. Cells were then incubated at 37^oC for 24h. Media containing viral supernatant and polybrene was aspirated and replaced with appropriate media. The cells were then re-incubated for a further 72h prior to assessment of trans-gene expression using flow cytometry. The entire process can be repeated by adding viral supernatant and polybrene if gene expression is found to be unsatisfactory.

NB. This process took place in antibiotic naïve cells as advised by Dr Jathoul. Trans-gene expression was confirmed using flow cytometry. Once performed cells were subsequently sorted using fluorescence-activated cell sorting (FACS) to maximize the density of highly expressing cells (see chapter 6). Subsequently flow cytometry was repeated to confirm the final level of trans-gene expression.

2.16 PDT/PCI EXPERIMENTS

The PDT and PCI experiments followed a standard format comprising the following:

1. Cells were trypsinised as described above and following centrifugation, they were counted using a haemocytometer. Cells were then diluted and plated into 96-well plates (Thermo Scientific® Nunc® clear, flat bottom 96-well plates, UK) at a cell number of 12 x 10^4 ml^{-1}. Each treatment group comprised a minimum of 16 x 100 µL wells. There was a minimum of five repeats for each PDT/PCI experiment.

2. Following 24h incubation at 37°C the various drug combinations (described in the results of the PCI chapter) were added. For the light-after protocol, each treatment combination was added at this time (fig. 2.6). For the light-before protocol, only photosensitiser and REDOX drugs (BSO/LH/SOD) were added (fig. 2.7). The entire process took place under dark conditions in the whole laboratory area. Plates were then wrapped in foil and re-incubated for 24h at 37°C.

3. 24h later the cells were washed twice in PBS. Subsequently, media or appropriate doses of the REDOX drugs were added to the appropriate treatment groups (for both light-after and light-before treatment regimens). In this way, excess photosensitiser and cytotoxin (SAP/MTX) were removed from the extracellular environment. Cells were then re-incubated at 37°C for a further 4h or immediately illuminated. The plates were then illuminated for the appropriate time (seconds) using a blue lamp, LumiSource® (PCI Biotech, Norway), which emits light uniformly from four fluorescence tubes (spectral region 375-450 nm) with a fluence rate of 7 mW cm^{-2} (fig. 2.4).

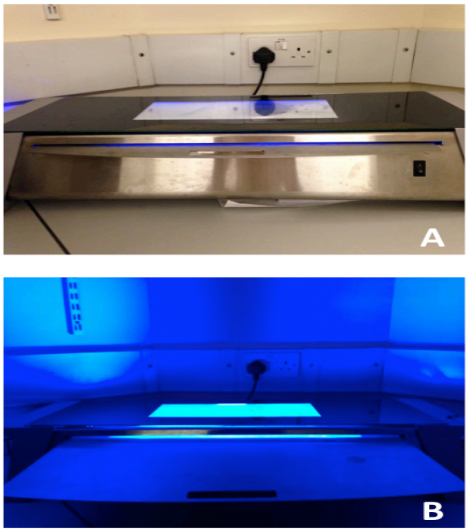

Figure 2.4 – Plate illuminator.
(A) LumiSource® OFF, (B) LumiSource® ON. Comprises a bank of 4 fluorescent tubes. In order to maximise illumination a light impermeable box is placed over the plate during illumination.

4. Cells were subsequently re-incubated at 37°C for 24h/72h (light-after) or media changed with the addition of cytotoxin +/- the appropriate REDOX drugs (either in combination or alone). Again, these were re-incubated for 24h/72h.

5. Cells were subsequently washed twice in PBS and treated with MTT (100 µL, 1mg/ml, made up in media) and incubated for 2h. At this point, the MTT was removed and the remaining crystals were dissolved in DMSO and placed on a plate shaker for 5 minutes prior to reading absorbance on the plate reader (fig. 2.5).

Figure 2.5 – Plate reader.
The absorbance of the formazan derivative (MTT) was quantified using a microplate reader (ELx800 Biotek 4).

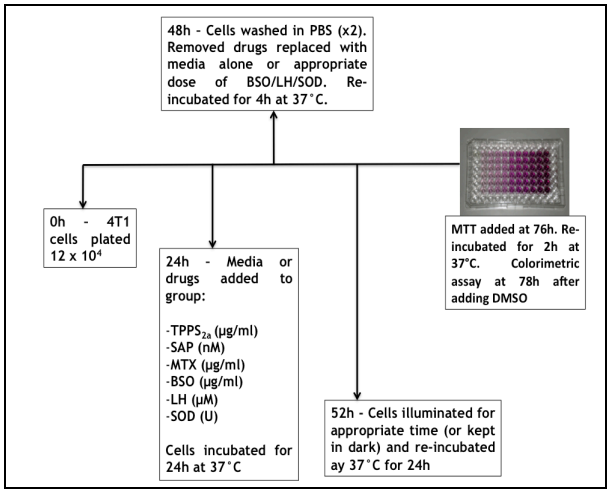

A

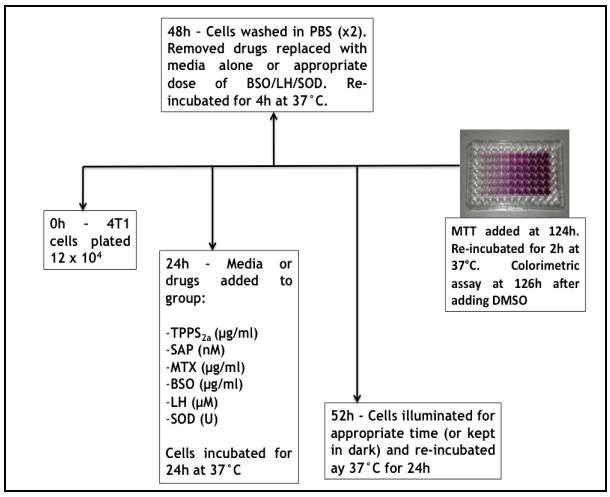

B

Figure 2.6 – Light 'after' cytotoxin treatment regimen timelines.
For this regimen, cells were treated with photosensitiser and cytotoxin +/- REDOX agent prior to illumination. Cells were exposed to MTT (cell viability assay) 24h (A) or 72h (B) following illumination. For the 'immediate' illumination group there was no 4h re-incubation following drug wash off at 48h. (MTT plate image from Wikipedia).

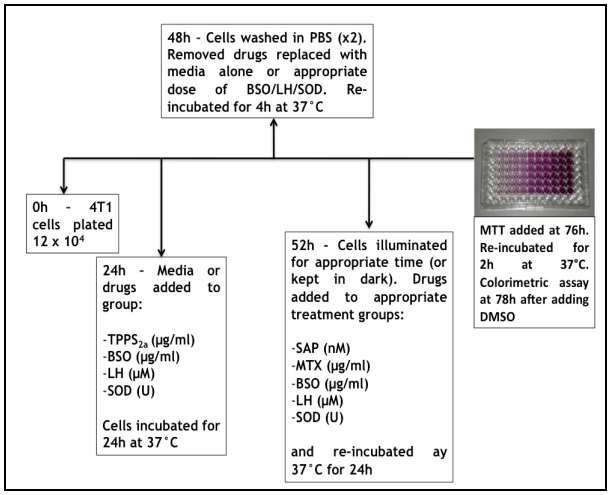

A

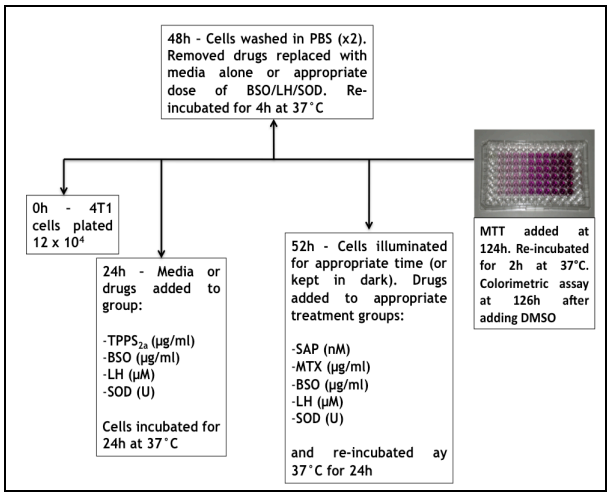

B

Figure 2.7– Light 'before' cytotoxin treatment regimen timelines.
For this regimen, cells were treated with photosensitiser +/- REDOX agent prior to illumination with cytotoxin added after exposure to light. Cells were exposed to MTT (cell viability assay) 24h (A) or 72h (B) following illumination. For the 'immediate' illumination group there was no 4h re-incubation following drug wash off at 48h. (MTT plate image from Wikipedia).

2.17 BIOLUMINESCENT PDT

The bioluminescent PDT experimental protocol was based upon the standard PDT/PCI protocol with a few alterations. Firstly, there is the consideration of adding D-luciferin or coelenterazine for light production, in particular the amount of time required. This was determined by performing emission kinetics work for the MCF7-GLuc species whereby, the intensity and duration of the bioluminescent signal was measured over time. This was achieved by adding coelenterazine (25µg/ml) to cells that had been growing for 24h (seeded at 15 x 10^4) in black 96-well plates (Thermo Scientific® Nunc® UK) and reading the

bioluminescence initially for spectral analysis before a kinetic measurement was taken for emission between 460 nm-490 nm (Varioskan Flash, Thermo Scientific, Loughborough, UK). Subsequently, a treatment time of 2 x 15 minutes (900 s) was decided upon. Furthermore, following the acquisition of initial data it was determined that the extracellular secretion of GLuc might necessitate the presence of photosensitiser in the media (phenol free RPMI-1640 or phenol free DMEM F-12) both without FBS (as this can bind the luciferin) at the time of bioluminescence. This was done to enhance the BRET effect(61-63) as described in chapter 6.

1. Cells were trypsinised as described above and following centrifugation, they were counted using a haemocytometer. Cells were then diluted and plated into 96-well plates (Thermo Scientific® Nunc® white (bioluminescence enhanced), flat bottom 96-well plates, UK) at a cell number of 8×10^4 ml^{-1}. Each treatment group comprised a minimum of 16 x 100 µL wells. There was a minimum of three repeats for each bioluminescent PDT experiment.

2. Following 48h incubation at 37°C the various drug combinations described later (chapter 6) were added. Each treatment combination was added at this time +/- SOD. The entire process took place under dark conditions in the lab. Plates were then wrapped in foil and re-incubated for 4h (hypericin) or 1.5h (TBR) at 37°C.

3. Cells were then washed twice in PBS. Subsequently, phenol free media or appropriate doses of the photosensitiser + luciferin (D-luciferin or coelenterazine) +/- SOD were added to the appropriate treatment groups for 15 minutes. The media was then removed and the same process repeated for a further 15 minutes. The media was removed again and replaced with media +/- SOD.

4. Following a 2h incubation period, cell viability was assessed using the MTT protocol described above.

2.18 CONFOCAL MICROSCOPY

Cell preparation: 4T1 (murine) breast cancer cells (1 x 10^4) were seeded on 35 mm diameter glass-bottomed, polylysine coated Fluorodishes™ WPI, UK). They were incubated for 48 to encourage adherence and optimal sub-confluent cell spreading for imaging. Pilot studies were performed to optimize cell seeding and incubation length pre-treatment. 4T1 cells were incubated with fully supplemented fresh RPMI-1640 Medium. At 48h-post seeding, the cells were treated with drug (SAP-488 or MTX) for 24h at 37°C. Cells were subsequently washed with PBS and bathed in appropriate phenol-free media for a further 4h. At which point cells were either: i) illuminated for 90 s (using the LumiSource® illuminator) with confocal images taken after a final 4 h incubation period; ii) Confocal images were taken initially followed by on-stage exposure to the 405 nm confocal laser for 15s before further images were taken at two time points (immediately and 240 s after 405 nm laser). Short exposures were employed in order to protect the integrity of the cell and so as not to perturb the fluorescence distribution. Appropriate controls were used throughout. Different combinations of excitation/detection wavelengths were used for Alexa – 488 (Ex 488 nm, Em 520 nm) and MTX (Ex 635 nm, Em 647 nm) compared to $TPPS_{2a}$ in order avoid crosstalk (controls were checked) and limit the excitation of $TPPS_{2a}$ (405 nm).

Saporin – Alexa 488 complex: This was prepared according to manufacturers' specification as described above. Final dose used for imaging was 40 nM (SAP-488).

Lysotracker® Green (LYG: Invitrogen, UK) experiment: Following 24h incubation with MTX, cells were washed and treated with LYG 50 nM (used to image endolysosomal compartments) for 30 min prior to confocal imaging (Ex 488 nm, Em 520 nm).

Monochlorobimane (mBCl, Life Technologies): this is a thiol probe that remains non-fluorescent until conjugated. It can react with low molecular weight thiols

including glutathione(64-66) and mercaptopurine. This probe was used to determine intracellular glutathione expression with or without BSO. The absorption/emission maximum for the glutathione-monochlorobimane conjugate is ~394/490 nm. Cells were treated with 40 μM mBCl in RPMI-1640 for 20 minutes prior to confocal microscopy as per previously reported protocol(66).

Confocal microscope: Cells were observed using an inverted Olympus Fluoview 1000 confocal laser-scanning microscope to determine intracellular localisation of MTX, LYG, mBCl or SAP-488. Fluorescence confocal images were obtained using a 60 x 1.35 NA oil immersion or a 20 x 0.75 NA objective (Olympus). Fluoview FV1000 (Olympus) and Image J software were used to analyse images. A minimum of five samples, of equal area, was taken in order to perform quantitative analysis of mean fluorescence. Each experiment was repeated twice.

2.19 Lipid peroxidation confocal studies

In order to assess the impact of ROS production on lipid peroxidation the Image-iT® Peroxidation Kit (Life Technologies, Molecular Probes®, UK). Oxidation of the fluorophore, within live cells, results in a shift in fluorescence from red to green(67), which enables ratiometric analysis(68) of lipid peroxidation as a result of photosensitiser mediated ROS production.

Cells were prepared as described above in polylysine-coated fluorodishes and treated with chosen doses and combinations of $TPPS_{2a}$, SAP and BSO. Appropriate controls were used throughout. However, the Cumene hydroperoxide positive control proved too toxic for the cells at the doses recommended by the manufacturer.

The lipid probe was prepared as per the manufacturers guidelines. The probe, which is pre-dissolved in DMSO to 10 mM, was diluted in media to a final concentration of 10 μM. This was added to cells that had already been treated for 24h with appropriate agents and illuminated using the LumiSource®

illuminator. These cells were incubated for 30 minutes at 37°C and subsequently washed in PBS three times. Following washing, phenol-free media was added to the cells prior to confocal imaging.

The confocal settings used:

- Reduced form of probe. Recommended excitation and emission maxima are 581/591 nm. Settings used 559/579-615 nm.
- Oxidised form of probe, 488/510 nm. Settings used 488/490-525 nm.

Appropriate controls were utilized including dark controls. Triplicate repeats were performed and quantitative analysis was performed as described above in order to provide ratiometric comparison between reduced and oxidized lipid.

2.20 SMoC confocal studies

Cells were prepared for confocal as described above and treated with appropriate SMoC, siRNA-Alexa-555, lipofectamine concentrations and combinations as described above. Original image files were analysed using Image J software. Image J software was again used to analyse the uptake of the labelled siRNA +/- 4G-BfSMoC-COOH, 2 in order to quantify the mean intracellular signal intensity in comparison to the background level of fluorescence(69). Appropriate controls were used throughout.

2.21 3D ARTIFICIAL CANCER MASS SYNTHESIS AND PCI STUDIES

The 3D artificial cancer masses (ACMs) were based on a type I collagen hydrogel, in to which 4T1 cancer cells were embedded and the complex placed under plastic compression with the aim of increasing both cell and matrix density. The methodology follows the model reported by Nyga et al. (2013)(50).

The first step was the preparation of the collagen hydrogel and 4T1 cell complex/artificial cancer mass (ACM). For this, rat-tail type I collagen, 2.04 mg ml^{-1} in 0.6% acetic acid (Fist Link UK) was complexed with 10x concentrated minimum essential Eagle's medium (0.4ml) (MEM, Life Technologies, Paisley, UK). In order to neutralise the acidic solution, initially 5 M NaOH was added as

individual drops. As the colour of the mixture changed to pink, 1 M NaOH was used until the correct colour was achieved (fig. 2.8), indicating ~pH 7.3 (the mixture was agitated throughout to facilitate mixing). Following this the mixture was put on ice to enable the dispersion of air bubbles present due to the mixing process. If the mixture was not rapidly cooled it would have set, rendering it not suitable for cell implantation.

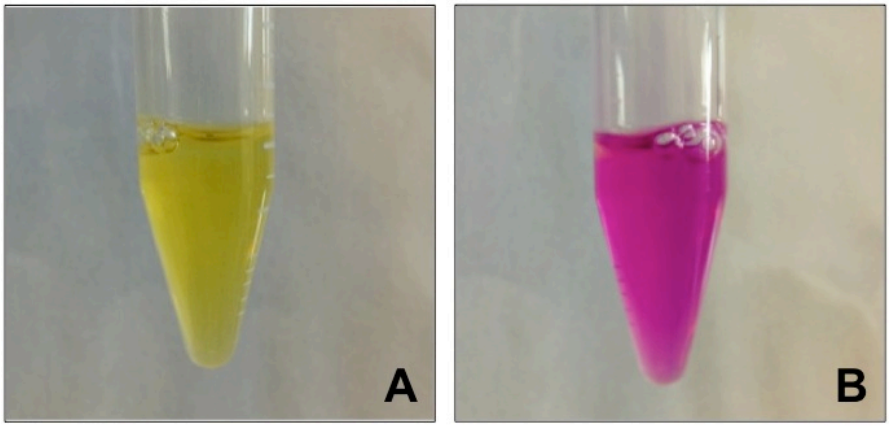

Figure 2.8 – Neutralisation of rat-tail collagen and acetic acid using NaOH.
(A) Type I collagen (2.4 mg ml^{-1}) with 0.6% acetic acid prior to addition of NaOH, (B) neutralised type I collagen/acetic acid following addition of NaOH. The bright pink colour indicates ~pH 7.3.

During this time a mould was set up with a 165 µm steel mesh and a nylon mesh on absorbent paper at the bottom. A 0.4ml (for a 4ml collagen gel) suspension of 4T1 cancer cells (6.4 million) was added to the collagen and gently mixed using a Pasteur pipette. The volume ratios of collagen:MEM:cell suspension were 8:1:1(50). This mixture (4 ml) was then poured into the rectangular mould resting on a glass slide, which is in turn on top of filter paper. Mixture was allowed to set for 30 minutes at room temperature. The steel mesh was placed on top of the filter paper, with the nylon mesh placed above the steel mesh. The 3 were then placed over the opening of the mould and the mould inverted. At which point the mould was placed under compression for 30 s using a 175g weight. The mould was then inverted, the mesh removed and placed on the other side and the process repeated for a further 30 s of compression. The whole process, undertaken under sterile conditions, enabled liquid expulsion and defined compression of the cell-populated gel (ACM).

The compressed ACM was cut in to 4 equal pieces using a sterile surgical blade. These were transferred to individual wells within a 12-well plate. The AMCs were then anchored on to an acellular collagen scaffold (hydrogel), using 10 ml of uncompressed collagen gel (collagen:MEM ratio 9:1) (fig. 2.9). The resultant 3D cultures comprising a central dense ACM surrounded by acellular collagen (to mimic cancer stroma) have been termed: tumoroids. Plates were incubated for 30 minutes at 37°C. Media was then added (DMEM F-12 + 10% (v/v) FBS and 10% penicillin/streptomycin) and the cells incubated for 24h. At this point the media was changed to (RPMI + 10% (v/v) FBS) and the ACM grown for a further 6 days prior to experimentation. Media was changed every 48h.

At day 7 tumoroid growth was assessed using a light microscope. Drugs were subsequently added to the tumoroids: Control (media, RPMI-1640), PDT ($TPPS_{2a}$ 0.8 μg/ml), Cytotoxin (SAP 60 nM) and PCI ($TPPS_{2a}$ + SAP). All of this performed under standard 'dark' conditions. These were subsequently wrapped in foil and incubated for 24 hours. Media was then carefully aspirated and the tumoroids washed three times with PBS. Media was then added and the ACMs were re-incubated for 4h at 37°C.

The tumoroids were then illuminated using the LumiSource® illuminator for 3 minutes, before being transferred back to the incubator. The tumoroids were then left to recover for 7 days (media changed every 48h). The 7-day delay was chosen based on advice given by colleagues at the Royal Free Hospital, Department of Surgery, who have a great level of experience in 3D-tumour models.

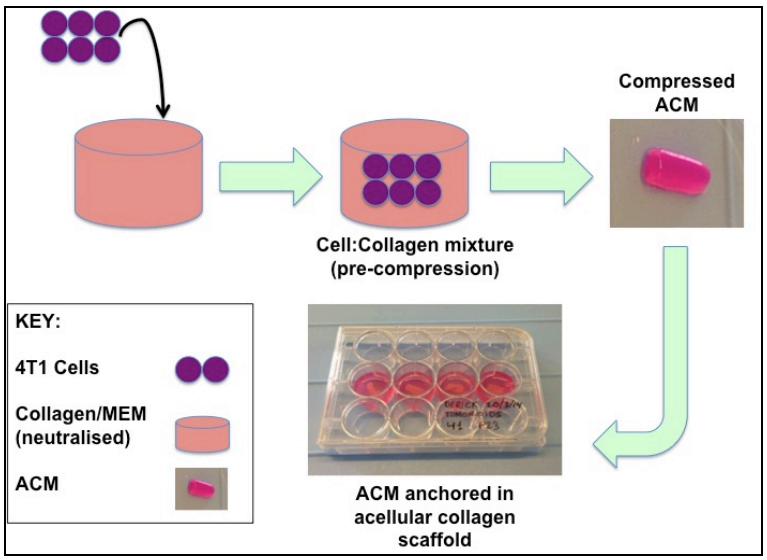

Figure 2.9 – Illustration of stepwise synthesis of 4T1 cell Artificial Cancer Mass. Following synthesis the ACM was grown for 7 days, and tumoroid growth assessed under light microscope prior to addition of drugs.

The timings used for *in vitro* experiments (24h or 72h) would not have been sufficient to detect a significant cytotoxic effect. AlamarBlue® toxicity assay, subsequently performed prior to fixation in formalin.

2.22 STATISTICS

Results generated from the work undertaken for this thesis were generally parametric, as befitting data derived from experimental repeat laboratory protocols. All statistical analysis was undertaken using Microsoft Excel and subsequently GraphPad PRISM.

Gaussian distribution was confirmed and analysis was undertaken by one-way ANOVA followed by post hoc analysis (Tukey's), non-parametric investigations were undertaken for data sets with small repeats per group <4).

Repeats for most experiments were n=6 per group, with a minimum of n=4. Routinely, each of these numbers were averages of multiple readings. For example, multiwell data were averaged as appropriate (for example 8 well readings = one average number, then used for statistical analysis). In addition all multiwall data was normalised (using GraphPad PRISM) to enable comparison. In other experiments (for example tumoroids/confocal), numbers were averages of duplicates. Significance was taken at $p<0.05$.

Chapter 3: The role of reduction and oxidation in Photochemical Internalisation

SCIENTIFIC BACKGROUND

Reduction-oxidation (REDOX) homeostasis is vitally important for the survival of mammalian cells. Physiological REDOX homeostasis is maintained by appropriately balancing the levels of pro-oxidants and antioxidants within a cell. The majority of reactive oxygen species (ROS) are produced by mitochondria in the electron-chain during aerobic respiration(70). Other sources of ROS production include the hepatic cytochrome P450 (CYP450) system, which is involved in the metabolism of toxic and non-toxic compounds; and the xanthine oxidase pathway during the formation of H_2O_2(71). The roles of ROS, at sub-micromolar levels, as secondary messengers for triggering cell proliferation, gene expression and apoptosis have also been described. Pi et al. (2007) (72) reported that H_2O_2 generated from glucose metabolism has an important role in triggering insulin secretion from β-cells of the pancreas. However, excessive or persistently elevated levels of H_2O_2 have been shown to disrupt mitochondrial activity(73) and alter macromolecules subsequently contributing to the pathogenesis of diabetes mellitus (74). ROS are also implicated in carcinogenesis and the development of the multidrug resistant (MDR) phenotype. For example ROS have been shown to modulate the structure(71), activity(75) and gene expression (via the activation of hypoxia-inducible factor)(76, 77) of cellular efflux pumps up-regulated in the MDR phenotype. Overexpression and/or increased activity of such pumps is an important feature in MDR. In order to manage higher levels of endogenous ROS, antioxidants are produced by a variety of enzymes including catalase, superoxide dismutase (SOD) glutathione peroxidase and glutathione S-tranferase(71, 78). If the balance is weighted in favour of oxidation it may result in intolerable and potentially mutagenic oxidative stresses. For example, Sies and Cadenas (1985)(79), described the potential detrimental effects of oxidative stresses on nucleic acids, lipids and structural carbohydrates. One of the well-described mechanisms for cellular protection against ROS damage is under the regulation of Nuclear Factor (erythroid-derived 2)-like 2 also known as NFE2L2 or Nrf2 (80, 81). Under normal REDOX conditions, Nrf2, is kept inactive following binding to Keap1 (Nrf2-Keap1), which prevents it acting as a transcription factor for the

antioxidant response element (ARE) associated genes that encode a range of antioxidants. However following oxidative attack Nfr2-Keap1 is cleaved, subsequently liberating Nfr2 to transcribe ARE associated genes to enhance the reducing power of the cell.

Lipid peroxidation is a very important consequence of ROS interactions with polyunsaturated fatty acids (PUFAs). PUFAs play a variety of important roles in cell signalling, membrane structure and function, regulation of gene expression notwithstanding energy provision(82). Linoleic acid (C18:2n-6) and α-linolenic acid are the two essential fatty acids that animals are entirely dependent on from plant sources. PUFAs are known to exhibit a particularly high sensitivity to oxidative stresses when compared to other cellular macromolecules. Of the PUFAs, phospholipids are particularly susceptible to oxidative damage not least owing to their proximity to enzymatic and non-enzymatic systems that can generate pro-oxidative-free radical species(83). Wagner et al (1994)(84) reported that the sensitivity of PUFAs to oxidative damage increases with the number of double bonds per fatty acid molecules, thus the more unsaturated a fatty acid the greater the reducing power it possesses. Of particular importance when considering the effect of photosensitiser mediated ROS generation in the membranes of organelles is the fact that 30-80% of the mass of the biological cell membrane is made up of lipids(82). The peroxidation of lipids, as described by Catala (2006)(83) is a 3 step process involving:

i) Initiation – this includes the abstraction of a hydrogen atom from a methylene group in PUFA, mainly phospholipids. This can be triggered by reaction with among others peroxyl (ROO•), hydroxyl (OH•) and alkoxyl (RO•) radicals but not H_2O_2 or superoxide (O_2-•)(85). The process involves the reaction between a free radical e.g. OH• with PUFAs resulting in the formation of a lipid radical, which subsequently reacts with O_2 forming lipid peroxyl radical (LOO•). Following this the lipid peroxyl can abstract hydrogen from -CH_2- forming a lipid hydroperoxide (LOOH) and a second lipid radical(83).

ii) Propagation – a chain reaction is set up as LOOH can undergo reductive cleavage by reduced transition metals such as Fe^{2+} forming LO• (alkoxyl radical)(82). Both LOO• and LO• can oxidise other unsaturated fatty acids in a process that is governed by the reactivity of free radicals thus, for example, the LOO• radical is more reactive than PUFA• thus will propagate the reaction (86). It is important to note at this point that there are different chemical reactions involved in forming LOOH, which occur with the different ROS, for example, with singlet oxygen there is the 'ene' reaction with unsaturated double bonds.

iii) Termination – this process is facilitated by the presence of transition metals and ascorbic acid (vitamin C). LOOH decomposes to yield a range of products including reactive aldehydes such as 4-hydroxynonenal, 4-hydroxyhexenal, and malonaldehyde.

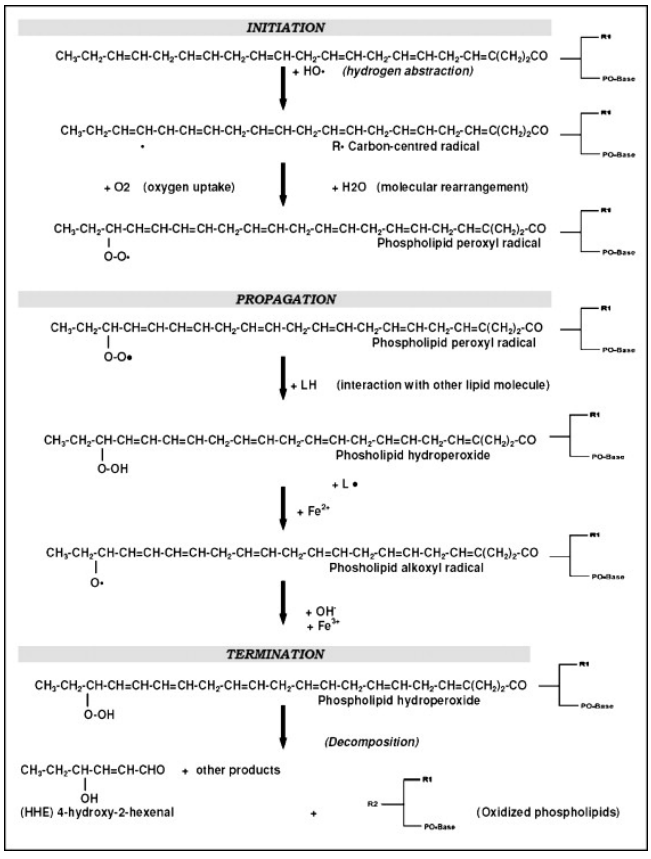

Figure 3.1 – Chemical steps for Lipid Peroxidation.
Diagrammatic representation of process for lipid peroxidation including docosahexaenoicacid (22:6*n*-3), R1=fatty acid, R2=fragmentation products of fatty acid oxidation. Catala 2009(82)

iv) Of the reactive aldehydes, 4-hydroxy-2-nonenal (HNE) is the main aldehyde formed from n-6 fatty acids including linoleic and arachadonic acid(83) and these have been shown to increase within membranes following oxidative insults(87). Whilst 4-hydroxy-2-hexenal (HHE) is formed following the decomposition of n-3 (e.g. α-linolenic and docosahexaenoic acid) lipid hydroperoxides. These aldehydes play an important role in prolonging the effects of oxidative attack as they can persist for longer than free radicals owing to their relative stability. Further more they can diffuse within or even out of a cell and covalently react with distant targets including proteins, DNA and phospholipids(83). Sub-lethal doses of the HNE and HHE have also been implicated in both physiological and pathophysiological processes where they can function as second messengers to regulate among other functions cell division(88), differentiation(89), and apoptosis(90). This indicates that the by-products of lipid peroxidation can have a significant effect of cell function even if the oxidative insult that initiated their formation is primarily non-lethal.

Given the preference in PCI to utilise amphiphilic photosensitisers that preferentially reside within the phospholipid bilayer(26) it is important to consider the potential effects of ROS generation within this lipid environment and potential generation of lipid hydroperoxides +/- reactive aldehydes.

3.1 Disulfonated meso-tetraphenylporphyrin ($TPPS_{2a}$)

The photosensitiser of choice in this study was $TPPS_{2a}$, owing to its amphiphilic properties making it an ideal photosensitiser for PCI(26). In addition to its ability to act as a photosensitiser for PDT, the suitability of $TPPS_{2a}$ for PCI is well described in the literature for both *in vitro* and *in vivo* studies(24, 43, 91). $TPPS_{2a}$ has a very similar structure to the chlorin-based photosensitiser, Amphinex® (fig. 3.2), which is currently undergoing clinical trials for PCI of bleomycin in head and neck cancer and cholangiocarcinomas. The 'targeting' of $TPPS_{2a}$ to the endo-lysosomal membranes is a product of its amphiphilic structure with sulfonation on adjacent phenyl rings and the methodology employed in this study (e.g. 4 hour wash out period).

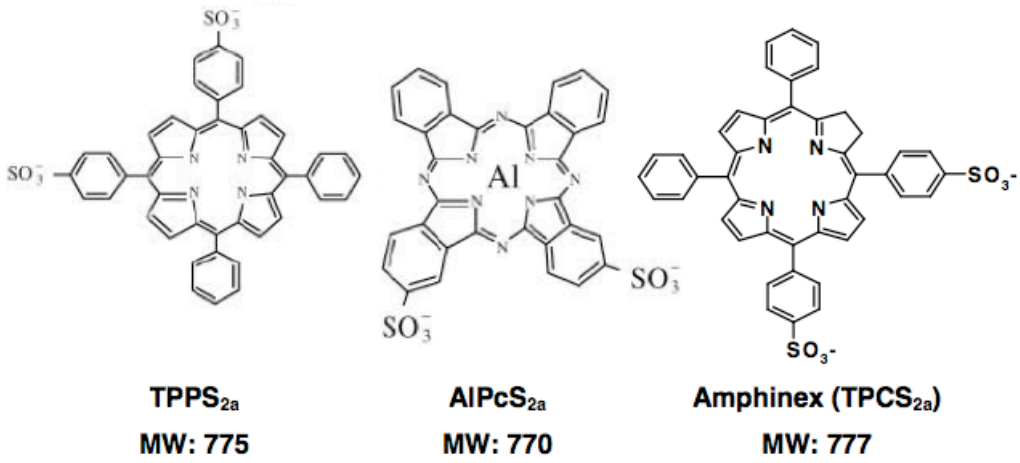

Figure 3.2 – Molecular weight and structure of three disulfonated amphiphilic photosensitisers.
Sulfonation of the photosensitisers confers amphiphilic properties. $TPPS_{2a}$ and $TPCS_{2a}$ (Amphinex®) share almost identical structures. Amphinex has been specifically synthesised for use in humans, therefore using $TPPS_{2a}$ (activated by blue-light) does not negate the relevance of this thesis to potential clinical application.

3.2 Saporin and the Ribosome Inactivating Proteins

The chosen cytotoxins are both good candidates for studying enhanced delivery. Saporin (SAP) is a 30kD plant ribosome inactivating protein (RIP, type I) isolated from the soapwort *Saporinaria officinalis(92)*. Being a type I RIP, SAP comprises a single, enzymatically active A-chain, whereas the type II RIPs such as Ricin comprise the A-chain, linked to a lectin B-chain via a disulfide bridge. The B-chain enables Type II RIPs to bind to carbohydrate-based cell surface receptors, which facilitates their entry in to the cell. Consequently, the Type II agents demonstrate enhanced selectivity and uptake(93). These toxic inhibitors of translation irreversibly disrupt ribosomal RNA ribosomal subunit(94). Adenine residues in large rRNAs are the *in vitro* targets for SAP, which catalyzes depurination reactions resulting in loss of function(95). Endo et al. (1987)(94, 96) demonstrated that the principal enzymatic activity of RIPs is an *N*-glycosidation to remove A4324 in the 28S rRNA in the 60 s subunit of the rat ribosome(97). This adenine is part of a tetranucleotide G(A4324)GA sequence within a highly conserved (among eukaryotic rRNA) region of large rRNAs known as the α-sarcin loop. Once the target adenine is irreversibly modified this consequently impairs ribosome interaction with elongation factor (EF) – 2, thus

blocking translation(98, 99). This is mediated by the inhibition of EF-1 and EF-2-dependent GTPases.

As described above, unlike the type II RIPs, SAP and other type I agents such as pokeweed antiviral protein (PAP), only possess a single A-chain(100), which significantly impairs the cytosolic uptake, retention and delivery to site of action. This effect has been shown in animal models and human trials where there has been a significant difference in the toxic effects associated with the use of type I versus type II RIPs. For example, Ricin (type II RIP) found in the seeds of *Ricinus communis* L. (from castor beans) is potently toxic to both humans and animals(93). The toxic side effects associated with castor beans include gastrointestinal upset (nausea, haematochezia, necrotic hepatitis), central nervous system disruption (depressed Glasgow Coma Score, seizures) and nephrotoxicity (glomerulonephritis)(101). In rats, high doses of type II RIPs have been shown to result in death within 6-10 hours. At such doses death preceded the detection of lethal lesions in parenchymal organs(93). Type I RIPs in comparison have been shown to exhibit limited, if any, fatal effects at therapeutic doses. For example, trichosanthin given as an antiretroviral agent in patients with Acquired Immune Deficiency Syndrome (AIDS) resulted in the development of prodromal symptoms including fevers, flu-like symptoms, rashes and join pain(93, 102).

Given that both types of RIPs have been shown to have similar levels of activity in cell-free systems(103). This coupled with the reported observations that modifications to type I RIPs, including conjugations to form immunotoxins, have been shown to enhance their toxicity e.g. SAP for Hodgkin's disease(104). Battelli et al. (1990)(105) demonstrated that IgG-conjugation or homopolymerisation reduced the Activity-toxicity index (10^{-3} x units x LD_{50}) for SAP by a factor of 277 and 48 respectively. Gelonin, another type I RIP, also had a significant reduction in Activity-toxicity index by a factor of 165 (IgG-conjugate) and 174 (homopolymer).

Although the lack of the lectin B-chain clearly limits the rate of internalisation for SAP and other type I RIPs(97), it would be incorrect to suggest there is no uptake and this is supported by the observations of many groups working with such agents. Although SAP based immunotoxins have seen promising results in experimental models there is a body of evidence to suggest that enhanced cell membrane binding is not the only factor that determines overall efficacy. Many mechanisms for internalisation have been described for type I RIPs including:

- Passive uptake such as fluid phase pinocytosis(106)
- Receptor-mediated via α_2-macroglobulin/low-density lipoprotein receptor-related protein (LRP)(107), however this school of thought has been challenged by observations indicating that LRP-positive or –negative cells showed comparable sensitivity to SAP. This indicates that receptor-independent endocytosis may play an important role (108). This view is supported by work performed by Bolognesi et al. (2012)(109) using confocal microscopy, utilising indirect immunofluorescence analysis and transmission electron microscopy utilising direct assay with gold conjugated SAP-S6 and indirect immunoelectron microscopy assay. They reported that SAP-S6 was taken up mainly by receptor-independent endocytosis in HeLa cells. Furthermore, they found that just fewer than 1 in 3 endocytosed SAP molecules ended up in endosomes compared to 1 in 10 ending up in the Golgi-apparatus. Studies on intracellular trafficking found progressive accumulation in perinuclear vesicular structures(109). However, it is important to stress that any such receptor-mediated uptake mechanisms for SAP and other type I RIPs are likely to be significantly inferior to those utilized by type II RIPs such as ricin.

SAP induced cell kill is likely to involve a combination of both apoptosis and necrosis. This reflects the cell type-dependent and multi-direction pathway of SAP trafficking once endocytosed. The effects of inhibiting protein synthesis within a cell will lead to variable consequences and modes of cytotoxicity in different cell lines. Furthermore, there is an emergence of evidence to support SAP induced DNA damage, either secondary to *N-glycosylase* activity or oxidative-stress induction(110). The latter mechanism is of particular interest in

this study given the oxidative stress the cell is put under following the activation of a photosensitiser. Polito et al. (2013)(97) concluded that "apoptosis seems to be the main detectable effect in several different cell lines."

Important chemico-physical properties of SAP include its resistance to high temperature, denaturation by urea or guanidine and attack by proteolytic enzymes(111). This may be of benefit in the potentially harsh microenvironment of photosensitised endosomes. The characteristics of SAP, as described above make it an ideal candidate for PCI:

- Relatively large protein (30kDa) requiring endocytic uptake.
- Poor endocytic uptake and delivery to intracellular site of action, thus potentially limiting systemic side effects.
- Highly potent cytotoxic activity exerted by A-chain upon reaching target.
- No phototoxic activity.
- Chemico-physical robustness.

3.3 Mitoxantrone

Mitoxantrone is an anthacenedione cytotoxin. Its principle mechanism of action is to inhibit topoisomerase II. The resultant intercalation between DNA bases impairs DNA synthesis and repair in both healthy and malignant cells. It is used for the treatment of malignancies including hormone-independent prostate cancer, metastatic breast cancer and haematological malignancies (non-Hodgkin's lymphoma and acute myeloid leukaemia). It also has a therapeutic role to reduce the rate of disease progression in secondary progressive multiple sclerosis. The selectivity of MTX is based on the accessibility of DNA thus fast dividing cells, which have more exposed DNA e.g. colorectal cells in the crypt of Lieberkuhn and leukocytes can often be innocent bystanders sensitive to the cytotoxic effects of MTX. The side effect profile varies in severity and is linked to total cumulative dose. Specific side effects include: gastrointestinal upset (nausea and vomiting), alopecia and immunosuppression. A major problem is the development of irreversible cardiomyopathy. Cardiomyopathy and myelosuppresssion represent two dose-limiting side effects(112, 113). MTX and similar drugs such as Adriamycin are retained within cytoplasmic vesicular

structures such as lysosomes(25, 114). Mitoxantrone has a weak-base structure, thus like other basic anticancer agents (e.g. doxorubicin) MTX appears to accumulate in acidic endosomes(115) and lysosomes owing to protonation of the amino groups, a process known as ion-trapping, which reduces their overall cytotoxicity (fig. 3.3).

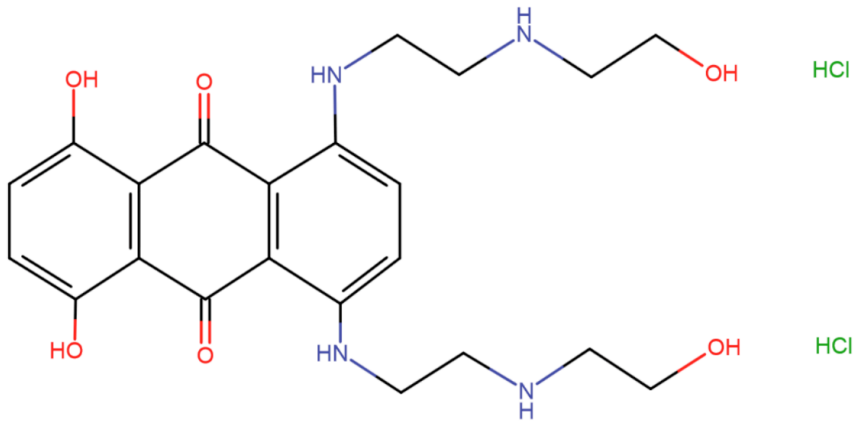

Figure 3.3 – Molecular structure of Mitoxantrone.

Furthermore, cells expressing resistant phenotypes, such as multidrug resistant MCF-7 (breast cancer) cell line have been shown to exclude MTX from the nuclear compartment where its DNA targets reside(25) a finding that is supports observations by Smith et al. (1992)(116) using EMT6/AR1.0 and EMT6/CR1.0 p-glycoprotein expressing murine breast cancer cell lines.

The characteristics of MTX including its potency, known resistant mechanisms, cytoplasmic vesicular-sequestration and previous observations as a suitable agent for PCI in resistant breast (MCF-7/R) and bladder (MGHU1/R) cell lines(25) has led to its nomination as a cytotoxin for PCI studies in this chapter.

AIMS

The studies performed in this chapter aim to take a closer look at the role of ROS in disulfonated meso-tetraphenylporphyrin ($TPPS_{2a}$)-mediated PCI of the type I ribosome inactivating protein SAP (SAP) and the topoisomerase II inhibitor Mitoxantrone (MTX). In particular to assess how manipulating the reducing capacity of the intracellular environment may affect the efficiency of PCI. Buthionine Sulfoximine (BSO) is a synthetic amino acid (fig. 3.4) that irreversibly inhibits gamma-glutamylcysteine synthetase, the enzyme required

in the first step of glutathione synthesis (117). In doing so BSO attenuates intracellular levels of the powerful reducing agent glutathione (GSH), thereby increasing susceptibility to oxidative damage. BSO has been shown to partially reverse drug-resistance in MRP_1 – overproducing cells associated with decreased levels of GSH and increased intracellular accumulation of daunorubicin(75).

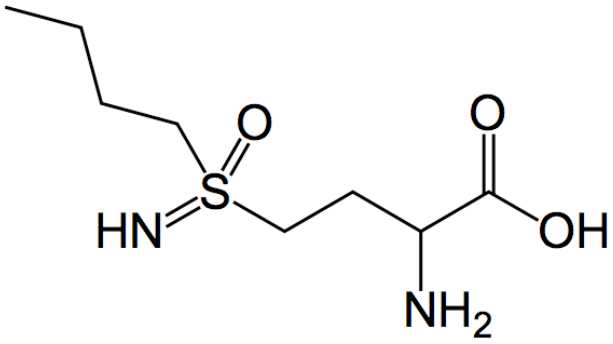

Figure 3.4 – Molecular structure of Buthionine Sulfoximine.

L-histidine (LH) is a naturally occurring amino acid that has been shown to interfere with REDOX reactions by scavenging hydroxyl and $^1O_2$ (118) free radicals. Pharmacological doses of histidine have also been shown to have an anti-inflammatory effect in animal models(119).

The ultimate aim of this chapter is to unpick the different factors that not only govern PCI but also influence the balance between PDT and PCI, specifically:

- Photosensitiser dose
- Cellular location of photosensitiser at time of ROS generation
- Chemotoxin dose
- Light dose
- Time following PS activation
- Effect of pro-oxidant and reducing conditions

3.4 PCI

The 'light-after chemotherapy' regimen can also be described as the standard PCI protocol. In this guise the photosensitiser and cytotoxin are co-incubated prior to activation of the photosensitiser using light, hence 'light-after'. At the intracellular level this theoretically enables the co-localisation of the cytotoxin (luminal) and photosensitiser (phospholipid membrane) within organelles including endosomes.

Figure 3.5 depicts the results of 'standard' PCI in the 4T1 cells, specifically the effects of combining TPPS2a (TP) with SAP (SAP) or Mitoxantrone (MTX) for 24hs prior to illumination. The 4h delay between washing off the drugs with phosphate buffered saline (PBS) and illumination represents the 'chasing' period (120). This effect will be further described in this chapter. The cells were illuminated for 2 minutes. Following a 24h-resting period the cells were assayed using the 3-(4,5-dimethylthiazol-2-yl)-2,5-diphenyltetrazolium (MTT) assay.

Following 120 s illumination, 0.6 μg/ml $TPPS_{2a}$ (TP) killed 23% of 4T1 cells compared to control ($p<0.01$, Fig 3.5a), which is the photodynamic therapy (PDT effect). The cytotoxic effect of SAP 15 nM alone (chemotherapy) was 4%. Upon combination of TP + SAP (PCI) there was 57% increased cytotoxicity compared to control ($p<0.01$). This corresponds to a 34% and 53% increase in cytotoxicity compared to PDT or chemotherapy alone, respectively ($p<0.01$).

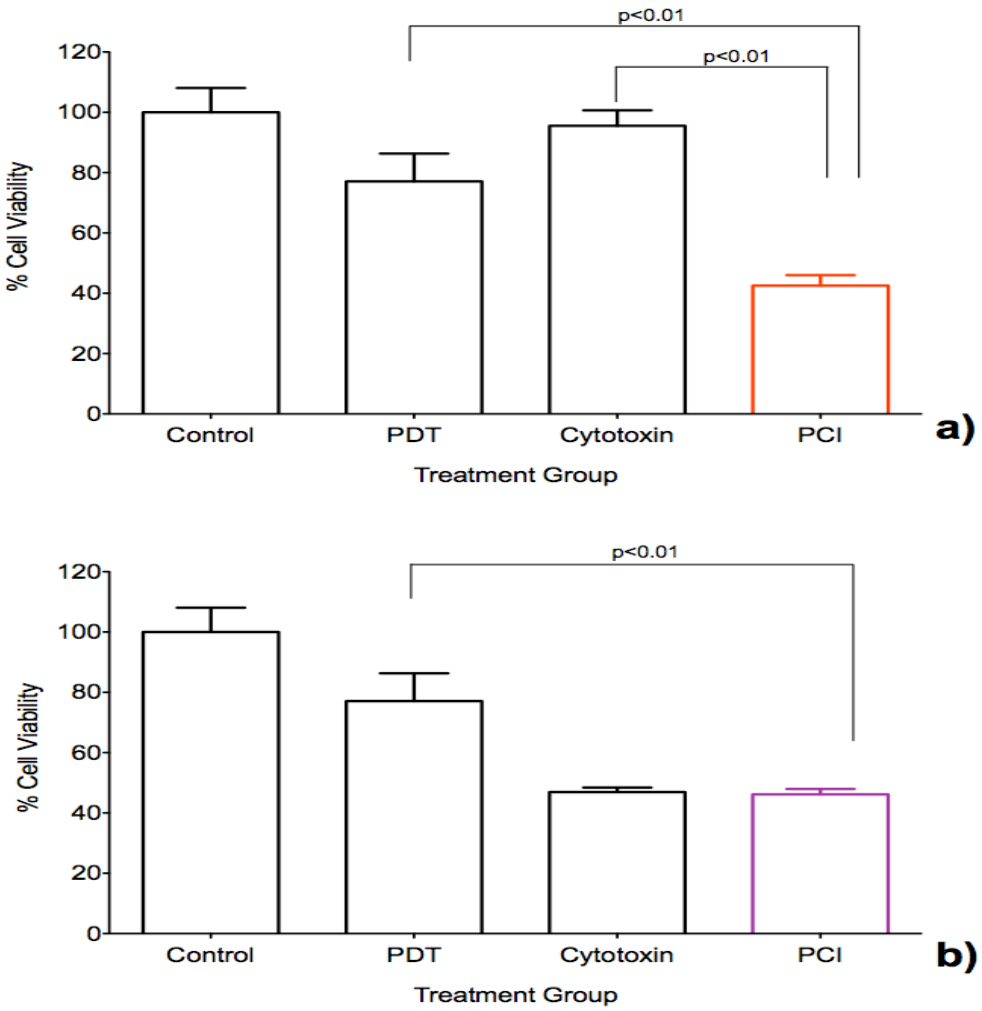

Figure 3.5 – $TPPS_{2a}$-mediated Photochemical Internalisation (higher dose).
4T1 breast cancer cells treated with $TPPS_{2a}$ 0.6 μg ml^{-1} alone (PDT) or plus: (a) SAP 15 nM, (b) MTX 0.4 μg ml^{-1} (PCI). Cells exposed to 120 s of light using LumiSource® illuminator 4h after drugs washed off. SAP-PCI killed 34% and 53% more cells than PDT or cytotoxin (SAP) alone ($p<0.01$). Cell viability measured using MTT assay 24h after illumination (absorbance read at 490 nm). Cytotoxin/PCI refers to SAP (a) and MTX (B).

Fig 3.5b shows results obtained from the same protocol as 3.5a, except in this instance, using the same fundamental protocol; SAP was exchanged for the topoisomerase inhibitor MTX (Fig 3.5b). The PDT effect was the same, however, MTX alone triggered 53% increased cytotoxicity compared to control ($p<0.01$). The combination of TP + MTX yielded 54% increased cytotoxicity compared to control ($p<0.01$). Thus the PCI group in 3.5b had a 31% increase in cytotoxicity compared to PDT alone ($p<0.01$) but there was no significant increase compared to MTX alone.

Combining TP + SAP in the presence of light appeared to increase the cytotoxicity of either agent on its own (fig. 3.5a). However, this effect is not mirrored with MTX (fig 3.5b) where under the conditions of this study, for example, TP dose, illumination time and MTX dose, combining the two agents (TP+MTX) had no effect beyond the inherent cytotoxicity of MTX alone.

In order to optimise any PCI effect the next step was to dissect the different variables that potentially play a role in determining the rate, total level and localisation of ROS generation following the activation of the photosensitiser (TP).

3.5 Variable 1: Photosensitiser Dose

Two different doses of TP were tested within a "light after" protocol. Figure 3.6a illustrates that 0.3 μg/ml of $TPPS_{2a}$ caused less than 10%, albeit significant, cytotoxicity when 4T1 cells were illuminated for 2 minutes (PDT). The combination of TP + SAP (15 nM) resulted in 49% cell kill, which translate into 41% and 44% increased cytotoxicity compared to PDT or chemotherapy alone, respectively ($P<0.01$). MTX (fig 3.6b) yielded a similar trend to that seen in cells treated with 0.6 μM of TP (fig 3.5b).

The effect that doubling the dose of TP from 0.3 μM to 0.6 μM had on the three treatment groups is also shown graphically (fig. 3.7). There was an observed 12% ($p<0.001$) and 8% ($p<0.001$) increase in PDT and SAP-PCI associated cytotoxicity for cells treated with 0.6 μg/ml compared to 0.3 μg/ml $TPPS_{2a}$. The importance of this ratio (PDT:PCI) will be addressed in the discussion.

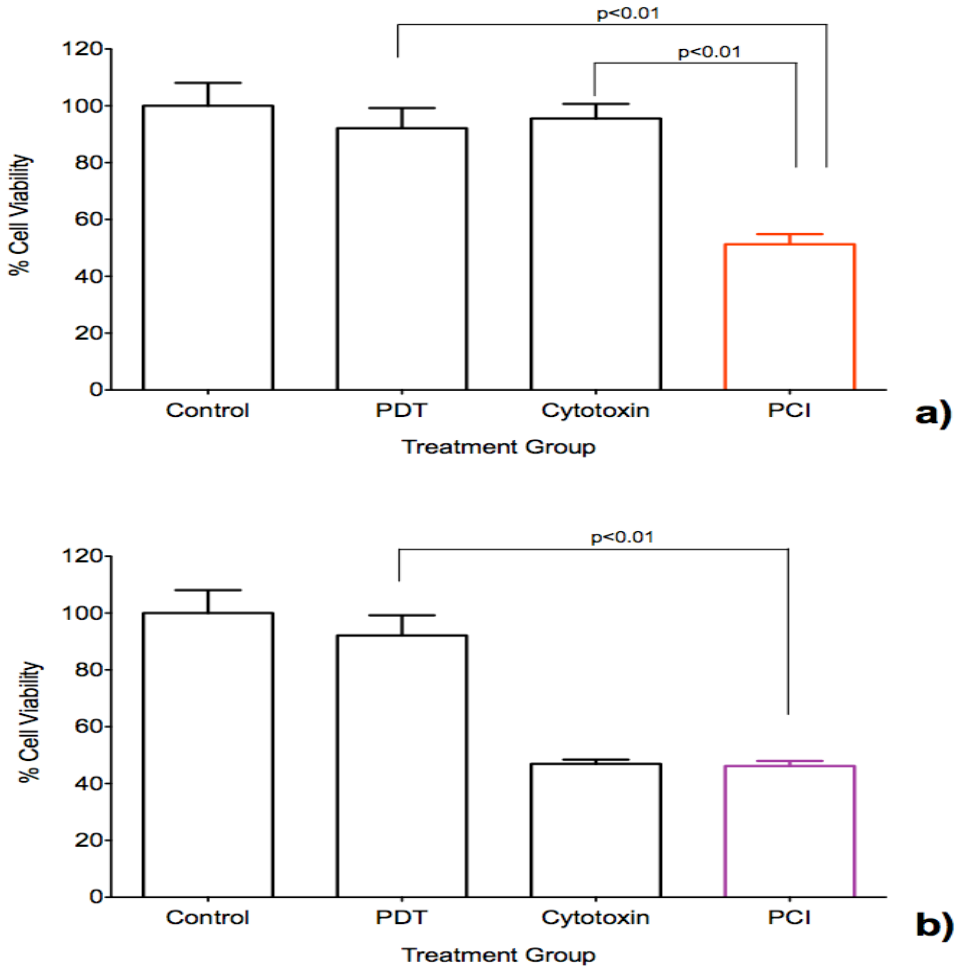

Figure 3.6 – $TPPS_{2a}$-mediated Photochemical Internalisation (lower dose).
4T1 breast cancer cells treated with $TPPS_{2a}$ 0.3µg ml^{-1} alone (PDT) or plus: (a) SAP 15 nM, (b) MTX 0.4 µg ml^{-1} (PCI). Cells exposed to 120 s of light using LumiSource® illuminator 4h after drugs washed off. SAP-PCI killed 41% and 44% more cells than PDT or cytotoxin (SAP) alone ($p<0.01$). Cell viability measured using MTT assay 24h after illumination (absorbance read at 490 nm). Cytotoxin/PCI refers to SAP (a) and MTX (B).

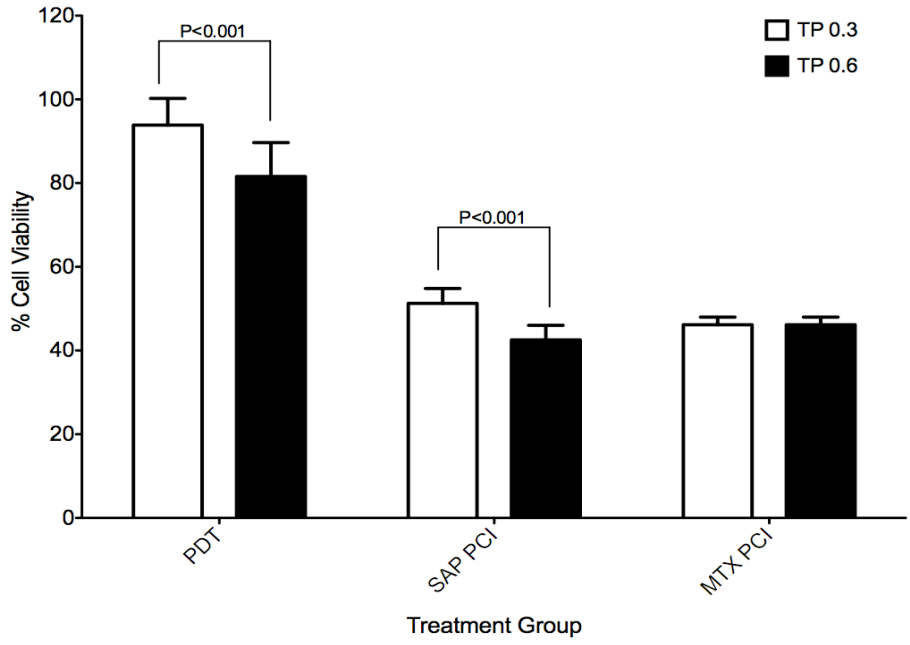

Figure 3.7 – $TPPS_{2a}$-mediated Photochemical Internalisation (lower dose versus higher dose).
4T1 breast cancer cells treated with $TPPS_{2a}$ 0.3μg ml^{-1} (white histogram) or o.6 μg ml^{-1} (black histogram) alone (PDT) or plus: SAP 15 nM (SAP-PCI) or MTX 0.4 μg ml^{-1} (MTX-PCI). Cells exposed to 120 s of light using LumiSource® illuminator 4h after drugs washed off. For SAP-PCI there was a 12% ($p<0.0001$) and 8% ($p<0.001$) increase in PDT and PCI for $TPPS_{2a}$ o.6 μg ml^{-1} compared to o.3μg ml^{-1}. Cell viability measured using MTT assay 24h after illumination (absorbance read at 490 nm).

3.6 Variable 2: Light Dose

Given the observed effects of doubling the photosensitiser dose on PDT/PCI, one possible theory is that the potential maximum ROS load generated within the cell, post-illumination, plays a pivotal role in the efficacy of either technique. However, although the photosensitiser is the substrate for ROS generation, oxygen and light are vital ingredients for successful initiation and subsequent propagation of ROS generation. In order to further assess the effect of varying light dose (duration of illumination) on PDT, PCI and the PDT:PCI ratio, illumination time studies were performed.

The effect of increasing illumination time, from 60 - 300 seconds, on PDT and PCI of SAP 30 nM was investigated (fig 3.8). TP (0.6 μg/ml) without illumination ('dark' PDT) resulted in no significant cell kill. TP (0.6 μg/ml)+ SAP (30 nM) without illumination ('dark' PCI) resulted in 12% cytotoxicity compared to control ($p<0.01$). However, this represented no significant difference when

compared to the residual toxicity of SAP (30 nM). For the standard PCI protocol, comprising a 4h incubation period prior to illumination the cytotoxicity for PDT ranged from 12% at 60 seconds ($p<0.01$) to a maximum of 43% at 240 seconds ($p<0.01$). Between 60 – 300 s, the only significant differences in PDT cytotoxicity (versus 60 s) occurred above 180 s.

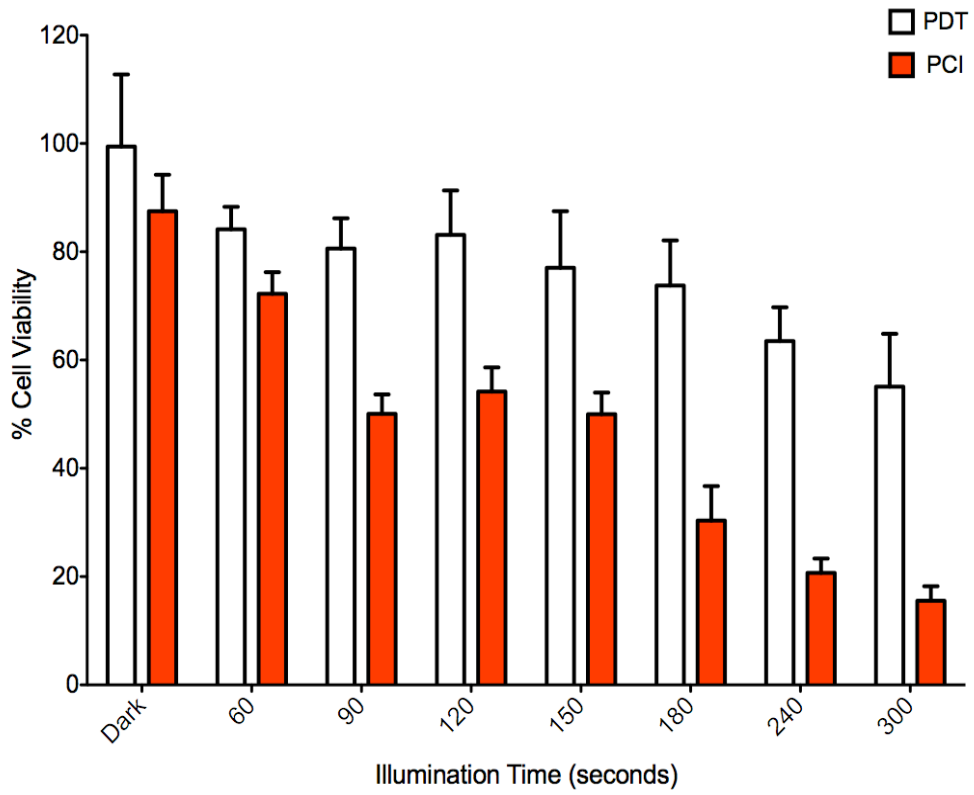

Figure 3.8 – Effect of increasing light dose on $TPPS_{2a}$-mediated Photochemical Internalisation of Saporin.
4T1 breast cancer cells treated with $TPPS_{2a}$ 0.6 μg ml^{-1} alone (PDT, white histogram) or 0.6 μg ml^{-1} + SAP 30 nM (PCI, red histogram). Cells exposed to increasing durations of light from no light (dark) to 300 s of light using LumiSource® illuminator 4h after drugs washed off. A light-dose dependent increase in cytotoxicity was observed for both PDT and PCI achieving 43% and 83% cell kill, respectively at 300 s illumination. Cell viability measured using MTT assay 24h after illumination (absorbance read at 490 nm).

The cytotoxicity of PCI–SAP-30 demonstrated a light-dose dependent increase in cytotoxicity of 83% ($p<0.01$) from no illumination ('dark') though to 300 s illumination. One trend that was observed is that as the light-dose increased, the differential between PDT and PCI also rose; for example, at 60 seconds

illumination there was a 12% ($p<0.01$) increase in cytotoxicity, which rose to 46% ($p<0.01$) at 300 s illumination.

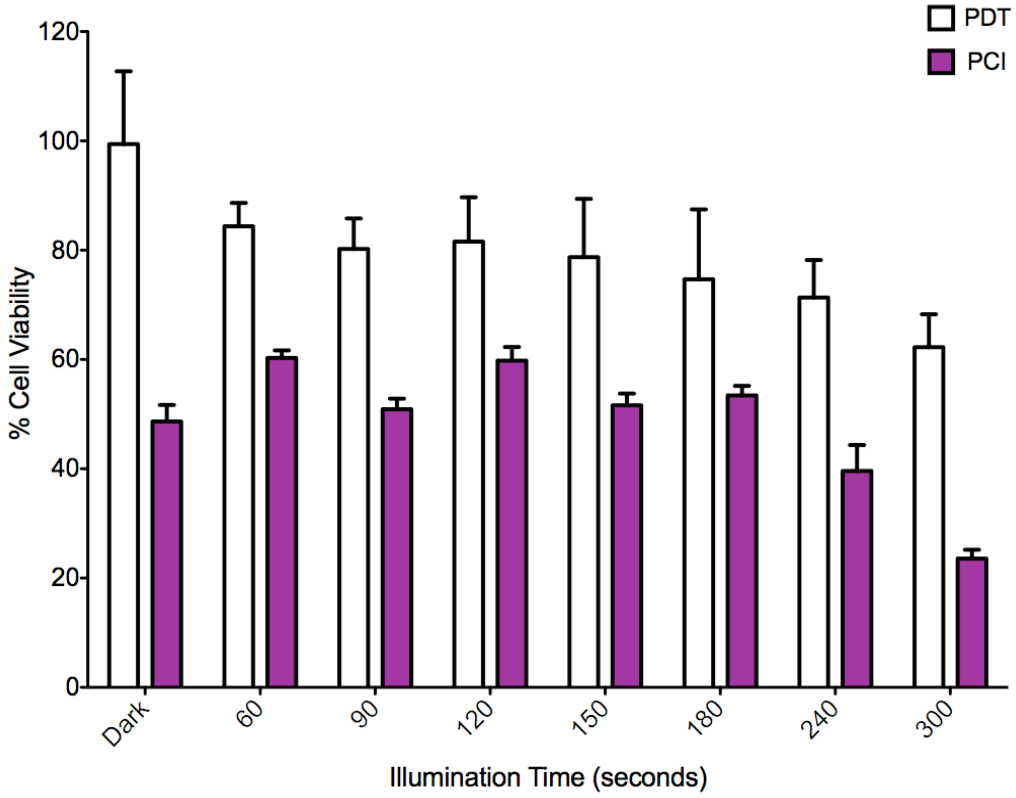

Figure 3.9 – Effect of increasing light dose on $TPPS_{2a}$-mediated Photochemical Internalisation of Mitoxantrone.
4T1 breast cancer cells treated with $TPPS_{2a}$ 0.6 μg ml^{-1} alone (PDT, white histogram) or 0.6 μg ml^{-1} + MTX 1.5 μg ml^{-1} (PCI, purple histogram). Cells exposed to increasing durations of light from no light (dark) to 300 s of light using LumiSource® illuminator 4h after drugs washed off. A light-dose dependent increase in cytotoxicity was observed for both PDT and PCI achieving 43% and 76% cell kill, respectively at 300 s illumination. Cell viability measured using MTT assay 24h after illumination (absorbance read at 490 nm).

The effect of increasing illumination time, from 60 – 300 seconds, was also investigated on PDT and PCI of MTX 1.5 μg/ml (fig. 3.9). The PDT results mirror those seen in figure 3.8. The 'dark' control for PCI – MTX demonstrated 51% cell kill ($p<0.01$). However, this observation was confounded by the background cytotoxicity that was exerted by MTX 1.5 μg/ml alone, which was 47% (data not shown, $p<0.01$). Thus, there was no significant difference observed between MTX alone and PCI – MTX 'dark' control. With this in mind it was interesting to observe that it was only after 240 s that PCI-MTX produced increased cytotoxicity compared to MTX alone or 'dark' control, though the 9% increase

was not statistically significant. After 300 s illumination, PCI-MTX increased cytotoxicity by 25% ($p<0.01$) and 29% ($p<0.01$) compared to 'dark' control and MTX alone, respectively.

3.7 Variable 3: Photosensitiser localisation

To investigate this variable the studies in this section take a closer look at the impact of the 'chasing' period prior to illumination(120). This chasing period of 4h enables the 'leak' of the photosensitiser from the cell membrane with accumulation in endo-lysosomal membranes.

The relative effect of the 4h 'chasing' period on TP-based PDT in 4T1 cells with increasing duration of illumination from 60 s-300 s is illustrated in figure 3.10a. The general trend is consistent with 'light' dose-dependent toxicity in both the 'immediate' and '4h' illumination groups. However, as illumination time increased, cells that were exposed to light immediately after wash-off of drug exhibited significantly greater sensitivity to PDT compared to those cells that were incubated for 4h prior to illumination. Consequently, resulting in progressive divergence of cell survival between the two groups. Following 60 seconds of illumination 1 in 4 cells in the immediate group were killed compared to 1 in 6 cells in the 4h group. This represents a 9% reduction in PDT-induced cytotoxicity if the cells were incubated for 4 hours prior to illumination ($p<0.01$). After 150 seconds of illumination more than 75% of cells in the immediate group were killed compared to just below 25% cells in 4h group. This corresponded to a 55% increase in cytotoxicity (immediate vs. 4h, $p<0.01$). 300 seconds of illumination resulted in over 95% cytotoxicity in the immediate group compared to 45% in the 4h group. This indicated that by illuminating cells immediately we were able to achieve PDT-related cytotoxicity at 150 seconds illumination, which was 22% greater than that achieved after 300 seconds illumination in cells that had been re-incubated for 4h prior to illumination ($p<0.01$). This is consistent with a hypothesis that PDT is more effective in this model when the photosensitizer is within the plasma membrane.

The effect of the 4h incubation time between drug wash-off and illumination on PCI-SAP is graphically expressed in figure 3.10b. As seen in figure 3.10b the general trend was consistent with 'light' dose-dependent toxicity in both treatment groups. Furthermore, between 60 – 300 s, cells in the immediate illumination group exhibited increased cytotoxicity compared to cells in the 4h group. However, unlike PDT, the average difference between the immediate and 4h group was reduced. For example, after 60 s illumination over 5 in every 8 cells in the immediate group were killed compared to over 2 in every 8 cells in the 4h group, representing a 39% increase in cytotoxicity ($p<0.01$). This differential remained relatively consistent at 150 seconds where the observed increase in cytotoxicity was 41% (immediate vs. 4h). After 300 s, this differential between the 'immediate' and '4h' groups had reduced to 11% with over 9 in every 10 cells in the 'immediate' group and over 8 in every 10 cells in the '4h' group dying ($p<0.01$).

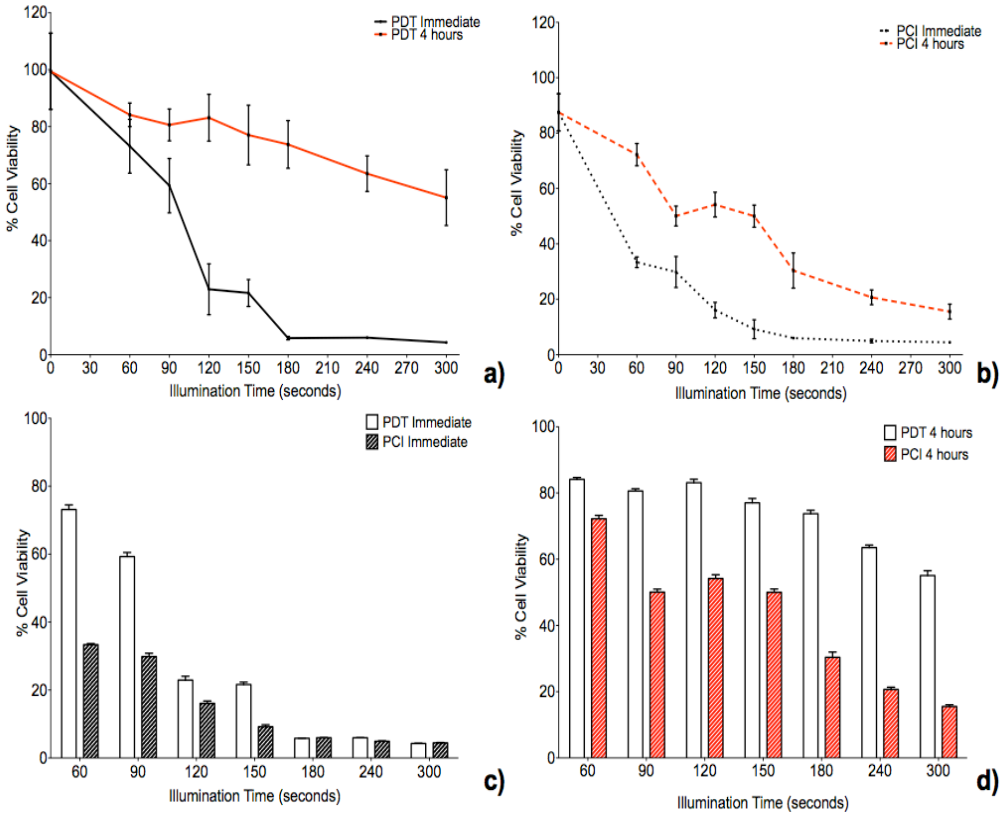

Figure 3.10 – Impact that timing of illumination following removal of $TPPS_{2a}$ has on Photochemical Internalisation of Saporin.
4T1 breast cancer cells treated with $TPPS_{2a}$ 0.6 μg ml^{-1} alone (PDT) or 0.6 μg ml^{-1} + SAP 30 nM (PCI,). (a) PDT treatment group – cells illuminated either immediately (black line) or 4h (red line) after wash off of TP; (b) PCI treatment group – cells illuminated either immediately (black line) or 4h (red line) after drugs washed off; (c) PDT (white histogram) versus PCI (grey histogram) – for cells illuminated immediately after drugs washed off; (d) PDT (white histogram) versus PCI (red histogram) – for cells illuminated 4h after drugs washed off Cells illuminated for increasing durations of time up to 300 s using LumiSource® illuminator. Cell viability measured using MTT assay 24h after illumination (absorbance read at 490 nm).

Figures 3.10c and 3.10d illustrate the difference between PDT and PCI within the immediate and 4h groups, respectively. The most striking observation is that for illumination times ≥ 180 seconds there was no significant difference in cytotoxicity between PDT vs. PCI (fig. 3.10c). The largest differential was at 60 s illumination where PCI induced cytotoxicity was 2.7 times greater than PDT with a 42% increase in cell kill ($p<0.01$). The differential reduced to 12% at 150 s ($p<0.01$) and subsequently <1% at 180 s illumination. This indicated that when illumination time was ≥ 180 s there is no difference between PDT versus PCI induced cell kill.

Figure 3.10d shows that unlike the 'immediate' illumination group (fig. 3.10c), cells that were exposed to light after a 4h incubation period consistently exhibited significantly increased cytotoxicity for PCI versus PDT. After 60 s, illumination the cytotoxic effect in the PCI group was 1.8 times greater than the PDT group with 12% increased cytotoxicity ($p<0.01$). After 150 s of illumination this ratio increased, such that the PCI group experienced 2.2 times greater cell kill than the PDT group with 27% increased cell kill ($p<0.01$). The greatest differential was observed after 240 s illumination when 43% increased cytotoxicity was observed in the PCI group compared to the PDT group. This represents 1.9 times increased cell kill ($p<0.01$).

The effect of immediate versus 4h-delayed illumination on the PCI of MTX is shown in figure 3.11. A similar trend to that seen with SAP is seen for the 'immediate' group (fig. 3.11a) whereby there is an initial light-dose dependent increase in cytotoxicity, prior to a flat nadir. At 60 s cells treated with TP + MTX experienced 37% increased cell kill compared to TP-alone ($p<0.01$), though the magnitude of this result is attenuated by the fact that after 60 s illumination PCI-MTX enhanced the cytotoxicity of MTX-alone by 15% ($p<0.01$). After 120 s illumination the impact of the photosensitiser both for PDT (alone) and PCI (+MTX) led to 27% and 38% increase in cytotoxicity, respectively ($p<0.01$). However, this represents a 28% decrease in the difference between PCI versus PDT cytotoxicity. In fact for illumination times >120 s there appeared to be no significant increase in cytotoxicity (PCI versus PDT).

No significant increase in cytotoxicity was seen, in cells that underwent a 4h incubation period prior to illumination, until cells were exposed to ≥ 240 s of light. The maximum cell kill achieved after 300 s of illumination was 76%, corresponding to a 29% increase compared to MTX-alone and 32% compared to PDT ($p<0.01$).

Figure 3.11c illustrates the differential effects observed between PCI when cells were illuminated either immediately after 24h incubation or following 4h

incubation in drug-free media. It was observed is that immediate illumination resulted in increased cell kill across all light-doses investigated. The greatest difference was observed following 120 s of light (45%, $p<0.01$), however after 300 s of illumination this reduced to 18% ($p<0.01$).

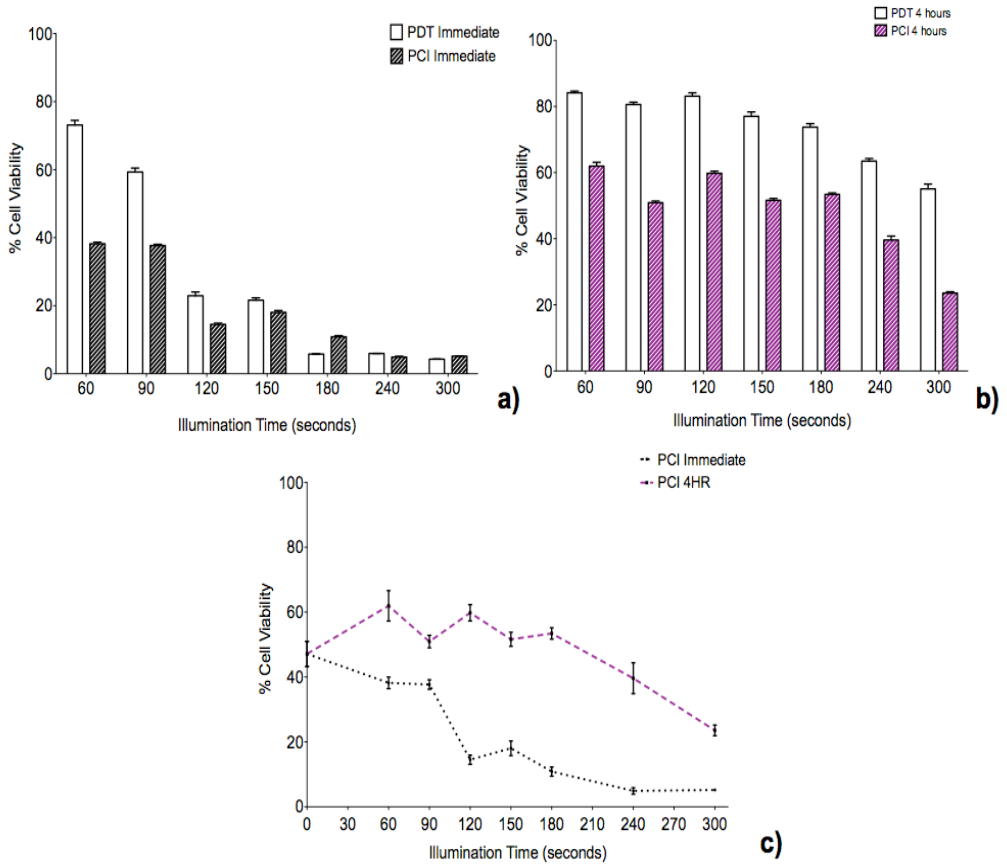

Figure 3.11 – Impact that timing of illumination following removal of $TPPS_{2a}$ has on Photochemical Internalisation of Mitoxantrone.
4T1 breast cancer cells treated with $TPPS_{2a}$ 0.6 μg ml^{-1} alone (PDT) or 0.6 μg ml^{-1} + MTX 1.5 μg ml^{-1} (PCI,). (a) PDT (white histogram) versus PCI (grey histogram) – for cells illuminated immediately after drugs washed off; (b) PDT (white histogram) versus PCI (purple histogram) – for cells illuminated 4h after drugs washed off; (c) PCI treatment group – cells illuminated either immediately (black line) or 4h (purple line) after drugs washed off. Cells illuminated for increasing durations of time up to 300 s using LumiSource® illuminator. Cell viability measured using MTT assay 24h after illumination (absorbance read at 490 nm).

3.8 Variable 4: Intracellular REDOX Environment

This section focuses on the effect alterations in the intracellular REDOX environment have on both PDT and PCI. Given the accepted important role that ROS play in photosensitiser-mediated cell damage this section investigates what

effect, if any, altering the intracellular REDOX environment has on both PDT and PCI.

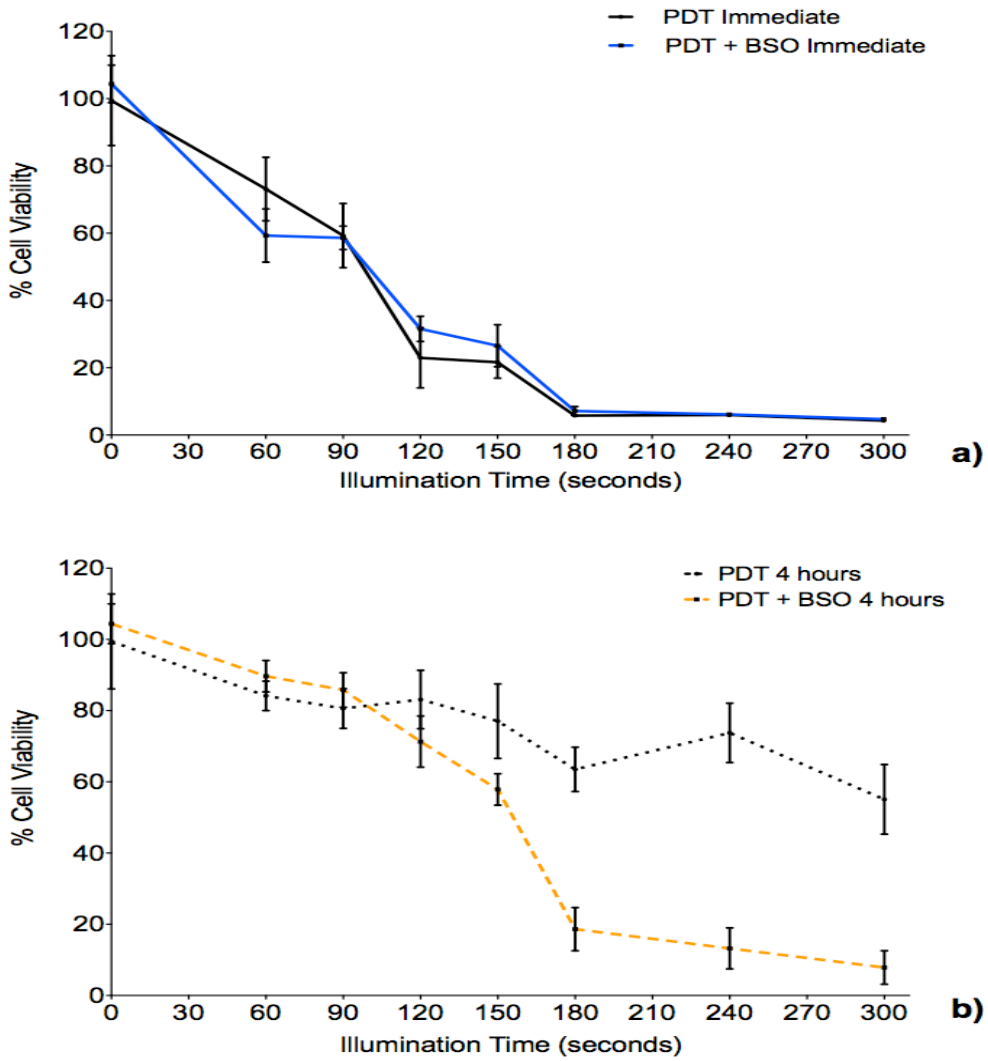

Figure 3.12 – Impact of Buthionine Sulfoximine on $TPPS_{2a}$-mediated Photodynamic Therapy.
4T1 breast cancer cells treated with $TPPS_{2a}$ 0.6 μg ml^{-1} alone. (a) Cells illuminated immediately after TP washed off with (blue line) or without (black line) BSO 1.0 μg ml^{-1}; (b) Cells illuminated 4h after TP washed off with (orange broken line) or without (black broken line) BSO 1.0 μg ml^{-1}. Cells illuminated for increasing durations of time up to 300 s using LumiSource® illuminator. Cell viability measured using MTT assay 24h after illumination (absorbance read at 490 nm).

Figure 3.12 illustrates the effect that treating cells with the glutathione synthase inhibitor, buthionine sulfoximine (BSO), has on PDT either when cells were illuminated immediately (3.11a) or 4h (3.11b) after washing off the photosensitiser. BSO alone killed 6% of cells ($p<0.01$).

under ‘dark’ conditions the combination of TP (0.6 μg/ml) + BSO (1.0 μM) caused no significant change in cytotoxicity compared to ‘dark’ PDT alone.

Figure 3.12a (immediate) shows that above 60 s illumination at which point there was a 15% increase in cytotoxicity ($p<0.01$), there was no difference between PDT and PDT + BSO.

Figure 3.12b (4h delay) shows that for illumination durations ≤ 120 s, there was no significant difference in cytotoxicity between PDT versus PDT + BSO. Those cells exposed to ≥150 s illumination experienced a non-linear increase in cytotoxicity compared to PDT alone. For example, after 150 s illumination, the addition of BSO resulted in a 19% increase in cell killing ($p<0.01$), representing a cytotoxicity ratio of 1 in 4.3 for PDT and 1 in 2.4 for PDT + BSO. After 180 s the addition of BSO enhanced the PDT effect by 55% ($p<0.01$), this represented a cytotoxicity ratio of 1 in 3.8 for PDT and 1 in 1.2 for PDT + BSO. The greatest difference was seen after 240 s illumination when the differential was increased to 61% ($p<0.01$). This may indicate that GSH prevents or reduces delayed PDT cytotoxicity.

Figure 3.13a shows the difference in cytotoxicity profiles between PDT + BSO for cells in the immediate versus 4h groups. Comparison with fig. 3.10a indicated that BSO had a significant effect on PDT when a 4h delay was utilised prior to illumination. Figure 3.13b further reinforces the enhancing effect of BSO on ‘4h delayed’ PDT compared to ‘immediate’ PDT.

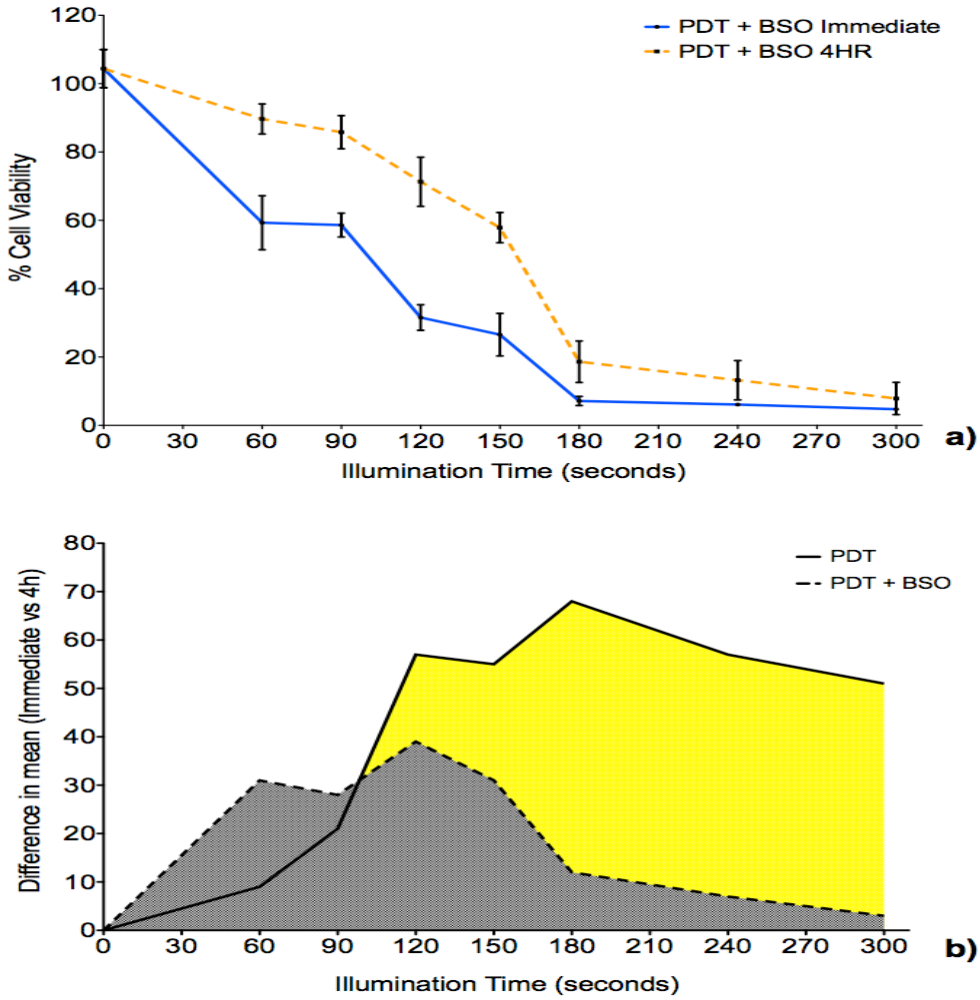

Figure 3.13 – Impact of Buthionine Sulfoximine on $TPPS_{2a}$-mediated Photodynamic Therapy (Immediate versus 4h protocol).
4T1 breast cancer cells treated with $TPPS_{2a}$ 0.6 μg ml^{-1} + BSO 1.0 μg ml^{-1}. (a) Cells illuminated immediately (blue line) or 4h (orange broken line) after TP washed off; (b) difference in mean cytotoxicity for immediate versus 4h-delayed illumination, grey area represents PDT + BSO, yellow area represents PDT. Cells illuminated for increasing durations of time up to 300 s using LumiSource® illuminator. Cell viability measured using MTT assay 24h after illumination (absorbance read at 490 nm).

Although up to 90 s illumination the difference between the mean cytotoxicity (Immediate minus 4h) is greater for PDT + BSO, at all time points beyond 90 s the difference in means is significantly less for PDT + BSO compared to PDT alone. For example, at 120 s the difference in mean cell viability is 57% and 39% for PDT and PDT + BSO respectively. After 180 s illumination this increases to 68% for PDT and 12% for PDT + BSO. The shape of the marginally negatively skewed PDT + BSO graph (fig. 3.13b) indicates that at higher illumination times BSO has a greater effect on '4h delay' PDT compared to 'immediate' illumination.

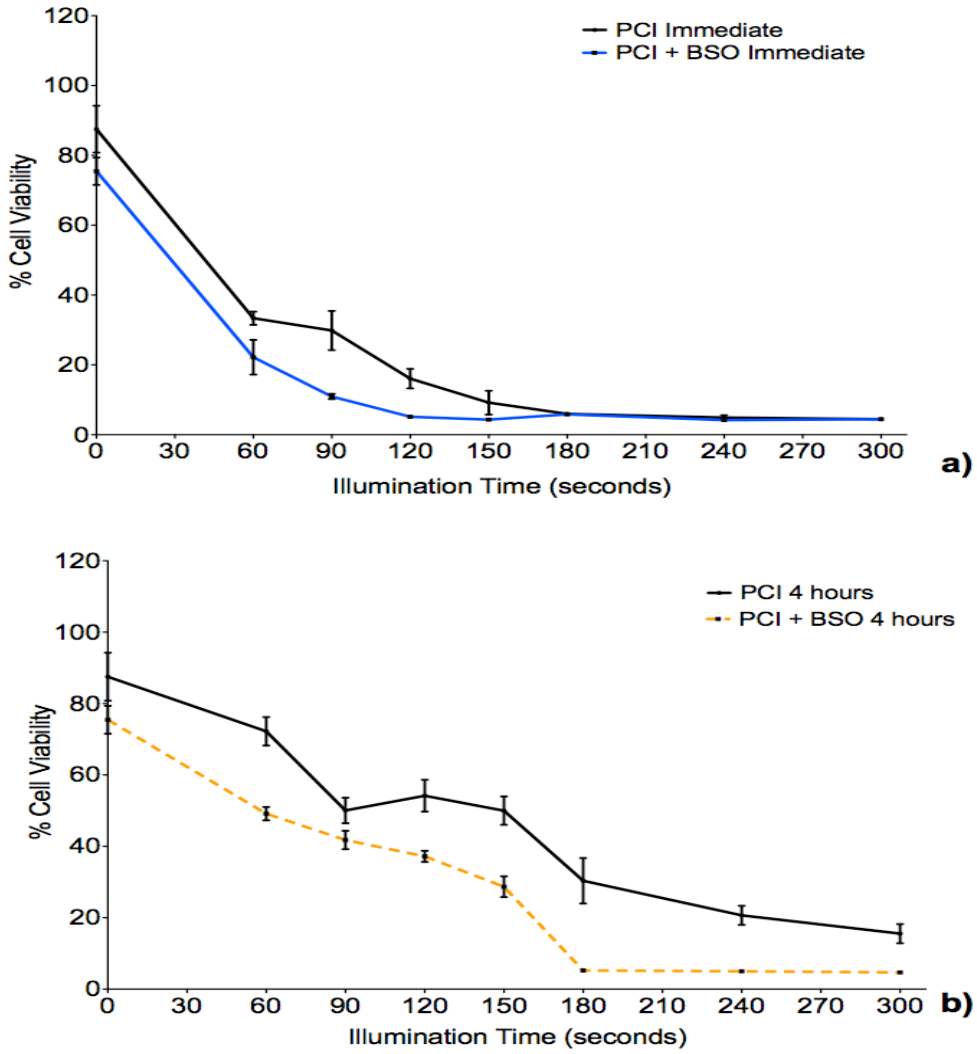

Figure 3.14 – Impact of Buthionine Sulfoximine on $TPPS_{2a}$-mediated Photochemical Internalisation of Saporin.
4T1 breast cancer cells treated with $TPPS_{2a}$ 0.6 μg ml^{-1} + SAP 30 nM (PCI). (a) Cells illuminated immediately after drugs washed off with (blue line) or without (black line) BSO 1.0 μg ml^{-1}; (b) Cells illuminated 4h after drugs washed off with (orange broken line) or without (black broken line) BSO 1.0 μg ml^{-1}. Cells illuminated for increasing durations of time up to 300 s using LumiSource® illuminator. Cell viability measured using MTT assay 24h after illumination (absorbance read at 490 nm).

The effect of BSO, for both 'immediate' (fig. 3.14a) and '4h delay' (fig 3.14b) regimens, on PCI is shown in figure 3.14. PCI + BSO in the absence of light ('dark' control) resulted in 24% cytotoxicity, which corresponded to a 12% increased compared to 'dark' PCI alone.

For the 'immediate' illumination group BSO enhanced PCI-mediated cytotoxicity by 11% ($p<0.01$) after 60 s illumination and 15% ($p<0.05$) after 90 s. However,

these findings need to be taken in the context of the 12% 'dark' toxicity seen with the addition of BSO to PCI. For illumination times longer that 90 s there was no significant increase in cytotoxicity associated with BSO treatment.

The effect of BSO on '4h delay' PCI is seen in figure 3.14b. After 60 s illumination there was a 22% increase in cytotoxicity associated with application of BSO ($p<0.01$). This increase was maintained after 150 seconds illumination (21%, $p<0.01$). The peak increase in cytotoxicity of 25% occurred after 180 s exposure to light ($p<0.01$).

Figure 3.15a shows the difference in cytotoxicity profiles between PCI + BSO for cells in the immediate versus 4h groups. This graph illustrates that for illumination times <180 s, there was a significant increase in cytotoxicity in the 'immediate' group compared to the '4h' group with a maximum difference of 32% seen when cells were illuminated for 120 seconds ($p<0.01$). Between 180 s – 300 s illumination there was no difference in cytotoxicity observed between the two groups with over 9.3 in every 10 cells being killed ($p<0.01$).

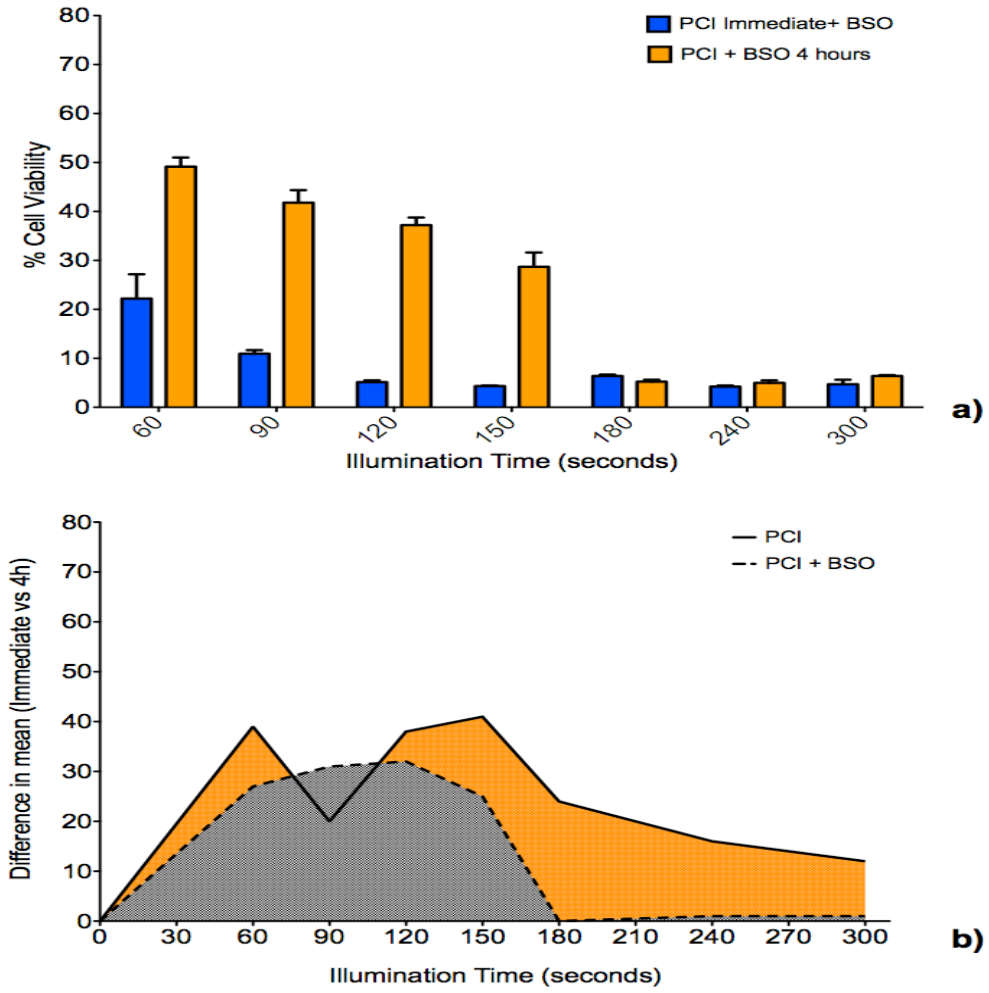

Figure 3.15 – Impact of Buthionine Sulfoximine on $TPPS_{2a}$-mediated Photochemical Internalisation of Saporin (Immediate versus 4h protocol).
4T1 breast cancer cells treated with $TPPS_{2a}$ 0.6 μg ml^{-1} + SAP 30 nM + BSO 1.0 μg ml^{-1} (enhanced PCI). (a) Cells illuminated immediately (blue histogram) or 4h (orange histogram) after drugs were washed off; (b) difference in mean cytotoxicity for immediate versus 4h-delayed illumination, grey area represents PCI + BSO, orange area represents PCI. Cells illuminated for increasing durations of time up to 300 s using LumiSource® illuminator. Cell viability measured using MTT assay 24h after illumination (absorbance read at 490 nm).

Comparison of the % viability after 180 s illumination in the '4h' group with the that in fig. 3.10b shows a 24% increase in cytotoxicity for PCI + BSO compared to PCI alone. Figure 3.15b shows that in the presence of BSO there was no significant difference in the mean survival of cells treated with TP 0.6 μg/ml + SAP 30 nM (PCI) and exposed to ≥180 illumination between the 'immediate' and '4h' groups. For example, PCI alone on cells exposed to 180 s illumination

resulted in 24% increased killing in the 'immediate' group compared to '4h' however; this difference was completely eradicated upon addition of BSO.

Figure 3.16 illustrates the effect of BSO on PCI of MTX 1.5 μg/ml. In figure 3.16a no significant increase in cytotoxicity was observed upon addition of BSO, across all the light durations, in the immediate illumination group. The maximum increase was 8.4% at 90 s illumination ($p>0.05$). Figure 3.16b shows that for illumination durations <180 s there was no significant increase in cytotoxicity in the '4h' group. However after 180 s and 240 s of light treatment there was 30% and 24% increased cell killing, respectively ($p<0.01$). The maximum cell kill achieved was 90%, achieved after 300 seconds of light exposure, though it is important to consider that MTX alone has about 47% cytotoxicity and TP (0.6 μg/ml) + MTX 'dark control' has 53% cytotoxicity +/- BSO.

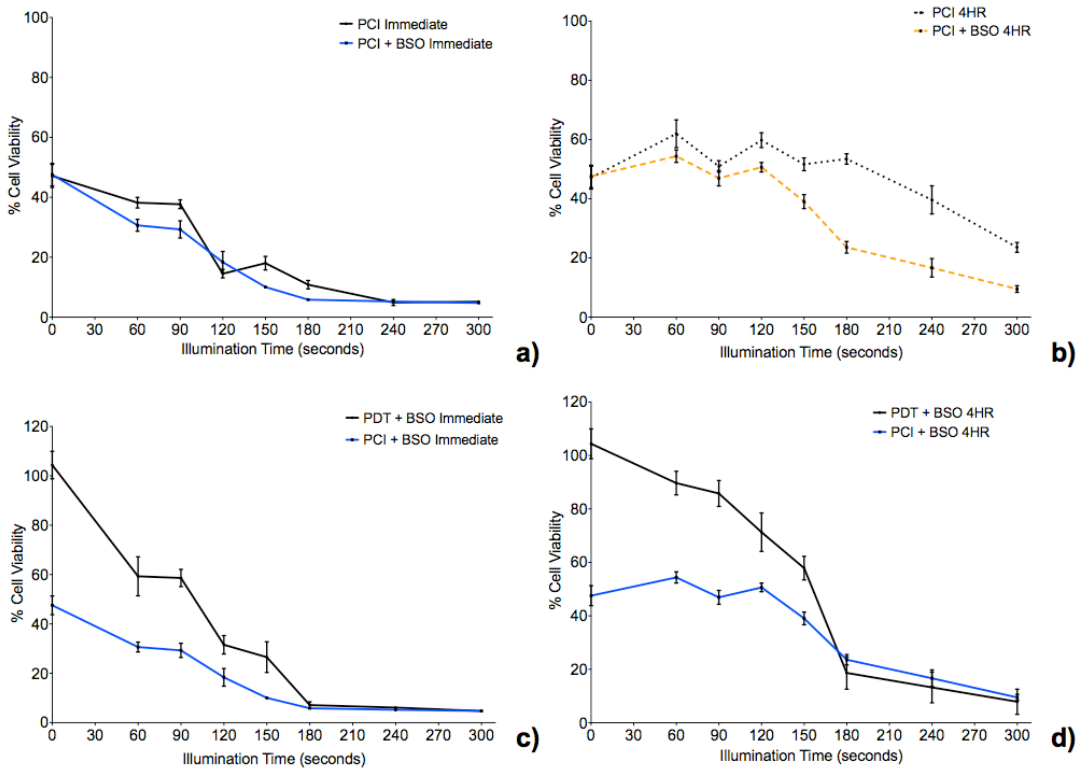

Figure 3.16 – Impact of Buthionine Sulfoximine on $TPPS_{2a}$-mediated Photochemical Internalisation of Mitoxantrone.
4T1 breast cancer cells treated with $TPPS_{2a}$ 0.6 μg ml^{-1} + MTX 1.5 μg ml^{-1} (PCI). (a) Cells illuminated immediately after drugs washed off with (blue line) or without (black line) BSO 1.0 μg ml^{-1}; (b) cells illuminated 4h after drugs washed off with (orange broken line) or without (black broken line) BSO 1.0 μg ml^{-1}; (c) cells illuminated immediately after TP (PDT, black line) or drugs (PCI, blue line) were washed off; (d) cells illuminated 4h after TP (PDT, black line) or drugs (PCI, blue line) were washed off. Cells illuminated for increasing durations of time up to 300 s using LumiSource® illuminator. Cell viability measured using MTT assay 24h after illumination (absorbance read at 490 nm).

Figure 3.16c compares the effect of BSO on PDT and MTX-PCI in the 'immediate' group. The graph illustrates a converging cytotoxicity profile between PDT+BSO and PCI+BSO. The former has significantly reduced 'dark' cytotoxicity compared to the latter (55%, $p<0.01$). This is almost entirely due to the cytotoxic effect of MTX. After 90 s illumination this difference reduces to 29% ($p<0.01$). At this time point there is a 46% increase in PDT+BSO cytotoxicity compared to 'dark' control. At the same time point the increase in PCI+BSO cytotoxicity is 18%, representing a 2.6-fold differential in improved PDT+BSO cytotoxicity between

0-90 s illumination and PCI+BSO. Illumination times >180 s were associated with >93% cytotoxicity with no difference between the two groups.

A very similar pattern of convergence between PDT+BSO and PCI+BSO induced cytotoxicity is seen in the '4h' group (fig. 3.16d). After 90 s illumination there was 39% increased cytotoxicity observed in the PCI+BSO group compared to PDT+BSO. However, this represents a 19% increase in PDT+BSO cytotoxicity compared to 'dark' control. In the PCI+BSO group a 1% increase in cytotoxicity in cytotoxicity was seen over the same illumination time period. Much like the 'immediate' group, there was no significant difference in cytotoxicity for illumination durations >180 seconds. However the ultimate level of cytotoxicity achieved was 92% compared to control.

3.9 Variable 5: Illumination 'before' versus 'after' cytotoxin treatment

In this section the investigation focuses on the effect of altering the timing of light treatment, either 'before' or 'after' treatment with the cytotoxin. The former regimen involved exposing cells treated with a photosensitiser to light prior to cytotoxin treatment. The latter was the 'standard' PCI protocol with light treatment following 24h co-incubation of photosensitiser and cytotoxin.

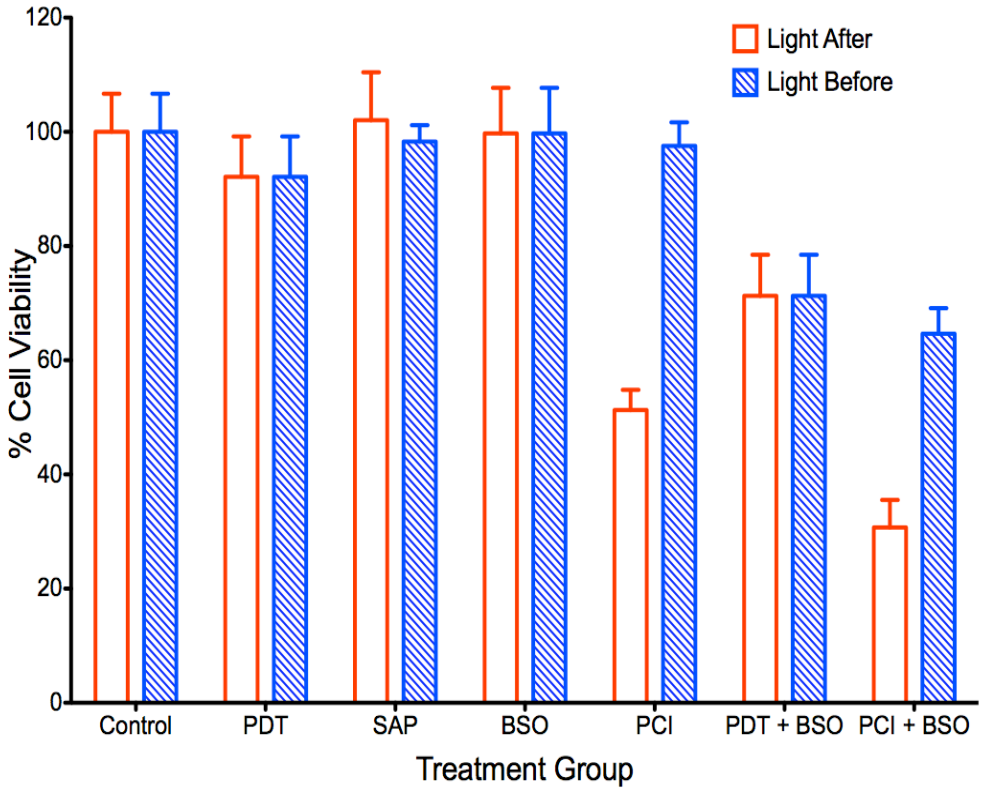

Figure 3.17 – Comparison of the light 'after' versus light 'before' Saporin Photochemical Internalisation protocols.
4T1 breast cancer cells treated with different combinations of $TPPS_{2a}$ 0.3 μg ml^{-1}, SAP 15 nM and BSO 1.0 μg ml^{-1}. Saporin was added to appropriate treatment groups either preceding (light 'after') or following (light 'before') illumination. Exposure to light took place 4h after drugs were washed off. Cells illuminated for 120 s using LumiSource® illuminator. BSO increased PCI cytotoxicity by 25% ($p<0.01$) in the light 'before' group (blue histogram). Cell viability measured using MTT assay 24h after illumination (absorbance read at 490 nm).

The two PCI protocols (light 'after versus light 'before') were compared when using TP 0.3 μg/ml and SAP 15 nM (fig. 3.17). The combination of TP, SAP and 120 s illumination (PCI) in the light 'after' cytotoxin protocol resulted in 41% and 47% increased cell kill compared to either PDT or SAP alone, respectively ($p<0.01$). In comparison there was no significant kill effect seen for PCI in the light 'before' group. Addition of BSO to the PCI group led to a 10% increase in cytotoxicity in the light 'after' group ($p<0.01$), whereas in the light 'before' group a 25% increase was observed ($p<0.01$). Furthermore, subsequent to the addition of BSO, the cytotoxic differential between the light 'after' versus 'before' groups narrowed from 46% ($p<0.01$) to 34% ($p<0.01$). Buthionine sulfoximine also enhanced the efficacy of photosensitiser alone (PDT) by 20% ($p<0.01$). The

greatest magnitude of cell kill was seen in cells treated with PCI+BSO in the light 'after' group, with 69% cytotoxicity achieved.

Figure 3.18 illustrates the comparison between the light 'before' versus light 'after' protocols for both SAP 15 nM-PCI (fig. 3.18a) and MTX 0.4 μg/ml (fig. 3.18b). In these experiments the $TPPS_{2a}$ dose was doubled to 0.6 μg/ml. An interesting point to note is the effect of increasing the photosensitiser dose on the light 'before' regimen. Specifically, comparison of the PCI group in figure 3.18a with that from figure 3.17 shows that the PCI effect in the 'before' group increases by 47% ($p<0.01$). There was only a marginal increase in PCI cytotoxicity for the light 'after' group after the photosensitiser was doubled.

The differential cytotoxicity between the two groups reduced from 20% ($p<0.01$) with 0.3 μg/ml TP to 8% ($p<0.05$) with 0.6 μg/ml TP. Addition of BSO to the PCI treatment group resulted in a 12% ($p<0.01$) increase in cytotoxicity compared to PCI alone. This is comparable to the increase seen using SAP 30 nM (17%, $P<0.05$, fig. 3.14b). No significant difference was observed between PCI versus PCI + BSO in the light 'before' group (fig. 3.18a).

Figure 3.18b shows a similar pattern to that seen in figure 3.18a. Specifically the light 'after' protocol achieved the highest overall level of cell kill, compared to control, for both PCI (54%, $p<0.01$) and PCI + BSO (71%, $P<0.01$).

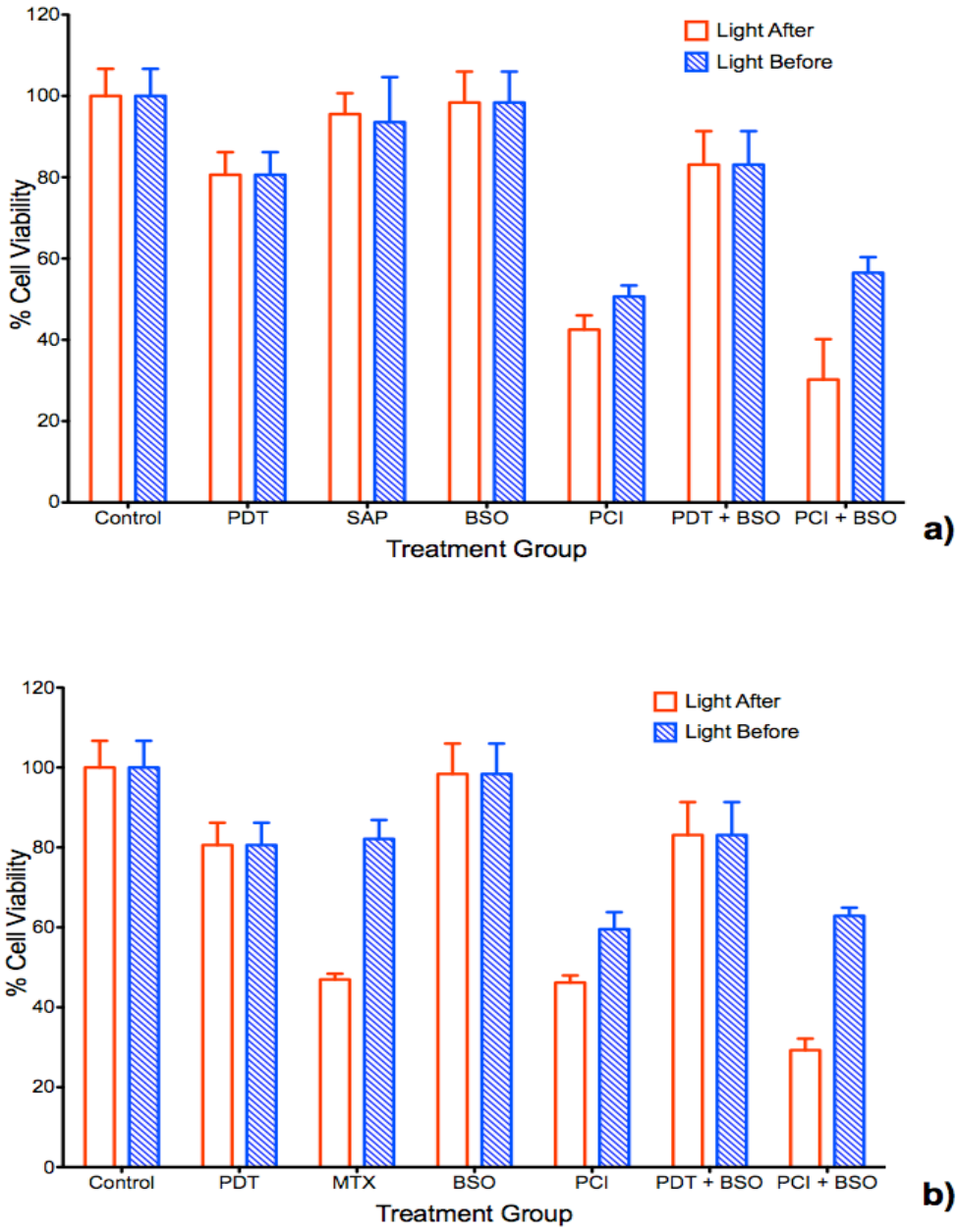

Figure 3.18 – Comparison of the light 'after' versus light 'before' Saporin or Mitoxantrone Photochemical Internalisation protocols.
4T1 breast cancer cells treated with different combinations of **(a)** $TPPS_{2a}$ 0.6 μg ml^{-1}, SAP 15 nM and BSO 1.0 μg ml^{-1}; **(b)** $TPPS_{2a}$ 0.6 μg ml^{-1}, MTX 0.4 μg ml^{-1} and BSO 1.0 μg ml^{-1}. SAP **(a)** or MTX **(b)** was added to the appropriate treatment groups either preceding (light 'after') or following (light 'before') illumination. Exposure to light took place 4h after drugs were washed off. Cells illuminated for 120 s using LumiSource® illuminator. Cell viability measured using MTT assay 24h after illumination (absorbance read at 490 nm).

However, an interesting observation can be made on closer inspection of the results. In the light 'after' protocol where MTX is added to the cells 24 hours after initial seeding, 53% cytotoxicity is observed. Indicating there is no

significant increase with PCI (1%). However, the light 'before' protocol involves treating the cells with MTX 48 hours after cell seeding. This resulted in 18% cytotoxicity, a full 35% less than in the light 'after' group. Consequently, despite achieving 13% ($p<0.01$) less ultimate cell kill than PCI in the light 'after' group, the light 'before' PCI-MTX regimen resulted in a 23% ($p<0.01$) increase in cytotoxicity compared to MTX alone.
Addition of BSO enhanced PCI in the light 'after' group by 17% ($p<0.01$), though there was no significant difference observed in the light 'before' group. The addition of BSO to PDT resulted in 17% ($p<0.01$) increased cytotoxicity.

In order to better simulate the clinical picture with regard to cancer therapeutics, where multiple therapeutics are often used in a single treatment regimen, SAP and MTX were given in combination to assess whether or not PCI would enhance the delivery of a combined therapy.

The relative toxicity associated with combining SAP + MTX for PCI (120 seconds illumination) was compared with single agent PCI +/- BSO in this investigation (fig. 3.19). In the light 'after' group, Combination (SAP + MTX)-PCI (Combo-PCI) resulted in 14% ($p<0.01$) and 17% ($p<0.01$) increased cell kill compared to SAP-PCI and MTX-PCI respectively. In the light 'before' group, Combo-PCI did not significantly increase cytotoxicity compared to SAP-PCI, though MTX-PCI was enhanced by 15% ($p<0.01$). Interestingly in the SAP + MTX (S/M, without TP) control (data not shown), there was a significant difference in cytotoxicity with the light 'after' (LA) regimen eliciting 52% ($p<0.01$) cytotoxicity compared to 22% ($p<0.01$) in the light 'before' (LB) group. Therefore, for Combo-PCI (LA) there was no significant increase in cell kill compared to S/M (LA). However, Combo-PCI (LB) increased cytotoxicity by 34% ($p<0.01$) compared to S/M (LB). Overall, Combo-PCI was more effective (for total cell kill) with the LA protocol, which produced 15% increased cell kill compared to the LB protocol.

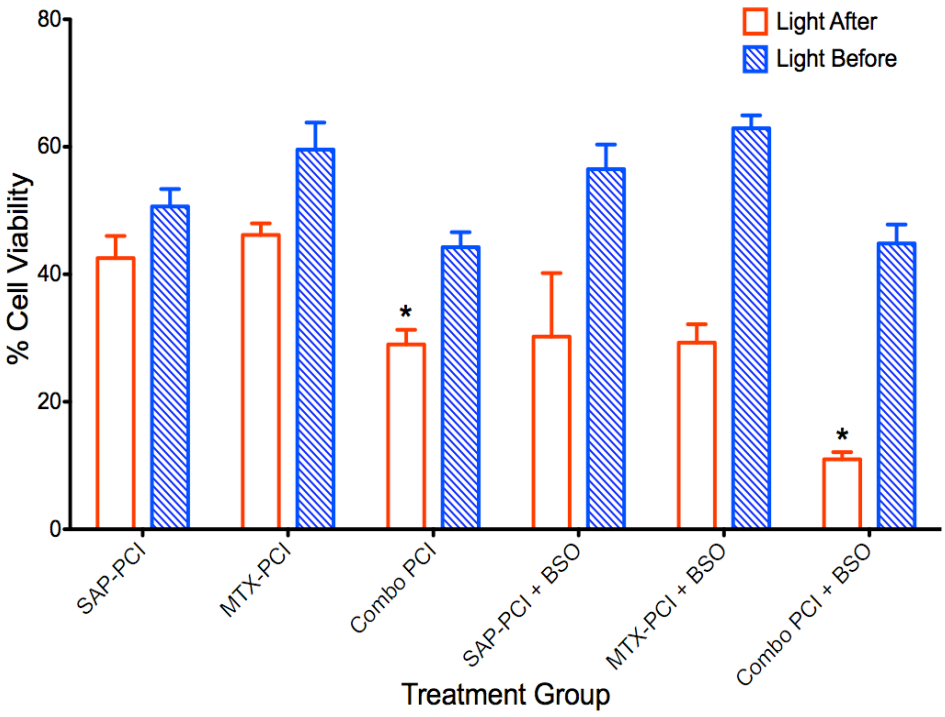

Figure 3.19 – Comparison of the light 'after' versus light 'before' Combination Photochemical Internalisation protocols.
4T1 breast cancer cells treated with different combinations of $TPPS_{2a}$ 0.3 μg ml^{-1}, SAP 15 nM, MTX 0.4 μg ml^{-1} and BSO 1.0 μg ml^{-1}. Saporin and or MTX was added to the appropriate treatment groups either preceding (light 'after') or following (light 'before') illumination. Exposure to light took place 4h after drugs were washed off. Cells illuminated for 120 s using the LumiSource® illuminator. **(*)** BSO increased combo-PCI cytotoxicity by 18% ($p<0.01$) in the light 'before' group (blue histogram). Cell viability measured using MTT assay 24h after illumination (absorbance read at 490 nm).

Addition of BSO to Combo-PCI (LA) resulted in 18% ($p<0.01$) increased cytotoxicity reaching a maximum of 89% cell kill compared to control. This also represents a 19% and 18% increase compared to BSO enhanced SAP-PCI (LA) and MTX-PCI (LA) respectively ($p<0.01$). The BSO + SAP + MTX (B/S/M, without TP) control (LA) produced 55% ($p<0.01$) cytotoxicity compared to control (no treatment). Thus BSO enhanced Combo-PCI (LA) produced 34% increased cell kill compared B/S/M (LA) ($p<0.01$). Addition of BSO to Combo-PCI (LB) had no effect on cytotoxicity. However, there was a 12% ($p<0.01$) and 18% ($p<0.01$) increase compared to BSO enhanced SAP-PCI (LB) and MTX-PCI (LB) respectively. B/S/M (LB) caused 23% cell kill compared to control (no treatment). Therefore, Combo-PCI + BSO (LB) killed 32% more cells than B/S/M (LB) ($p<0.01$).

It is important to note that there was <3% increase in cytotoxicity upon addition of BSO to S/M for both LA and LB protocols.

3.10 Variable 6: Time between photosensitiser activation and survival assay

In this study the effect of prolonging the time to MTT-assay from 24 hours post-light to 72 hours post-light was investigated.

Figure 3.20 shows four graphical comparisons in cell viability at 24h and 72h post-light for both LB (blue) and LA (red) PCI protocols. Figure 3.20a represents the light 'after' protocol for SAP-PCI. In the PDT alone group, a 6% ($p<0.01$) increase in cell kill was observed at 72h compared to 24h. For SAP 15 nM alone the increase was 13% ($p<0.01$) at 72h, therefore, 18% ($p<0.01$) cytotoxicity compared to control. There was no significant increase in cytotoxicity for BSO between 24h and 72h; therefore, it remained <10% compared to control. At 72h, the cytotoxicity of SAP-PCI increased by 28% ($p<0.01$) compared to 24h to achieve a total of 85% ($p<0.01$) compared to control. This represented a 2.4-fold and 3.7-fold increase in cytotoxicity compared to PDT alone (72h) or SAP alone (72h) respectively ($p<0.01$). In contrast, at 24h there was a 2-fold and 13-fold increase in cytotoxicity compared to PDT alone or SAP alone respectively. In the PDT-BSO group a 13% ($p<0.01$) increase in cell kill was observed at 72h compared to 24h, corresponding to a maximal 30% ($p<0.01$) cell kill compared to control.

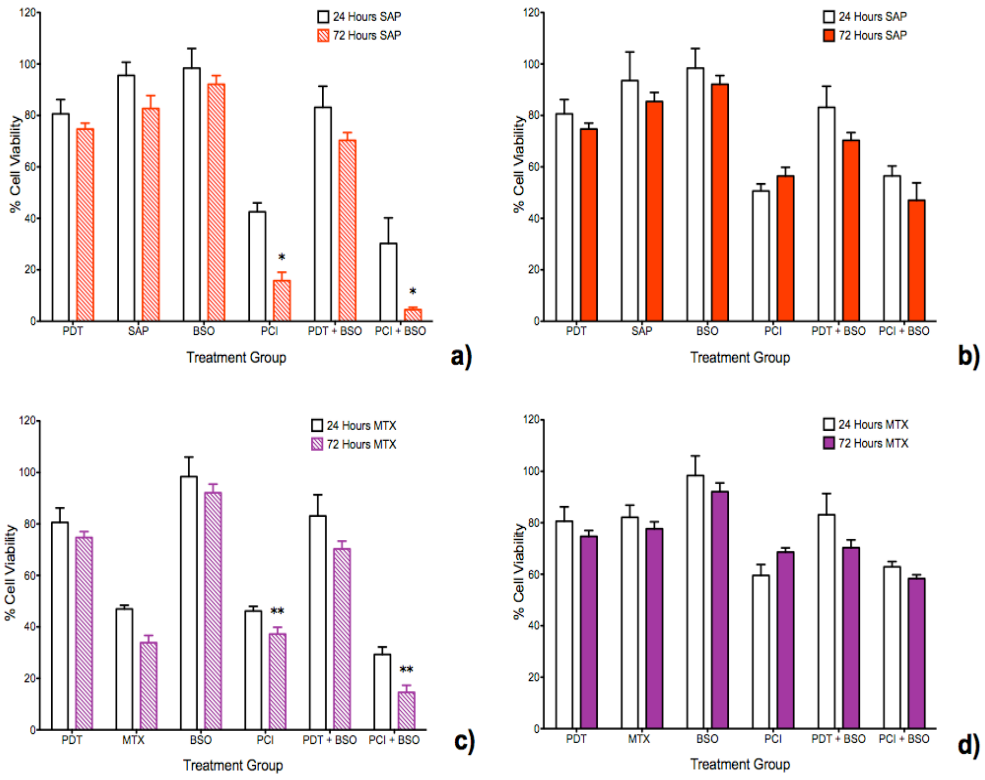

Figure 3.20 – Investigation into the impact on cytotoxicity of waiting 72h versus 24h post-illumination for Buthionine Sulfoximine enhanced Photochemical Internalisation of Saporin or Mitoxantrone.
4T1 breast cancer cells treated with different combinations of $TPPS_{2a}$ 0.6 μg ml^{-1}, SAP 15 nM, MTX 0.4 μg ml^{-1} and BSO 1.0 μg ml^{-1}. **(a)** Cells were treated with TP or SAP or BSO alone or in combination and illuminated for 120 s at a time point 4h after drugs were washed off, MTT performed 24h (white histogram) or 72h (red striped) after illumination; **(b)** cells were treated with TP and/or BSO and illuminated for 120 s at a time point 4h after drugs were washed off, SAP and/or BSO added after illumination (light 'before'), MTT performed 24h (white histogram) or 72h (red solid) after illumination; **(c)** same protocol as (a) except SAP replaced with MTX, MTT performed 24h (white histogram) or 72h (purple striped) after illumination; **(d)** same protocol as (c) (light 'before) except SAP replaced with MTX, MTT performed 24h (white histogram) or 72h (purple solid) after illumination. **(*)** addition of BSO, enhanced SAP-PCI cytotoxicity by 11% at 72h ($p<0.01$) resulting in >95% cell kill, **(**)** addition of BSO, enhanced MTX-PCI cytotoxicity by 23% at 72h ($p<0.01$). Cell viability measured using MTT assay (absorbance read at 490 nm).

The PCI + BSO group experienced the highest level of cell kill at 72h. A 26% ($p<0.01$) increase in cytotoxicity was observed compared to 24h, which corresponds to 96% ($p<0.01$) cell kill compared to control. This also represents an 11% ($p<0.01$) increase in cell kill compared to PCI in the absence of BSO at 72h SAP + BSO at 72h produced 10% ($p<0.01$) increased cell kill compared to

24h. This corresponded to 59% ($p<0.01$) less cytotoxicity than SAP-PCI (72h) and 70% ($p<0.01$) less than SAP-PCI + BSO (72h).

Figure 3.20c illustrates the results for the (LA) protocol for PCI-MTX. At 72h MTX 0.4 μg/ml elicited 66% ($p<0.01$) cell kill compared to controls, which represents a 13% increase compared to 24h. MTX-PCI (LA) produced 62% ($p<0.01$) cell kill, thus there was no difference observed compared to MTX alone at 72h. Addition of BSO to PCI-MTX (LA) resulted in 85% cell kill, a 14% ($p<0.01$) increase compared to PCI-MTX + BSO at 24h and a 23% ($p<0.01$) increase compared to PCI-MTX at 72h. A 15% rise in cytotoxicity was observed between MTX + BSO at 72h compared to 24h. This translates into 32% increase compared to MTX alone at 72h and this is equivalent to the level of cytotoxicity seen with MTX-PCI at 72h, as there is no significant difference. However, MTX + BSO (72h) produced 16% ($p<0.01$) less cell kill than MTX-PCI + BSO (72h).

Figure 3.20b shows the histogram for the light 'before' protocol for SAP-PCI. There was an 8% ($p<0.01$) increase in cytotoxicity for SAP alone 72h compared to 24h. SAP-PCI (LB, 72h) achieved 44% ($p<0.01$) cytotoxicity. This represents no difference compared to 24h. SAP-PCI + BSO (72h) increased cytotoxicity by 12% ($p<0.01$) compared to SAP-PCI (72h) and SAP-PCI + BSO (24h). There was no difference in cytotoxicity between SAP + BSO (LB) at 24h versus 72h. However, SAP + BSO (LB, 72h) killed 16% less cells that SAP-PCI (LB, 72h) and 28% less than SAP-PCI + BSO (LB, 72h) ($p<0.01$).

Figure 3.20d illustrates the difference in cytotoxicity at 24h versus 72h in light 'before' MTX-PCI. There was no difference in cell kill for MTX alone between 24h and 72h. MTX-PCI (LB, 72h) elicited 10% ($p<0.01$) increased cell kill compared to MTX alone (LB, 72h). MTX-PCI (LB, 72h) killed 8% ($p<0.01$) less cells compared to 24h (LB). MTX-PCI + BSO (LB) produced 43% ($p<0.01$) cell kill compared to control, which equates to an 11% increase compared to MTX-PCI (LB, 72h). However, there is no difference in cytotoxicity in the MTX-PCI + BSO groups at 24h versus 72h. MTX + BSO (LB, 72h) produced 11% ($p<0.01$)

increased cell kill compared to 24h. There is a 12% increase in cell kill in the MTX + BSO (LB, 72h) compared to MTX alone (LB, 72h), however there is no difference between MTX + BSO and MTX-PCI in the LB-group at 72h. Treatment of cells with MTX-PCI +BSO resulted in 9% ($p<0.01$) increased cytotoxicity (data not shown).

Figure 3.21 illustrates the effect of waiting 72h post-light before assessing cell viability for Combo-PCI for LA (fig. 3.21a) and LB (fig. 3.21b) protocols. Figure 3.21a shows a 19% ($p<0.01$) increase in cell kill for Combo-PCI at 72h compared to 24h, reaching 90% ($p<0.01$) overall cytotoxicity. However, there was no significant increase in cell kill compared to SAP-PCI (72h, LA). Combo-PCI (72h, LA) killed 15% ($p<0.01$) more cells than SAP + MTX under the same conditions. However, at 72h SAP + MTX (LA) killed 22% ($p<0.01$) (74% in total) more cells than at 24h (LA). Addition of BSO to the Combo-PCI protocol (72h, LA) resulted in maximum cytotoxicity of 97% ($p<0.01$) compared to control and 8% ($p<0.05$) compared to Combo-PCI alone (72h, LA). Combo-PCI + BSO (72h, LA) killed 21% more cells than SAP + MTX + BSO (B/S/M, 72h, LA).

Figure 3.21b shows there is no significant difference in cell kill for Combo-PCI (LB protocol) at 72h compared to 24h. This corresponds to reaching 56% ($p<0.01$) overall cytotoxicity compared to control. Combo-PCI (72h, LB) killed 27% ($p<0.01$) more cells that SAP + MTX under the same conditions. However, at 72h (LB) SAP + MTX killed 24% ($p<0.01$) (29% in total) more cells than at 24h (LB). Addition of BSO to the Combo-PCI protocol (72h, LB) resulted in 11% ($p<0.01$) increased cytotoxicity

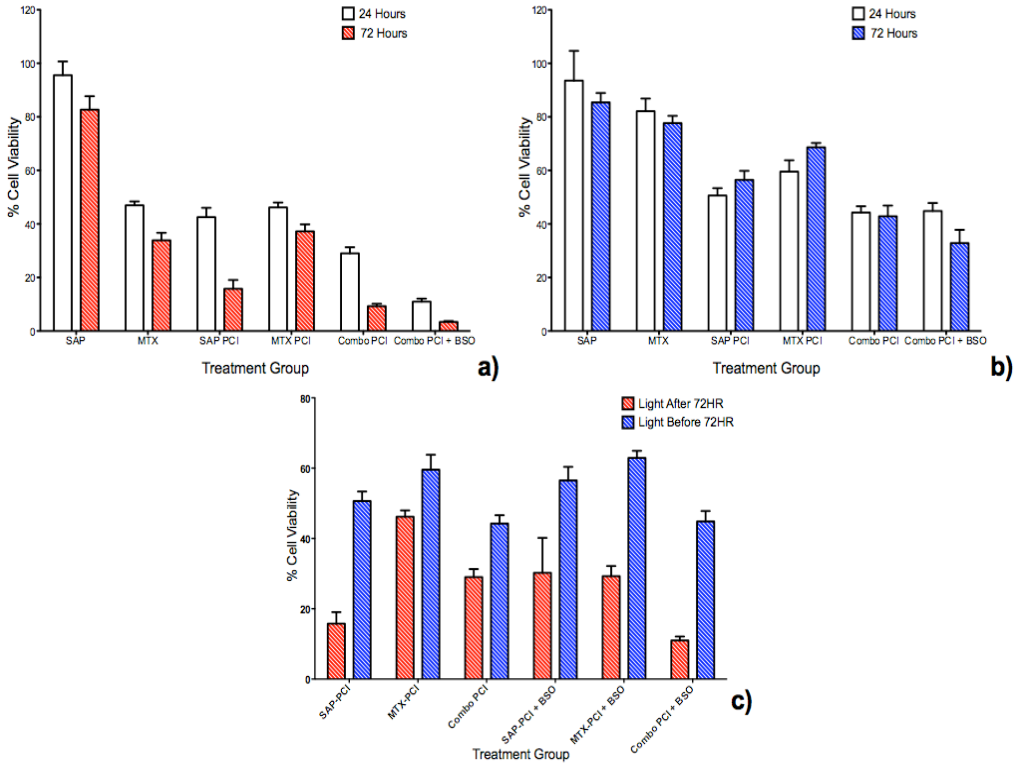

Figure 3.21 - Investigation into the impact on cytotoxicity of waiting 72h versus 24h post-illumination for Buthionine Sulfoximine enhanced combination Photochemical Internalisation of Saporin and Mitoxantrone.
4T1 breast cancer cells treated with different combinations of $TPPS_{2a}$ 0.6 μg ml^{-1}, SAP 15 nM, MTX 0.4 μg ml^{-1} and BSO 1.0 μg ml^{-1}. **(a)** Cells were treated with TP or SAP or MTX alone or in combination +/- BSO and illuminated for 120 s at a time point 4h after drugs were washed off using the light 'after' protocol, MTT performed 24h (white histogram) or 72h (red striped) after illumination; **(b)** Cells were treated with TP +/- BSO and illuminated for 120 s at a time point 4h after drugs were washed off using the light 'before' protocol, SAP and/or MTX +/- BSO were added following illumination, MTT performed 24h (white histogram) or 72h (blue striped) after illumination; **(c)** cells were treated with TP or SAP or MTX alone or in combination +/- BSO (light 'after', red striped histogram) and illuminated for 120 s at a time point 4h after drugs were washed off or treated with TP +/- BSO and illuminated for 120 s at a time point 4h after drugs were washed off using the light 'before' protocol, SAP and/or MTX +/- BSO were added following illumination (blue striped histogram). Cell viability measured using MTT assay 72h after illumination (absorbance read at 490 nm).

compared to Combo-PCI alone (72h, LB), corresponding to maximum cytotoxicity of 67% ($p<0.01$). Combo-PCI + BSO (72h, LB) killed 31% more cells than B/S/M (72h, LB).

Comparison between LA vs. LB after 72h shows that overall LA achieved significantly greater cell kill than the LB protocol (fig 3.21c). For SAP-PCI + BSO the LA protocol achieved 40% ($p<0.01$) increased cytotoxicity compared to LB.

For MTX-PCI + BSO the LA protocol achieved 43% increased cytotoxicity compared LB (72h). At 72h combo-PCI + BSO using the LA protocol achieved 97% cytotoxicity. In comparison, the LB protocol achieved 67% cytotoxicity, representing a 30% increase in cell kill using the LA protocol.

3.11 Confocal Imaging – alexa-488 labeled saporin

Confocal microscopy was used to assess the intracellular localisation of Alexa-labeled SAP prior to and following 'on-stage' exposure to a 405 nm laser (15s), to excite TP, for 4T1 cells treated with SAP-488 alone (fig. 3.22a-c) and SAP-488 + TP 0.6 μg/ml (fig. 3.23a-c). The SAP-488 alone group is shown as controls for the any potential photobleaching or redistributive effects of the 405 nm laser on the fluorescently labeled protein. The images are a z-stack of two slices taken at three different time points (before, immediately following and 240 s after exposure to the 405 nm laser). Figure 3.22a shows the intracellular distribution of SAP-488 prior to exposure to the 405 nm laser. The image shows a granular pattern of uptake, 28h after cells were initially treated with SAP-488. Immediately following exposure to the laser there was no observable change in the intracellular distribution of SAP-488 (fig. 3.22b). Figure 3.22c was taken 240 s after treatment with the laser and again shows very little if any visual change in SAP-488 intensity or distribution. Quantitative analysis of the images shows a 3% reduction in average signal intensity between fig. 3.22a and fig. 3.22c.

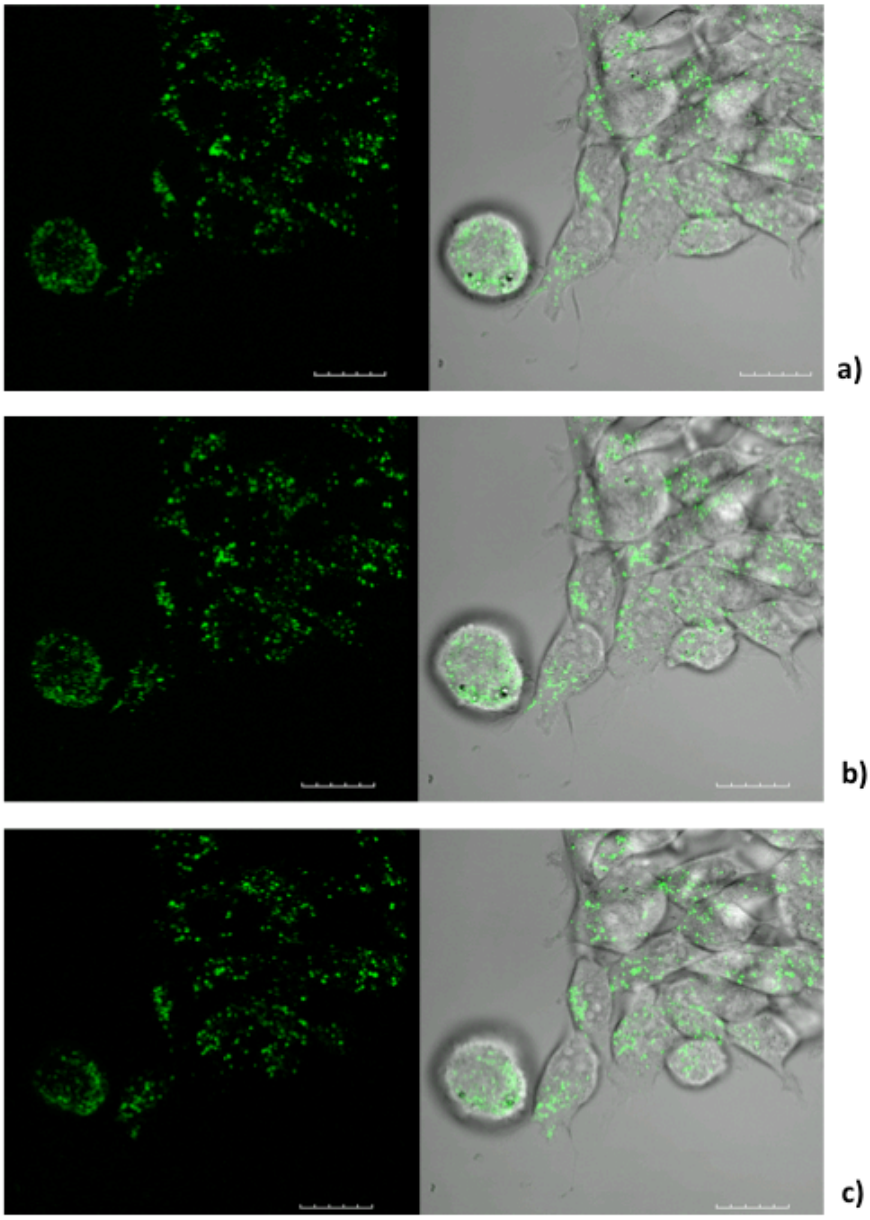

Figure 3.22 – Confocal imaging of Alexa-488 labeled Saporin (alone).
1 x 10^4 4T1 (murine) breast cancer cells were seeded on 35 mm diameter glass-bottomed fluorodishes and grown for 48h. Cells treated with SAP-488 400 nM for 24h and washed three times with PBS prior to imaging. **(a)** pre-laser treatment, **(b)** immediately following exposure to 405 nm laser, **(c)** 240 s after exposure to 405 nm laser. Quantitative analysis of images using ImageJ revealed a 3% reduction in intracellular signal intensity at 240 s. *Ex 488 nm, Em 520 nm, 60X NA:1.35 Objective Lens, zoom x1.0, scale 20 microns.*

Cells in figure 3.23 were treated with both SAP-488 and TP prior to imaging and exposure to the 405 nm laser using the same protocol described above for figure

3.22. Much like 3.22a, figure 3.23a shows granular uptake of SAP-488, 28h after drugs were initially added to the 4T1 cells.

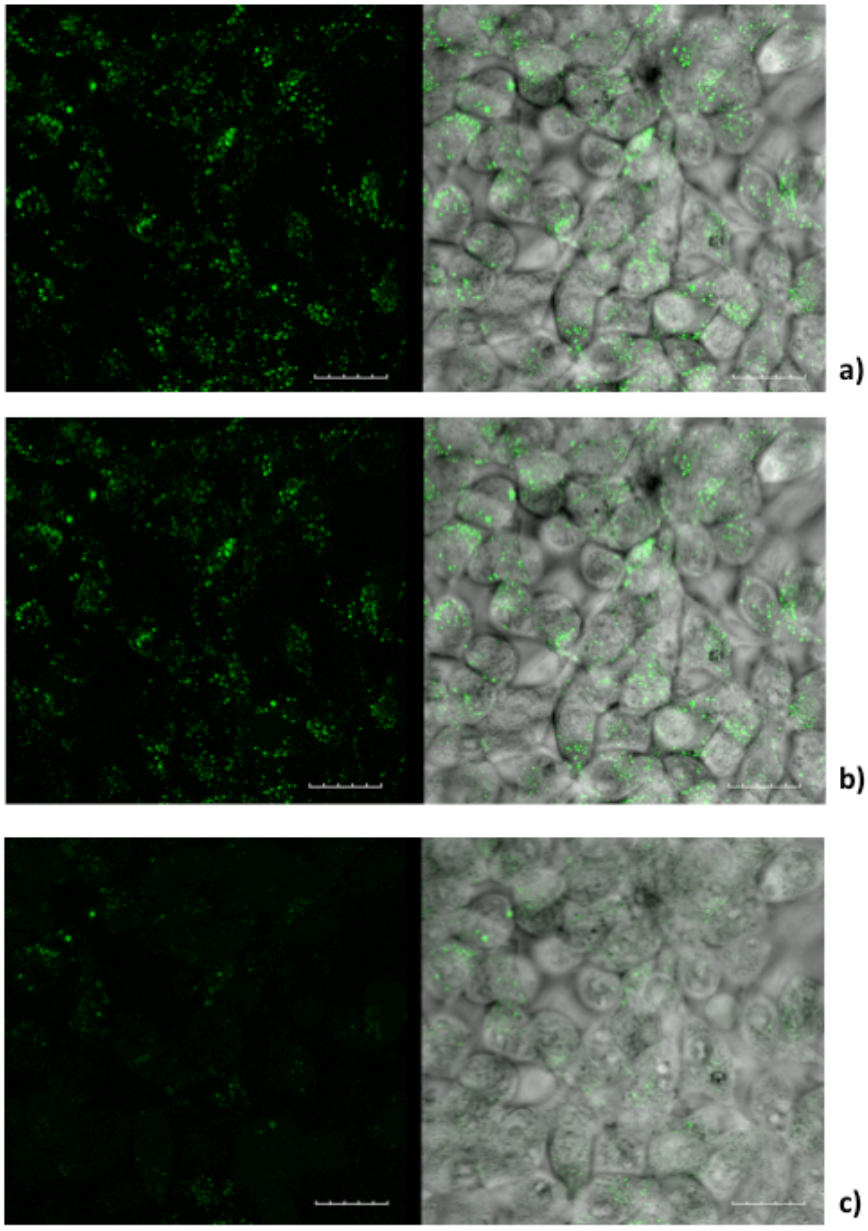

Figure 3.23 – Confocal imaging of Alexa-488 labeled Saporin.
1 x 10^4 4T1 breast cancer cells were seeded on 35 mm diameter glass-bottomed fluorodishes and grown for 48h. Cells treated with $TPPS_{2a}$ 0.6 µg ml^{-1} + SAP-488 400 nM for 24h and washed three times with PBS prior to imaging. **(a)** pre-laser treatment, **(b)** immediately following exposure to 405 nm laser, **(c)** 240 s after exposure to 405 nm laser. Quantitative analysis of images using ImageJ revealed a 30% reduction in intracellular signal intensity at 240 s ($p<0.01$). *Ex 488 nm, Em 520 nm, 60X NA:1.35 Objective Lens, zoom x1.0, scale 20 microns.*

Immediately following the treatment with the 405 nm laser, little if any visual change in SAP-488 signal intensity or distribution was observed (fig. 3.23b). However, 240 s following exposure to the 405 nm laser there was an apparent loss of signal in the 2-slice z-series associated with phenotypic features that are consistent with a pre-apoptotic state (seen in the bright field image, fig. 3.23c). Quantitative analysis showed a 30% reduction in SAP-488 signal intensity in figure 3.23c compared to figure 3.23a. This represents a 10-fold greater loss of signal intensity in cells treated with SAP-488 + TP compared to SAP-488 alone. This would be consistent with the re-localisation of SAP-488, as treatment with the 405 nm laser alone does not trigger this change in the absence of $TPPS_{2a}$ (fig. 3.22a).

3.12 Confocal Imaging – mitoxantrone and lysotracker green

The intracellular localisation of the cytotoxin mitoxantrone (MTX, 1.2 μg/ml) was also assessed using confocal microscopy. Uptake into the endo-lysosomal system was observed, as detected by co-localisation with Lyso-Tracker Green (50 nM) (fig. 3.24c). In order to make a real time assessment of the effect of PCI on the redistribution of MTX from endo-lysosomal vesicles, 'on-stage' illumination of the cells was performed using the 405 nm laser. Prior to use of the laser (fig. 3.24a) MTX was localised in discrete intracellular vesicles (similar to SAP-488 above). Following application of the 405 nm laser, the treated cells were assessed after 10 minutes (fig. 3.24b). We observed a significant change in the pattern of distribution of MTX with fewer discrete vesicles, increased membrane uptake and mobilisation into the nucleus of the 4T1 cells (white arrows). This is consistent with findings in previously published data, which showed the redistribution and nuclear mobilisation of MTX following PCI treatment(25).

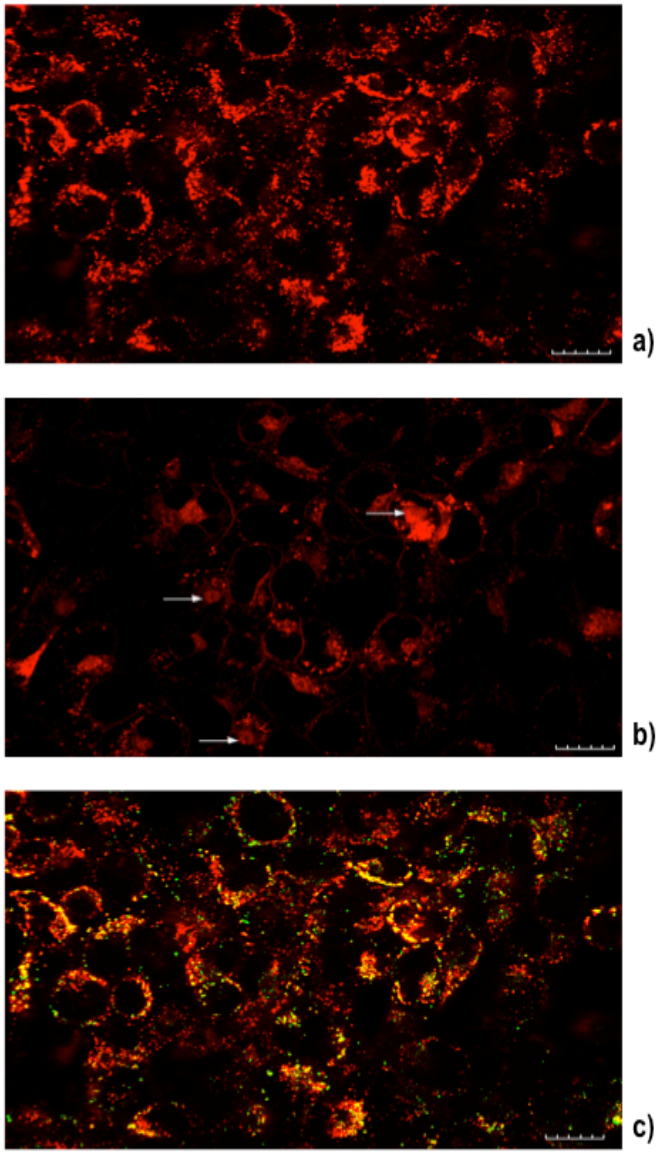

Figure 3.24 - Endolysosomal localization and Photo-induced redistribution of intracellular Mitoxantrone following $TPPS_{2a}$-mediated PCI.
Cells were treated with $TPPS_{2a}$ 0.6 μg ml^{-1} + MTX 1.2μg ml^{-1} for 24h. Images were taken 4h after drugs were washed off. **(a)** was taken prior to laser treatment and shows the distribution of MTX in a granular pattern. Image **(b)** was taken 10 minutes after exposing the cells to a 405 nm laser resulting in redistribution of MTX. The white arrows indicate areas of nuclear mobilisation. **(c)** PCI drugs were washed off and Lysotracker® green (LYG) 50 nM added for 30 minutes prior to confocal imaging (these cells were not treated with the laser. Areas in Red = MTX, Green = LYG, Yellow = CO-LOCALISATION. *60X NA:1.35 Objective Lens, zoom x1.0, scale 20 microns.*

3.13 Confocal Imaging – Effect of buthionine sulfoximine on intracellular glutathione synthesis

The effect of buthionine sulfoximine (BSO) on the expression of intracellular reduced glutathione (GSH) stores was assessed by detection of the GSH fluoro-probe monochlorobimane (mBCl) using confocal microscopy (fig. 3.25). Figure 3.25a shows 4T1 cells that have not been treated with BSO prior to exposure to mBCl. We observed a high mBCl signal indicating intracellular expression of GSH. Cells in figure 3.25b were treated with BSO 1.0 μg/ml for 24h prior to exposure to mBCl. The confocal image shows a visually significant reduction in the mBCl signal, indicating a reduced level of intracellular GSH expression. Using quantitative image analysis (of 4 separate cell clusters per treatment group), a 4-fold reduction in the mBCl signal in cells treated with BSO compared to controls was determined ($p<0.001$).

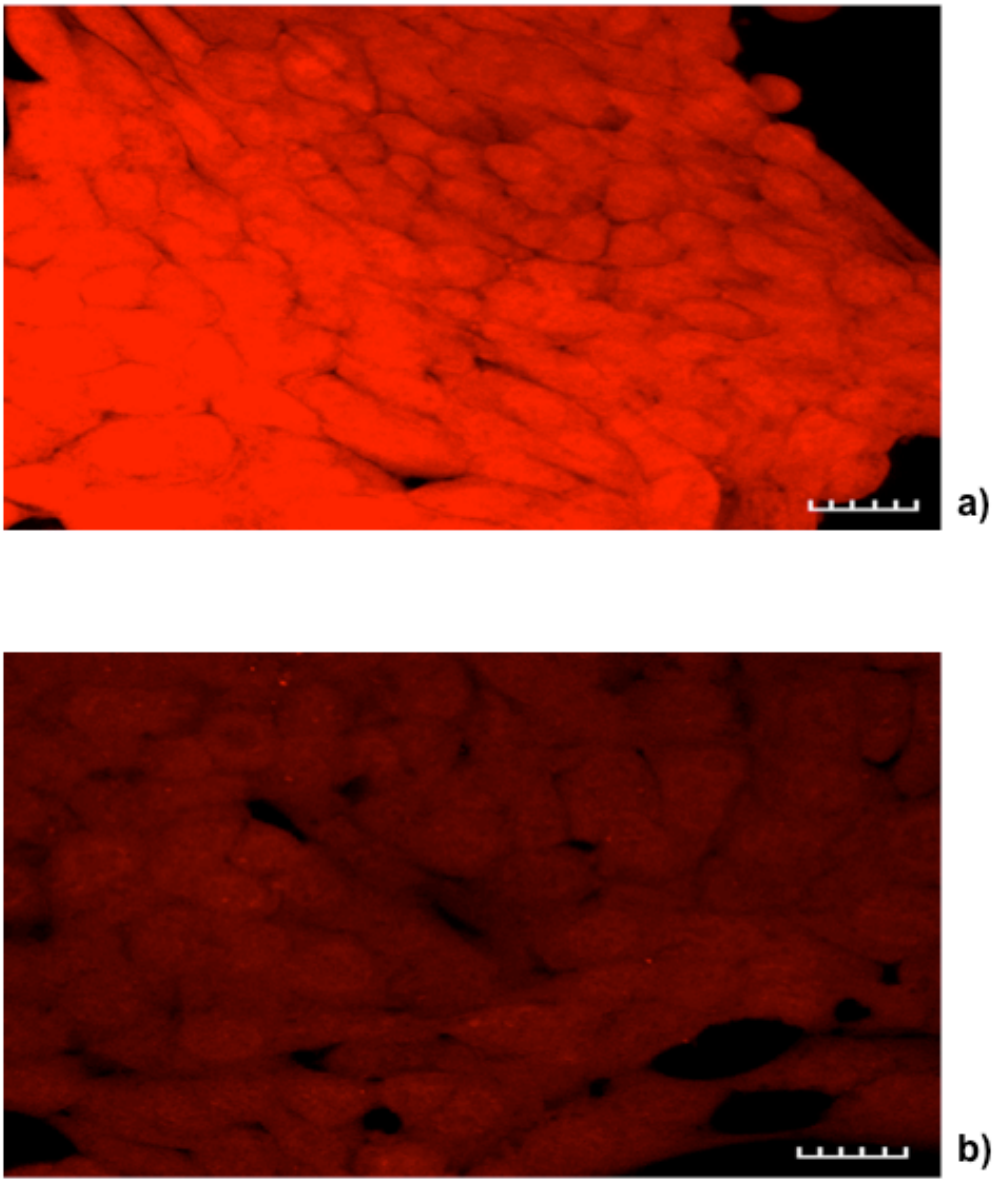

Figure 3.25 - Monochlorobimane-glutathione detection.
4T1 cells were treated with mBCl 40 µM for 20 minutes prior to confocal microscopy either **(a)** alone or **(b)** following 24h incubation with BSO 1.0 µg ml^{-1}**.** Quantitative analysis (Image J) revealed a 4-fold reduction in the mBCl-GSH signal in cells pre-treated with BSO ($p<0.001$). *20X NA:0.75 Objective Lens, zoom x2.1, scale 20 microns*

3.14 Confocal Imaging – Lipid peroxidation studies

This section investigates the effect of photoactivation and the different compounds used thus far in the chapter on the level of lipid peroxidation taking place within the intracellular environment. Cells were treated with SAP, $TPPS_{2a}$ and BSO either alone or in different combinations +/- light. Subsequently they were treated with a lipid peroxide probe, Image-iT® Peroxidation Kit, which is

based on the BODIPY® 581/591 C11 reagent, that has two emission peaks, one pre-lipid peroxidation at ~590 nm and the other post-lipid peroxidation at ~610 nm (figure 3.26).

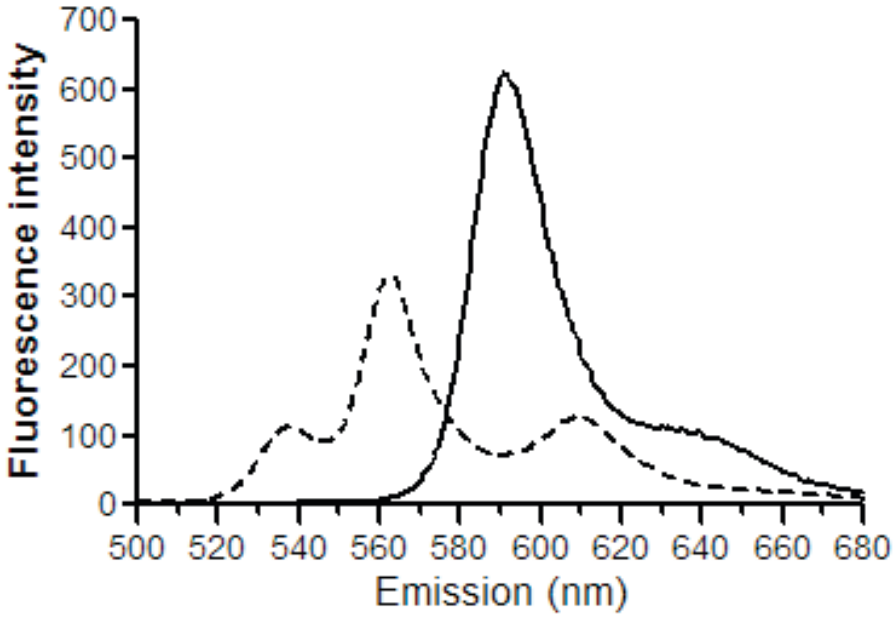

Figure 3.26 - Fluorescence emission spectra of the Image-iT® Lipid Peroxidation Sensor.
Before and after lipid peroxidation(121).

Figure 3.27 shows confocal images of negative control groups (untreated cells with no lipid peroxide probe, fig. 3.27a) and (untreated cells with lipid peroxide probe, fig. 3.27b). The comparison between the two upper quadrants of fig 3.27b shows the relative fluorescence of lipid peroxide (green) compared to lipid pre-peroxidation (red). The ratio of green:red is 1:4.7, indicating that in untreated cells there is relatively low level of lipid peroxidation. The bottom left quadrant shows the overlay of the two separate fluorescence signals, while the bottom right quadrant shows the live cells in a transmitted light view.

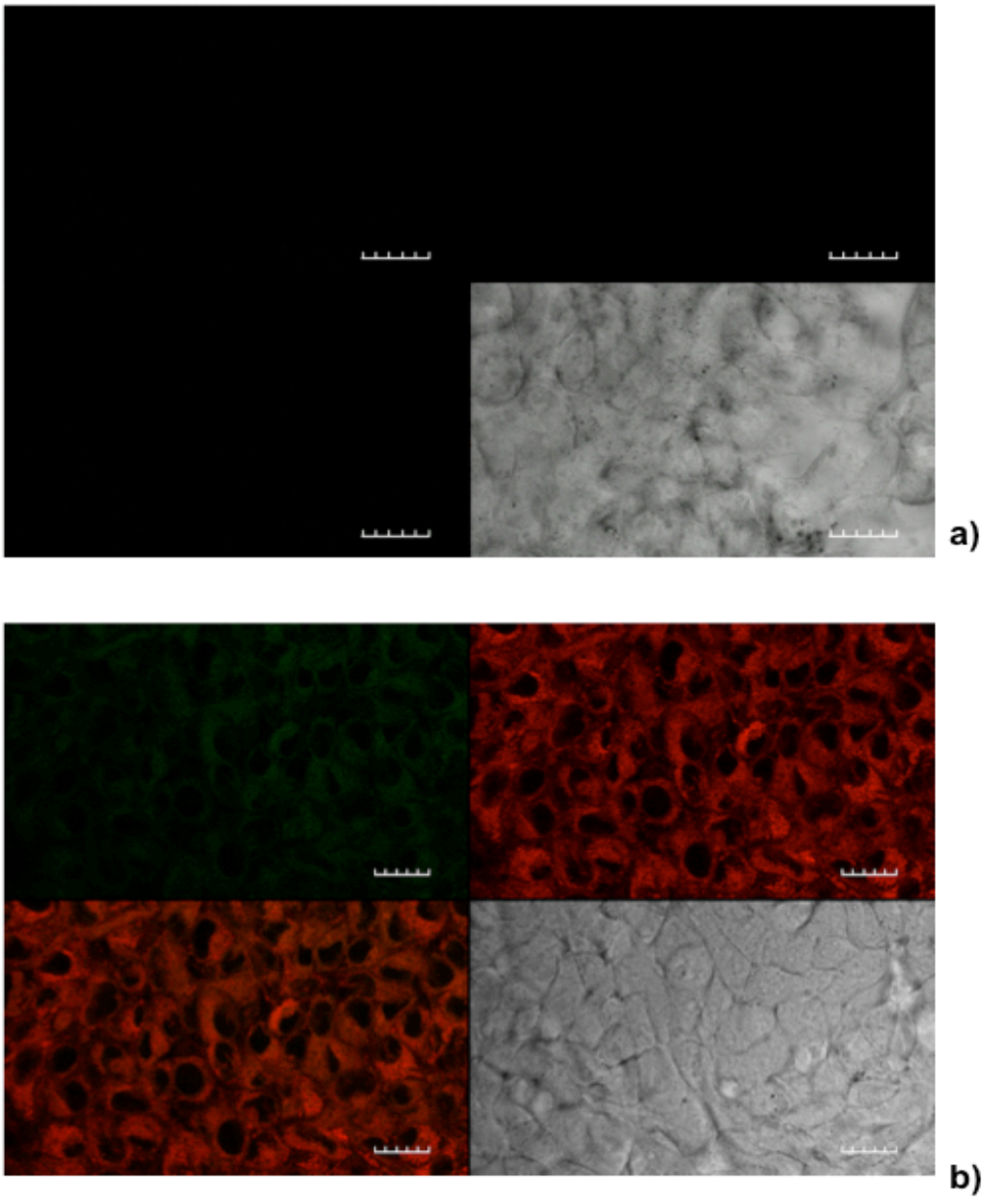

Figure 3.27 – Confocal Microscopy Lipid Peroxidation Studies (untreated controls). 1 x 10^4 4T1 breast cancer cells were seeded on 35 mm diameter glass-bottomed fluorodishes and grown for 48h. Cells were re-incubated with media alone for a further 24h. Cells were then illuminated for 150 s using the LumiSource® illuminator **(a)**. Subsequently, **(b)** Image-IT lipid peroxidation probe was added to the cells to make a final concentration of 10 μM and incubated at 37°C for 30 minutes. Images then taken using confocal microscope. RED = reduced lipid, Ex 581 nm Em 591 nm; GREEN = oxidized lipid, Ex 488 nm Em 510 nm; ORANGE = overlaid image. *60X NA:1.35 Objective Lens, zoom x1.0, scale 20 microns.*

Figure 3.28 illustrates the effects of TP on the level of intracellular lipid peroxidation both under 'dark' conditions (fig. 3.28a) and following 150 s of illumination using the LumiSource® illuminator (fig. 3.28b). Under 'dark' conditions, there was a three-fold increase in the red fluorescence signal compared to the green signal. Interestingly the maximum intensity of the red signal is reduced compared to untreated cells (fig. 3.27b). Following exposure to 150 seconds of light there was a shift in the ratio between red and green signal, reducing from 1:3.4 under 'dark' conditions to 1:0.9 (fig. 3.28b). The latter indicated that activation of the photosensitiser increased the level of lipid peroxidation compared to reduced lipid. The maximum signal intensity (green) increased 2.6-fold following illumination (fig. 3.28b) compared to 'dark' controls (fig. 3.28a). The transmitted light image (fig. 3.28b) showed features of pre-apoptotic cells with a significant change in morphology, particularly when compared to untreated (fig. 3.27b) and dark (fig. 3.28a) controls.

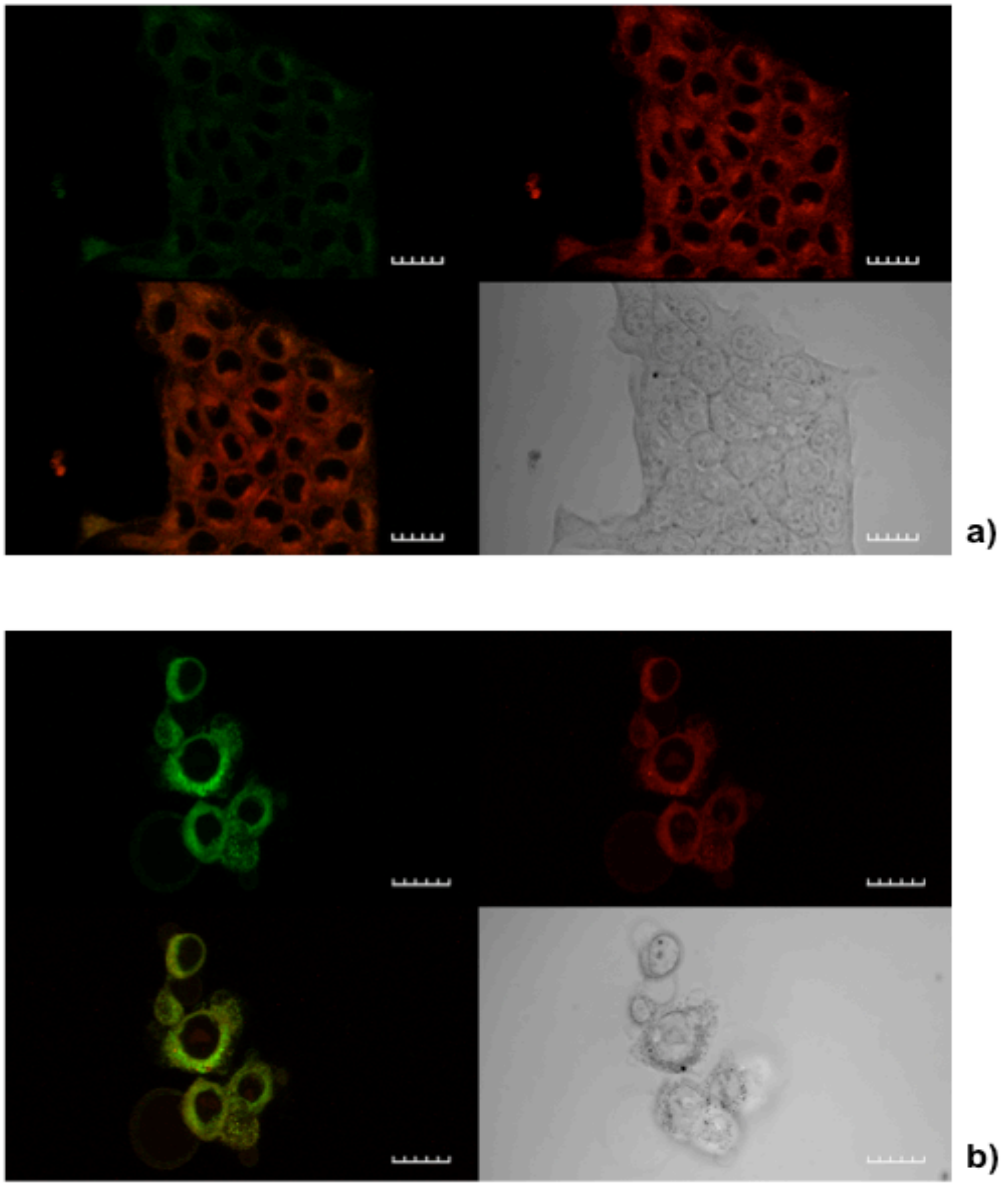

Figure 3.28 – Confocal Microscopy Lipid Peroxidation Studies (PDT treated controls).

1 x 10^4 4T1 breast cancer cells were seeded on 35 mm diameter glass-bottomed fluorodishes and grown for 48h. Cells were re-incubated with $TPPS_{2a}$ 0.6 μg ml^{-1} alone (PDT) for a further 24h. Cells in **(b)** were then illuminated for 150 s using the LumiSource® illuminator, while those in **(a)** were kept 'dark'. Subsequently, Image-IT lipid peroxidation probe was added to the cells to make a final concentration of 10 μM and incubated at 37°C for 30 minutes. Images were then taken using confocal microscope. A 2.6-fold increase in oxidised lipid was observed in the illuminated group (b) compared to 'dark' control (a). RED = reduced lipid, Ex 581 nm Em 591 nm; GREEN = oxidized lipid, Ex 488 nm Em 510 nm; ORANGE = overlaid image. *60X NA:1.35 Objective Lens, zoom x1.0, scale 20 microns.*

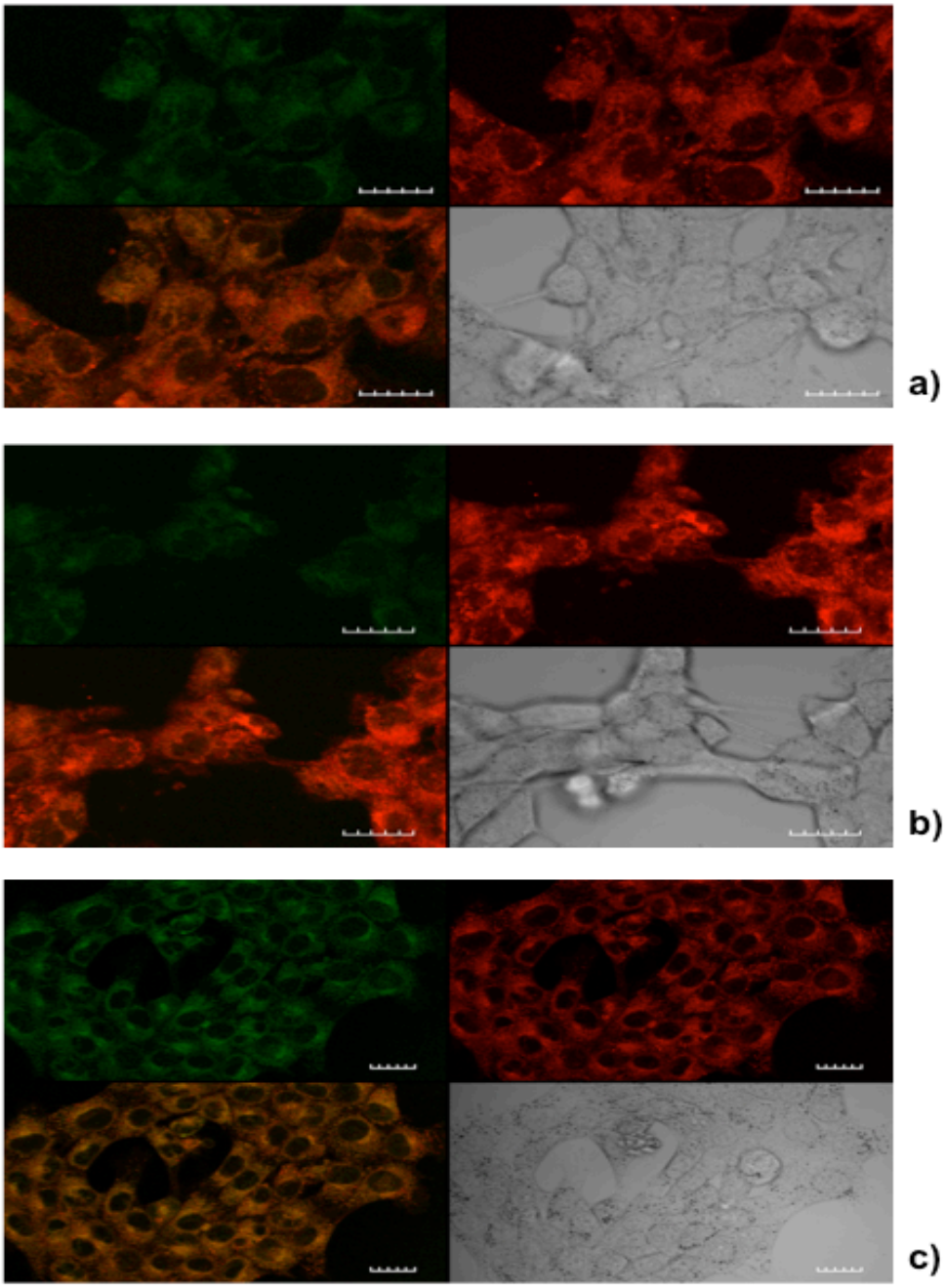

Figure 3.29 – Confocal Microscopy Lipid Peroxidation Studies (Buthionine Sulfoximine or Saporin treated controls).

1 x 10^4 4T1 breast cancer cells were seeded on 35 mm diameter glass-bottomed fluorodishes and grown for 48h. Cells were re-incubated with **(a)** BSO 1.0 µg ml^{-1} alone, **(b)** SAP 30 nM alone, **(c)** BSO + SAP for a further 24h. Cells in were then illuminated for 150 s using the LumiSource® illuminator. Subsequently, Image-IT lipid peroxidation probe was added to the cells to make a final concentration of 10 µM and incubated at 37°C for 30 minutes. Images were then taken using confocal microscope. The combination of BSO + SAP resulted in 19% and 31% increase in lipid peroxidation compared to BSO or SAP alone respectively ($p<0.01$) RED = reduced lipid, Ex 581 nm Em 591 nm; GREEN = oxidized lipid, Ex 488 nm Em 510 nm; ORANGE = overlaid image. *60X NA:1.35 Objective Lens, zoom x1.0, scale 20 microns.*

Figure 3.29 illustrates the effects of treating cells with buthionine sulfoximine 1.0 μg/ml (BSO, fig. 3.29a), SAP 30 nM (fig. 3.29b) and BSO + SAP (fig. 3.29c). In cells treated with BSO alone ('dark') a ratio of 1:2.8 (green:red) was observed, indicating that BSO may have an effect on the rate of lipid-peroxidation when compared to untreated cells (fig. 3.27b). However, the maximum intensity of the green signal was less the 50% of that observed in cells treated with TP + light (150 s). SAP alone treatment resulted in a ratio of 1:3.3 (green:red), indicating that although SAP does appear to increase lipid-peroxidation compared to untreated controls, this represented a 14% relative reduction in green fluorescent signal. The combination of BSO + SAP resulted in a green:red ratio of 1:1.9 (fig. 3.29c). This indicated the combination of these two agents had a greater positive effect on the rate of lipid-peroxidation compared to either agent alone. There was a 19% and 31% increase in the maximum green signal intensity compared to BSO or SAP alone, respectively ($p<0.01$). There was a concomitant 7% decrease in the maximum red signal intensity compared to either agent alone.

Figure 3.30 illustrates the effect treating cells with TP + SAP + BSO + light (150 s) has on the relative production of lipid peroxides. Figure 3.30a shows the relative fluorescence signals for peroxidised (green) and non-peroxidised (red) lipids within a large group of 4T1 cells. The ratio of green:red is 1:1.9, which is equivalent to that seen with BSO + SAP (fig. 3.29c). However, it is important to note that the maximum green signal was 36% greater than that observed with BSO + SAP ($p<0.01$). Figure 3.30b shows a smaller group of 4T1 cells after the same treatment regimen of figure 3.30a. The first point to note is that these cells appear to be in the early phases of dying. Second that they have a significantly greater intensity of both green and red signals, compared to the other confocal images. The ratio of green:red is 1:1.5, thus indicating a significant increase in lipid peroxidation compared to untreated controls.

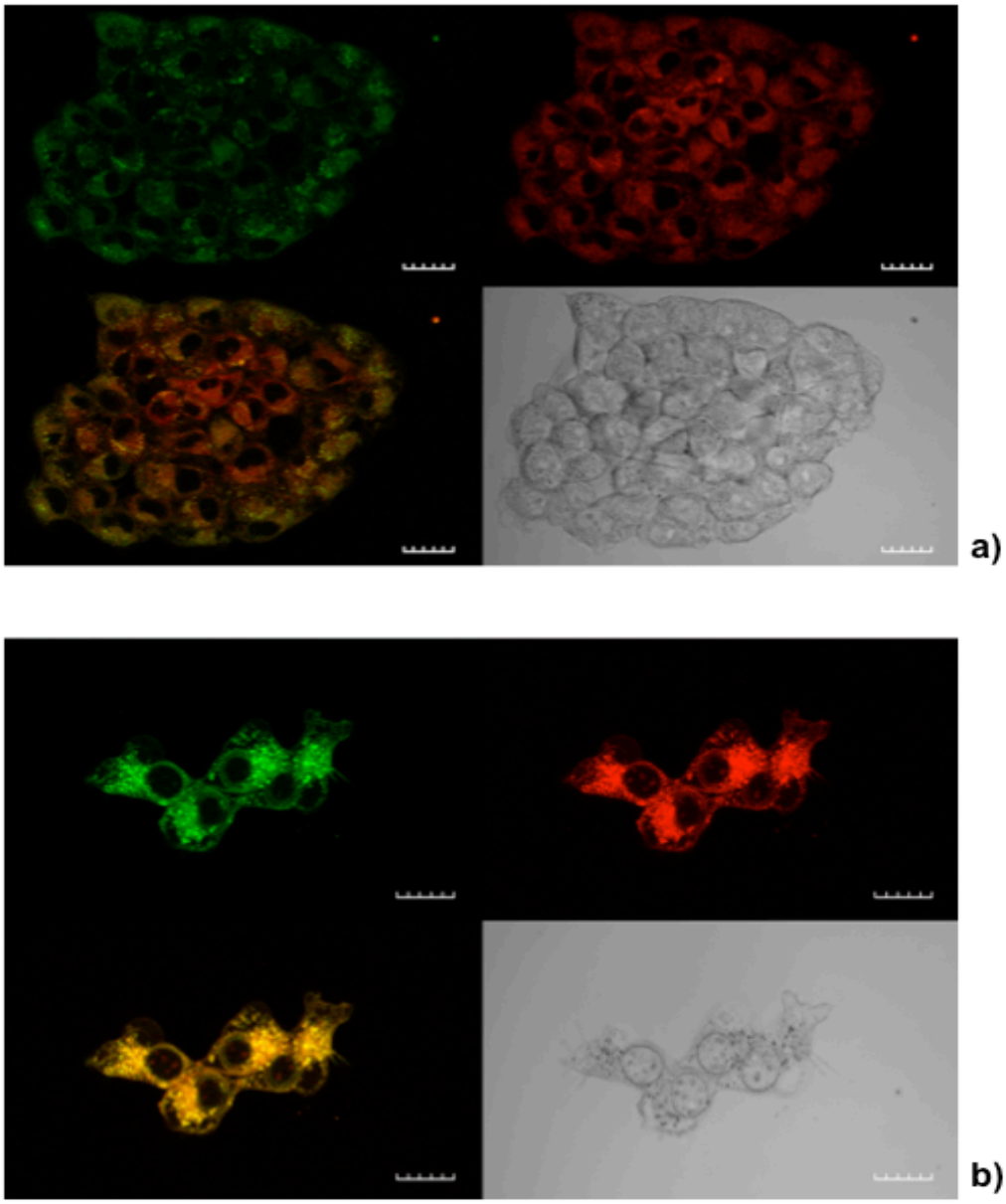

Figure 3.30 – Confocal Microscopy Lipid Peroxidation Studies (Buthionine Sulfoximine or Saporin treated controls).
1 x 10^4 4T1 breast cancer cells were seeded on 35 mm diameter glass-bottomed fluorodishes and grown for 48h. Cells were re-incubated with $TPPS_{2a}$ 0.6 μg ml^{-1} + SAP 30 nM + BSO 1.0 μg ml^{-1} for a further 24h. Cells in were then illuminated for 150 s using the LumiSource® illuminator. Subsequently, Image-IT lipid peroxidation probe was added to the cells to make a final concentration of 10 μM and incubated at 37°C for 30 minutes. Images were then taken using confocal microscope. **(a)** cluster of cells **(b)** dying group of cells. RED = reduced lipid, Ex 581 nm Em 591 nm; GREEN = oxidized lipid, Ex 488 nm Em 510 nm; ORANGE = overlaid image. *60X NA:1.35 Objective Lens, zoom x1.0, scale 20 microns.*

3.15 Antioxidants and Reducing Enzymes

This section reports on investigations looking at the potential impact of antioxidants on PCI. In particular, the effects of superoxide dismutase (SOD) and L-histidine (LH).

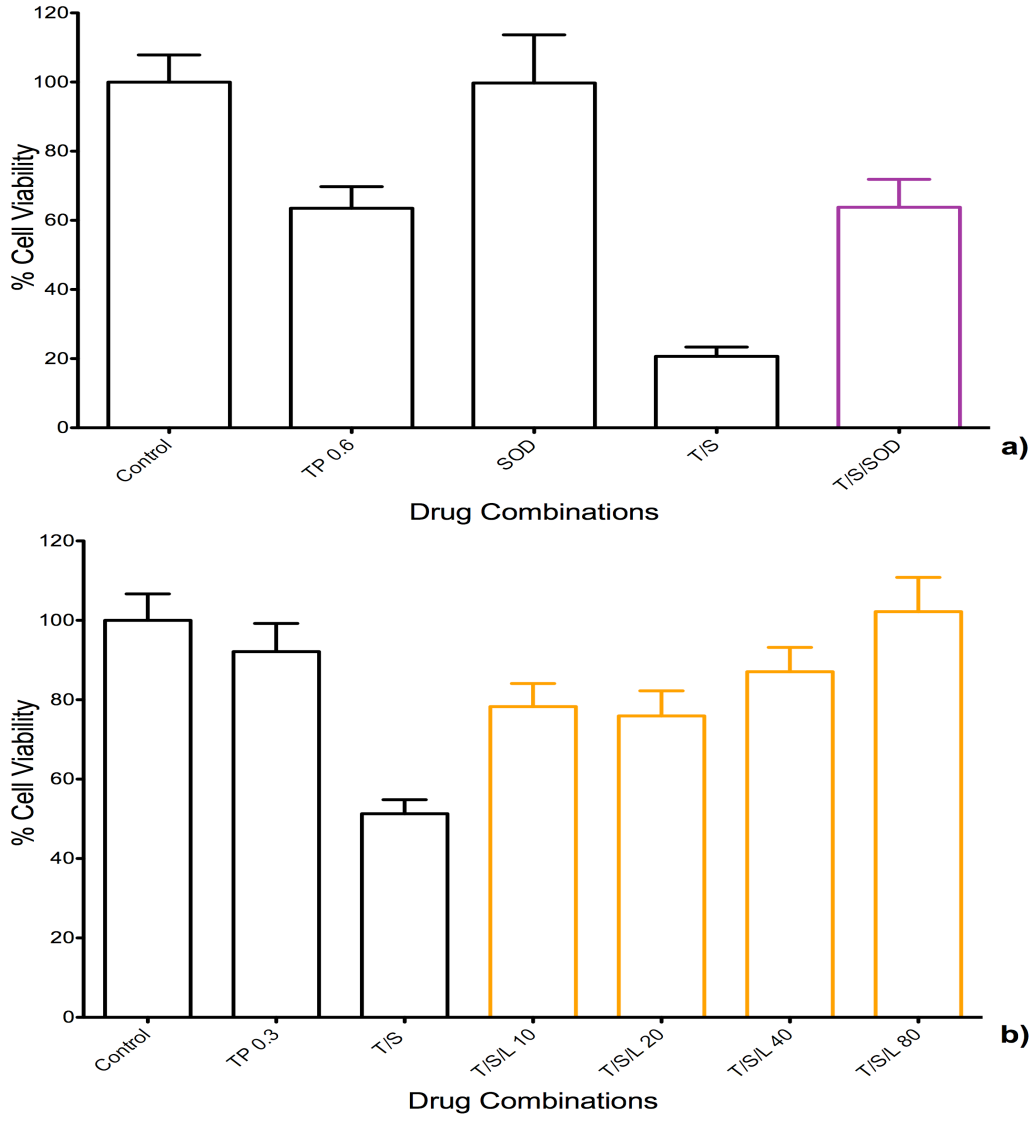

Figure 3.31 – Effect of antioxidants/reducing enzymes (L-histidine and superoxide dismutase) on Photochemical Internalisation of Saporin.
4T1 breast cancer cells treated with **(a)** TP 0.6 µg/ml + SAP 30 nM + light (180 s) +/- SOD 100U, **(b)** TP 0.3 µg/ml + SAP 15 nM + light (90 s) +/- LH (increasing doses up to 80 µM). Cells were illuminated using the LumiSource® illuminator. (a) SOD reduced PCI cytotoxicity by 43% ($p<0.01$). (b) LH 80 µM caused 51% reversal of the PCI effect ($p<0.01$). Cell viability measured using MTT assay 72h after illumination (absorbance read at 490 nm).

Figure 3.31 shows the histograms for TP 0.6 μg/ml + SAP 30 nM + light (180 s) +/- SOD 100U (fig. 3.31a) and TP 0.3 μg/ml + SAP 15 nM + light (90 s) +/- LH (increasing doses, fig. 3.31b).

Figure 3.31a shows that cells that were treated with SOD 100U for 24h pre- and 24 hours post-light experienced a 43% ($p<0.01$) reduction in PCI cytotoxicity. This is equivalent to PDT (TP 0.6 μg/ml) induced cytotoxicity following 180 s of exposure to light, therefore essentially reversing the PCI effect. SOD 100U (alone) had no significant effect on PDT based cytotoxicity.

Figure 3.31b shows, cells that were treated with increasing doses of LH (10-80 μM) for 24h pre- and 24h post-light, there was a dose dependent reduction in PCI induced cytotoxicity. This ranged from 27% ($p<0.01$) reversal for LH (10 μM) to 51% ($p<0.01$) for 80 μM. The latter completely reversed PCI induced cytotoxicity with no statistically significant difference from control. Interestingly no significant reversal effect was seen for PDT + LH even at 80 μM.

DISCUSSION

The ultimate aim of the studies performed in this chapter was to test the null hypothesis that the intracellular REDOX environment has no effect on the efficacy of PCI. The experiments performed were designed to initially determine whether or not $TPPS_{2a}$ based PCI could be used to enhance the delivery and consequently the cytotoxic efficacy of two cytotoxic agents (SAP and MTX). The balance between oxidation and reduction is vital to the normal functioning of a cell and abnormal REDOX states have been shown to confer resistance to cytotoxic agents in cancer chemotherapy(122). The reducing capacity of a cell is determined by the expression of reducing agents/enzymes including glutathione (GSH), glutathione peroxidase ($GSHP_x$), catalase and superoxide dismutase (SOD); relative to the oxidative load. These reducing agents act to prevent the toxic and mutagenic effects of ROS, for example, SOD catalyses the conversion of the reactive $O_2^{\cdot-}$ to $H_2O_2 + O_2$, the former being subsequently detoxified by catalase(123). Many clinical conditions are associated with imbalances with intracellular REDOX tending towards an oxidative state that can result in cell death, for example in the haemolytic anaemia's, such as glucose-6-phosphate dehydrogenase deficiency and pyruvate kinase deficiency. In situations where overwhelming levels of ROS are achieved, including ionizing radiation and cytotoxic anthacycline antibiotics such as doxorubicin, the probability of observing increased DNA damage; lipid peroxidation and protein modification are enhanced(122, 123). Photosensitiser activation results in the formation of ROS including $O_2^{\cdot-}$, $^1O_2$ and $OH^{\cdot}$. These free radical species can be formed by direct reaction between the excited photosensitiser and a substrate (Type I) or (Type II) energy transfer from the excited photosensitiser to ground state molecular oxygen ($^3O_2$) forming $^1O_2$. Both PDT and PCI are believed to favour Type II reactions whereby $^1O_2$ oxidises substrates in close proximity e.g. nucleic acids, enzymes and cell membranes(124). The latter are rich in unsaturated fatty acids, which readily react with $^1O_2$. By investigating the relationship between photosensitiser activation in PCI and the intracellular REDOX environment of a cell a greater understanding of the influence reactive oxygen species (ROS) production had on PDT/PCI was elucidated. PCI represents a developmental step of PDT, retaining its fundamental properties of light,

photosensitiser and oxygen dependent ROS production, but with the effect restricted to subcellular domains(28, 125, 126). In particular, the phospholipid membranes of intracellular vesicles including, endosomes and lysosomes. The most consistent observation in this study is that the factors that theoretically influence the production of ROS, some of which are tested in the current body of work, the photosensitiser, light dose and the chronological point at which the photosensitiser is activated appear to have a correlative effect on the efficacy of PCI.

3.16 PCI

As previously described, the 'light-after' (LA) protocol involved pre-treating cells with photosensitiser (TP) plus chemotherapeutic (SAP or MTX) prior to light exposure. In doing so both the amphiphilic, TP(26, 30), and the chosen chemotherapeutic will be taken up by the cell to assimilate in endosomes, with TP in the membrane and chemotherapeutic within the lumen. Berg et al. (2011)(20) described the endocytic vesicular-membrane localisation of a photosensitiser as 'a prerequisite' for PCI. Thus, activation of the photosensitiser leads to localised ROS production and release of the luminal toxin into the cytosol.

In these experiments, the combination of the photosensitiser and cytotoxin (TP 0.6 μg/ml + SAP 15 nM) (PCI) plus 120 s illumination, resulted in a statistically significant increase in cytotoxicity, 24h after light exposure, whereby PCI enhanced the PDT effect by a factor of 1.5 ($p<0.01$) and the chemotherapeutic effect by a factor of 12.5 ($p<0.01$) (fig. 3.5). These observations support those of Berg et al. (2011)(20) who reported a significant increase in the cytotoxicity of SAP for cells treated with SAP + $TPCS_{2a}$ + light (PCI), compared to SAP +/- light. This indicates that the combination of photosensitiser + chemotherapeutic enhances the cytotoxicity of the chosen photosensitiser. The 12.5-fold increase in cytotoxicity for TP + SAP + light (PCI) compared to SAP + light also supports the school of thought that despite lacking a B-chain lectin-based binding domain that Type I RIPs such as SAP retain potency in their enzymatically active A-chain

that is comparable to the Type II RIPs once they are delivered to the cytosol, as described in the Scientific Background section of this chapter(97, 103, 105). It is for this reason that SAP was the 1st-choice candidate for the experiments carried out in this chapter. Another important point of comparison is the relatively low level of cytotoxicity achieved by PDT alone (fig. 3.5), with less than 1 in 4 cells killed. As will be discussed further in this chapter this low level of direct ROS-induced death is very important for PCI, particularly when delivering non-stable compounds, such as siRNA.

MTX was studied using the same LA protocol for PCI (MTX 0.4 μg/ml + light +/- TP). The dose of MTX chosen for experimentation was partly based on previously published data(25) and pilot experiments (data not shown). In comparison to SAP 15 nM, MTX 0.4 μg/ml alone exerted a significant level of cytotoxicity (53%, $p<0.01$). In this instance the addition of TP + light (PCI) yielded no significant additional cytotoxicity 24h after illumination. One potential explanation for the apparent lack of effect is that the basic chemical composition of MTX facilitates its accumulation and ion-trapping within acidic compartments such as endosomes and lysosomes. Lee and Tannock (2004)(115) reported in an abstract that by raising the pH of endosomes with agents including the antibiotic chloroquine and the proton-pump inhibitor omeprazole, they were able to enhance the penetration of MTX using a multi-cell layer technique. Given that a basic compound will be protonated in an acidic environment a possible hypothesis is that unless the level of ROS generated within the endo-lysosomal membranes is sufficient, the severity of damage achieved will not permit the escape of hydrophilic (protonated) molecules though the phospholipid bilayer. Hence, the reduced potency of MTX-PCI under the conditions used.

3.17 Redistribution studies for SAP-488 and mitoxantrone

The importance of ROS production as a rate-limiting step in PCI is supported by the lack of cell toxicity in non-illuminated ('Dark controls') and this has been described in previous *in vitro* and *in vivo* studies: Selbo *et al.*(29) evaluated the therapeutic potential of photochemical internalisation of gelonin (type I

ribosome inactivating protein) using the photosensitiser aluminum phthalocyanine disulfonate ($AlPcS_{2a}$) for the treatment of human adenocarcinoma (WiDr) in athymic female BALB/c nude mice. They observed that WiDr cells from tumours exposed to 15 min of light exposure *in vivo* had diffuse perinuclear fluorescence of $AlPcS_{2a}$ compared to granular fluorescence in 'light-protected' (dark control) cells. The granular pattern of fluorescence was hypothesized to be indicative of lysosomal uptake of the amphiphilic $AlPcS_{2a}$. Given the light-dose dependent manner of $AlPcS_{2a}$ re-localisation, in addition to the synergistic cytotoxic effect of gelonin plus $AlPcS_{2a}$, the authors concluded that this effect is consistent with PCI(43). Thus, it is the release of endocytosed molecules and subsequent redistribution within the cytosol that enables the therapeutic effect. The dynamics and photobleaching characteristics of $AlPcS_{2a}$ have been shown to be dependent on an aerobic environment(127), which further supports the importance of ROS production via type II reactions in PCI. The confocal study (figure 3.23), presents evidence supporting the redistribution of SAP-488, in PCI treated cells. Preliminary experiments performed using the SAP-488, demonstrated that despite achieving a stable construct, only a weak signal was detectable at lower doses (30 nM), consequently, a higher dose of SAP-488 was chosen. Interestingly, there was very little effect on cell viability, which supports pilot dose-response data using SAP. Furthermore, in order to minimise any photobleaching effects, only two slices were taken for each image. These were subsequently converted into z-stacks for comparison. The control experiment (figure 3.22) demonstrated there was only a 3% reduction in signal, 240 seconds after application of the laser. By comparison, there was a 30% reduction in the signal for cells treated with SAP-488 + $TPPS_{2a}$ (fig. 3.23), 240 seconds after application of the laser. This represented a 9-fold decrease in signal intensity for PCI compared to cytotoxin alone. The loss of signal intensity was most likely due to release of SAP-488 from endosomal stores into the cytoplasm leading to its spread and concurrent drop in signal intensity. The likely endosomal sequestration of SAP-488 is supported by work performed by Bolognesi et al. (2012)(109) using confocal-based indirect immunofluorescence analysis to detect the intracellular trafficking of labeled-SAP. They reported just below 1 in 3 SAP molecules end up in

endosomes. This coupled with the amphiphilic nature of TP and the imaging observations (fig. 3.2) supports the hypothesis that PCI induces the release of SAP from endosomal stores in to the cytoplasm.

The inherent fluorescent signal of MTX is of benefit with regards to mapping out its intracellular localisation in cells. Figure 3.24 illustrates the intracellular localisation of TP-MTX pre- (fig. 3.24a) and post (fig. 3.24b) exposure to the 405 nm laser (15s). A longer laser exposure time was selected, compared to SAP-488, following preliminary experiments that demonstrated that MTX re-localisation required a longer exposure. The post exposure image (Fig 3.24b) clearly demonstrated a loss of the granular pattern, which was present prior to exposure (fig. 3.24a), to a more diffuse, membranous localisation with evidence of nuclear uptake, which is the site of action for MTX. The granular pattern of distribution pre-laser is likely to represent endo-lysosomal storage, supported by the evidence of co-localisation seen with lysotracker (fig. 3.24c). These findings are consistent with previously published data regarding MTX uptake into lysosomes and subsequent nuclear mobilisation following PCI treatment using hypericin as a photosensitiser(25). In 4T1 cells treated with MTX alone, there was no redistribution following treatment with the 405 nm laser (data not shown). This, as with the SAP-488 data above, indicated that the change in the signal of both compounds was less likely to be due to any direct effects or photobleaching.

The data from the 'light after' study along with the confocal imaging support the rejection of the null hypothesis that TP - mediated PCI does not enhance the delivery and consequently the efficacy of SAP as a cytotoxin in 4T1 cells. However, under the chosen experimental conditions the null hypothesis cannot be rejected for TP-mediated MTX-PCI in 4T1 cells.

3.18 Variable 1: Photosensitiser Dose

As described in the results section, in order to reach an excited state a photosensitiser must absorb a photon of light of the appropriate wavelength. A proposed mechanism is that activation of the photosensitiser generates ROS,

damaging endosomes and liberating the endocytosed cytotoxin, thus enhancing delivery to the intracellular compartment. This is based on the understanding that the ground state photosensitiser (PS), prior to exposure to light, can exert a cytotoxic effect in dose dependent(25, 128) and cell-specific manner; an effect often referred to as 'dark' cytotoxicity. Following absorption of a photon of light the PS can be excited to a number of higher-energy states(129). Ultimately, the excited photosensitiser may go on to chemically alter a substrate in a time and proximity dependent manner. The formation of reactive oxygen species (ROS) may occur following the donation of an electron to a substrate (type I); resulting in the oxidation of the photosensitiser. Alternatively ROS, more specifically $^1O_2$, formation may be secondary to direct transfer of energy from the excited photosensitiser to ground state molecular oxygen, resulting in the preservation of ground-state photosensitiser (type II) (fig. 3.32). The efficiency of this process is often dependent on the rate of decay for the excited photosensitiser, the availability of oxygen and the reducing capacity of the local environment. Consequently, oxygen rich environments will support a type II mediated process, which is associated with increased decay of the more stable triplet state. Whereas, oxygen depleted environments will encourage a type I mediated process with formation of other reactive species, including superoxide and hydroxyl free radicals, associated with reduced decay of the triplet state. Therefore the availability of substrate (TP) may play an important role in overall efficacy of photoactivation.

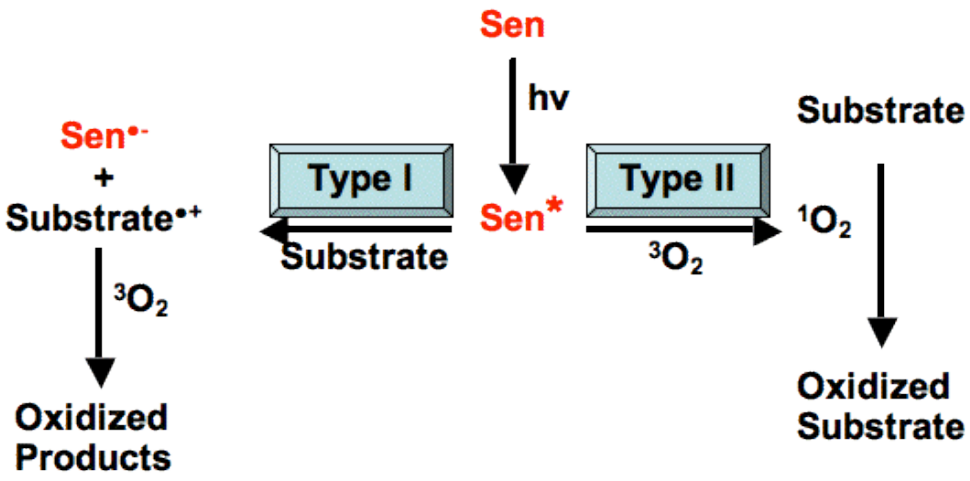

Figure 3.32 – The development of reactive oxygen species.
Type I versus Type II reactions (129).

This section of the study was carried out in order to test the null hypothesis that photosensitiser dosing does not have a significant effect on the efficacy of TP - mediated PCI of SAP and/or MTX.

The results showed that doubling the dose of photosensitiser from 0.3 μg/ml to 0.6 μg/ml does not result in a proportionate rise in PDT or PCI efficacy i.e. these are not doubled (fig. 3.7). This dosing range was chosen as pilot experiments showed that at 0.8 μg/ml the PDT effect of TP, for the light doses and experimental conditions employed, produced an inappropriately high level of PDT killing reducing the power for comparative analysis. As the results showed, PDT cytotoxicity (0.6 μg/ml) was increased to 18%, representing a 12% ($p<0.001$) increase compared to 0.3 μg/ml. In comparison, an 8% rise in PCI cytotoxicity (using SAP 15 nM) was observed over the same dosing range. The increased cytotoxicity observed for PDT and PCI of SAP is consistent with previously published work by Selbo et al. (2006)(120). Throughout these studies, a constant aim was to ensure that PDT based toxicity was kept to a minimum. The two effects (PDT and PCI) are on a spectrum and if the PDT effect is too great there would be an increased risk of damaging the molecule that is being internalised. Thus the relatively small, albeit statistically significant, rise in both PDT and PCI cytotoxicity in this instance may not justify the doubling of photosensitiser dose with the increased potential for unwanted side effects.

For MTX there was no significant difference in 'PCI' cytotoxicity between 0.3 μg/ml and 0.6 μg/ml (TP).

Taken together these results indicate that when the illumination time is constant, a significant increase in concentration of photosensitiser does not produce a proportionate rise in PDT or PCI cytotoxicity. This is not to discount the fact that there was a statistically significant increase in cytotoxicity, which is in keeping with the reported results from other groups(120). However, the relatively small increase suggests that the rate and/or total amount of ROS

produced upon activation of a photosensitiser is only partially limited by the concentration of photosensitiser available.

3.19 Variable 2: Light Dose

The light dose studies were performed in order to gain a better understanding of what impact increasing duration (dose) of illumination would have on PDT and PCI. Light is an absolute requirement for photoactivation and this school of thought is supported by the significant decrease in cytotoxicity that was observed in this (fig. 3.8) and previous studies on 'dark cytotoxicity'(25). Figure 3.8 illustrates the impact of increasing illumination time from 60-300 seconds for PDT (TP) and PCI (TP + SAP); in addition to non-illuminated 'dark' controls. There was no significant 'dark' cytotoxicity for PDT. PCI did exhibit 12% cell kill compared to control; however, when this is compared to the residual toxicity of SAP 30 nM no difference was observed. This indicates that the 'dark' toxicity observed for PCI is most likely due to the effect of SAP. Thus, when comparing to other illumination times one can be confident that the any difference is at least in part related to the activation of the photosensitiser.

For SAP-PCI a light dose-dependent increase in cytotoxicity was observed from 'dark' control to a peak level of cytotoxicity at 300 s when a 6-fold increase is achieved compared to 'dark' controls (fig. 3.8). A similar trend, albeit of significantly reduced magnitude was observed for PDT, with peak cytotoxicity at 300 seconds (26%), which represented a 12-fold increase. Throughout all light doses, the level of cell kill achieved for PCI was significantly greater than for PDT. The mean increase was 34%, with the smallest difference at 60 s (12%) and the greatest difference at 240 s (53%). Close analysis of the two sets of data showed that the stepwise rise in cytotoxicity tended to increase for PDT as illumination time prolonged, with the largest difference occurring between 240 s and 300 s (10%). Conversely, for PCI the largest difference occurred between 60 s and 90 s (22%) with a general trend of reducing difference as illumination time increased. Selbo et al. (2006)(120) observed similar results for PCI/PDT using the type I RIP gelonin + $TPPS_{2a}$ in a human multidrug-resistant (MDR) uterine cancer cell line (MES-SA/Dx5) with incremental light doses. A potential

hypothesis for the differing trends is that at lower light doses/reduced energy levels, the comparatively modest level of ROS production is sufficient to damage endo-lysosomal vesicles, resulting in the release of SAP and a consequent rate-limiting rise in cytotoxicity; for PDT however, this level of ROS production is insufficient to kill the cell via direct phototoxicity. Conversely, at high light doses/energy levels, the likelihood that further SAP release will take place and exert a cytotoxic effect above and beyond that of PDT is less likely. This may go some way to explaining why the differential between PDT and PCI reduces at 300 s compared to 240 seconds.

Although the overall trend for MTX-PCI was loosely similar to that for SAP-PCI, with the highest level of cell kill occurring after 300 s of light exposure (fig. 3.9), the dose-dependent effect only occurred for light durations that were greater than 180 s. This is illustrated by the following:

- Between 60 s-180 s, there was no significant (statistical) increase in cytotoxicity.
- At 180 s, MTX-PCI toxicity was no different to 'dark' cytotoxicity.
- The only significant rise occurred between 180 s-300 s when a 30% rise in cytotoxicity was observed ($p<0.01$).

Thus for MTX-PCI the light dose progressively became a more important factor as it increased. Furthermore, a closer look at the differential between PDT and MTX-PCI, with increasing light dose, reveals that the gap between PDT and PCI induced cytotoxicity widened with increasing light dose. At 60 s illumination the differential was 22% in favour of PCI; there was a minimal rise to 25% at 150 s and a peak differential of 40% at 300 s. Given that the light dose-dependent effect only occurred after 180 s, this illumination time may represent the true start point for MTX-PCI as prior to this it is likely that the cytotoxicity observed was due to the inherent cytotoxicity of MTX 1.5 μg/ml. This would suggest that MTX-PCI requires a greater load of ROS production compared to SAP-PCI. A possible explanation is that given MTX is a weak base, therefore charged in the acidic environment of endosomes and lysosomes(115). In this charged state, the endo-lysosomal membranes will provide both a physical and electrostatic

barrier to MTX release. Consequently, whereas 'minor' membrane damage may be sufficient for SAP release, a greater level of damage is required in order for MTX to overcome the physical and electrostatic resistance to its release. This is further supported by the fact that the PDT:MTX-PCI differential continued increase; hence, it is unlikely that the augmented cytotoxicity was due to PDT.

Light dose appears to play a pivotal role in both PDT and PCI. However, under the conditions chosen for the study described here, in particular the 4h 'chasing' period prior to illumination, there is a disproportionate favoring of PCI cytotoxicity compared to PDT for both SAP- and MTX-PCI.

3.20 Variable 3: Photosensitiser localisation

The biochemical properties of a photosensitiser play a significant role in determining its suitability for PCI. Any photosensitiser that is taken up and retained by a cell can potentially exert photodynamic therapy (PDT) based cytotoxicity via site non-specific generation of ROS. For example, the dye tetrabromorhodamine-123 selectively localises to mitochondria(130), thus upon photoactivation, ROS-generation would be restricted to this intracellular compartment. Hypericin on the other hand is retained within endolysosomes (25)and mitochondria(131); the former making it a good candidate for PCI. Though it is important to note that although hypericin starts in the endolysosomes it can migrate to other organelles, hence a shorter incubation time is beneficial for hypericin-mediated PCI. Newer photosensitisers have been designed to accumulate within the phospholipid bilayer of the cell membrane. Thus when compounds are taken up by endocytosis the resultant endosomes contain photosensitiser within their membrane. Examples of such photosensitisers include $TPPS_{2a}$(26, 120) and $TPCS_{2a}$(20). The latter has been specifically designed for use as a potential therapeutic for clinical application for PCI-based treatment in humans.

The consistent property of general photosensitisers and those optimized for PCI is the generation of ROS; for example $TPPS_{2a}$, has an amphiphilic nature that enables it to reside in both the cell membrane and endo-lysosomal

compartments. Consequently, it can potentially act as both a PDT (cell membrane) and/or PCI (endolysosomal membranes) agent.

The location of the photosensitiser at the point of illumination plays a determinant role in PDT and PCI cytotoxicity. The null hypothesis is that the relative localisation of the photosensitiser at time of illumination has no bearing on the likelihood of achieving PDT versus PCI. It is important to consider this, as one potential application of PCI is to facilitate the intracellular delivery of non-toxic therapeutics such as siRNA. In such instances, it would be beneficial to limit the proportion of ROS contributing to PDT compared to PCI.

The two illumination protocols utilised were chosen as a means to compare the relationships between PDT and PCI cytotoxicity when cells are illuminated either 'immediately' following the washing off of drugs (after a 24 hour incubation period) or following a further '4h' incubation period in drug-free media. This delay has previously been described as a 'chase' period(120). The concept is based on the theory that after a period of incubation with an amphiphilic photosensitiser such as $TPPS_{2a}$ there will be indiscriminate accumulation in lipid bi-layers such as the cell membrane. By washing off the drug and re-incubating cells in drug-free media a concentration gradient is set up either side of the cell membrane enabling the diffusion of photosensitiser into the media and also accumulation within intracellular vesicular membranes. The former leads to a reduction in total photosensitiser load. Such an effect has previously been reported in 2006(120) when $TPPS_{2a}$ fluorescence was measured in lysed cellular material that had undergone a 4h 'chase' protocol versus immediately after incubation. Consequently, the total level and location of ROS production may be significantly different between the two protocols. This is evident in the observations made during this study whereby for cells that were illuminated immediately after 24h incubation, there is no difference in cytotoxicity for PDT or SAP-PCI for illumination times ≥ 180 s (fig 3.10c). Using the 'immediate' protocol, the greatest differential of PCI versus PDT was a 2.7-fold (42%, $p<0.01$) increased cytotoxicity, which was observed in cells treated with 60 s of illumination. In fact, between 60 s-90 s illumination the average PCI-

induced increase in cytotoxicity, compared to PDT, was 36%; between 120 s-150 s this reduced to 11%; between 180 s-300 s there was no difference (0.3%). This indicated that when the photosensitiser load was relatively high, immediately after incubation for example, the time to illumination is a major factor in determining PDT versus PCI induced cytotoxicity. Thus with shorter illumination times the total level of ROS production is insufficient to cause enough global cellular damage to induce >40% cytotoxicity. However, this is sufficient to trigger release of SAP, therefore mediate PCI-induced killing. As the illumination time increases the level of ROS production significantly increases to facilitate PDT induced killing, hence for light durations ≥180 s almost all the cytotoxicity can be attributed to PDT. The limited sensitivity of the MTT assay for cytotoxicity above 90% makes it very difficult to see any true difference. This in comparison to the 4h protocol where, as discussed in the light dose section above, as illumination time increased the difference between PDT and PCI induced cytotoxicity was divergent in favour of PCI with the largest differential of 53% is observed at 240 s (fig. 3.10d).

A very similar trend was observed for MTX-PCI versus PDT for the 'immediate' protocol whereby between 60 s-90 s there was a 30% increase in cytotoxicity for PCI; 120 s-150 s (8%); 180 s-300 s there was a 1.3% reduction in PCI cytotoxicity compared to PDT, though this is unlikely to represent any significant difference (fig. 3.11a).

The effect of photosensitiser localisation on PDT is reinforced when 'immediate' versus 4h protocols are compared (fig. 3.10a). The pattern of cytotoxicity suggests that 'immediate' - PDT (for illumination times between 60 s-300 s) is consistently more potent than the 4h protocol. A significant step for increased effect appears to take place between 90 s-120 s (immediate group) when a 33% increase occurs. This may represent the point at which a critical level of ROS production occurs. In comparison, there is no true difference in cytotoxicity, for the 4h group, between 90 s-120 s. In fact, comparison of the total increase in cytotoxicity between 60 s-300 s reveals a significant difference with a 71% increase for the 'immediate' group versus a 29% increase for the 4h group. This

represents a 2.8-fold ('immediate') versus 1.9-fold (4h) increase across the illumination times.

The differential for SAP-PCI (fig 3.10b) and MTX-PCI (fig. 3.11c) 'immediate' versus 4h shows a different light-dose trend to PDT in that despite the immediate group achieving greater cell kill at each time point, the two groups converge as illumination time increased with the major step occurring between 150 s-240 s for both SAP-PCI and MTX-PCI (4h group). As discussed above, from 180 s onwards the cytotoxicity observed was almost all down to PDT. Thus, the convergence is likely due to the increased proportion of PCI induced cytotoxicity occurring in the 4h group. This would indicate that the 4h protocol is superior when aiming to achieve the greatest PCI effect. In terms of photosensitiser localisation, this suggests that the 'chase' period facilitates the accumulation of photosensitiser in endo-lysosomal membranes in synchrony with the loss of photosensitiser from the cell membrane. Thus upon activation of the photosensitiser the localised ROS generation favours endo-lysosomal disruption while preserving overall cell integrity. Consequently, the cytotoxicity observed is likely to be due to the mechanistic effects of SAP (RIP) or MTX (topoisomerase inhibitor). Therefore, from these results it is possible to conclude that photosensitiser location at the time of activation is a determining factor for PDT versus PCI cytotoxicity.

3.21 Variable 4: Intracellular REDOX Environment

This section of the study aimed to test the null hypothesis that the intracellular REDOX environment has no effect on the efficacy of PCI. As described earlier in the discussion REDOX homeostasis is vital for normal cellular function and is believed to play an important role in the ageing process. Sandana et al. (132) performed studies to further understand the role of oxidation resistance-1 (OXR1) gene in humans using a homolog LMD-3 which is found in the nematode *Caenorhabditis elegans* (*C. elegans*). The group concluded that in conjunction with mitochondrial superoxide dismutase, LMD-3 contributes to regulating oxidative damage and ageing in the C. elegans nematode.

Buthionine sulfoximine (BSO) is an irreversible inhibitor of γ-glutamylcysteine synthase that causes depletion of GSH in tumours and normal tissues. Thanislass et al. (133) have demonstrated that sustained treatment (several days) using BSO in male rats resulted in chronic suppression of GSH levels, which was associated with an overall reduction in antioxidant defenses owing to diminishing activity of catalase, superoxide dismutase, and glutathione peroxidase among other scavengers of ROS. In this chapter, monochlorobimane (mBCl) was chosen as a fluorescent probe for intracellular glutathione levels. However, it is important to state that mBCl will emit a fluorescent signal when conjugated to a range of thiols including N-acetylcysteine and mercaptopurine; the glutathione conjugate of mBCl has a specific absorption/emission maxima ~394/490 nm, which was used in this chapter. The 4-fold reduction in the mBCl signal for 4T1 cells treated with BSO (24h) versus untreated (fig. 3.24) supports the findings of Thanislass et al.

BSO appeared to have very little if any effect on PDT using the immediate illumination protocol, with the only true difference being observed at 60 seconds illumination. However, following the 4h 'chase' period BSO, significantly, enhanced PDT for illumination durations ≥150 s. This is highlighted by the following observations whereby between 60 s-90 s there was no difference in cytotoxicity between PDT versus PDT+BSO; 120 s-150 s the mean increase effect of BSO on PDT cytotoxicity was 16%; 180 s-300 s was 57% with the largest increase of 61% occurring at 240 s (fig. 3.12b). The maximum level of cell kill was 92% ($p<0.001$) compared to control. This is comparable to the cytotoxicity achieved using the 'immediate' protocol for both PDT and PDT+BSO (fig. 3.12a; fig 3.13a). Another important point of note is the relative impact of BSO on PDT (4h group) at longer illumination times compared to shorter time. At longer illumination times BSO appears to have a greater effect on 4h-delayed PDT compared to 'immediate', hence the narrowing gap in the difference between their means as the light-dose increased. However, it is important to acknowledge that this is likely to be confounded by the fact that 'immediate' protocol PDT/PDT+BSO kills almost all the cells at lower light doses. Nevertheless, under the conditions within this set of experiments PDT+BSO

produces greater cytotoxicity at illumination durations >150 s than SAP-PCI/MTX-PCI. However at lower light doses 60 s-150 s, SAP-PCI has a mean increase in cytotoxicity of 24% compared to PDT+BSO. This indicates that for PDT (4h protocol), by impairing the ability of the cell to cope with increased oxidative stress exerted following the activation of a photosensitiser it is possible to achieve sufficient levels of ROS production to induce cytotoxicity that is comparable to 'immediate' protocol PDT+/-BSO. However, for the dose of BSO used (1.0 μg/ml) in this study the effect is only apparent at higher light doses, which is in keeping with the rate-limiting effect that light-dose has on PDT. The overall enhancing effect of BSO on PDT is supported by findings in work performed by Jiang et al. (2003)(134) using BSO to enhance Photofrin PDT in glioma cells *in vitro* and glioma tumours *in vivo* (Fisher Rats).

Unlike for 'immediate' PDT, BSO appeared to have significantly enhanced effect on 'immediate' SAP-PCI cytotoxicity however only at light durations ≤90 s (fig. 3.14a). This suggests that at the lower light doses the attenuated reducing capacity of the intracellular environment does have a significant effect on ROS production/survival time, consequently enabling a greater degree of endo-lysosomal disruption and release of SAP. However, this conclusion is confounded by the residual 'dark' cytotoxicity seen (12%, data not shown) for SAP-PCI+BSO. Thus at present there is not enough evidence to conclude that BSO enhances 'immediate' protocol SAP-PCI. The same can be said of MTX-PCI + BSO ('immediate' group) where no significant increase in cytotoxicity is observed. Both sets of results may be affected by the sensitivity of the MTT assay to delineate relatively small differences in cell viability accurately. It is likely that a greater sample size or alternative viability assays would be required in order to improve the power of this part of the study.

The effect of BSO on the 4h protocol was significantly more positive when compared to the 'immediate' protocol. The mean increase in cytotoxicity for cells treated with SAP-PCI + BSO was 17% across all light doses. The greatest effect observed was between 150 s-180 s with a 23% increase in cytotoxicity. This represented a 0.4-fold increase compared to SAP-PCI alone. BSO had a

comparable effect at lower light doses (60 s-120 s) when a 0.5-fold increase in cytotoxicity was observed. An important point to consider is the effect of BSO on the contribution of PDT induced cytotoxicity to PCI; the question being whether or not the enhanced PCI effect is in fact due to an enhancement of PDT. For illumination times ≤150 s PCI + BSO induced cytotoxicity was significantly greater (statistically) than for PDT + BSO. The mean increase in cell kill for (PCI + BSO) versus (PDT + BSO) between 60 s-90 s was 43% (3.6-fold) and 120 s-150 s (32%, 1-fold). However, between 180 s-300 s the mean increase dropped to 7.3% ($p>0.05$), which represented a 0.1-fold increase. This indicates that as light dose increases BSO acts to significantly increase ROS production and survival which given the increasing activation of photosensitiser tips the scales in favour of PDT. However, importantly at lower light doses BSO has a greater effect on ROS production favouring PCI compared to PDT. PCI appeared to have the greater effect.

The effect of BSO on MTX-PCI appeared to be misleading. Although comparison between MTX-PCI versus MTX-PCI + BSO showed that statistically significant increases in cytotoxicity are only achieved at illumination times ≥180 s (fig. 3.16b). However, when PDT + BSO was compared to MTX-PCI + BSO, it became apparent that at illumination times ≥180 s there was no difference in cytotoxicity between the two treatment groups (fig. 3.16d). Thus, the increased effect is most likely due to the enhancement of PDT and not PCI. Another possible explanation is that the cytotoxic effects of mitoxantrone have been shown, in part, to be mediated by toxic metabolites formed via oxidation in by P450-dependent mixed function oxidase (MFO) system(135). Therefore, the increased level of ROS produced under the conditions of suppressed glutathione levels may lead to modification of MTX, rendering it less toxic. Given MTX has been shown to be an effective candidate for PCI using hypericin as a photosensitiser(25), the results of this study may indicate that the choice of photosensitiser, beyond preference for amphiphilic structure, is of significant importance when considering PCI. If for example the structure of a photosensitiser brings ROS generation closer to the lumen of the endosome

containing the internalised agent (MTX) then the likelihood of ROS-mediated damage is increased.

Overall, these results indicated that using the 4h protocol, BSO effectively reduced the dose of light required to achieve a particular level of cytotoxicity. For example, at 180 s SAP-PCI + BSO achieved 15% ($p<0.05$) and 13% ($p<0.05$) increase cytotoxicity compared to SAP-PCI at 240 s and 300 s respectively. However, MTX-PCI does not appear to be enhanced under the conditions utilised during the study. Thus, in the case of SAP, the addition of BSO creates an intracellular REDOX environment that facilitates the generation of sufficient ROS to enhance SAP release at a scale beyond that achieved with up to 120 seconds additional illumination. In this way, BSO enhances SAP-PCI. Drawing such a conclusion highlights an important role of GSH in regulating the rate of production and survival time of ROS generated following the activation of a photosensitiser. Consequently, GSH levels within a cell are likely to have a significant impact on the success of both PDT and PCI; however, owing to the reduced levels of ROS production in PCI this effect will likely be greater in the latter. Thus, GSH modulation may be an important consideration when developing PCI protocols.

3.22 Variable 5: Illumination 'before' versus 'after' cytotoxin treatment.

The 'classical' PCI model involves pre-treating cells with an appropriate photosensitiser prior to exposing them to light of a specific wavelength(26). Using this protocol, endosomes containing the internalized compound in the lumen and photosensitiser in the membrane will release the luminal

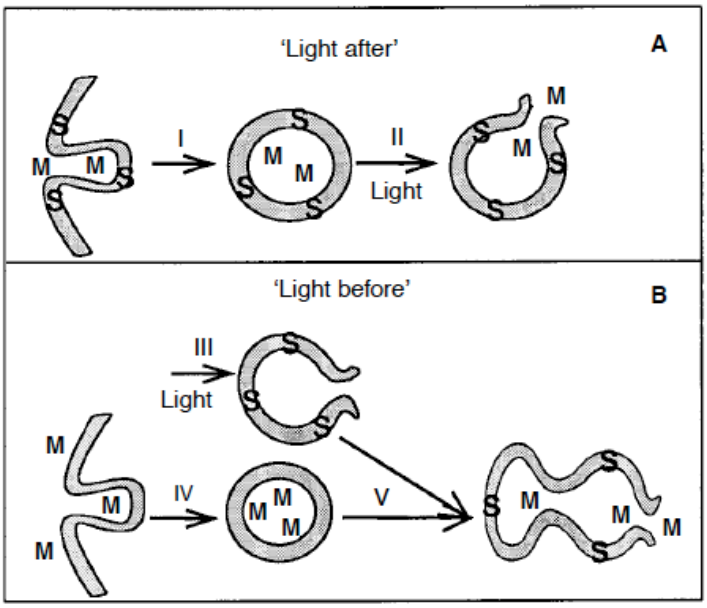

Figure 3.33 – Diagrammatic representation of light 'after' versus light 'before' PCI protocols.
Prasmickaite et al. (2002)(34)

compound following activation of the photosensitiser (fig. 3.33A). An alternative regimen has been reported by Prasmickaite et al. (2002)(34) whereby cells are pre-treated with photosensitiser and then exposed to light treatment. Subsequently they are treated with the compound to be internalised. The school of thought for the 'light before' regimen that preformed vesicles (no drug within the lumen) will contain photosensitiser in the membranes which once activated will causes ROS-induced damage, including lipid peroxidation. The compound to be internalised is given afterwards, thus the new endosomes formed will likely be of normal structure. However, these may subsequently come in to contact with pre-damaged vesicular membranes containing reactive lipid peroxides +/- aldehydes that can damage the endosomal membranes, leading to the release of the internalised drug. In doing so, the light before regimen may provide a second mechanism for PCI.

This study, the light 'before' cytotoxin protocol was used for both SAP- and MTX-PCI using two doses of $TPPS_{2a}$ (0.3 and 0.6 µg/ml). The results indicated that when the illumination time was fixed at 120 seconds, doubling the dose of photosensitiser had a disproportionate effect on the light 'before' regimen compared to the light 'after' for SAP (15 nM)-PCI. When the photosensitiser dose

was doubled the differential between light 'before' and light 'after' regimens reduced from 20% ($p<0.01$) to 8% ($p<0.05$). This represented a 24-fold increase in LB SAP-PCI compared to a 0.2-fold increase in LA SAP-PCI. BSO had a significant enhancing effect on the LB SAP-PCI ($TPPS_{2a}$ 0.3 μg/ml), however almost all of the effect is likely to be explained by the enhanced PDT effect (fig. 3.17).

Using the LB protocol, an interesting observation was made for MTX (0.4 μg/ml). There appeared to be a significant reduction in residual cytotoxicity (35%), which is likely to be due to the increased cell density and consequent reduction in doubling time, hence MTX has less access to replicating DNA and therefore a reduced therapeutic effect (fig. 3.18b). This resulted in a significantly improved LB PCI effect of 23% ($p<0.01$) improved cytotoxicity compared to LA PCI (no increase). This is in keeping with the results reported by Prasmickaite et al. (2002)(34) who found that the light 'before delivery' protocol using Aluminium Phthalocyanine ($AlPcS_{2a}$) "exhibited much stronger toxicity" compared to light after. Whilst it is correct to observe, in this study that the greatest cytotoxic effect was achieved using LA MTX-PCI, the differential change was far greater for the LB group compared to the LA group. There was no increase in cytotoxicity upon addition of BSO for both SAP-PCI and MTX-PCI for the LB protocol. Interestingly there was no increase for PDT+BSO compared to PDT alone (fig. 3.18). Based on the findings of this section of the study it would appear that the light 'before' regimen does enhance drug delivery, which under conditions of increased photosensitiser dose appears to be comparable to the light after protocol. These observations are further supported by Prasmickaite et al. (2002)(34) who report from their studies that both the light 'before' and light 'after' strategies enhanced "*in vitro* transfection with reporter genes delivered by non-viral and adenoviral vectors" by more than 10- and six-fold, respectively. A possible explanation for this proposed mechanism can be found when looking at the propagation phase of lipid peroxidation(82) as described in the introduction to this chapter, whereby formed lipid peroxide radicals such as LOO• and LO• (as a result of photosensitiser activation pre-cytotoxin treatment) may react with PUFA within newly formed endosomes containing drug. If the

burden of lipid peroxides is sufficient, this will cause sufficient damage for drug release from the lumen of the endosomes. Lipid peroxidation appears to be a consequence of photosensitiser activation when the relative level of lipid peroxide compared to non-oxidised lipid within the cytoplasm increases by 60%. BSO has a significant effect on intracellular lipid peroxidation, even in the absence of light and photosensitiser (fig. 3.29a). This indicates that impairing the reducing capacity of the intracellular compartment alone can increase the level of lipid peroxidation. However, in the results obtained in cytotoxicity studies, BSO alone did not increase cell kill significantly compared to control. The same can be said of BSO + SAP compared to SAP alone. The mean signal intensities (green/peroxide) for cells treated with BSO or BSO + SAP are significantly reduced compared to cells treated with $TPPS_{2a}$ + light or $TPPS_{2a}$ + BSO + light. Taken together with the increased level of cytotoxicity observed for the latter groups, this indicates that the level of lipid peroxidation achieved in the absence of photosensitiser activation may not be sufficient to facilitate cytotoxin release in SAP or MTX + BSO alone. This further supports the hypothesis that there is a critical load of ROS required to cause sufficient damage to endo-lysosomal membranes and trigger the release of the endocytosed molecule. A potential confounding factor here is that lipid peroxidation has been reported as a potential indicator/secondary messenger of the cellular stress response, for example 4-hydroxynonenal (4-HNE) is believed to play a role in the cell cycle and differentiation/apoptosis(136). Therefore, the rise in lipid peroxidation may in part be due to a stress response hence the increase in background level seen with the treatment of all the agents: $TPPS_{2a}$ (dark/light), SAP and BSO).

The findings for the light 'before' protocol are important as it may prove a more suitable mechanism for the internalisation of certain molecules such as genetic material and non-toxic therapeutic molecules when other factors are taken into account such as the extinction coefficient of the photosensitiser, light dose, and stability of the molecule to be internalised.

The combination-PCI experiments were performed to investigate whether this mechanism of drug delivery would be suitable for the internalisation of more than one cytotoxin. The importance of this is that in clinical practice, medical management of malignancy commonly requires the administration of more than on and often multiple therapeutic agents. The question to be addressed was could PCI enhance dual-drug chemotherapy in 4T1 cells? The observations made during the study overall indicate that combination PCI is more effective than either cytotoxin-PCI alone. However, this is only the case for the LA Combo-PCI protocol where the combination of both agents resulted in a significant increase in cytotoxicity, compared to SAP-PCI or MTX-PCI alone +/- BSO. In fact, LA Combo-PCI produced cell kill equivalent to SAP-PCI/MTX-PCI +BSO. The addition of BSO to combo PCI resulted in 89% cell kill. In comparison to SAP-PCI and SAP-PCI + BSO this represents an increase in cell kill ratio from 5.7 in 10 cells and 7 in 10 cells, respectively, to 8.9 in 10 cells with no increase in PDT toxicity. Whereas compared to MTX-PCI and MTX-PCI + BSO the increase in cell kill ratio is from 5.3 in 10 and 7.1 in 10, respectively, to 8.9 in 10. The increased toxicity in comparison to single agent PCI is significant, however it is important to put this into context when compared to SAP alone when a 13.8-fold increase in cytotoxicity is observed.

Combination PCI is an area that certainly requires further evaluation in order to have any true relevance to clinical practice in cancer therapeutics. This study has shown that LA PCI can be used to facilitate the internalisation of two structurally and mechanistically different cytotoxins in unison and that this is significantly better than single-agent PCI alone when the light dose is fixed. Furthermore, that when the REDOX environment of the cell is altered to favour oxidation, under the action of BSO, it is possible to see as much as an 83% increase in cytotoxicity (compared to SAP alone). The benefit of such a regimen is that it is possible to achieve magnitudes of cytotoxicity at significantly lower doses of cytotoxin. In doing so, it is possible to effectively widen the therapeutic index of chemotherapeutic agents, which will be of great benefit to both clinicians and patients. The lack of enhanced killing with the LB PCI regimen further supports the hypothesis that LA and LB PCI have two distinct

mechanisms. It is possible that when both agents are trapped within endosomes an even greater level of ROS production is required to cause sufficient lipid peroxidation, enabling adequate disruption of subsequently formed vesicle when they react.

3.23 Variable 6: Time between photosensitiser activation and survival assay

The time between illumination and MTT assay represents the period during which the different phases of PCI will take place. Initially, photosensitiser activation and ROS generation; lipid peroxidation leading to endosomal membrane rupture and release of internalised agent (in this case cytotoxin) in to the cytoplasm; trafficking of the released drug to site of action (SAP to rough endoplasmic reticulum and MTX to nucleus); exerting cytotoxic effect (SAP inhibition of protein synthesis and MTX inhibition of DNA replication); apoptosis +/- necrosis. Thus it is not without reason to challenge the null hypothesis that prolonging the time between illumination and MTT assay has no effect on overall cytotoxicity for PCI.

In order to challenge the null hypothesis experiments were performed to evaluate the effect of increasing the time between illumination and MTT assay from 24h to 72h. This time period was chosen due to the practicalities of completing PCI-based experiments in the laboratory. Other groups have been known to wait longer periods of up to 7-10 days post illumination(137). The results for LA PCI are positive, with regard to an increased effect when waiting 72h compared to 24 hours, for SAP, MTX and Combo-PCI. SAP based PCI +/- BSO exhibited the greatest magnitude of increased cytotoxicity at 72h compared to 24h; for SAP-PCI there is a 0.6-fold increase in cytotoxicity; SAP-PCI + BSO there is a 0.8-fold increase achieving 95% cytotoxicity. Therefore, by enabling further time for the release of SAP from endosomal stores and/or prolonged time for cytotoxic effect to take place, the overall cytotoxicity is increased. A potential mechanism for this is that by waiting 72h post-illumination there is a combination of light ‘after’ and light ‘before’ PCI. In both protocols photosensitiser will initially become incorporated into the cell membrane and subsequently accumulate into endolysosomal membranes. In the LA protocol

this will be accompanied by the random, non-receptor mediated endocytosis of SAP therefore the co-localisation of both TP and SAP will be dependent on the total concentration of both agents along with their uptake kinetics. If these are not equivalent then a mismatch may occur with a proportion of endosomes containing both; some containing SAP but little or no TP; others containing TP without SAP; and finally some with neither. Thus when the light (randomly) activates photosensitiser and ROS-mediated lipid damage leads to rupture of the endolysosomal membranes only those cells with a high proportion of co-localised agents will undergo apoptosis that can be observed at 24h (LA protocol). However, waiting an extra 48h enables those damaged endosomes that contained TP alone to react with undamaged vesicles containing SAP alone or co-localised drugs, enabling their release and thus killing a cell that may otherwise have survived if assayed at 24h.

MTX had showed a slightly different trend in that although there was an increase in cytotoxicity for LA MTX-PCI at 72h compared to 24h, this was no different to the level of cytotoxicity reached with MTX alone at 72 hours. However, in support of the hypothesis that TP mediated PCI of MTX requires a higher level of ROS production to facilitate the endosomal escape; the addition of BSO did result in a 9% ($p<0.05$) and 15% ($p<0.01$) increase in cytotoxicity compared to MTX and MTX-PCI + BSO, respectively. Importantly this rise was not explained by an enhancement of the PDT effect alone.

There was no true increase in PCI or PCI + BSO (LB), for the experimental conditions chosen (in particular cytotoxin and light dose). The LB protocol appears to suffer from what might be described as a narrow operating window. Pilot experiments showed that by increasing the illumination time it was possible to significantly enhance this protocol, however, this comes at the cost of an increased PDT/PDT + BSO effect. Furthermore, when the dose of SAP is increased to 30 nM, the level of cytotoxicity achieved is comparable to the LA protocol (fig. 3.18a). Given that a higher dose of TP (0.6 μg/ml) + SAP 30 nM (LB) at 24h achieved a greater ultimate level of cytotoxicity and had a greater differential to PDT or SAP alone compared to TP (0.6 μg/ml) + SAP 15 nM (LB)

(same light dose, 120 s) at 24h and 72h suggests that the dose of cytotoxin might be the rate limiting step for this protocol. A potential explanation for this is that the pre-treatment of the cell (TP + light) attenuated the efficiency of endocytosis/pinocytosis(138). Consequently, higher doses are required to increase the probability of endocytosis and subsequent cytosolic delivery following interaction between pre-damaged and newly formed endo-lysosomal membranes to a degree that supports significant enhancement in cell kill; even if more time is given for lipid peroxidation (i.e. 72h). This may also explain why no significant increase in cytotoxicity, independent of an enhanced PDT effect, is observed following the addition of BSO. Such a hypothesis is supported by the findings of LB Combo-PCI +/- BSO where an overall greater level of cytotoxicity and differential is observed versus SAP + MTX (data not shown) chemotherapy alone (fig. 3.21b). Therefore, the overall increased concentration of cytotoxin increases the likelihood of successful endocytosis, post-light, therefore greater probability of endosomes containing drug reacting with pre-damaged vesicular membranes and release into the cytoplasm. However, overall the light 'after' therapy, using lower doses of cytotoxin (SAP 15 nM/MTX 0.4 μg/ml) appears to elicit a more efficacious PCI effect at both 24h and 72h following illumination.

3.24 Effect of Antioxidants

As described in the introduction, varieties of antioxidants/reducing enzymes exist within a cell to enable survival within dynamic REDOX environments. A good example of how cells have adapted and retained protective reducing capabilities can be seen in erythrocytes, which are exposed to both oxygen-rich (pulmonary circulation) and oxygen-deplete (respiring tissues) regions of the body. Enzymes such as G6PD and pyruvate kinase play a vital role in stabilizing the erythrocyte membrane and thus preventing oxidation induced membrane damage that results in inappropriate and premature haemolysis as a sequelae of their absence or ineffective function. The ability of a cell to enhance its reducing capabilities has been implicated in the development of drug resistance. Wang et al. (1999)(139) reported that multi-drug resistant MCF-7/ADR breast cancer cells, which are 30-65-fold more resistant to doxorubicin than wild type and this was associated with 23-fold elevated glutathione-S-transferase (GST) activity

within the cytoplasm. In addition, Goto et al. (2001)(140) reported that levels of nuclear-targeted GSTπ are not only elevated in doxorubicin-resistant cancer cells but dynamically rose in response to treatment; they conclude that GSTπ protects DNA from anticancer drugs. This supports the findings in this study whereby cells treated with SOD both pre- and post-illumination exhibited perceptible inhibition of the PCI effect. SOD catalyses the simultaneous reduction and oxidation of superoxide into oxygen (O_2) + hydrogen peroxide (H_2O_2), and in doing so SOD exerts an antioxidant effect within a cell. Golab et al. (2003)(141) demonstrated that use of the MnSOD inhibitor 2-methoxyestradiol (2-MeOE(2)) potentiated *in vivo* PDT in a murine tumour model. This indicates that O_2^- may play a role in mediating the ROS associated damage that is triggered by photosensitiser activation. Therefore, by making the intracellular environment more susceptible to the generation and persistence of O_2^- by inhibiting SOD we can enhance this effect. Interestingly, in this study, under the experimental conditions used, SOD did not have a statistically significant effect on PDT but did for PCI. This is in keeping with the effect of BSO on PDT versus PCI, whereby under certain conditions it appears to favour PCI. This is consistent with the hypothesis that the amount of ROS required to liberate endocytosed drugs from their cytosolic vesicles in PCI is significantly less than that required for PDT-induced cell killing; in the former the cytotoxic agent released causes the step in cytotoxicity. Consequently, a relatively small increase in the ROS-quenching capacity of a cell using SOD may be sufficient to inhibit the low ROS-burden for PCI but have little effect on PDT.

A similar effect is seen using the amino acid L-Histidine (LH), which is known to quench singlet oxygen(142). The dose-dependent reversal of PCI indicates that TP photo-activation, in part at least, is likely to involve the Type II reaction with the generation $^1O_2$.

The findings of the ROS quencher experiments add further credibility to the importance of ROS generation and survival in PDT and PCI. In the case of LH, it is important to consider that a non-enzymatic anti-oxidant can potentially enhance ROS production and this was observed at higher doses.

SUMMARY

Throughout this chapter the roles of ROS in PDT and PCI, have been investigated in order to determine which variables exert the greatest influence on the relationship between the two technologies. The findings certainly do not support the theory that PDT and PCI are mutually exclusive. Rather, they highlight that certain variables play a vital role in determining what proportion of cell killing will be attributable to PDT or PCI. Furthermore, a recurrent theme throughout the results was that SAP-PCI regimen appears to superior to MTX-PCI despite the inherent toxicity of MTX. This important observation demonstrates the potential of PCI with regard to enhancing the efficacy of a drug. However, it must be noted that clearly in this thesis the magnitude of such an effect is dependent on the compound to be internalised.

The process of photosensitiser activation is an energy transfer process, whereby visible/non-visible light energy is converted into ROS with subsequent physical and chemical damage to cellular structures resulting in potential organelle disruption, vesicle rupture and/or cell death.

It would appear that the three most important determinants for PDT versus PCI are:

1. Light dose
2. Photosensitiser dose
3. Immediate versus delayed illumination

(1) and (3) are of significant importance with regard to optimising the PCI effect. If the light dose is too high, PDT will inevitably predominate as the probability of activating the photosensitiser increases, and in these studies, this does not appear to be proportionate as illustrated by the 'step' in cytotoxicity seen at 180 seconds illumination. Delaying the time to illumination is vital for PCI. The location and density of the photosensitiser at time of photo-activation (2) and (3) will ultimately determine whether ROS production is localised within specific cellular compartments such as endocytic vesicles (favouring PCI) or indiscriminately throughout the cell (favouring PDT).

Altering the REDOX environment appears to mainly benefit fine-tuning the technique. BSO and other ROS facilitators may have a role to play in enhancing the PCI and/or PDT effect, particularly when maximum cell kill is the desired outcome. BSO is already utilized in the clinical arena to help reverse drug resistance driven by enhanced cellular robustness to oxidative damage.

Photochemical internalisation as a tool for enhanced *in vitro* drug delivery certainly merits further investigation. By facilitating drug delivery in cancer, PCI has the potential to:

1. Circumvent multi drug resistance: this has been demonstrated by multiple groups. The 'early' release of endocytosed drug helps negate resistance mechanisms including enzymatic degradation and increased drug efflux.
2. Reduced systemic toxicity: localised drug activation will reduce systemic side effects.
3. Widen the therapeutic index of drugs: this is particularly important as many cytotoxic agents have very narrow therapeutic windows. By enabling clinicians to start drugs at lower doses (but with comparable therapeutic effect) PCI could have a particularly significant impact in cancer therapeutics. Strategies such as enhancing the oxidative state of the cell could further improve this effect.

The possible limitations of PCI mainly centre on the time and labour intensive process of optimisation. There are significant variations in treatment success with varying agents both photosensitiser and cytotoxin. However, strategies such as those described in this chapter may help the development of greater understanding of the mechanisms that underpin PCI. Consequently, more reproducible protocols may be developed for PCI.

Chapter 4: Small Molecule Carriers and Photochemical Internalisation

SCIENTIFIC BACKGROUND AND AIMS

Conventional chemotherapeutic agents have been the mainstay of cancer therapeutics for many years. The narrow therapeutic windows of mutagens/cytotoxic agents designed to induce DNA damage has limited the effectiveness and successes of such anticancer regimens. Consequently, the last 20 years has seen the advent of a range of targeted and/or non-mutagenic agents, which are targeted against the underlying cellular abnormality driving the malignancy. The monoclonal antibody trastuzumab targets the constitutively active erbB2 receptor in breast cancer; imatinib targets the constitutively active tyrosine kinase that is formed following the *bcr-abl* fusion (t9:22) in chronic myeloid leukaemia. Other forms of targeted therapies that are being investigated in pre-clinical and clinical settings include photosensitive compounds such as quantum dots(143).

One of the major obstacles faced when developing novel therapeutic agents in oncology is to synthesize a molecule that can achieve efficient uptake within the target tissue. Therapeutic proteins and peptides are a good example of novel agents, which based on structure habitually suffer from inefficient transport into the cytoplasm and subsequently a blunted therapeutic effect. Mechanisms developed to enhance the delivery of peptides include microinjection and complexing with membrane-permeablising agents such as lipids(48). However, the former is limited by time- and labour-intensity whereas the latter technologies are not uncommonly toxic to cells. A well known solution to this problem is the use of protein transduction domains (PTDs), which are short peptides that can be used for classical endocytosis-independent ferrying of larger molecules across the cell membrane and into the cytoplasm(144). These PTDs are known to bind commonly expressed cell surface markers including Heparan Sulphate Proteoglycans, thus their potential use across many different cell types make them a very useful delivery tool. Some of the more commonly used PTDs include the basic region of HIV-1 Tat peptide, third helix of antennapedia homeodomain (penetratin)(145, 146). A benefit of many PTDs is that that they are able to interact with membranes owing to the multiple basic

amino acid residues in their structure, which affords them amphipathic properties. The first major PTD-conjugate was the Tat fusion protein used to deliver β-galactosidase to multiple organs in murine models(147). This demonstrated the effectiveness of PTDs, in particular HIV-1 Tat, to facilitate the delivery of a protein into cells. Li et al (2006)(148) have reported on the use of antennapedia homeodomain to facilitate the transduction of rat brains with the anti apoptotic X-linked inhibitor of apoptosis protein (XIAP) to reduce cell death following brain injury induced by seizures. The observations of the group led to their conclusion that PTD-XIAP provides a neuroprotective effect versus brain injury. Another example of the use of PTDs, in this case HIV-1 Tat, is shown by Choi et al. (2006)(149) who demonstrated that a wild-type Tat-alpha-synuclein fusion protein (produced from bacteria) was able to attenuate paraquat induced cell death in astrocytes *in vitro* and *in vivo.* The mechanism is believed to involve the anti-oxidant properties associated with increased expression of heat shock protein-70 (HSP70). This is thought to be of potential benefit for the prevention of cell death in the basal ganglia in Parkinson's disease.

In all the examples given above PTDs were able to significantly enhance the delivery of their 'cargo' in to the cell and consequently to their target of action.

4.1 Small-molecule Carriers (SMoCs)

The minimal size and molecular weight of SMoCs affords them the added benefit of avoiding the intracellular biodegradation processes to which peptide linkers may be subjected. A further benefit of SMoCs is that they are able to react with native proteins, thus these can be delivered into the cell without need for further processing and without disruption of protein function (fig. 4.1).

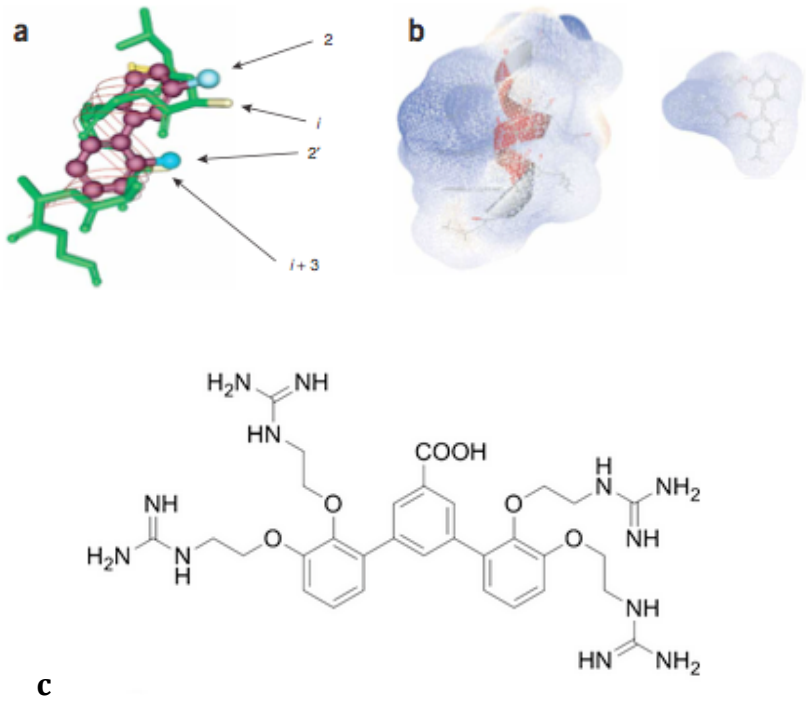

Figure 4.1 – Molecular modeling of SMoCs.
A Molecular model of a typical alpha helix overlaid with a biphenyl ring from a SMoC. **B** The amphipathic nature of the helix mimic 2G-SmoC is shown to the alpha helix of antennapedia 44-57 (penetratin). ***(Okuyama et al., 2007)***(48). **C** The molecular structure of 4G-BfSMoC-COOH (69)(4G-SmoC). The amino groups provide potential reactive domains to enable coupling with, for example, proteins for transport.

SMoCs have been shown to be effective in facilitating the delivery of a range of molecules including dyes, proteins(148) and siRNA(47, 69). Okuyama et al. (2007)(48) complexed di-guanidine (2G-SmoC) and tetra-guanidine (4G-SmoC) with fluorescein (FITC) to assess uptake in U2OS osteosarcoma cells. Using Tat-FITC and FITC alone as comparators the group observed that at low magnification SMoC-FITC treated cells appeared strongly fluorescent and this was comparable to Tat-FITC; cells treated with FITC alone were not fluorescent. The same group went on to demonstrate the ability of SMoCs to enhance uptake of protein based molecules. They coupled 4G-SmoC to the relatively large (23.5kDa) protein, Geminin, which blocks DNA replication licensing by competitively binding Cdt1(150). Using an Alexa-fluorophore (488), they showed that 4G-SmoC enhanced the overall uptake of Geminin with perinuclear and nuclear accumulation. The uptake of SMoCs was assessed using reduced temperature (4°C) incubation and a range of inhibitors for differing endocytic pathways. The group concluded that SMoCs alone are taken up in an energy-

dependent but endocytosis-independent manner. However 4G-SmoC-Geminin-Alexa 488 was dependent upon clathrin-mediated endocytosis (therefore an active process). These findings demonstrate the versatility of SMoCs with regard to their mechanism of facilitated cell entry, both with and without 'cargo'. SMoCs have also been used to enhance siRNA delivery in to cancer cells(69).

AIM

The aim of this chapter is to assess the efficacy of SMoC enhanced delivery of siRNA in to human (MCF-7) and murine (4T1) breast cancer cells.

4.2 SMoC enhanced siRNA transfection observed using fluorescent siRNA oligomers

This study was performed to test the null hypothesis that 4G-BfSMoC-COOH does not enhance the siRNA transfection in MCF-7 (human) and 4T1 (murine) breast cancer cells. In order to monitor the level of transfection in a manageable way within our lab, an Alexa Fluor® 555-labelled siRNA oligonucleotide was used, with uptake and localisation monitored using confocal microscopy. The findings of this study have undergone peer-reviewed publication(69).

Controls for SMoC facilitated uptake (siRNA-588 alone) showed undetectable uptake within the 4T1 cell line (fig. 4.2a) and non-significant uptake in the MCF-7 cell line (fig. 4.2b). For negative controls with SMoC alone, no fluorescent signal was detected, suggesting that the background uptake of siRNA-588, albeit not significant, seen with the MCF-7 cell line is likely to be a cell type-dependent process.

Treatment of cells with 10 μM 4G-BfSMoC-COOH resulted in a 4.9-fold ($p<0.01$) increase in the fluorescent signal for the siRNA-588 (4T1 cells), indicating significantly increased uptake. In addition, nuclear accumulation was also observed in the 4T1 cell line (fig. 4.2c).

There is also increased uptake in the MCF-7 cell line albeit, at 2.6-fold (fig. 4.2d, $p<0.01$) compared to siRNA-588 alone, somewhat of a lesser effect than observed in the 4T1 cell line; indicating a that uptake of siRNA-588 with or without SMoC is likely to be a cell specific process. For the purpose of comparison the gold standard transfection reagent, Lipofectamine®, was used in place of SMoC. 14.4-fold ($p<0.01$) increased uptake of siRNA-588 is observed in the 4T1 cell line; a 3.3-fold ($p<0.01$) increase is observed in the MCF-7 cell line. Nuclear uptake is observed in both cells lines (white arrows).

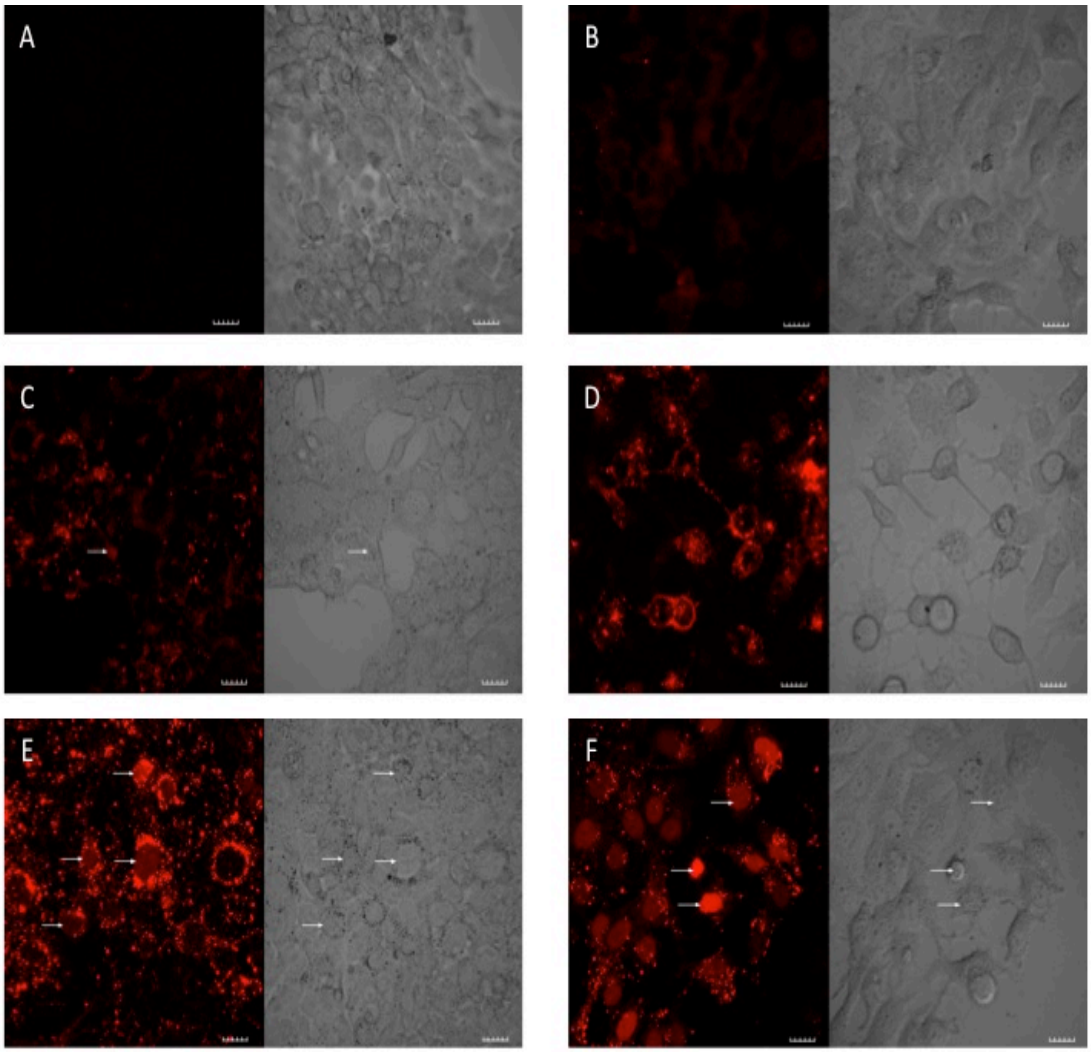

4T1 *MCF-7*

Figure 4.2 – Cellular uptake of fluorescent siRNA.
Confocal microscopy of cells treated with AlexaFluor® Red Fluorescent Oligonucleotide +/- 4G-BfSMoC-COOH. Cells were treated with oligonucleotide-fluorophore alone – **A** 4T1 and **B** MCF7; or treated with oligonucleotide-fluorophore (1.0 μM) – 4G-Bf-SmoC-COOH (10 μM) – **C** 4T1 and **D** MCF-7 or oligonucleotide (1.0 μM) plus Lipofectamine – **E** 4T1 and **F** MCF-7. Quantitative analysis of the relative cellular uptake demonstrates that addition of the 4G-BfSMoC-COOH, resulted in 4.9-fold ($p<0.01$) increased uptake of the oligonucleotide-fluorophore (siRNA) in the 4T1 cells; and a 2.6-fold ($p<0.01$) increase in the MCF7 cell line. There was evidence of nuclear uptake in the 4T1 cell line (**C**, white arrow). In cells treated with Lipofectamine plus siRNA, we observed 14.4-fold and 3.3-fold increase uptake in 4T1 and MCF-7 cell lines respectively. There was significant nuclear uptake in both cell lines following treatment with Lipofectamine (**D** and **E**, white arrows). The differing level of background uptake (siRNA-alone) is likely due to the differing characteristics of the two cell lines including doubling times and uptake kinetics. *Ex 559 nm, Em 572 nm, 60X NA:1.35 Objective Lens, zoom x1.0, scale 20 microns*(69).

The observed results showed that in the 4T1 cell line, Lipofectamine achieved 1.9-fold greater siRNA uptake compared to SMoC, which in turn facilitated

significantly greater uptake than siRNA alone. In the MCF-7 cell line, this differential reduced to a 0.3-fold increase in uptake for Lipofectamine compared to SMoC.

4.3 Photochemical Internalisation of 4G-BfSMoC-COOH – siRNA oligonucleotide complex.

Given the results in the siRNA-588 uptake study above, the following set of experiments were carried out to determine if $TPPS_{2a}$ based PCI could be used to enhance the SMoC-facilitated uptake of siRNA-588 in the MCF-7 cell line. The observations presented by Okuyama et al. (2007)(48) demonstrated that SMoCs could facilitate various modes of active uptake including endocytosis. Thus, the null hypothesis to test is PCI does not enhance the intracellular delivery 4G-BfSMoC-COOH – siRNA complex.

MCF-7 cells were treated with a combination of 4G-BfSMoC-COOH – siRNA-588 complex (final concentration of SMoC 10 μM and siRNA 1 μM) for 24 hours prior to washing and a 4-hour re-incubation in media alone. Cells were given a 15 second exposure to a 405 nm laser (as a negative control for PCI to ensure the laser alone did not affect the signal intensity or distribution of cytoplasmic siRNA-588). Confocal Images were taken prior to laser treatment (fig. 4.3a), immediately after (fig. 4.3b), 300 seconds after (fig. 4.3c), and a final image 600 seconds after laser treatment. Visually there appeared to be little if any significant change in the signal intensity or distribution.

Quantitative analysis found that there was <10% reduction in signal intensity at 600 seconds post laser treatment. This suggests that there is no significant effect exerted by laser alone on the siRNA-588 signal. The addition of $TPPS_{2a}$ (0.4 μg/ml) enabled assessment of the impact of PCI on the overall cellular uptake of siRNA-588, in the presence of 4G-BfSMoC-COOH. The same experimental format was used as for that described in figure 4.3. The first observation to make is that the intracellular localization of the siRNA-588 appeared to be different when administered with photosensitiser compared to without. In figure 4.4a, the intracellular distribution appears to be juxta-opposed to the membrane, in

comparison to figure 4.3a where there is more diffuse spread throughout the cytoplasm.

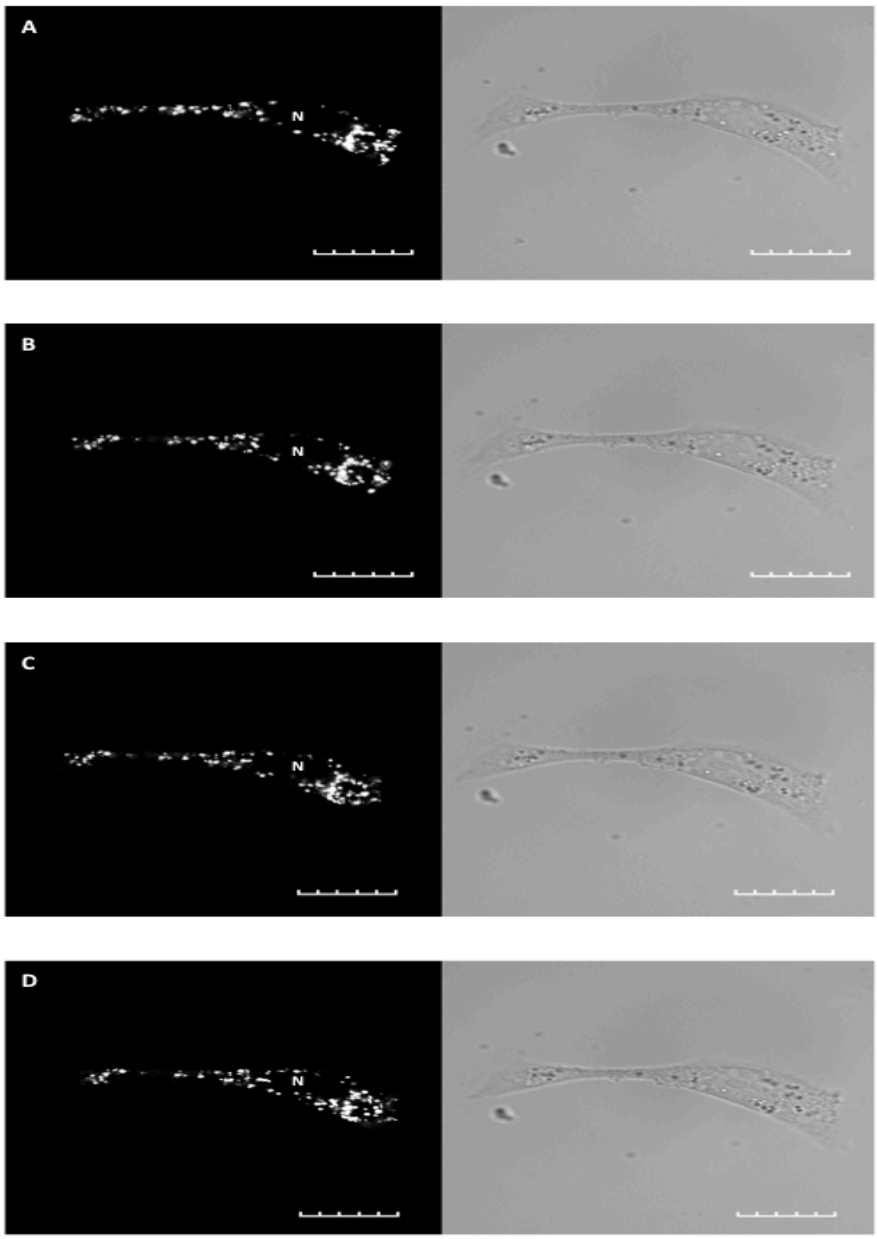

Figure 4.3 – Intracellular distribution of siRNA Alexa-555 fluorophore pre- and post- 405 nm laser treatment.
Single slice confocal microscopy of a single MCF-7 cell treated with AlexaFluor®-555 Red Fluorescent Oligonucleotide + 4G-BfSMoC-COOH. Cells were treated with oligonucleotide-fluorophore (1 µM) – 4G-BfSMoC-COOH (10 µM). Confocal images were taken at four different time points: **A –** Pre treatment with a 405 nm laser; **B –** Immediately after 15s 'on-stage' exposure to the 405 nm laser; **C –** 300 s after laser; **D –** 600 s after laser. Quantitative analysis using ImageJ shows there was <10% reduction in the signal of the oligonucleotide-fluorophore 600 s after treatment with the 405 nm laser. * N = nucleus. *Ex 559 nm, Em 572 nm, 60X NA:1.35 Objective Lens, zoom x1.0, scale 20 microns.*

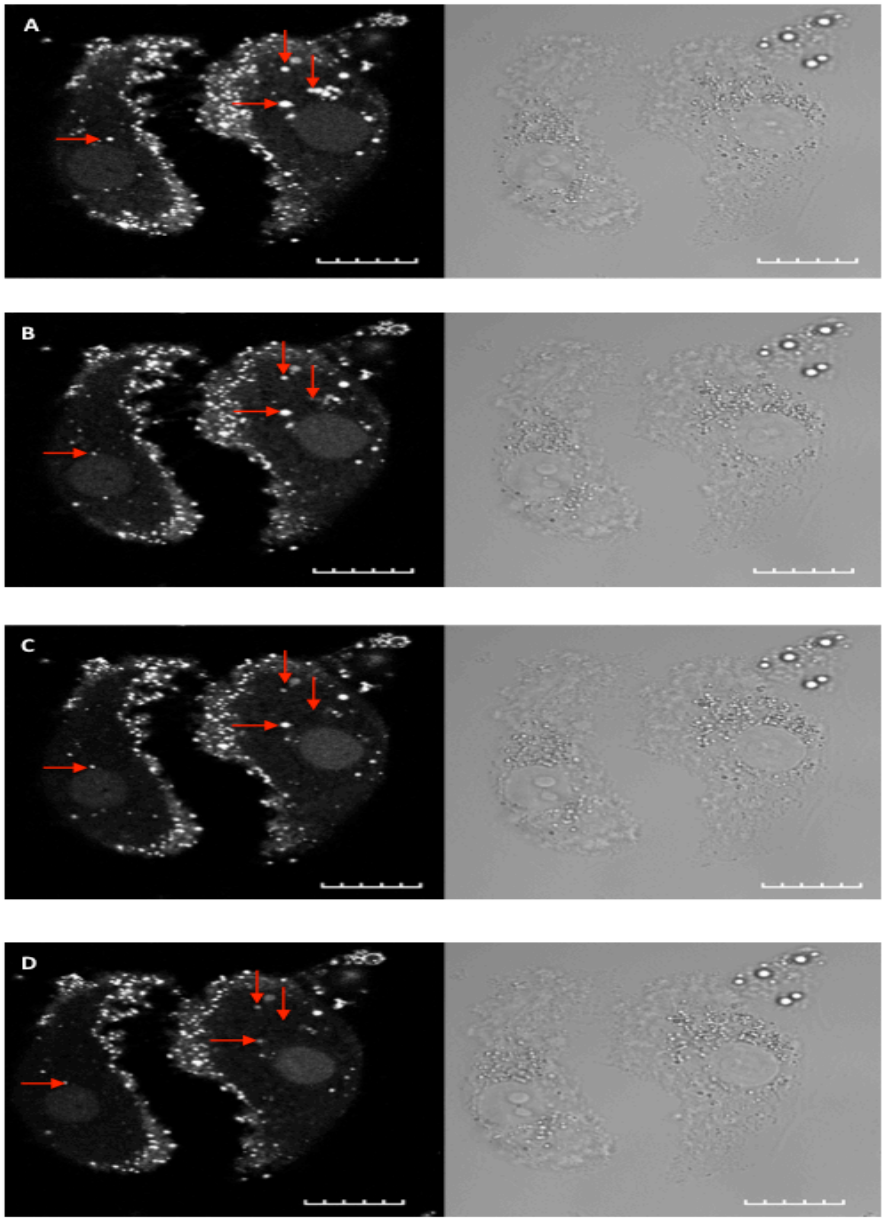

Figure 4.4 – Intracellular distribution of siRNA Alexa-588 fluorophore pre- and post- PCI treatment.

Single slice confocal microscopy of two MCF-7 cells treated with AlexaFluor® Red Fluorescent Oligonucleotide – 4G-BfSMoC-COOH complex + $TPPS_{2a}$. Cells were treated with oligonucleotide-fluorophore (1 µM) – 4G-BfSMoC-COOH (10 µM) plus $TPPS_{2a}$ 0.4 µg ml^{-1} for 24h. Confocal images were taken at four different time points: **A –** Pre treatment with a 405 nm laser; **B –** Immediately after 15s 'on-stage' exposure to the 405 nm laser; **C –** 300 s after laser; **D –** 600 s after laser (scale = 20 microns). Quantitative analysis using ImageJ shows there was a 0.5-fold reduction in the signal of the oligonucleotide-fluorophore and a simultaneous 0.23-fold rise in nuclear uptake, 600 s after treatment with the 405 nm laser. * N = nucleus. *Ex 559 nm, Em 572 nm, 60X NA:1.35 Objective Lens, zoom x1.0, scale 20 microns.*

However, what is consistent is that the internalized siRNA appear to be distributed in discrete vesicles, which is consistent with an endocytic process. Evaluation of the signal intensities across the four time points before and after application of the 405 nm laser, indicate the following:

- There was a steady decline of the mean signal intensity as time progressed following exposure to the 405 nm laser. Specifically, a 0.5-fold reduction was observed at 600 seconds post-laser (fig. 4.4b) compared to pre-laser (fig. 4.4a).
- There is a loss of signal from the 'vesicular' structures that are seen in the cytoplasm (red arrows, fig. 4.4).
- As the overall signal intensity decreases, there is a rise in the intensity of the nuclear signal. This peaks and plateaus 300 seconds after laser treatment when a 0.23-fold increase is observed.

The results are consistent with the previously published data available on SMoCs in the literature(48). The impact of PCI on the efficiency of this process will be addressed on the discussion. Parallel experiments using a different type of SMoC did not appear to significantly impact on the uptake or localization of siRNA (data not shown). No experiments were performed to determine the effect of PCI alone on the uptake of siRNA-588. This was due to the limited amount of siRNA available for experimentation.

DISCUSSION

The main aim of this study was to determine if PCI can enhance SMoC-facilitated siRNA delivery in breast cancer cells. Previous work has demonstrated that both techniques can be used to facilitate *in vitro* delivery of genetic material. Bonsted et al. (2004)(151) used $TPPS_{2a}$ to mediate photochemical internalisation of adenovirus serotype 5 (*Ad5*)-vectored gene transfection. The group reported that when complexed with *poly-L-lysine* and *Superfect®,* PCI-mediated *Ad5*-vectored gene transfection achieved "a substantial increase in reporter gene expression" with a maximum of 75% positive cells (using flow cytometry). In this study PCI appears to have a beneficial effect on the overall transfection efficiency of the SMoC-siRNA complex. The finding that the 405 nm laser-alone does not appear to have a significant effect on the fluorescent signal of siRNA is important with regard to interpretation of the results for PCI. The vesicular pattern of distribution within the cytoplasm was promising, with regard to suitability for PCI as it was consistent with an endocytic mode of uptake and subsequent trafficking into the endo-lysosomal pathway as described in chapter 3.

The residual level of background uptake for 4G-BfSMoC-COOH – siRNA-588 complex appeared to be a cell specific process. This is likely to be a multi-factorial effect. Overall, it appeared that the 4T1 cells, under the chosen experimental conditions including drug dose, were less able to internalize the siRNA-588 (fig. 4.2a and 4.2b). Consequently, the facilitating effect of SMoC appeared more pronounced in the 4T1 cells compared to the MCF-7 cell line. Possible explanations for this could include the two cell lines express different cell surface receptors; have differing preferences for modes of uptake for exogenous compounds; are able to degrade or efflux the siRNA at different rates. The second explanation is particularly interesting where SMoC-assisted delivery is concerned owing to previously described evidence by Okuyama et al. (2007)(48) whereby SMoCs are able to support multiple forms of energy-dependent uptake. If for example, one form of uptake is better suited to a particular SMoC than another then this may lead to a discrepancy in effect when comparing two separate cell lines. However, it could also be that the relatively

good level of background uptake seen in the MCF-7 cell line means that any SMoC effect is likely to appear blunted versus the relatively poor background uptake in the 4T1 cell line. Nuclear mobilisation of siRNA is an important finding as this is where its effect will be exerted, thus it is relevant that 4g-BfSMoC-COOH triggered nuclear mobilisation at the time-point measured in the study (fig. 4.2c and 4.2d). Lipofectamine presents an interesting comparator to SMoC as a means to enhance gene transfection in both mechanism and efficiency. Lipofectamine comprises a cationic liposomal structure, which via complexing with anionic nucleic acid enables it to overcome the repulsive forces exerted by interaction with phospholipid bilayer(152). In doing so Lipofectamine achieves gold-standard level of gene expression. This is supported by the findings in this study, whereby Lipofectamine facilitated increased uptake in 4T1 cells (1.9 times) compared to SMoC. Interestingly, this differential was significantly reduced to 0.3-times increase in the MCF-7 cell line, which suggests that SMoC in this cell line may be very effective. In both cell lines, there was an increase in nuclear mobilisation and accumulation, which was particularly pronounced in the MCF-7 cell line. Overall, 4G-BfSMoC-COOH appeared to significantly enhance the uptake of siRNA in both cell lines. In the case of the MCF-7 cell line, this appeared to be comparable to the transfection efficiency achieved by Lipofectamine.

One of the main considerations that may limit the use of PCI as a means to enhance the delivery of non-robust compounds, including genetic material, is the potential for ROS damage due to proximity at the time of photosensitiser activation. Although in this series of experiments, gene expression was not measured as a marker of successful transfection, fluorescent signal intensity and localisation were used as surrogate markers. Therefore, the lack of change in signal intensity or distribution following cell exposure to the 405 nm laser is important as it enables interpretation of gene delivery if the assumption is made that the siRNA 'survives' exposure to the laser at the dose utilized. This is the main reason 0.4 μg/ml of $TPPS_{2a}$ was chosen for this set of experiments. The results from the PCI study indicate that upon activation of the photosensitiser there was evidence of cytoplasmic redistribution and increased nuclear

accumulation. The mechanism for PCI as described by Adigbli and MacRobert (2012)(26) is supported in this study by the apparent loss of signal observed in some of the vesicular 'clumps' as shown by the red arrows (fig. 4.4). This indicated that photosensitiser activation might lead to rupture of the endo-lysosomal membranes and subsequent release of siRNA into the cytoplasm and facilitation of delivery into the nucleus. One area that was not adequately investigated during this study was whether the presence of $TPPS_{2a}$ in the absence of light would enhance SMoC-siRNA delivery. Although the level of increased nuclear uptake was not spectacular, it must be taken into account that the majority of PCI experiments in this thesis are assayed at least 24 hours after initial activation of the photosensitiser. Therefore, it would be important to follow this up and perform confocal imaging at later time-points. Another important point of note is that cellular integrity appears to be preserved following 405 nm laser treatment. Pilot studies using longer durations of laser exposure were associated with cellular swelling and death. Overall, there appears to be insufficient evidence at present to justify the rejection of the null hypothesis. However, at the very least the evidence is consistent with PCI having an enhancing effect on SMoC-facilitated delivery of siRNA in breast cancer cells. The findings also support an endocytic process of SMoC-siRNA uptake and at the very least makes this an intriguing target for PCI based therapy. The combination of SMoC + PCI may also enable the adoption of less harsh conditions (ROS) as a similar level of transfection or drug delivery may be achieved with a lesser load of total ROS production. The benefits would be a lower probability of ROS-mediated damage to the compound/drug to be internalised. The combination of the two therapies is an exciting prospect as if a true symbiosis exists it could further widen the therapeutic windows of multiple agents. This is further supported by the versatility of the two techniques, being amenable to a range of compounds and molecular structures. Further work in this area will be described in the closing summary.

Chapter 5: Photochemical Internalisation in a 3D Tumour Model

SCIENTIFIC BACKGROUND

The tumour stroma is the basis upon which a micro-collection of cells may establish preferential conditions to assist and promote tumour growth and progression. The development of hypoxia within this environment results in the release of hypoxia-inducible factor (among other molecules), which in turn results in the increased expression of genes that will promote tumour survival and growth. These include growth factors (fibroblast growth-factor (FGF), vascular endothelial growth factor (VEGF), colony-stimulating factor (CSF) and inflammatory cytokines. The result is the activation of a host of stromal cells such as fibroblasts; macrophages and endothelial cells that can help the micro-tumour proliferate, whilst supplying a route for nutrient delivery and waste excretion, and remodeling of the tumour mass to a point when invasion and metastasis become possible. The make up of the stroma is driven by the demands of the malignant cells and capabilities of the host tissue, resulting in varying ratios of non-cellular components of the stroma including collagen and glycoproteins(50).

In order to make a more representative analysis of cancer cell response to treatment, pre-clinical researchers are often forced to opt for *in vivo* studies, which no doubt provide a far more dynamic and characteristic tumour model. The necessary and justified restrictions on *in vivo* work along with the demands of the Animals (Scientific Procedures) Act (ASPA) 1986 (revised 2013) for researchers to look into alternative modes of biological investigations has placed the onus on scientists to develop new models that can at least act as a bridge between *in vitro* and *in vivo* studies.

The bulk of work looking into alternatives to 2-D models has fallen under the umbrella of 3-D scaffolds, which include the development of multicellular tumour spheroids(153). Hirschhaeuser et al. (2010)(154) reviewed the potential use of spheroids, stating that they "strikingly mirror the 3D cellular context and therapeutically relevant pathophysiological gradients of *in vivo* tumors." Another strategy for 3D modeling that has been employed is growing tumours in tissue-engineered structures(155). The choice of natural or synthetic

constituents for the matrices is of further benefit both in terms of versatility in construction and suitability for different cell types. The non-synthetic matrices typically comprise a structure rich in the trimeric glycoprotein laminin and Type I collagen or hyaluronic acid(155, 156). Laminin is a particularly important extracellular matrix (ECM) component found within the basal lamina, which plays an important role in multiple cell functions including differentiation, adhesion, motility and survival(157). Therefore, a matrix rich in such a glycoprotein will possess many of the structural and biologically active characteristics necessary to support the growth of a 3D tumour. The biocompatible and biodegrading polymer, polyethylene glycol (PEG) is commonly used in synthetic matrices(50). Such constructs have the added benefit of increased versatility with regards to the type of extra molecules, such as RGD (Arg-Gly-Asp) sequences(158) that can bind cell-ECM adhesion molecules such as integrins. Integrins are a group of essential cell adhesion molecules that act as anchors, 'wheels' and proprioceptors for cells and play a vital role in division, survival, invasion and metastasis. Such attributes and characteristics are of significant benefit when aiming to mimic or simulate the 'normal' environment of a developing tumour. Another important component of the tumour stroma are catalytic enzymes that can degrade the ECM. The main class is a group of serine proteases known as matrix-metalloproteinases (MMPs). A good example of the advantage of synthetic matrices is the inclusion of engineered polymers with specific MMP sites, which potentially can aid biodegradation and remodeling of the stroma(49).

The different types of matrices described above highlight the potentially positive impact that 3D models could have in the fields of cancer biology and therapeutics. The flexibility and versatility afforded by the range of different structures, in theory at least, makes it possible to mimic a small tumour stroma that can provide a growing mass with structural support, a reservoir of growth factors and the potential to embed active stromal cells such as fibroblasts, endothelial cells and immune cells. One of the more commonly used collagen matrices is the Type I collagen hydrogel, however the relatively high water

content of the gel is not an optimal model for tumour growth, which is preferentially suited to a more densely packed collagen scaffold(159).

In this chapter, pilot studies into the potency of $TPPS_{2a}$ and SAP-PCI have been investigated using a 3D tumour model. The model chosen was based on the plastic compression model first described by Brown et al. (2005)(160). This method is a forward step from previous hydrogel matrices that are restricted by their high water density, which does not closely mimic the denser collagen scaffold of a tumour mass. To negate this the hydrogel and cellular components (cancer cells +/- stromal cells e.g. fibroblasts) are placed under plastic compression with the consequent removal of H_2O resulting in shrinkage reported to be >100-fold(160). This technique has been shown to have beneficial effects for closer tumour mimicking including:

- Comparable cell viability.
- Increased strength and compliance of the collagen matrix, associated with significantly increased collagen density.
- Spatial heterogeneity that better mimics a natural tumour stroma.
- Variable cell and matrix densities throughout the scaffold, which again is a closer fit to a growing tumour mass.

AIM

The aim of this study was to determine if pilot experiments can challenge the null hypothesis that $TPPS_{2a}$ based PCI of SAP is not a plausible therapy for enhanced cytotoxicity in a 3-D tumour model. This model was to be based upon the partial plastic compression technique described above but will not contain any stromal cells as the focus will be proof of principal.

RESULTS

The 3D tumour construct (fig. 5.1) was grown in media for 7 days prior to the addition of either $TPPS_{2a}$ 0.8 μg/ml (PDT), SAP 60 nM (cytotoxin) or a combination of the two (PCI) and treated for 24 hours and subsequently washed and re-incubated in media for 4-hours prior to illumination for 180 seconds. Cytotoxicity and emission spectra were analysed seven days after illumination using the AlamarBlue® assay.

5.1 Spectral Analysis (AlamarBlue®)

Analysis of cytotoxicity was also performed by fluorescence analysis of aspirated AlamarBlue® following a 4-hour incubation period with a mean calculated from 12 (n=3) 100 μL samples. PDT resulted in a 21% increase in mean signal intensity compared to control ($p<0.001$), whereas treatment with SAP alone was associated with <10% increase in mean signal intensity (fig. 5.2).

Spectral analysis of the four experimental groups (Control, PDT, Saporin, PCI) investigated in this study was performed. Fluorescence intensity was normalized to enable a more representative comparison (fig. 5.2). The peak emission remained consistent across the three treatment groups, compared to control. However, tumoroids treated with $TPPS_{2a}$ alone + light (180 seconds) produced the greatest fluorescence intensity (40% increase) compared to control group. In the PCI tumoroid group, however, an 85% reduction in the fluorescence signal was observed. The fluorescence intensity was proportional to the amount of resorufin produced via the reduction of the nonfluorescent resazurin, which is freely taken up and reduced by active cells.

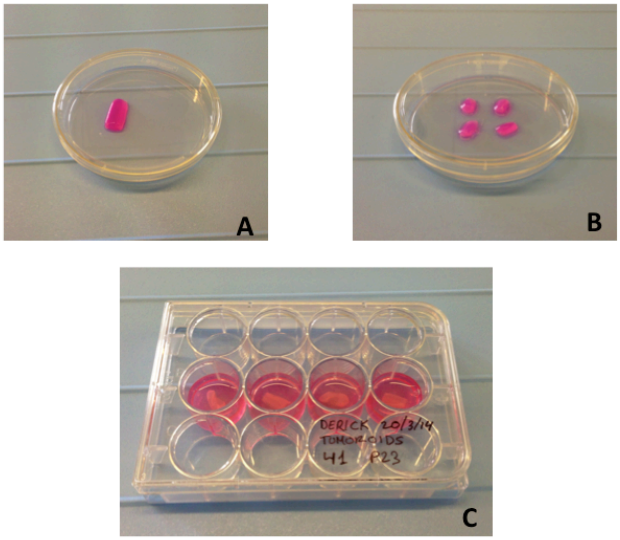

Figure 5.1 – Tumoroid preparation.
A – Compressed collagen scaffold containing 4T1 cells (5 x 10^5 ml^{-1}), **B –** x4 equal pieces of tumoroid cut from initial piece (A), **C –** tumoroids in media following insertion into acellular collagen hydrogel for anchorage. Tumoroids were subsequently grown for 7 days (media changed every 48 hours) prior to experimentation.

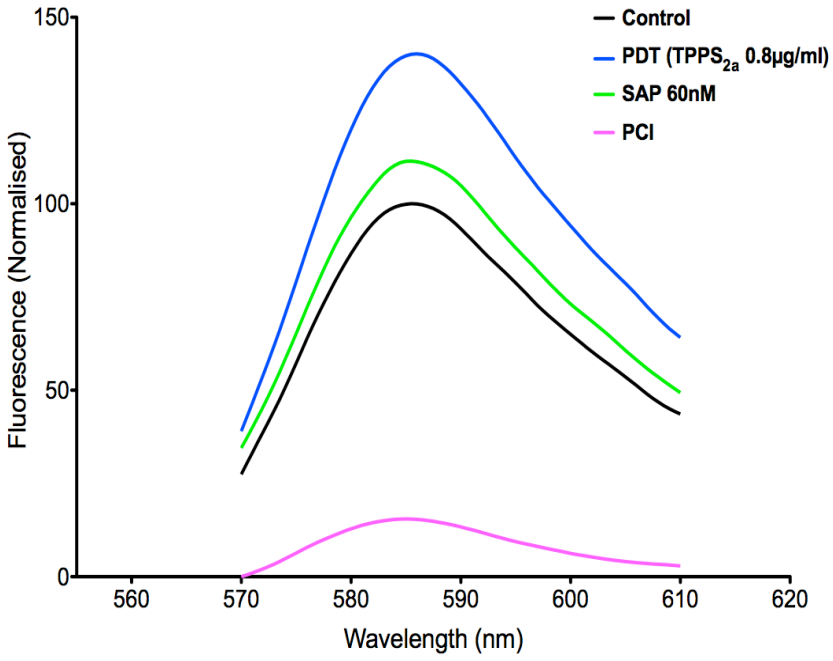

Figure 5.2 – 4T1 Tumoroids AlamarBlue® emission spectra.
4T1 cells were seeded into collagen constructs at 5 x 10^5 ml^{-1} and grown for 7 days at 37°C prior to 24h incubation with either $TPPS_{2a}$ (PDT, 0.8 µg ml^{-1}), SAP (60 nM) or both (PCI). Cells were incubated with AlamarBlue® for 4 hours at 37°C, 7 days after light exposure (180 seconds). Peak emission at 585 nm. (n=3)

5.2 Cytotoxicity Assay (AlamarBlue®)

Analysis of cytotoxicity was also performed by fluorescence analysis of aspirated AlamarBlue® following a 4-hour incubation period with a mean calculated from 12 (n=3) 100 µL samples. PDT resulted in a 21% increase in mean signal intensity compared to control ($p<0.001$), whereas treatment with SAP alone was associated with <10% increase in mean signal intensity (fig. 5.3). Treatment with $TPPS_{2a}$ + SAP (PCI) caused a 69% reduction in signal intensity, which corresponds to 90% and 77% reduction compared to PDT or SAP alone, respectively ($p<0.001$) (fig 5.3 and 5.4).

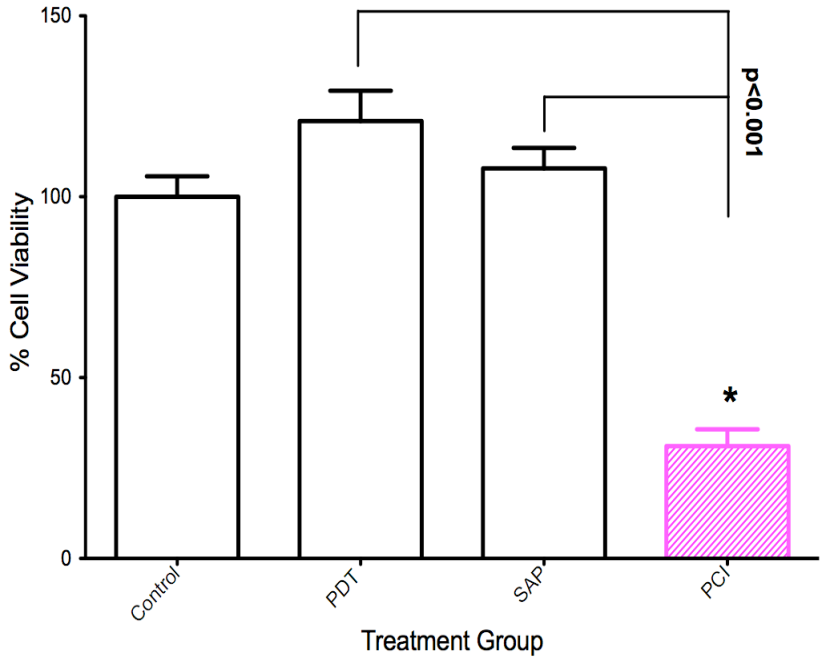

Figure 5.3. 4T1 Tumoroids $TPPS_{2a}$ + SAP Photochemical Internalisation.
4T1 cells were seeded into collagen constructs at 5 x 10^5 ml^{-1} and grown for 7 days @ 37°C prior to 24h incubation with either $TPPS_{2a}$ (PDT, 0.8µg ml^{-1}), SAP (60 nM) or both (PCI). Cells were incubated with AlamarBlue® for 4 hours at 37°C, 7 days after light exposure (180 seconds). Ex. 570 nm, Em. 610 nm. *69% cytotoxicity ($p<0.001$). n=3

5.3 Histological Analysis

Planned histological studies on the samples that had been fixed with formalin and stored unfortunately had to be curtailed as the samples were mistakenly destroyed within the multi-user laboratory. Therefore, it was not possible to perform H&E staining to visually assess cytotoxicity.

DISCUSSION

This chapter focused on the development of a novel 3-D cancer model from 4T1 murine breast cancer cells, grown in a dense artificial tumour mass, surrounded by a non-dense hydrogel in the guise of previously published data(50). The compression model utilised in this study appears to be a suitable method for 3D tumour development with 4T1 cells in support of evidence in the literature about the versatility of this technique(160). Within the artificial tumour mass, the formation of spheroids could be seen at day 7 on light microscopy, with the greatest rate and density of growth at the margins of the mass. This may indicate more favourable growth conditions at the periphery and supports the findings in the literature where oxygen measurements found the centre of the mass to be hypoxic(50).

These cytotoxicity results support the *in vitro* findings of the main PCI chapter, where cells treated with a combination of SAP and $TPPS_{2a}$ exhibited a greater level of cytotoxicity compared to control or either agent alone. This novel piece of work not only supports the need for further studies into the 3-D tumour masses as a platform for evaluating cancer growth and therapeutics, but supports the findings of *in vivo* studies where PCI has been shown to be effective in delaying tumour growth and progression(43, 44). Such work using 3-D compressed collagen tumour scaffolds for PCI experimentation has never been investigated. The level of cell death achieved is particularly interesting, especially in the context of what appears to be a growth response to SAP or PDT alone. Given the cytotoxicity assay was performed 7 days after activation of the photosensitiser with light, the results shown in figure 5.3 may actually show a picture of tumour regrowth in all treatment groups. Thus, it may be possible that PCI in fact delayed regrowth and this has been postulated following the findings of previous *in vivo* data where the PCI was used to enhance the deliver of bleomycin into implanted HT1080 tumour mass(44). Nevertheless, the regrowth phenomenon, beyond control, has been reported(25) and may represent the activation of survival and proliferative second messenger pathways in response to a sub-lethal therapeutic 'insult'. Such a response highlights the importance of maximizing drug delivery, particularly at relatively

low doses of drugs with narrow therapeutic indices in order to avoid such a phenomenon.

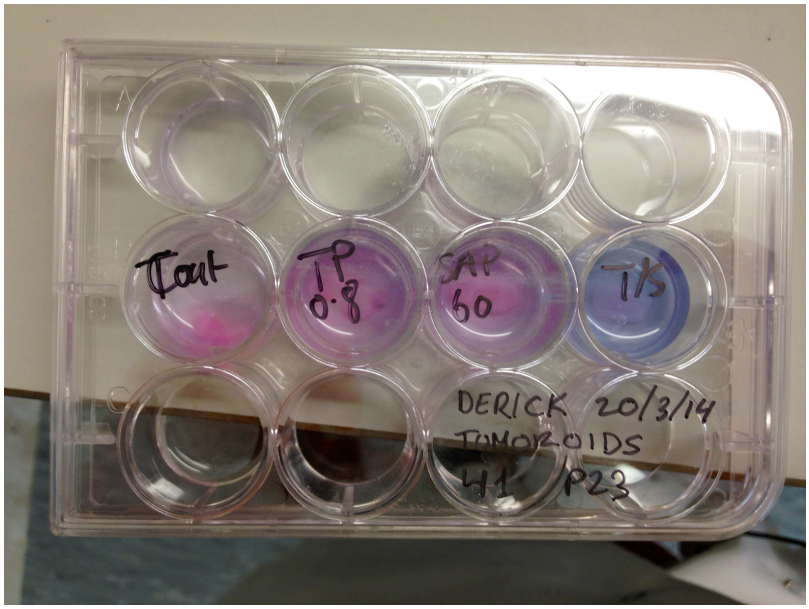

Figure 5.4 – Visualisation of AlamarBlue® assay.
Cells were incubated with AlamarBlue® for 4 hours at 37°C, 7 days after light exposure (180 seconds). **Cont** = Control, **TP 0.8** = $TPPS_{2a}$ (0.8 µg/ml) + light (PDT group), **SAP 60** = Saporin 60 nM, **T/S** = $TPPS_{2a}$ (0.8 µg/ml) + SAP 60 nM + light (PCI group). Live cells reduce AlamarBlue® causing a shift in fluorescence from Blue to red/pink. Therefore, the blue in the T/S well indicates reduced live cell density/number.

Despite the promising results from the AlamarBlue® assay, the lack of histological data does limit the impact of the data presented in this study. Figure 5.5 shows an example of what can be observed following H&E staining of colorectal cancer tumoroids(50).

The clarity of the images obtained indicates that this might be a suitable initial stain to visually assess the impact of PCI treatment on tumoroid density and distribution compared to control, PDT and SAP alone. There is no dispute that further work is required, in particular the development of an active tumour stroma as this would enable further investigation of the impact of PCI on the stroma including anti-tumour immunomodulation and angiogenesis(26).

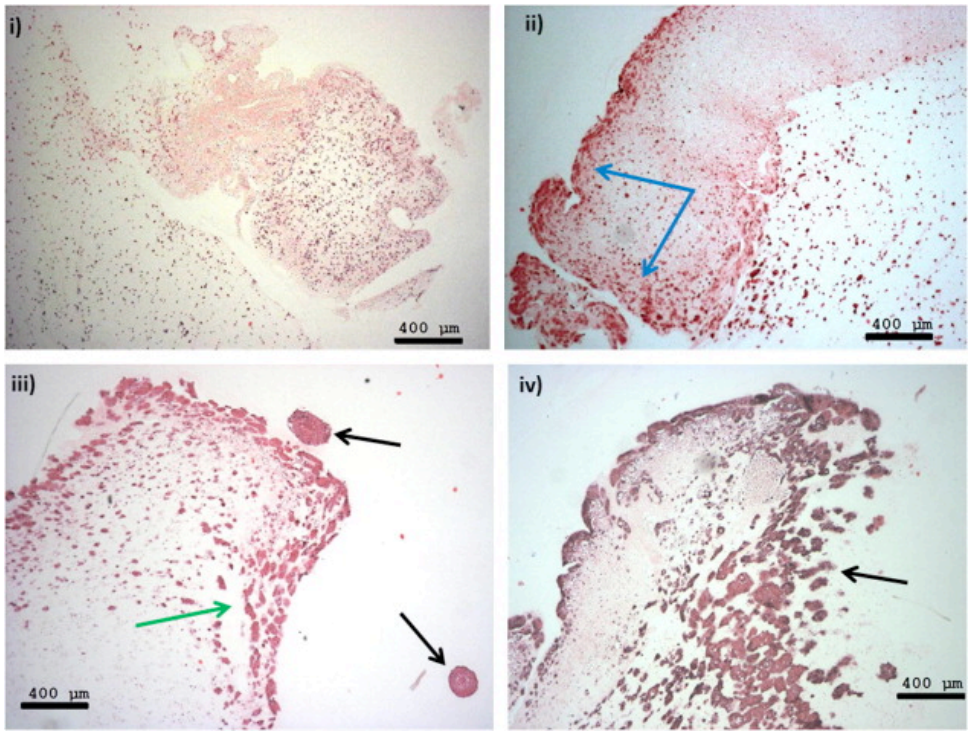

Figure 5.5 – Morphology of HT29 colorectal cancer cells (2,000,000 cells ml^{-1}) in an ACM situated within an uncompressed acellular collagen gel (H&E staining).
Day 1 showing an equal distribution of cells within the ACM; (ii) day 7 showing accumulation of cells at the edge of the ACM (blue arrows); (iii) day 14 showing formation of cell spheroids (green arrows) and migration into the surrounding matrix (black arrows); (iv) day 21 showing escape of the cell spheroids into the surrounding matrix (black arrow). Scale bar 400 µm. Image and legend from Nyga et al. (2013)(50)

Chapter 6: Bioluminescent Photodynamic Therapy

SCIENTIFIC BACKGROUND

The activation of photosensitisers following absorption of light energy has been described in chapter 3 and will only be briefly described here for the sake of clarity. Photodynamic therapy (PDT) utilises the unique properties of photosensitive compounds, which upon excitation with light of specific wavelengths in the presence of molecular oxygen results in the formation of reactive oxygen species. These free radicals, including singlet oxygen, are highly reactive and can trigger apoptosis following reactions with cellular organelles, leading to cell death. The photosensitisers tend to possess a similar basic structure comprising a heterocyclic ring comparable to chlorophyll and haem(161).

Clinically, PDT has been utilised in the treatment of various conditions including: localised dermatological lesions (including tumours). The premalignant lesion actinic keratosis was the first approved dermatological condition for which PDT was indicated. The use of the endogenous photosensitiser protoporphyrin IX (PpIX) via administration of exogenous 5-aminolaevulinic acid (ALA)(162) resulted in beneficial effects seen at long-term follow-up with projected disease free rates of 71%(163, 164). PDT is currently one of the recommended therapeutic options (National Institute of Clinical Excellence, NICE) for the premalignant condition, Barrett's oesophagus; for patients with high-grade dysplasia(165). It is also used for the treatment of ophthalmological conditions (including proliferative retinopathy).

Photochemical internalisation is an evolution of PDT that makes use of the localised toxicity of PDT to facilitate the delivery of macromolecules into cellular organelles. The potential applications of PCI include gene delivery and cytotoxic drug delivery; the latter has been demonstrated to help reverse the multidrug-resistant phenotype in cancer cells *in vitro*/*in vivo*(26).

A specific drawback of PDT/PCI is the limited level of tissue penetrance of light that can be achieved(2). Strategies that have been tested to reduce the limiting effect of this includes the use of fibre-optic light sources and the use of red emitting photosensitisers as light > 600 nm wavelength enables deeper tissue penetration(36). However, at present, deep lying tumours and distant

metastases lie outside of the therapeutic range of both PCI and PDT. Although strategies aimed at circumventing the problems with tissue penetrance have been developed, such as fibre optic light sources(2), technical limitations to their use still apply. Therefore, the challenge is to optimise the cytotoxic profile of PDT and PCI for both topical and deep lying tumours and distant metastases.

6.1 Bioluminescence

Firefly Luciferase (Fluc) is a 61 KD monomeric enzyme that catalyses the above reaction using D-Luciferin as a substrate(166). Although Fluc is the leading bioluminescent system utilised in scientific investigations, particularly animal imaging studies, others do exist including:

- Luciferase produced by the click beetle (*Pyrophorus plagiophthalamus*) – catalyses D-Luciferin emits green-orange @ 540 nm and red @ 611 nm(167)
- *Gaussia luciferase* from the marine copepod and *Renilla luciferase* from sea pansy – catalyse coelenterazine to emit blue light (480 nm)(51).

Bioluminescent systems, particularly those based on Fluc have a variety of applications that have been developed in recent years. The use of Fluc as molecular probes has been exploited to aid the detection of toxins and bacteria found in the natural environment(168, 169). Fluc has also been used for bioluminescence resonance energy-transfer (BRET) to assay a range of biomolecular interactions including red-fluorescent protein to monitor glutathione S-tranferase(170).

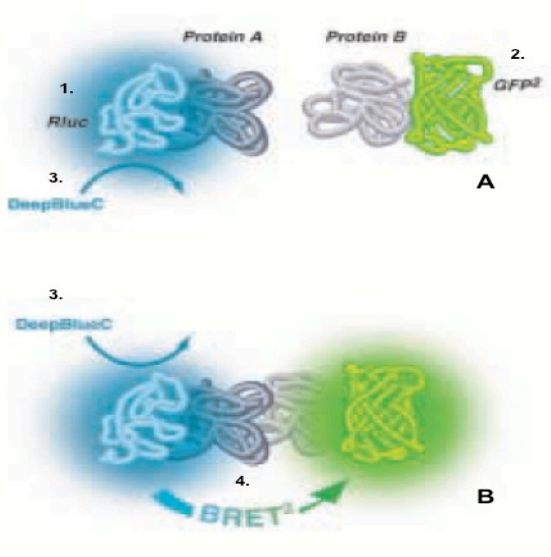

Figure 6.1 – Illustration of Bioluminescence Resonance Energy-transfer.
1. *Renilla luciferase*. **2.** Green fluorescent protein (GFP), **3.** DeepBlueC (coelenterazine-like luciferin), **4.** BRET process. In **A.** the donor and acceptor are too far apart for BRET to occur efficiently, therefore there is no activation of GFP. However, in **B.** the close proximity enables efficient energy transfer and subsequent activation of GFP. Image from Packard Bioscience (BioSignal Packard Inc. (171)

BRET is a naturally occurring phenomenon(172), which has been developed into a biochemical tool that is based on efficient resonant energy transfer (RET) between a bioluminescent (luciferase) donor molecule and a fluorescent acceptor molecule such as green fluorescent protein (GFP) (fig. 6.1). RET is a form of radiationless energy transfer from a donor to acceptor(173). Important factors to consider when aiming to enhance the efficiency of BRET are to limit the distance between the donor and acceptor molecule(61-63) and aim for good donor emission and acceptor absorption spectral overlap.
Of particular relevance to cancer biology, Fluc has been used to monitor *in vivo* growth(174) and metastasis(175) of tumours. It is the availability of such technology that led to the choice of the 4T1 (Luc1) breast cancer cell line for the majority of studies in this thesis as it could potentially be used to monitor tumour growth and treatment response in bioluminescent *in vivo* models.

The aim of the studies in this chapter was to challenge the null hypothesis that bioluminescence cannot sufficiently activate a photosensitiser to mediate PDT

or PCI in 4T1 (Fluc) and MCF7 (Gluc) breast cancer cells. The work using Gluc expressing cells for PDT is novel.

Initial work was performed using the Gluc expressing MCF7 cells. However, given the blue-shifted emission of these transduced cells along with the difficulties associated with using the unstable compound coelenterazine in the lab, the more suitable 4T1 cells with a stable Fluc transduction were purchased and used.

6.2 Photosensitisers

The chosen photosensitisers for bioluminescent studies in the genetically modified cell lines will be described below.

6.3 Hypericin

Hypericin is an anthraquinone, which is synthesised by the *hypericum* genus of plants(176) and is believed to be one of the most powerful naturally occurring photosensitisers(25). Agostinis et al. (2002)(177) described hypericin as exhibiting fundamental characteristics that are beneficial to its use as a photosensitiser, specifically i) high singlet oxygen yield following photoactivation, ii) intense fluorescence and iii) minimal dark cytotoxicity. It is important to note that it is reported in the literature that hypericin can also induce other ROS production such as superoxide(178), albeit at lesser amounts. Hypericin has been shown to be an efficacious photosensitiser when used for PDT on a range of cell types including fibroblasts(179), keratinocytes(180) and malignant human breast (MCF7) and bladder (MGHU1) cancer cells(25). The photodynamic efficacy of Hypericin was first observed in sheep and cattle grazing on the *Hypericum* species, which resulted in cutaneous lesions(180, 181). Furthermore, it has been reported that much like sulfonated aluminium phthalocyanine, hypericin appears to exhibit lipophilic properties that enable it to become incorporated into cellular lipid membrane structures(177) and, more specifically, by liposomes(180). This property was exploited by Adigbli et al.(25) who demonstrated that hypericin can be used for PCI in breast and bladder cancer cells. Finally, hypericin has multiple absorption peaks at wavelengths

including ~475 nm, ~540 nm and ~590 nm(182), which is a good overlap with the Fluc emission to be used in this study.

6.4 Tetrabromorhodamine-123

Tetrabromorhodamine-123 (TBR) is a halogenated form of the mitochondrial probe (dye) rhodamine-123(130). Substitution of hydrogen with bromine results in the formation of a photosensitiser that is more likely to induce efficient formation of singlet oxygen(183), in terms of the light energy absorbed (also known as the 'quantum yield'). The efficiency is enhanced by intersystem crossing, a process whereby there is non-radiative transition between the excited singlet state and excited triplet state. Intersystem crossing is more rapid in the presence of a heavy atom such as iodine or bromine, thereby increasing the efficiency of triplet state formation(184). The efficiency of generating singlet oxygen and other ROS (such as superoxide) is in turn increased with efficient generation of the triplet state. This consequently significantly increases the phototoxicity of TBR compared to rhodamine-123, rendering the latter a less suitable option for PDT. Tetrabromorhodamine 123 can be used to generate singlet oxygen ($^1O_2$) in mitochondrial membranes. The dye has a quantum yield for singlet oxygen generation of 0.65-0.7 and is particularly toxic to carcinoma cells. Ex\em(MeOH) = 524/550 nm, ε (MeOH) = 91,000(185).

RESULTS

6.5 Flow cytometry for MCF7 Luciferase transduction

Following fluorescence-activated cell sorting (FACS) of the three different cell samples: wild type MCF7, MCF7-Fluc and MCF7-Gluc, flow cytometry was performed in order to determine the transduction efficiency. The control (MCF7, wild-type), were appropriately negative for Fluc or Gluc expression (fig. 6.2). Those cells that underwent Fluc transduction were shown to be 91% expressive for the tagged CD34 biomarker (fig. 6.3). The Gluc cells were found to be were found to have a transduction efficiency of 85%.

Unfortunately, due to problems encountered with the growth of the MCF7-Fluc cells following transduction and FACS it was decided to abandon this cell line for further experimentation.

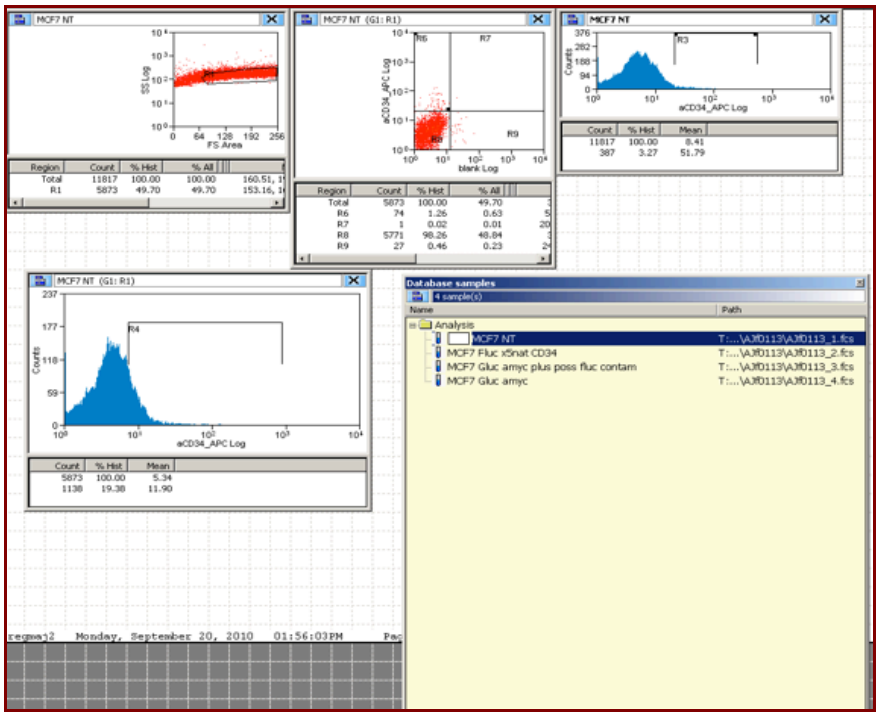

Figure 6.2 – Flow cytometry of wild type MCF7 (breast cancer) cells.
Over 98% of cells were identified as wild type. This was determined by positive bio-detection of neurotensin with no detection of CD34 (Fluc) or a-myc-FITC (Gluc).

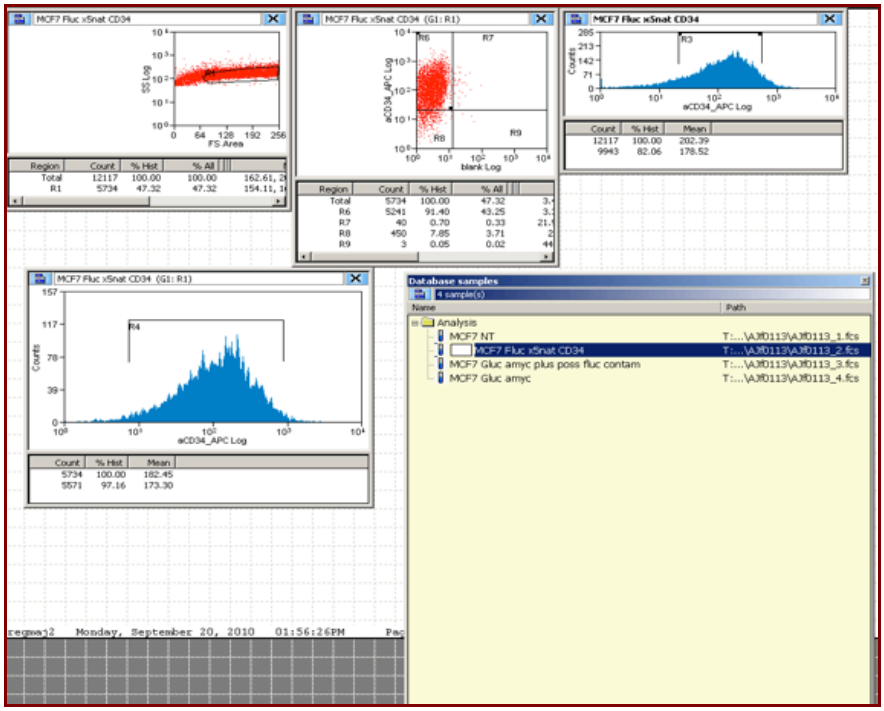

Figure 6.3 – Flow cytometry of wild type MCF7-Fluc (*firefly* luciferase) cells.
Over 90% of cells were positive for the CD34 biomarker indicating successful Fluc transduction.

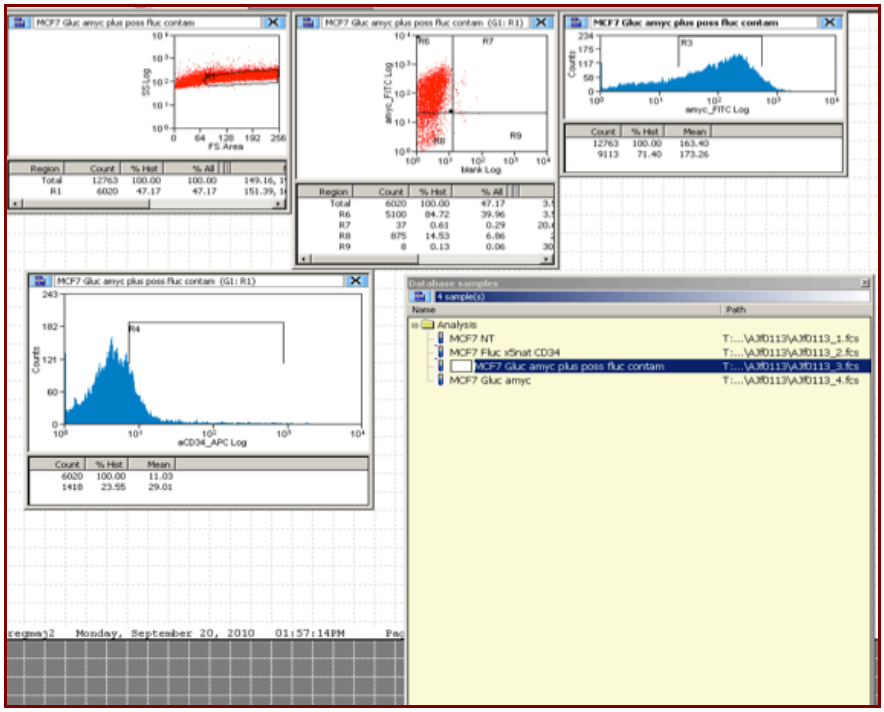

Figure 6.4 – Flow cytometry of wild type MCF7-Gluc (*Gaussia* luciferase) cells.
85% of cells were positive for the a-myc-FITC biomarker indicating successful Gluc transduction.

6.6 MCF7-Gaussia Luciferase emission spectra and kinetics

Following assessment of the transduction efficiency, spectral analysis was performed for the Gaussia luciferase. The analysis was commenced using coelenterazine as a substrate for Gluc. Two peaks were observed at ~460 nm and ~490 nm, which may indicate two distinct cell populations (fig. 6.5). Analysis of the emission kinetics was also performed on the MCF-Gluc cells. The graph shows that the intensity of the bioluminescent signal reduces by a factor of >8.5-fold within the first 180 s (fig. 6.6).

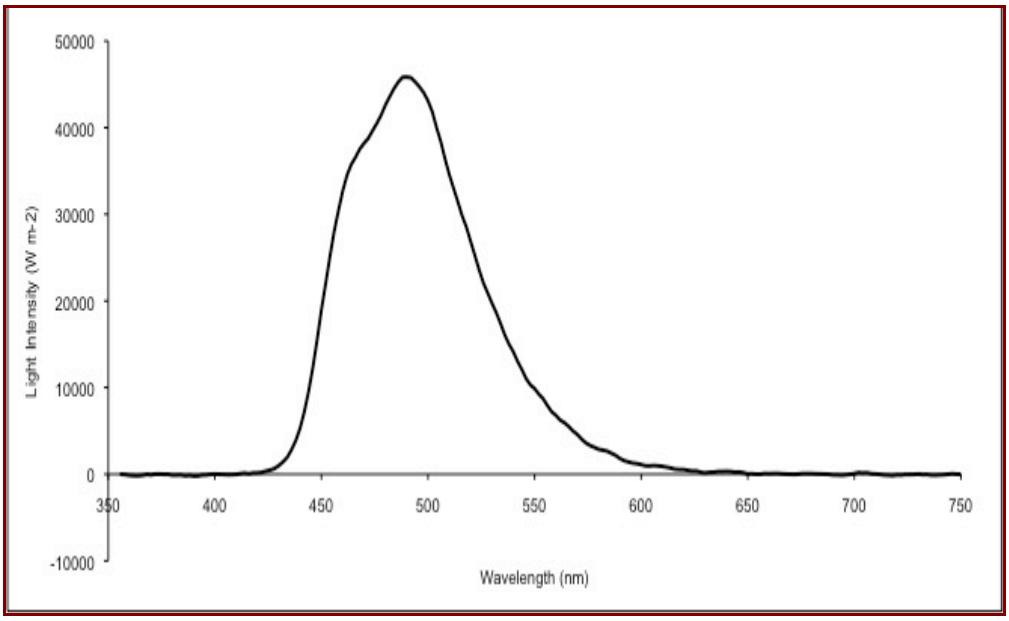

Figure 6.5 – Gaussia Luciferase emission spectrum.
The emission spectrum of Gaussia luciferase was assessed using MCF7-GLuc (transduced breast cancer cell line). Spectra acquired following the addition of coelenterazine (25 μg ml^{-1}). Two peaks: (1) at ~460 nm, (2) at ~490 nm (the graph plots a moving average).

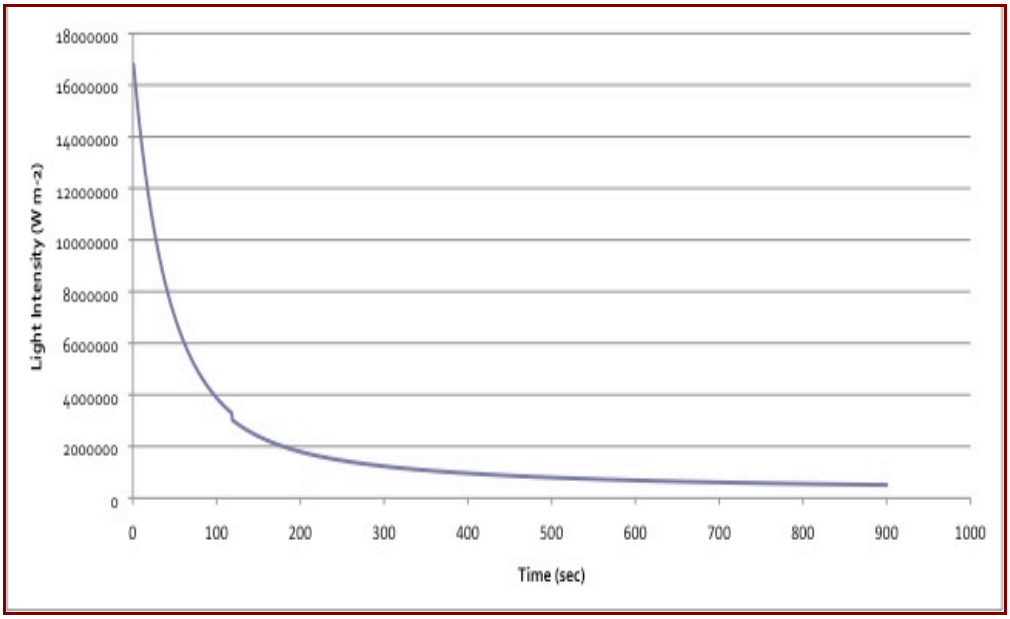

Figure 6.6 – MCF7-Gluc emission kinetics.
The emission kinetics of Gaussia luciferase expressing MCF7-GLuc cells was assessed. Data acquired over 900 s following the addition of coelenterazine (25 µg ml^{-1}).

6.7 MCF7 Gaussia luciferase mediated Photodynamic Therapy

Modified PDT experiments were carried out to assess the level of cytotoxicity that could be elicited using the bioluminescent model. Cytotoxicity was calculated using the MTT assay, 4 hours after treatment with coelenterazine (light).

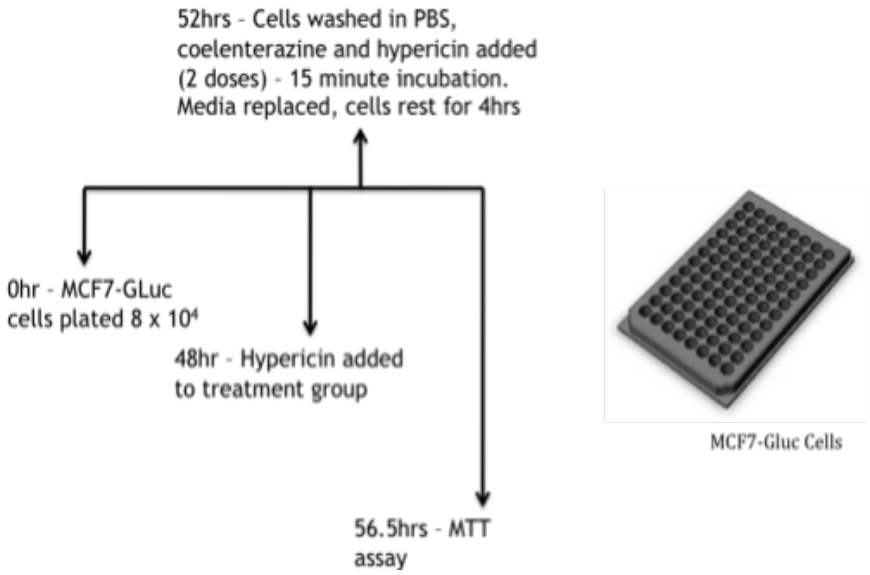

Figure 6.7 – Experimental timeline for Gluc-Hypericin bioluminescent PDT

Two back-to-back 15-minute incubation periods were used to treat the cells with coelenterazine (fig. 6.7). This was chosen following pilot experiments and based on the emission kinetics of the MCF7-Gluc (fig. 6.6).

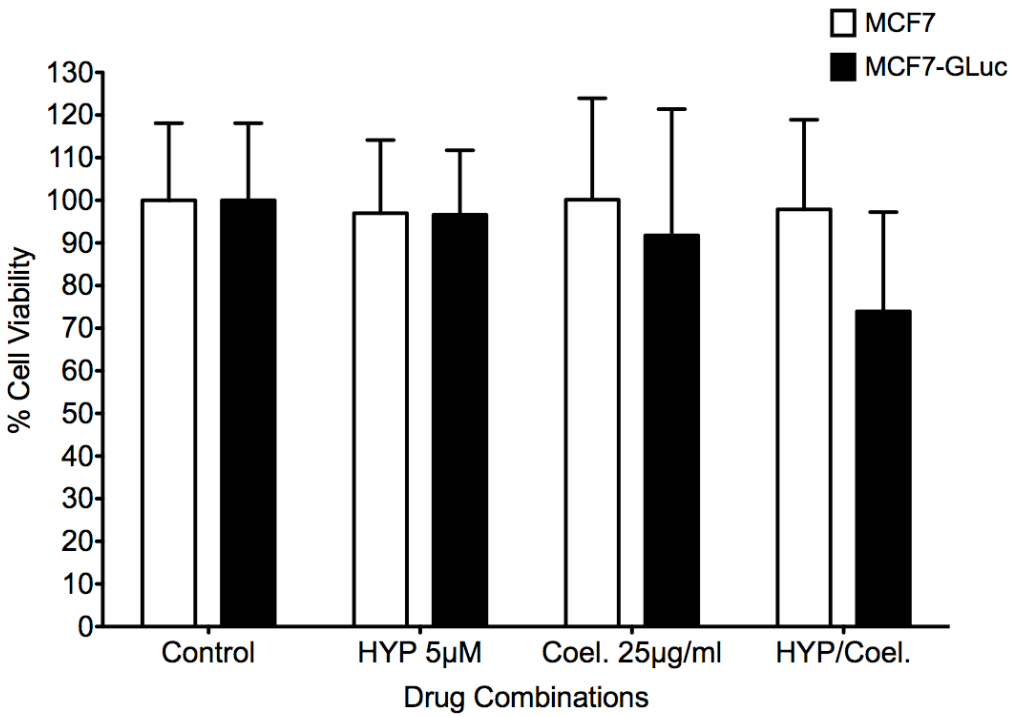

Figure 6.8 – MCF7 wild type vs. MCF7-Gluc – mediated PDT.
Both cell lines were treated with either hypericin ('dark' control, 5μM) or coelenterazine (25μg/ml) alone or in combination (PDT). Combination of HYP/Coel. Achieved <2% cell kill (MCF7) compared to 27% (MCF7-Gluc, $p<0.05$).

Both cell lines had no measurable cytotoxicity in response to treatment with HYP (4h, 5 μM) alone without light. There was no significant difference in cell kill following exposure to coelenterazine (2 x 900 s, 25 μg/ml) with both exhibiting <10% cytotoxicity. The combination of HYP + coelenterazine (PDT-group) did however result in significant cell kill within the Gluc group, with 27% and 25% increased cytotoxicity compared to MCF7-Gluc (control) and MCF7 respectively ($p<0.05$). The greatest level of cytotoxicity observed for MCF7-Gluc (PDT-group) compared to HYP or coelenterazine alone was not statistically significant, albeit achieving 23% and 18% increased cell kill respectively (fig. 6.8).

Despite repeated attempts to optimise the coelenterazine-Gluc system, due to the pressures of time and the difficulty in limiting the oxidation of coelenterazine during experimentation the decision was made to abandon this line of investigations and search for an alternative Fluc-based cell model that would enable the use of the more stable D-luciferin. To this end, it was decided to purchase a stable Fluc expressing murine breast cancer cell line (4T1-luc2) from Caliper Lifesciences.

6.8 4T1-Firefly Luciferase emission spectrum

This was performed to confirm the emission for the 4T1 cell line. Peak emission was at ~549 nm (fig. 6.9). In order to enhance the potential of the 4T1 model a second photosensitiser, tetrabromorhodamine-123 (peak excitation ~514 nm), was also tested for bioluminescence-induced PDT.

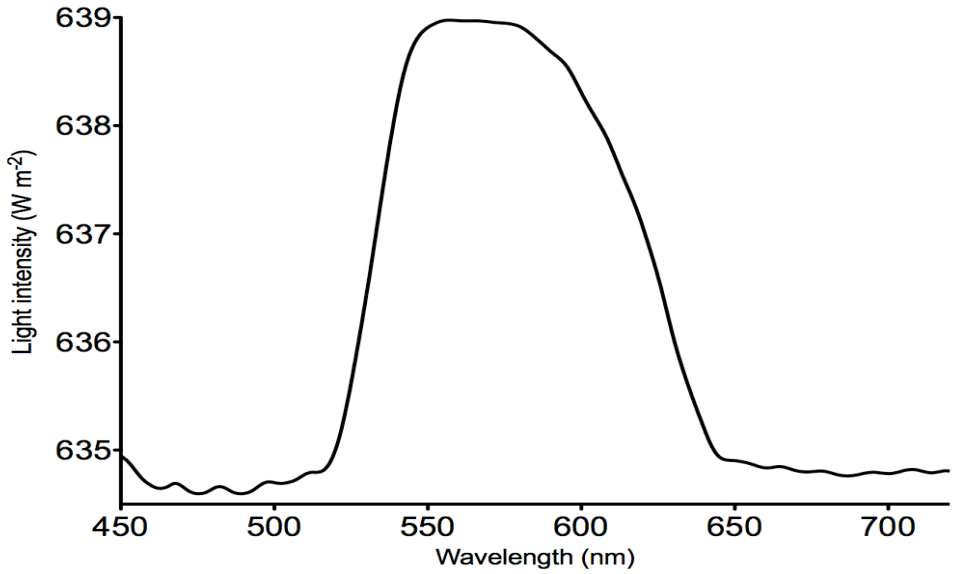

Figure 6.9 – 4T1-Firefly Luciferase emission spectrum.
The emission spectrum of Firfly luciferase expressing 4T1 (stably transfected murine breast cancer cell line) was assessed. Spectra acquired following the addition of addition of D-luciferin (20 μM). Peak at ~549 nm (the graph plots a moving average).

6.9 Tetrabromorhodamine-123 mediated bioluminescent PDT in 4T1 cells

PDT experiments were carried out using a similar protocol to that employed for Gluc-coelenterazine protocol described above (fig. 6.10). The main differences included the use of D-luciferin and TBR *in lieu* of coelenterazine and hypericin respectively.

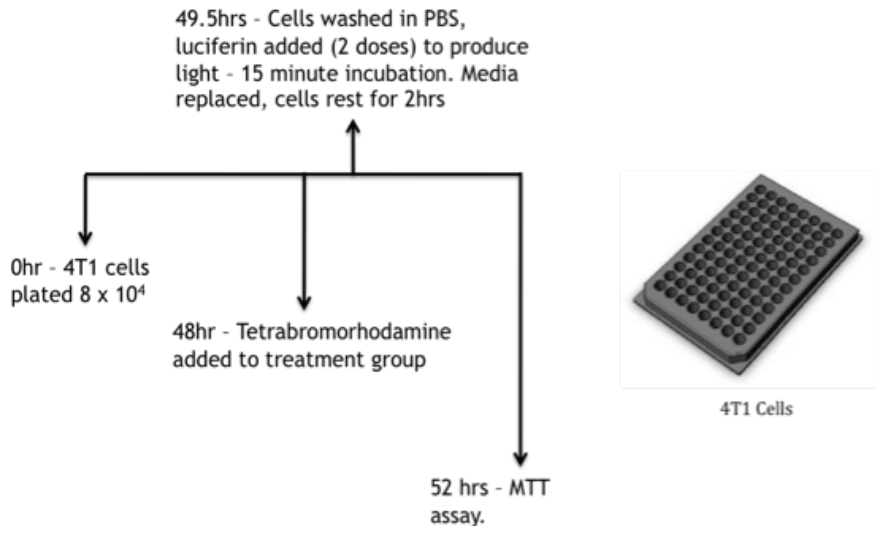

Figure 6.10 – Experimental timeline for 4T1-TBR bioluminescent PDT.

A set of studies looking into the effect of increasing the concentration of TBR (1.0, 3.0 and 5.0, μM) demonstrated a dose dependent rise in cytotoxicity when the concentration of D-luciferin (D-Luc) was kept constant (20 μM) (fig. 6.11). These were performed both in the absence of ('dark' control) and the presence of D-luciferin. At 1 μM TBR the addition of D-Luc resulted in <10% increase ($p>0.05$) in cytotoxicity compared to TBR 1 μM alone. However, in comparison to control this represents 14% cytotoxicity ($p<0.01$). At 3 μM TBR the cytotoxicity within the D-Luc group increased to 39% ($p<0.01$), which correlates to a 22% increase compared to TBR 3 μM alone. Finally, at 5μM TBR cytotoxicity further increased to 69% ($p<0.01$) compare to control. This translates to a 34% increase ($p<0.01$) in cytotoxicity compared to TBR 5 μM alone. D-luciferin (20 μM) alone exerted a cytotoxic effect of 7% ($p<0.05$) compared to control. The importance of this is that it indicates that cytotoxicity seen at TBR 3 μM and 5 μM in the D-Luc group is not due to D-luciferin toxicity alone.

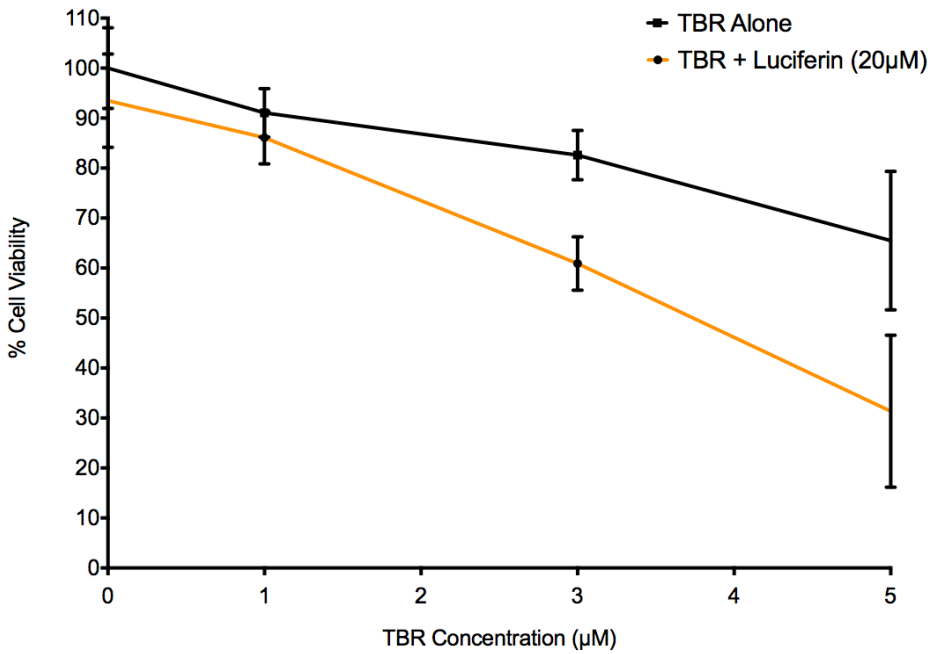

Figure 6.11 – 4T1-TBR bioluminescence PDT dose response.
Cells were treated with increasing concentrations of TBR for 90 minutes prior to addition of D-luciferin (2 x 900 s, 20 μM). Cell viability quantified using MTT assay 2hrs after cells exposed to D-Luciferin. At 5 μM TBR + 20 μM D-luciferin cytotoxicity = 69% ($p<0.01$). Background D-luciferin toxicity = 7% ($p<0.05$).

6.10 Role of Reactive Oxygen Species in TBR-mediated bioluminescent PDT

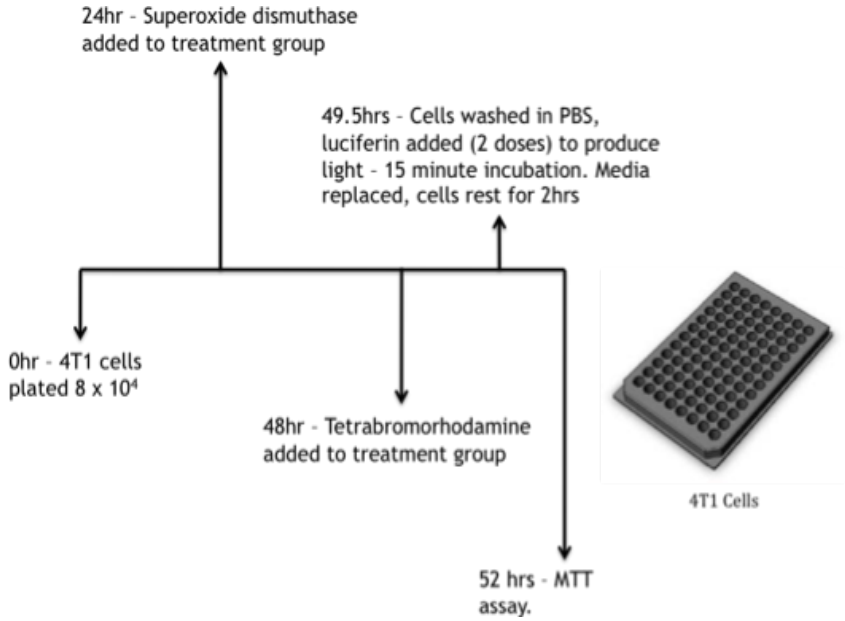

Figure 6.12 – Experimental timeline for 4T1-TBR bioluminescent PDT +/- superoxide dismutase.

Work discussed within the PCI chapter of this thesis considered the role of ROS in PDT and PCI, specifically investigating the role of the REDOX environment with regard free radical potentiation and quenching. In this section of the bioluminescence studies, the effect of ROS quenching on the cytotoxicity of potential bioluminescent PDT will be assessed as a means for proof of principal (fig. 6.12).

The chosen antioxidant/reducing enzyme, superoxide dismutase (SOD), has previously been discussed in the PCI chapter. When SOD treated cells underwent bioluminescent PDT using TBR 0.5 μM + Luc 25 μM a 12% ($p<0.01$) reduction in cytotoxicity was observed compared to TBR + Luc (PDT) alone, which equated to a 2.2-fold reduction (fig. 6.13, $p<0.01$). This protection resulted in a level of cell kill that statistically was no different from control, TBR 0.5 μM or Luc 25 μM alone.

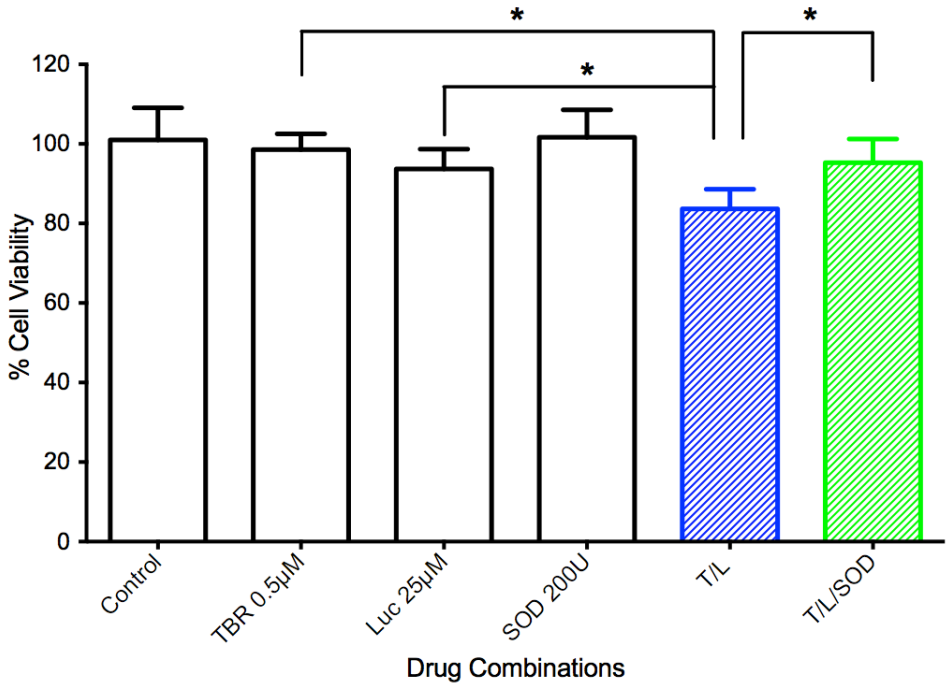

Figure 6.13 – 4T1 low dose TBR bioluminescent PDT +/- superoxide dismutase.
Cells were treated with variable drug combinations to assess the efficiency of SOD-mediated reduction of the bioluminescent PDT effect. Cells in the SOD or TBR + Luc + SOD (T/L/SOD) groups were treated with SOD for 24h prior to addition of TBR and during the 2h post-Luc incubation time prior to MTT. 2.2-fold reduction was observed for T/L/SOD compared to T/L. * = $p<0.01$

6.11 Hypericin-mediated bioluminescent PDT in 4T1 cells

An identical protocol to the HYP study with the MCF7-GLuc cells was used for the 4T1 cells. Figure 6.14 illustrates that upon combining HYP + Luc, 27% of cells were killed ($p<0.01$) compared to control. Adjusted for background levels of toxicity exerted by D-luciferin (5%, $p>0.05$), this represented a 4-fold increase in cytotoxicity. HYP alone ('dark' control) killed <10% of cells ($p<0.01$), whilst the addition of D-luciferin resulted in a 17% increase ($p<0.01$) in cytotoxicity (fig. 6.14).

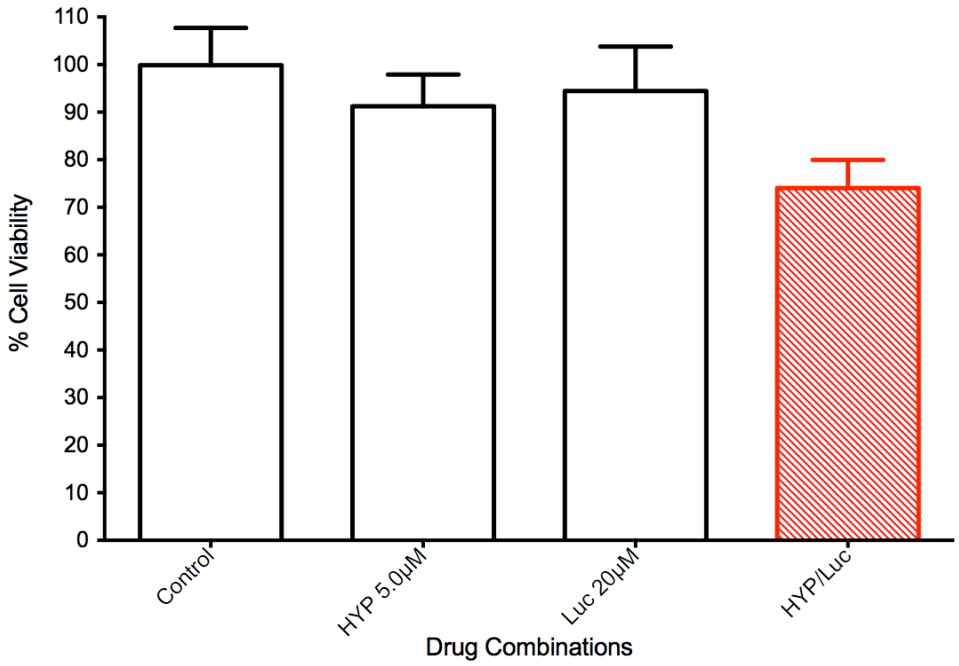

Figure 6.14 – Hypericin-mediated bioluminescent PDT in 4T1 cells.
Cells were treated with either hypericin (HYP, 'dark' control, 5 μM) or D-luciferin (Luc, 20 μg ml^{-1}) alone or in combination (PDT). Combination of HYP/Luc achieved 27% and 17% cell kill compared to control (no treatment) and 'dark' control (HYP alone), respectively ($p<0.01$).

DISCUSSION

PDT is a relatively well-developed technique with a reasonable evidence base both in the pre-clinical and clinical arenas(2). The mechanisms that underpin light-activation of photosensitisers, which in the presence of molecular oxygen results in the formation of ROS that can subsequently cause oxidative damage to cellular structures leading to repair, mutation or death of a cell. In the USA, Porfimer sodium (Photofrin®) is licensed for the treatment and to relieve symptoms of oesophageal and non-small cell lung cancer(2); in addition to the treatment of the premalignant lesions in Barrett's oesophagus(186). Three of the most well described limitations of PDT are:

I. Low tissue penetrance, with red light only able to pass through approximately 1 cm of tissue, restricting the use of PDT to luminal organs and the skin(187).

II. Limited efficacy for large tumours, again due to inability of light to penetrate deep into tissue(188-190).

III. No indication for non-focal/metastatic disease spread(190).

These limitations are partially negated with the development of tools to enhance accessibility to the tumour site, such as fibre optic light sources. However, the potential of generating light from either within on around the target cell could potentially go some way to circumventing these limitations. In this study, MCF7 breast cancer cells were successfully transduced with two types of Luciferase. This initial step of any gene therapy is fundamental in order to determine the feasibility such therapeutic options. Many examples exist in the literature including transfection of the Herpes Simplex Virus thymidine kinase (HSVtk), a target for antiviral agents such as ganciclovir to trigger death of an infected host cell *in vitro*(191). Such a technology has also been combined with neurotensin targeted nanoparticles carrying the HSVtk and ganciclovir for the transfection of HSVtk into adenocarcinoma xenografts grown in athymic mice where HSVtk expression plus ganciclovir treatment resulted 55-60% reduced tumour growth(192).

The main difficulty faced during the planning phase for these bioluminescent studies was to find a suitable photosensitiser that had an absorption peak to match the emission of the transduced cells. Hypericin was chosen due to its appropriate absorption/emission overlap and evidence of its suitability for PDT in MCF7 cells in previously published work(25). The failure of MCF7-GLuc – coelenterazine model to achieve cytotoxicity that was significantly superior to coelenterazine or HYP (fig. 6.8) could in part be due to the preparation of coelenterazine, which was dissolved in 100% ethanol prior to dilution. Furthermore, given that GLuc is secreted by the cells into the surrounding media(193), whereas hypericin has been shown to accumulate within intracellular organelles including the endoplasmic reticulum and Golgi apparatus(194); this may result in inefficient photosensitiser activation, owing to too great a distance between luciferase and photosensitiser for efficient BRET(61-63). To overcome this it might be advisable to repeat the experiment with hypericin present in the media, thus increasing the likelihood of photoactivation.

The 4T1-luc2 cell line afforded a more robust and reproducible model for bioluminescence-activated PDT. The stable transfection in this cell line showed that this study is a step forward from previous bioluminescent PDT studies performed when less stable transfection constructs were utilised(195). Given the 4T1-luc2 cell line was harvested from a murine model also presented the opportunity for using bioluminescence as a means for non-invasive monitoring of tumour growth and treatment response. The dose-dependent rise in TBR-mediated – Fluc bioluminescent PDT represents a very promising finding. In addition, the dose-dependent rise in toxicity appears to be greater than the effect of a rise in TBR concentration alone. This is illustrated by a 2.9-fold increase in 'dark' toxicity between 1 μM-5 μM, whereas a 3.9-fold increase is observed between the same dose-range in the presence of D-luciferin. This was supportive of photoactivation of TBR, resulting in a disproportionate rise in cell kill compared to TBR alone. Of particular importance is that this cytotoxic effect appeared to be independent of background D-luciferin cytotoxicity. It is important to put this finding in comparison with other novel systems that aim to

overcome the challenges faced by conventional PDT. One such example is fluorescence resonance energy transfer (FRET) where the initial fluorescence of one molecule (donor) is used to photoactivate another (acceptor), a similar model to the BRET system explained in the scientific background section. Li et al. (2012) demonstrated that quantum dots could act as donors to trigger singlet oxygen production from sensitised sulfonated aluminium phthalocyanines for PDT in cancer cells(196).

The experiment looking at the ability of SOD to reduce the apparent phototoxic effect of bioluminescence activated PDT was performed in order to obtain evidence supportive of ROS production within this bioluminescence PDT model. Given that these experiments were performed at the very beginning of the PhD, the L-histidine model for ROS-quenching had not yet been developed. As described in chapter 3, SOD plays an important role in scavenging superoxide radicals, thus the inhibitory effects observed for low-dose TBR-mediated bioluminescent PDT support the presence of ROS and consequently the photoactivation of TBR via the oxidation of D-luciferin by FLuc expressed within the cytoplasm of 4T1 cells (fig. 6.13). The cytoplasmic localisation of FLuc to organelles including peroxisomes(197) may explain the improved cytotoxic efficacy when used with hypericin (fig. 6.14).

Overall, it is not possible to conclude from this study that bioluminescence-mediated PDT is an active solution to the problems faced with conventional PDT but it certainly provides an exciting and challenging avenue that could potentially prove extremely useful. However, there have been positive reports regarding the use of bioluminescence to mediate PDT in cancer, including *in vivo* melanoma(198).

One of the first hurdles that must be overcome is that of efficient transfection that does not trigger an immune response in the host, which would otherwise render the vector and genetic material inactive. Furthermore, the bioluminescence signals must be enhanced to boost tissue penetrance, though at present further red-shifted luciferases are being engineered, for example firefly

Luciferase with peak emission at 617 nm(199). Given the relatively reduced level of ROS production required for PCI versus PDT as described in chapter 3 bioluminescence may have a more applicable role in PCI, however, this work was not achievable within the scope of this PhD but is certainly worth investigating for further work. Another potential avenue to explore is utilising quantum dots for BRET to boost the bioluminescence signal and this may prove particularly useful if constructs could be made that bring the photosensitiser into close proximity with the luciferase, which should enhance the efficiency of energy transfer from donor to acceptor(61-63). A potential solution may be found by using genetically encoded photosensitisers such as KillerRed (Evrogen, Moscow, Russia). This protein, the first of its kind(200), can be expressed in cells with the photosensitiser targeted to different cellular compartments including membrane or mitochondria. Although activated by green light, such a construct may be the first steps to developing blue (GLuc-activated on membrane) or red (FLuc-activated within cytoplasm) BRET-KillerRed systems for PCT/PCI *in vitro*. Unfortunately, although this experiment was investigated, the logistical and funding restrictions meant it wasn't a viable option for this PhD study.

Chapter 7: Concluding remarks

7.1 CHALLENGES OF CELLULAR DRUG DELIVERY

Inefficient delivery of therapeutic molecules to their site of action is a significant limiting factor in the medical treatment of cancer(25). Conventional anticancer drugs mainly exert their cytotoxic effect by gaining access to the nucleus or mitotic machinery of a cell, for example, mitoxantrone (anti topoisomerase) and docetaxel (anti-microtubule). In order to reach such a target many obstacles must be overcome including the bioavailability and systemic metabolism of the therapeutic molecule and at the cellular level, gaining access to the intracellular compartment. Highly lipophilic agents including steroids, which do form part of many anti-cancer treatment regimens, have excellent cellular absorption kinetics, however, bulky hydrophilic agents such as saporin require assistance for delivery(104, 108). One such way to overcome inefficient delivery is to increase the dosage of the drug being administered. However, such practices lead to narrow therapeutic indices for agents where the difference between the minimum therapeutic and toxic dose is small(26).

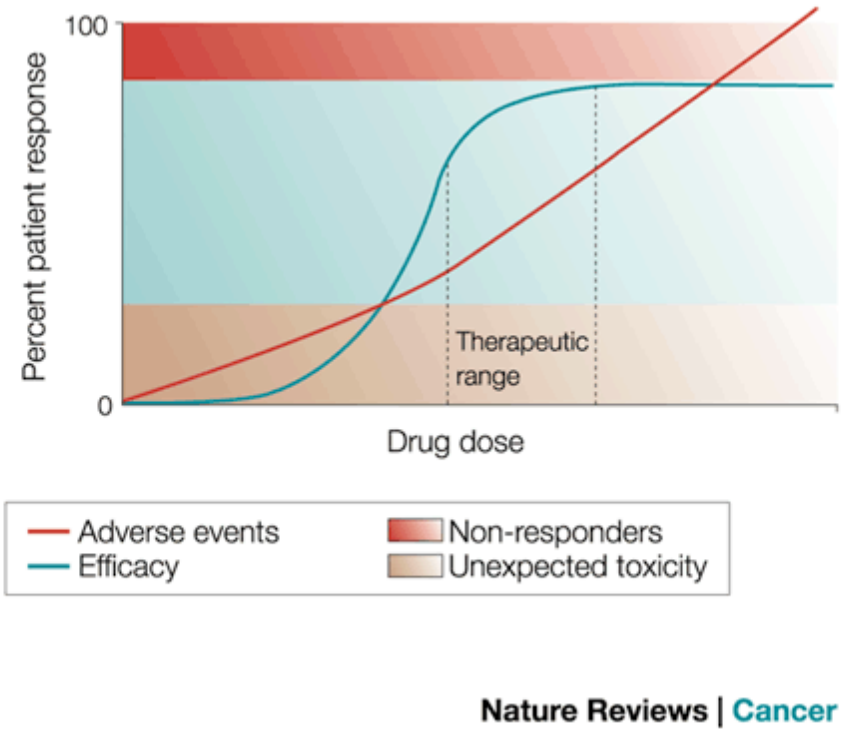

Figure 7.1 – Therapeutic index of drugs.
Graphical representation of the relationship between drug dose, efficacy, toxicity and the therapeutic range (index)(201)

The consequence of this includes reduced patient tolerance of treatment regimens and increased risk of developing multidrug resistance, which is a major impediment to cancer therapy(25). Therefore, strategies designed to enhance drug delivery have many potential benefits, not least of all the fact that technologies such as PCI and SMoCs often demonstrate reasonable versatility when it comes to agents they can potentiate the delivery of(23, 25, 26, 47, 48, 69, 104, 125, 138).

In this thesis, some of the mechanisms that mediate and factors that affect PCI have been investigated in 4T1 cells. PCI benefits from the fact that it is targeted (by light) and is based on administering low doses of agents for additive or synergistic effect. Such factors play a vital role in helping to widen the therapeutic index of a given agent. The benefits to patients are not limited to enhanced therapeutic effect but potentially include better toxicity profiles (leading to better compliance with treatment plans) and reduced probability of developing MDR as PCI has been shown to reverse MDR in previous studies(25).

PCI is currently undergoing multicenter clinical trials in the UK/Europe using bleomycin for the treatment of cutaneous head and neck cancer(46), and gemcitabine/cisplatin for the treatment of cholangiocarcinoma(202). Steps toward clinical application are vital for the continued growth of this sector of cancer therapeutics and support the potential of PCI to make the journey from bench towards the bedside application. The findings from the phase I safety trials were encouraging(46) and the phase II trials are underway. Concurrently, pre-clinical data continues to be created to help further develop the understanding and efficiency of the technique. For example, combining PCI with nanoparticles to enhance the intracellular trafficking and release of anticancer compounds(203). In this thesis, the intracellular REDOX environment was found to play a very important role in modulating the PCI and PDT effect. Given that buthionine sulfoximine is already used to reverse drug resistance, manifest by enhanced resistance to oxidative damage, it is an interesting and potential adjunct to PCI going forward. Many cancer clinical trials looking into BSO as an adjunct to established therapeutics have taken place such as the *Phase I Clinical*

and Pharmacokinetic Investigation of Intravenous Buthionine Sulfoximine/Melphalan in Patients with Refractory Advanced Solid Tumors (National Cancer Institute, USA).

Another area of potential development in the sphere of PCI/PDT is in bioluminescence. Although the findings in this thesis are very much preliminary, the development of more suitable luciferases and conjugation with nanoparticles such as quantum dots (QDs) for BRET(204). Such technologies benefit from eliminating the need for fluorescent excitation and utilizes the blue-increasing extinction coefficient of QDs. Further more it enables the exploitation of tissue-penetrating near-infrared wavelengths for fluorescence emission(205). Combining such technologies with PCI may help overcome two of the main limitations of PCI, namely accessing deep/irregularly shaped tumours and distant metastases. The benefit of using QDs as 'transformers' is that it helps bridge the discrepancy that often exists between blue-emitting luciferases and absorption maxima for porphyrin based photosensitisers.

7.2 CONCLUSION

In conclusion the options for developing PCI are wide ranging, however, in order for this technology to have any lasting, therapeutic and cost –effective impact in the clinical arena it must be refined and this requires a better understanding of the mechanics of PCI. This thesis aimed to address part of this and the natural progression for further work would be to test the BSO-PCI model further in both 3D tumoroids and *in vivo*. For the latter in particular, the FLuc expressing 4T1 cell line could be used to enable bioluminescent monitoring of tumour growth and treatment response.

Appendices

PUBLISHED PAPERS

1. Chem Biol Drug Des. 2014 Jul;84(1):24-35. doi: 10.1111/cbdd.12295. Epub 2014 May

A bifurcated proteoglycan binding small molecule carrier for siRNA delivery.
Gooding M(1), Adigbli D, Edith Chan AW, Melander RJ, MacRobert AJ, Selwood DL.

Author information:
(1)The Wolfson Institute for Biomedical Research, UCL, Gower Street, London, WC1E, 6BT, UK.

Abstract:
A wider application of siRNA- and miRNA- based therapeutics is restricted by the currently available delivery systems. We have designed a new type of small molecule carrier (SMoC) system for siRNA modeled to interact with cell surface proteoglycans. This bifurcated SMoC has similar affinity for the model proteoglycan heparin to an equivalent polyarginine peptide and exhibits significant mRNA knockdown of protein levels comparable to Lipofectamine and the previously reported linear SMoC.

PMID: 24472581 [PubMed - in process]

2. Curr Opin Pharmacol. 2012 Aug;12(4):434-8. doi: 10.1016/j.coph.2012.04.005. Epub 2012 May 17.

Photochemical internalisation: the journey from basic scientific concept to the threshold of clinical application. **Adigbli DK(1), MacRobert AJ.**

Author information:
(1)National Medical Laser Center, UCL Division of Surgery and Interventional Science, University College London, UK. d.adigbli@ucl.ac.uk

Abstract:
Efficient delivery of therapeutic agents to subcellular targets is a major challenge in pharmacology. Physical properties including size and charge may adversely affect the cellular uptake of molecules, and consequently reduce the accessibility of intracellular targets. For example macromolecules, which do not pass freely through the phospholipid membrane, are internalised via endocytosis and subsequently retained in endosomes or lysosomes before enzymatic degradation or cell efflux. Photochemical internalisation (PCI) is a novel drug delivery technology based on light-activated release of biologically active compounds retained within endosomes/lysosomes. PCI is founded upon the principle of photodynamic therapy (PDT), which uses light to activate photosensitisers to ultimately produce reactive oxygen species (ROS) and cause local damage/cell death. In PCI, photosensitisers are selectively localised in endosomal/lysosomal membranes. PCI triggers membrane rupture facilitating release and delivery of endocytosed molecules to intracellular targets.

PMID: 22608856 [PubMed - indexed for MEDLINE]

3. Br J Cancer. 2007 Aug 20;97(4):502-12. Epub 2007 Jul 31.

Photochemical internalisation of chemotherapy potentiates killing of multidrug-resistant breast and bladder cancer cells. **Adigbli DK(1), Wilson DG, Farooqui N, Sousi E, Risley P, Taylor I, Macrobert AJ, Loizidou M.**

Author information:
(1)Department of Surgery, Royal Free and University College Medical School, UCL, London, UK.

Abstract:
Multidrug resistance (MDR) is the major confounding factor in adjuvant solid tumour chemotherapy. Increasing intracellular amounts of chemotherapeutics to circumvent MDR may be achieved by a novel delivery method, photochemical internalisation (PCI). PCI consists of the co-administration of drug and photosensitiser; upon light activation, the latter induces intracellular release of organelle-bound drug. We investigated whether co-administration of hypericin (photosensitiser) with mitoxantrone (MTZ, chemotherapeutic) plus illumination potentiates cytotoxicity in MDR cancer cells. We mapped the extent of intracellular co-localisation of drug/photosensitiser. We determined whether PCI altered drug-excreting efflux pump P-glycoprotein (Pgp) expression or function in MDR cells. Bladder and breast cancer cells and their Pgp-overexpressing MDR subclones (MGHU1, MGHU1/R, MCF-7, MCF-7/R) were given hypericin/MTZ combinations, with/without blue-light illumination. Pilot experiments determined appropriate sublethal doses for each. Viability was determined by the 3- [4,5-dimethylthiazolyl]-2,5-diphenyltetrazolium bromide assay. Intracellular localisation was mapped by confocal microscopy. Pgp expression was detected by immunofluorescence and Pgp function investigated by Rhodamine123 efflux on confocal microscopy. MTZ alone (0.1-0.2 microg ml(-1)) killed up to 89% of drug-sensitive cells; MDR cells exhibited less cytotoxicity (6-28%). Hypericin (0.1-0.2 microM) effects were similar for all cells; light illumination caused none or minimal toxicity. In combination, MTZ /hypericin plus illumination, potentiated MDR cell killing, vs. hypericin or MTZ alone. (MGHU1/R: 38.65 and 36.63% increase, $P<0.05$; MCF-7/R: 80.2 and 46.1% increase, $P<0.001$). Illumination of combined MTZ/hypericin increased killing by 28.15% ($P<0.05$ MGHU1/R) compared to dark controls. Intracytoplasmic vesicular co-localisation of MTZ/hypericin was evident before illumination and at serial times post-illumination. MTZ was always found in sensitive cell nuclei, but not in dark resistant cell nuclei. In illuminated resistant cells there was some mobilisation of MTZ into the nucleus. Pgp expression remained unchanged, regardless of drug exposure. Pgp efflux was blocked by the Pgp inhibitor verapamil (positive control) but not impeded by hypericin. The increased killing of MDR cancer cells demonstrated is consistent with PCI. PCI is a promising technique for enhancing treatment efficacy.

PMCID: PMC2360354
PMID: 17667930 [PubMed - indexed for MEDLINE]

PRESENTATIONS

D. K. Adigbli, J. Seebaluck, M. Loizidou, A. J. MacRobert. Modification of the intracellular Redox environment can modulate *in vitro* photochemical internalisation. Oral presentation at The 6th Asia & Oceania Conference on Photobiology, Sydney (Australia) 10-13th November 2013.

D. K. Adigbli, J. Seebaluck, M. Loizidou, A. J. MacRobert. Varying the intracellular redox environment modulates photochemical internalisation in cancer cells. Abstract accepted for oral presentation at 14th World Congress of the International Photodynamic Association, Seoul (Republic of Korea) 28-31st May 2013.

D. K. Adigbli, J. Seebaluck, M. Loizidou, A. J. MacRobert. Disruption of glutathione synthesis enhances the photochemical potential of disulfonated meso-tetraphenylporphyrin ($TPPS_{2a}$) in combination with saporin in breast cancer cells. (Poster presentation at 9th International Symposium on Photodynamic Therapy and Photodiagnosis in Clinical Practice, Brixen (Italy) 16-20th October 2012)

D. K. Adigbli, J. Seebaluck, M. Loizidou, A. J. MacRobert. Photochemical Internalisation reverses saporin and mitoxantrone resistance in breast cancer cells. (Poster presentation at Third NIHR BRC/BRU/CLAHRC Experimental Medicine Research Training Camp 4-6 July 2012).

D. K. Adigbli, J. Seebaluck, M. Loizidou, A. J. MacRobert. Disulfonated meso-tetraphenylporphyrin ($TPPS_{2a}$) potentiates the cytotoxicity of saporin both as a monotherapy and in combination with Mitoxantrone in breast cancer cells (abstract). Poster presentation at 36th Meeting of the American Society for Photobiology 40th Anniversary.

D. K. Adigbli, J. Seebaluck, A. J. Macrobert, M. Loizidou. Bioluminescence mediated photodynamic therapy in breast cancer cell line. *British Journal of Surgery*, 2012;99(Suppl. 4):6-40. Presented (oral presentation) at SARS meeting January 2012 (University of Nottingham).

E. Sousi, **D. K. Adigbli**, D. G. Wilson, N. Farooqui, A., J. Macrobert, I. Taylor, M. Loizidou. Photochemical internalisation potentiates the killing of multi-drug resistant cancer cells without any change in the function of P-GP drug-efflux pumps. *Colorectal Disease, 2008;10(s1):1-12.* I presented this abstract at the 2008 Association of Coloproctology of Great Britain and Ireland Annual Meeting 2008 (30 June – 3 July), ICC,

D Wilson**, D Adigbli,** A Macrobert, P Risley, M Loizidou. Photochemical internalization of chemotherapy increases killing of multidrug resistant cancer cells. 2007, *British Journal of Surgery*, in press (Abstract). Presented at the Society of Academic and Research Surgeons (Cambridge), by my colleague, Jan 2007.

D Wilson, **D Adigbli**, P Risley, I Taylor et al. Photochemical internalisation of chemotherapy potentiates killing of resistant cancer cells. *European Journal of Surgical Oncology* (2006). 32, 1023 (Abstract)**.** Presented at the British Association of Surgical Oncology (BASO) ~ The Association For Cancer Surgery (ACS) conference (Royal College of Surgeons of England), by my colleague, Nov 2006.

D Adigbli, A Macrobert, N Farooqui, M Loizidou. Photochemical internalisation of chemotherapeutic agents to circumvent multidrug resistance. *European Journal of Surgical Oncology* (2005). 31(9), 1061 (Abstract). Presented at the British Association of Surgical Oncology (BASO) ~ The Association for Cancer Surgery (ACS) conference, Oct 2005.

D Adigbli, A Macrobert, N Farooqui, M Loizidou. Photochemical internalization of chemotherapeutic agents to circumvent multidrug resistance. *European Journal of Cancer Supplements* (2005); 3(2), 431 (Abstract). European Cancer Conference (ECCO), Paris. 30 October - 3 November 2005

ACADEMIC PRIZES

December 2013 – UCL Medical School Top Teacher award (2012-2013). This award is presented by the Director of UCL Medical School (Professor Jane Dacre). The awards are voted for by the students over the duration of the academic year. Over 1800 votes were cast.

November 2013 – Best oral presentation (student) at the 6th Asia & Oceania Conference, Sydney (Australia).

September 2013 – Runner up for The Eleanor Davies-Colley Prize (for PhD students in Division of Surgery and Interventional Science). Awarded by the Dean of Faculty of Medical Sciences following selection by executive committee to give a 5-minute presentation entitled 'Modification of the intracellular Redox environment can modulate *in vitro* photochemical internalisation'.

May 2013 – UCL Medical School Excellence in Medical Education Award. I was the most junior of five awardees. Awards are presented by the Vice-Provost (Health) Professor Sir John Tooke to reward those making an outstanding commitment to students and their education. Nominated by the Director of the Division of Medicine (Professor Raymond MacAllister).

November 2012 – runner up at UCL Faculty of Medical Sciences Dean's Research Prize presentation (top 8 research students in Faculty of Medical Sciences. Oral presentation title: Photochemical Internalisation as a mediator for enhanced drug delivery in cancer cells. Nominated by the Director of the Division of Surgery and Interventional Science (Professor Mark Emberton).

July 2012 - Poster Prize at the Third NIHR BRC/BRU/CLAHRC Experimental Medicine Research Training Camp 4-6 July 2012. Participants were nominated by their biomedical research centre and invited to the conference. 70 delegates submitted abstracts with 25 picked for a poster presentation. Three poster prizes were given.

July 2012 – Runner up prize for oral presentation at the Third NIHR BRC/BRU/CLAHRC Experimental Medicine Research Training Camp 4-6 July 2012.

June 2012 – awarded the Urbach Prize at the 36th meeting of the American Society for Photobiology (ASP), Montreal, Canada.

April 2012 – awarded Winners Prize at the UCL Grand Challenge Studentship 'Thinking Den' event. All studentship holders (21) were invited to write a one-page proposal explaining why their project should receive extra funding. The top 6 proposals were selected to give a 5-minute presentation to a panel comprising 4 Dean's from the Faculty of Medical Sciences, UCL. Top prize was awarded £250 to assist with conference fees.

September 2010 – Successfully applied for a UCL Grand Challenges Studentship for a 3 year PhD. The award provides me with funding for tuition fees, and incremental stipend starting at £18000 p.a. and bench fees of £5000 p.a. This highly prestigious award was very competitive being open Europe wide there were well over 200 applicants for 21 awards.

July 2008 – Invited to a prize presentation at the Association of Coloproctology in Birmingham. Was one of 8 speakers invited to this international conference where I presented the work from my group on photochemical internalisation. I was the most junior speaker there and went up against specialist registrars and PhD students. I was awarded the runner-up prize and was given special praise by the chair of the event for an accomplished presentation in spite of my more senior competition.

REFERENCES

1. Green B, Cobb AR, Hopper C. Photodynamic therapy in the management of lesions of the head and neck. The British journal of oral & maxillofacial surgery. 2013;51(4):283-7.

2. Master A, Livingston M, Sen Gupta A. Photodynamic nanomedicine in the treatment of solid tumors: perspectives and challenges. Journal of controlled release : official journal of the Controlled Release Society. 2013;168(1):88-102.

3. Finsen N. Phototherapy. Edward Arnold (Publisher). 1901.

4. Dolmans DE, Fukumura D, Jain RK. Photodynamic therapy for cancer. Nature reviews Cancer. 2003;3(5):380-7.

5. Jesionek H, von Tappeiner H. Zur Behandlung der Hautcarcinome mit fluoreszierenden Stoffen. Dtsch Arch Klin Med. 1905;82:223-6.

6. Hausmann W. Die sensiblisierende Wirkung des Hematoporphyrins. Biochem Zeitung. 1911;30:276-316.

7. Mayer-Betz F. Untersuchungen uber die biologische photodynamische Wirkung des Hematoporphyrins und anderer Derivative des Blutund Galenfarbstoffs. Dtsch Arch Klin 1913;112:476-503.

8. Schwartz SK, Ablon K, Vermund H. Some relationships of porphyrins, X-rays and tumours. Minn Med Bull. 1955;27:7-8.

9. Lipson RL, Baldes EJ, Olsen AM. The use of a derivative of haematoporphyrin in tumour detection. J Natl Cancer Inst. 1961;26:1-11.

10. Dougherty TJ, Grindey GB, Fiel R, Weishaupt KR, Boyle DG. Photoradiation therapy. II. Cure of animal tumors with hematoporphyrin and light. Journal of the National Cancer Institute. 1975;55(1):115-21.

11. Kelly JF, Snell ME, Berenbaum MC. Photodynamic destruction of human bladder carcinoma. Br J Cancer. 1975;31(2):237-44.

12. Kelly JF, Snell ME. Hematoporphyrin derivative: a possible aid in the diagnosis and therapy of carcinoma of the bladder. The Journal of urology. 1976;115(2):150-1.

13. McCaughan JSJ, Hicks W, Laufman L, May E, Roach R. Palliation of esophageal malignancy with photoradiation therapy. Cancer. 1984;54:2905-10.

14. Hayata Y, Kato H, Okitsu H, Kawaguchi M, Konaka C. Photodynamic therapy with haematoporphyrin derivative in cancer of the upper gastrointestinal tract. Semin Surg Oncol. 1985;1:1-11.

15. Byrne CJ, Marshallsay LV, Ward AD. The composition of Photofrin II. Journal of photochemistry and photobiology B, Biology. 1990;6(1-2):13-27.

16. Barolet D. Light-emitting diodes (LEDs) in dermatology. Seminars in cutaneous medicine and surgery. 2008;27(4):227-38.

17. Miller JD, Baron ED, Scull H, Hsia A, Berlin JC, McCormick T, et al. Photodynamic therapy with the phthalocyanine photosensitizer Pc 4: the case experience with preclinical mechanistic and early clinical-translational studies. Toxicology and applied pharmacology. 2007;224(3):290-9.

18. Scott LJ, Goa KL. Verteporfin. Drugs & aging. 2000;16(2):139-46; discussion 47-8.

19. Agency EM. Foscan http://www.ema.europa.eu/ema/index.jsp?curl=pages/medicines/human/medicines/000318/human_med_000801.jsp&mid=WC0b01ac058001d124: European Medicines Agency; 2014 [cited 2014]. Information about how Foscan has been studied].

20. Berg K, Nordstrand S, Selbo PK, Tran DT, Angell-Petersen E, Hogset A. Disulfonated tetraphenyl chlorin (TPCS2a), a novel photosensitizer developed for clinical utilization of photochemical internalization. Photochemical & photobiological sciences : Official journal of the European Photochemistry Association and the European Society for Photobiology. 2011;10(10):1637-51.

21. Ali H, Langlois R, Wagner JR, Brasseur N, Paquette B, van Lier JE. Biological activities of phthalocyanines--X. Syntheses and analyses of sulfonated phthalocyanines. Photochemistry and photobiology. 1988;47(5):713-7.

22. Berg K, Bommer JC, Moan J. Evaluation of sulfonated aluminum phthalocyanines for use in photochemotherapy. Cellular uptake studies. Cancer letters. 1989;44(1):7-15.

23. Berg K, Berstad M, Prasmickaite L, Weyergang A, Selbo PK, Hedfors I, et al. Photochemical internalization: a new tool for gene and oligonucleotide delivery. Topics in current chemistry. 2010;296:251-81.

24. Berg K, Western A, Bommer JC, Moan J. Intracellular localization of sulfonated meso-tetraphenylporphines in a human carcinoma cell line. Photochemistry and photobiology. 1990;52(3):481-7.

25. Adigbli DK, Wilson DG, Farooqui N, Sousi E, Risley P, Taylor I, et al. Photochemical internalisation of chemotherapy potentiates killing of multidrug-resistant breast and bladder cancer cells. Br J Cancer. 2007;97(4):502-12.

26. Adigbli DK, MacRobert AJ. Photochemical internalisation: the journey from basic scientific concept to the threshold of clinical application. Current opinion in pharmacology. 2012;12(4):434-8.

27. Hogset A, Prasmickaite L, Selbo PK, Hellum M, Engesaeter BO, Bonsted A, et al. Photochemical internalisation in drug and gene delivery. Advanced drug delivery reviews. 2004;56(1):95-115.

28. Prasmickaite L, Hogset A, Tjelle TE, Olsen VM, Berg K. Role of endosomes in gene transfection mediated by photochemical internalisation (PCI). The journal of gene medicine. 2000;2(6):477-88.

29. Selbo PK, Sandvig K, Kirveliene V, Berg K. Release of gelonin from endosomes and lysosomes to cytosol by photochemical internalization. Biochimica et biophysica acta. 2000;1475(3):307-13.

30. Norum OJ, Selbo PK, Weyergang A, Giercksky KE, Berg K. Photochemical internalization (PCI) in cancer therapy: from bench towards bedside medicine. Journal of photochemistry and photobiology B, Biology. 2009;96(2):83-92.

31. Moan J, Berg K. The photodegradation of porphyrins in cells can be used to estimate the lifetime of singlet oxygen. Photochemistry and photobiology. 1991;53(4):549-53.

32. Niedre MJ, Patterson MS, Giles A, Wilson BC. Imaging of photodynamically generated singlet oxygen luminescence in vivo. Photochemistry and photobiology. 2005;81(4):941-3.

33. Jimenez-Banzo A, Sagrista ML, Mora M, Nonell S. Kinetics of singlet oxygen photosensitization in human skin fibroblasts. Free radical biology & medicine. 2008;44(11):1926-34.

34. Prasmickaite L, Hogset A, Selbo PK, Engesaeter BO, Hellum M, Berg K. Photochemical disruption of endocytic vesicles before delivery of drugs: a new strategy for cancer therapy. Br J Cancer. 2002;86(4):652-7.

35. Berg K, Selbo PK, Weyergang A, Dietze A, Prasmickaite L, Bonsted A, et al. Porphyrin-related photosensitizers for cancer imaging and therapeutic applications. Journal of microscopy. 2005;218(Pt 2):133-47.

36. Rice BW, Cable MD, Nelson MB. In vivo imaging of light-emitting probes. Journal of biomedical optics. 2001;6(4):432-40.

37. Wang JT, Giuntini F, Eggleston IM, Bown SG, MacRobert AJ. Photochemical internalisation of a macromolecular protein toxin using a cell penetrating peptide-photosensitiser conjugate. Journal of controlled release : official journal of the Controlled Release Society. 2012;157(2):305-13.

38. Weyergang A, Selbo PK, Berstad ME, Bostad M, Berg K. Photochemical internalization of tumor-targeted protein toxins. Lasers in surgery and medicine. 2011;43(7):721-33.

39. Selbo PK, Rosenblum MG, Cheung LH, Zhang W, Berg K. Multi-modality therapeutics with potent anti-tumor effects: photochemical internalization enhances delivery of the fusion toxin scFvMEL/rGel. PloS one. 2009;4(8):e6691.

40. Weyergang A, Selbo PK, Berg K. Photochemically stimulated drug delivery increases the cytotoxicity and specificity of EGF-saporin. Journal of controlled release : official journal of the Controlled Release Society. 2006;111(1-2):165-73.

41. Yip WL, Weyergang A, Berg K, Tonnesen HH, Selbo PK. Targeted delivery and enhanced cytotoxicity of cetuximab-saporin by photochemical internalization in EGFR-positive cancer cells. Molecular pharmaceutics. 2007;4(2):241-51.

42. Raemdonck K, Naeye B, Høgset A, Demeester J, De Smedt S. Prolonged gene silencing by combining siRNA nanogels and photochemical internalization. J Controlled Rel. 2010;145(3):281-8.

43. Selbo PK, Sivam G, Fodstad O, Sandvig K, Berg K. In vivo documentation of photochemical internalization, a novel approach to site specific cancer therapy. International journal of cancer Journal international du cancer. 2001;92(5):761-6.

44. Norum OJ, Gaustad JV, Angell-Petersen E, Rofstad EK, Peng Q, Giercksky KE, et al. Photochemical internalization of bleomycin is superior to photodynamic therapy due to the therapeutic effect in the tumor periphery. Photochemistry and photobiology. 2009;85(3):740-9.

45. Woodhams J, Lou PJ, Selbo PK, Mosse A, Oukrif D, MacRobert A, et al. Intracellular re-localisation by photochemical internalisation enhances the cytotoxic effect of gelonin--quantitative studies in normal rat liver. Journal of controlled release : official journal of the Controlled Release Society. 2010;142(3):347-53.

46. Hopper C. Phase I, Dose-escalating Study to Evaluate Safety and Tolerance of Amphinex Based Photochemical Internalisation (PCI) of Bleomycin in Patients with Local Recurrence or Advanced/Metastatic, Cutaneous or Sub-cutaneous Malignancies: PCI Biotech AS; 2011. Available from: http://clinicaltrials.gov/ct2/show/NCT00993512?term=Photochemical+internalisation&rank=1.

47. Gooding M, Tudzarova S, Worthington RJ, Kingsbury SR, Rebstock AS, Dube H, et al. Exploring the interaction between siRNA and the SMoC biomolecule transporters: implications for small molecule-mediated delivery of siRNA. Chemical biology & drug design. 2012;79(1):9-21.

48. Okuyama M, Laman H, Kingsbury SR, Visintin C, Leo E, Eward KL, et al. Small-molecule mimics of an alpha-helix for efficient transport of proteins into cells. Nature methods. 2007;4(2):153-9.

49. Nyga A, Cheema U, Loizidou M. 3D tumour models: novel in vitro approaches to cancer studies. Journal of cell communication and signaling. 2011;5(3):239-48.

50. Nyga A, Loizidou M, Emberton M, Cheema U. A novel tissue engineered three-dimensional in vitro colorectal cancer model. Acta biomaterialia. 2013;9(8):7917-26.

51. Li J, Chen L, Du L, Li M. Cage the firefly luciferin! - a strategy for developing bioluminescent probes. Chemical Society reviews. 2013;42(2):662-76.

52. Haddock SH, Moline MA, Case JF. Bioluminescence in the sea. Annual review of marine science. 2010;2:443-93.

53. Inouye S. Firefly luciferase: an adenylate-forming enzyme for multicatalytic functions. Cellular and molecular life sciences : CMLS. 2010;67(3):387-404.

54. Widder EA. Bioluminescence in the ocean: origins of biological, chemical, and ecological diversity. Science. 2010;328(5979):704-8.

55. Branchini BR, Ablamsky DM, Davis AL, Southworth TL, Butler B, Fan F, et al. Red-emitting luciferases for bioluminescence reporter and imaging applications. Analytical biochemistry. 2010;396(2):290-7.

56. Kim JB, Urban K, Cochran E, Lee S, Ang A, Rice B, et al. Non-invasive detection of a small number of bioluminescent cancer cells in vivo. PloS one. 2010;5(2):e9364.

57. Bolin C, Sutherland C, Tawara K, Moselhy J, Jorcyk CL. Novel mouse mammary cell lines for in vivo bioluminescence imaging (BLI) of bone metastasis. Biological procedures online. 2012;14(1):6.

58. Sciences CL. Bioware Ultra Cell Line 4T1-luc2. http://wwwperkinelmercom/CMSResources/Images/44-155413DTS_Bioware_4T1-luc2_124087pdf.

59. Aldrich S. Cell Damage http://www.sigmaaldrich.com/life-science/metabolomics/enzyme-explorer/cell-signaling-enzymes/superoxide-dismutase.html [cited 2014].

60. Lancaster MV, Fields RD. Antibiotic and Cytotoxic Drug Susceptibility Assays using Resazurin and Poising Agents. 1996;U.S. Patent No. 5,501,959.

61. Förster VT. Versuche zum zwischenmolekularen Übergang von elektronenanregungsenergie. Naturwissenschaften. 1948;33:93-100.

62. Stryer L, Haugland RP. Energy transfer: a spectroscopic ruler. Proceedings of the National Academy of Sciences of the United States of America. 1967;58(2):719-26.

63. Lakowicz JR. Principles of fluorescence spectroscopy. New York: Plenum Press; 1983.

64. Sathishkumar K, Gao X, Raghavamenon AC, Murthy SN, Kadowitz PJ, Uppu RM. Determination of glutathione, mitochondrial transmembrane potential, and cytotoxicity in H9c2 cardiomyoblasts exposed to reactive oxygen and nitrogen species. Methods in molecular biology (Clifton, NJ). 2010;610:51-61.

65. Saitoh S, Kiyooka T, Rocic P, Rogers PA, Zhang C, Swafford A, et al. Redox-dependent coronary metabolic dilation. American journal of physiology Heart and circulatory physiology. 2007;293(6):H3720-5.

66. Stevenson D, Wokosin D, Girkin J, Grant MH. Measurement of the intracellular distribution of reduced glutathione in cultured rat hepatocytes using monochlorobimane and confocal laser scanning microscopy. Toxicology in vitro : an international journal published in association with BIBRA. 2002;16(5):609-19.

67. Pap EH, Drummen GP, Post JA, Rijken PJ, Wirtz KW. Fluorescent fatty acid to monitor reactive oxygen in single cells. Methods Enzymol. 2000;319:603-12.

68. Pap EH, Drummen GP, Winter VJ, Kooij TW, Rijken P, Wirtz KW, et al. Ratio-fluorescence microscopy of lipid oxidation in living cells using C11-BODIPY(581/591). FEBS letters. 1999;453(3):278-82.

69. Gooding M, Adigbli D, Edith Chan AW, Melander RJ, Macrobert AJ, Selwood DL. A Bifurcated Proteoglycan Binding Small Molecule Carrier for siRNA delivery. Chemical biology & drug design. 2014.

70. Yagi T, Seo BB, Di Bernardo S, Nakamaru-Ogiso E, Kao MC, Matsuno-Yagi A. NADH dehydrogenases: from basic science to biomedicine. Journal of bioenergetics and biomembranes. 2001;33(3):233-42.

71. Kuo MT. Redox regulation of multidrug resistance in cancer chemotherapy: molecular mechanisms and therapeutic opportunities. Antioxidants & redox signaling. 2009;11(1):99-133.

72. Pi J, Bai Y, Zhang Q, Wong V, Floering LM, Daniel K, et al. Reactive oxygen species as a signal in glucose-stimulated insulin secretion. Diabetes. 2007;56(7):1783-91.

73. Maechler P, Jornot L, Wollheim CB. Hydrogen peroxide alters mitochondrial activation and insulin secretion in pancreatic beta cells. The Journal of biological chemistry. 1999;274(39):27905-13.

74. Evans JL, Goldfine ID, Maddux BA, Grodsky GM. Are oxidative stress-activated signaling pathways mediators of insulin resistance and beta-cell dysfunction? Diabetes. 2003;52(1):1-8.

75. Versantvoort CH, Broxterman HJ, Bagrij T, Scheper RJ, Twentyman PR. Regulation by glutathione of drug transport in multidrug-resistant human lung tumour cell lines overexpressing multidrug resistance-associated protein. Br J Cancer. 1995;72(1):82-9.

76. Pouyssegur J, Mechta-Grigoriou F. Redox regulation of the hypoxia-inducible factor. Biological chemistry. 2006;387(10-11):1337-46.

77. Taylor CT. Mitochondria and cellular oxygen sensing in the HIF pathway. The Biochemical journal. 2008;409(1):19-26.

78. Sharma R, Yang Y, Sharma A, Awasthi S, Awasthi YC. Antioxidant role of glutathione S-transferases: protection against oxidant toxicity and regulation of stress-mediated apoptosis. Antioxidants & redox signaling. 2004;6(2):289-300.

79. Sies H, Cadenas E. Oxidative stress: damage to intact cells and organs. Philosophical transactions of the Royal Society of London Series B, Biological sciences. 1985;311(1152):617-31.

80. Giudice A, Arra C, Turco MC. Review of molecular mechanisms involved in the activation of the Nrf2-ARE signaling pathway by chemopreventive agents. Methods in molecular biology (Clifton, NJ). 2010;647:37-74.

81. Jaganjac M. Possible involvement of granulocyte oxidative burst in Nrf2 signaling in cancer. The Indian journal of medical research. 2010;131:609-16.

82. Catala A. Lipid peroxidation of membrane phospholipids generates hydroxy-alkenals and oxidized phospholipids active in physiological and/or pathological conditions. Chemistry and physics of lipids. 2009;157(1):1-11.

83. Catala A. An overview of lipid peroxidation with emphasis in outer segments of photoreceptors and the chemiluminescence assay. The international journal of biochemistry & cell biology. 2006;38(9):1482-95.

84. Wagner BA, Buettner GR, Burns CP. Free radical-mediated lipid peroxidation in cells: oxidizability is a function of cell lipid bis-allylic hydrogen content. Biochemistry. 1994;33(15):4449-53.

85. Gutteridge JM. Lipid Peroxidation: some problems and concepts. In: Halliwell, B. (Ed.). Oxygen Radicals and Tissue Injury (Symposium), FASEB. 1988:9-19.

86. Buettner GR. The pecking order of free radicals and antioxidants: lipid peroxidation, alpha-tocopherol, and ascorbate. Archives of biochemistry and biophysics. 1993;300(2):535-43.

87. Esterbauer H, Schaur RJ, Zollner H. Chemistry and biochemistry of 4-hydroxynonenal, malonaldehyde and related aldehydes. Free radical biology & medicine. 1991;11(1):81-128.

88. Uchida K. 4-Hydroxy-2-nonenal: a product and mediator of oxidative stress. Progress in lipid research. 2003;42(4):318-43.

89. Friguet B, Szweda LI. Inhibition of the multicatalytic proteinase (proteasome) by 4-hydroxy-2-nonenal cross-linked protein. FEBS letters. 1997;405(1):21-5.

90. Ji C, Amarnath V, Pietenpol JA, Marnett LJ. 4-hydroxynonenal induces apoptosis via caspase-3 activation and cytochrome c release. Chemical research in toxicology. 2001;14(8):1090-6.

91. Berg K, Moan J. Lysosomes as photochemical targets. International journal of cancer Journal international du cancer. 1994;59(6):814-22.

92. Lai PS, Pai CL, Peng CL, Shieh MJ, Berg K, Lou PJ. Enhanced cytotoxicity of saporin by polyamidoamine dendrimer conjugation and photochemical

internalization. Journal of biomedical materials research Part A. 2008;87(1):147-55.

93. Battelli MG. Cytotoxicity and toxicity to animals and humans of ribosome-inactivating proteins. Mini reviews in medicinal chemistry. 2004;4(5):513-21.

94. Endo Y, Mitsui K, Motizuki M, Tsurugi K. The mechanism of action of ricin and related toxic lectins on eukaryotic ribosomes. The site and the characteristics of the modification in 28 S ribosomal RNA caused by the toxins. The Journal of biological chemistry. 1987;262(12):5908-12.

95. Ferreras JM, Barbieri L, Girbes T, Battelli MG, Rojo MA, Arias FJ, et al. Distribution and properties of major ribosome-inactivating proteins (28 S rRNA N-glycosidases) of the plant Saponaria officinalis L. (Caryophyllaceae). Biochimica et biophysica acta. 1993;1216(1):31-42.

96. Endo Y, Tsurugi K. RNA N-glycosidase activity of ricin A-chain. Mechanism of action of the toxic lectin ricin on eukaryotic ribosomes. The Journal of biological chemistry. 1987;262(17):8128-30.

97. Polito L, Bortolotti M, Mercatelli D, Battelli MG, Bolognesi A. Saporin-S6: a useful tool in cancer therapy. Toxins. 2013;5(10):1698-722.

98. Nilsson L, Asano K, Svensson B, Poulsen FM, Nygard O. Reduced turnover of the elongation factor EF-1 X ribosome complex after treatment with the protein synthesis inhibitor II from barley seeds. Biochimica et biophysica acta. 1986;868(1):62-70.

99. Nielsen K, Boston RS. RIBOSOME-INACTIVATING PROTEINS: A Plant Perspective. Annual review of plant physiology and plant molecular biology. 2001;52:785-816.

100. Barbieri L, Battelli MG, Stirpe F. Ribosome-inactivating proteins from plants. Biochimica et biophysica acta. 1993;1154(3-4):237-82.

101. Balint GA. Ricin: the toxic protein of castor oil seeds. Toxicology. 1974;2(1):77-102.

102. Byers VS, Levin AS, Waites LA, Starrett BA, Mayer RA, Clegg JA, et al. A phase I/II study of trichosanthin treatment of HIV disease. Aids. 1990;4(12):1189-96.

103. Ferreras JM, Citores L, Iglesias R, Jimenez P, Girbes T. Use of ribosome-inactivating proteins from Sambucus for the construction of immunotoxins and conjugates for cancer therapy. Toxins. 2011;3(5):420-41.

104. Battelli MG, Buonamici L, Bolognesi A, Stirpe F. In vivo and in vitro uptake of an anti-CD30/saporin immunotoxin by rat liver parenchymal and nonparenchymal cells. Hepatology. 1994;20(4 Pt 1):940-7.

105. Battelli MG, Barbieri L, Stirpe F. Toxicity of, and histological lesions caused by, ribosome-inactivating proteins, their IgG-conjugates, and their homopolymers. APMIS : acta pathologica, microbiologica, et immunologica Scandinavica. 1990;98(7):585-93.

106. Colaco M, Bapat MM, Misquith S, Jadot M, Wattiaux-De Coninck S, Wattiaux R. Uptake and intracellular fate of gelonin, a ribosome-inactivating protein, in rat liver. Biochemical and biophysical research communications. 2002;296(5):1180-5.

107. Cavallaro U, Nykjaer A, Nielsen M, Soria MR. Alpha 2-macroglobulin receptor mediates binding and cytotoxicity of plant ribosome-inactivating proteins. European journal of biochemistry / FEBS. 1995;232(1):165-71.

108. Bagga S, Hosur MV, Batra JK. Cytotoxicity of ribosome-inactivating protein saporin is not mediated through alpha2-macroglobulin receptor. FEBS letters. 2003;541(1-3):16-20.

109. Bolognesi A, Polito L, Scicchitano V, Orrico C, Pasquinelli G, Musiani S, et al. Endocytosis and intracellular localisation of type 1 ribosome-inactivating protein saporin-s6. Journal of biological regulators and homeostatic agents. 2012;26(1):97-109.

110. Daniels-Wells TR, Helguera G, Rodriguez JA, Leoh LS, Erb MA, Diamante G, et al. Insights into the mechanism of cell death induced by saporin delivered into cancer cells by an antibody fusion protein targeting the transferrin receptor 1. Toxicology in vitro : an international journal published in association with BIBRA. 2013;27(1):220-31.

111. Santanche S, Bellelli A, Brunori M. The unusual stability of saporin, a candidate for the synthesis of immunotoxins. Biochemical and biophysical research communications. 1997;234(1):129-32.

112. Faulds D, Balfour JA, Chrisp P, Langtry HD. Mitoxantrone. A review of its pharmacodynamic and pharmacokinetic properties, and therapeutic potential in the chemotherapy of cancer. Drugs. 1991;41(3):400-49.

113. Dunn CJ, Goa KL. Mitoxantrone: a review of its pharmacological properties and use in acute nonlymphoblastic leukaemia. Drugs & aging. 1996;9(2):122-47.

114. Lin CW, Shulok JR, Kirley SD, Cincotta L, Foley JW. Lysosomal localization and mechanism of uptake of Nile blue photosensitizers in tumor cells. Cancer research. 1991;51(10):2710-9.

115. Lee CM, Tannock IF. Modulation of uptake of doxorubicin and mitoxantrone in acidic endosomes of cancer cells: A strategy to increase drug penetration through tumor tissue. Proc Amer Assoc Cancer Res. 2004;45.

116. Smith PJ, Sykes HR, Fox ME, Furlong IJ. Subcellular distribution of the anticancer drug mitoxantrone in human and drug-resistant murine cells analyzed

by flow cytometry and confocal microscopy and its relationship to the induction of DNA damage. Cancer research. 1992;52(14):4000-8.

117. Reliene R, Schiestl RH. Glutathione depletion by buthionine sulfoximine induces DNA deletions in mice. Carcinogenesis. 2006;27(2):240-4.

118. Mendez-Hurtado J, Lopez R, Suarez D, Menendez MI. Theoretical study of the oxidation of histidine by singlet oxygen. Chemistry. 2012;18(27):8437-47.

119. Wade AM, Tucker HN. Antioxidant characteristics of L-Histidine. J Nutritional Biochem. 1998;9(6):308-15.

120. Selbo PK, Weyergang A, Bonsted A, Bown SG, Berg K. Photochemical internalization of therapeutic macromolecular agents: a novel strategy to kill multidrug-resistant cancer cells. The Journal of pharmacology and experimental therapeutics. 2006;319(2):604-12.

121. Technologies L. Image-IT® Lipid peroxidation Kit. http://toolslifetechnologiescom/content/sfs/manuals/mp10445pdf.

122. Hirose K, Longo DL, Oppenheim JJ, Matsushima K. Overexpression of mitochondrial manganese superoxide dismutase promotes the survival of tumor cells exposed to interleukin-1, tumor necrosis factor, selected anticancer drugs, and ionizing radiation. FASEB journal : official publication of the Federation of American Societies for Experimental Biology. 1993;7(2):361-8.

123. Doroshow JH. Role of hydrogen peroxide and hydroxyl radical formation in the killing of Ehrlich tumor cells by anticancer quinones. Proceedings of the National Academy of Sciences of the United States of America. 1986;83(12):4514-8.

124. Ochsner M. Photophysical and photobiological processes in the photodynamic therapy of tumours. Journal of photochemistry and photobiology B, Biology. 1997;39(1):1-18.

125. Berg K, Selbo PK, Prasmickaite L, Tjelle TE, Sandvig K, Moan J, et al. Photochemical internalization: a novel technology for delivery of macromolecules into cytosol. Cancer research. 1999;59(6):1180-3.

126. Hogset A, Prasmickaite L, Tjelle TE, Berg K. Photochemical transfection: a new technology for light-induced, site-directed gene delivery. Human gene therapy. 2000;11(6):869-80.

127. Kunz L, Connelly JP, Woodhams JH, MacRobert AJ. Photodynamic modification of disulfonated aluminium phthalocyanine fluorescence in a macrophage cell line. Photochemical & photobiological sciences : Official journal of the European Photochemistry Association and the European Society for Photobiology. 2007;6(9):940-8.

128. Stamati I, Kuimova MK, Lion M, Yahioglu G, Phillips D, Deonarain MP. Novel photosensitisers derived from pyropheophorbide-a: uptake by cells and

photodynamic efficiency in vitro. Photochemical & photobiological sciences : Official journal of the European Photochemistry Association and the European Society for Photobiology. 2010;9(7):1033-41.

129. Oleinick NL. Basic Photosensitization http://www.photobiology.info: American Society for Photobiology; [updated February 2014].

130. Shea CR, Chen N, Wimberly J, Hasan T. Rhodamine dyes as potential agents for photochemotherapy of cancer in human bladder carcinoma cells. Cancer research. 1989;49(14):3961-5.

131. Ali SM, Olivo M. Bio-distribution and subcellular localization of Hypericin and its role in PDT induced apoptosis in cancer cells. International journal of oncology. 2002;21(3):531-40.

132. Sanada Y, Asai S, Ikemoto A, Moriwaki T, Nakamura N, Miyaji M, et al. Oxidation resistance 1 (OXR1) is essential for protection against oxidative stress and participates in the regulation of aging in Caenorhabditis elegans. Free radical research. 2014:1-27.

133. Thanislass J, Raveendran M, Devaraj H. Buthionine sulfoximine-induced glutathione depletion: Its effect on antioxidants, lipid peroxidation and calcium homeostasis in the lung. Biochemical Pharmacology. 1995;50(2):229-34.

134. Jiang F, Robin AM, Katakowski M, Tong L, Espiritu M, Singh G, et al. Photodynamic therapy with photofrin in combination with Buthionine Sulfoximine (BSO) of human glioma in the nude rat. Lasers in medical science. 2003;18(3):128-33.

135. Duthie SJ, Grant MH. The role of reductive and oxidative metabolism in the toxicity of mitoxantrone, adriamycin and menadione in human liver derived Hep G2 hepatoma cells. Br J Cancer. 1989;60(4):566-71.

136. Yang Y, Sharma R, Sharma A, Awasthi S, Awasthi YC. Lipid peroxidation and cell cycle signaling: 4-hydroxynonenal, a key molecule in stress mediated signaling. Acta biochimica Polonica. 2003;50(2):319-36.

137. Bostad M, Berg K, Hogset A, Skarpen E, Stenmark H, Selbo PK. Photochemical internalization (PCI) of immunotoxins targeting CD133 is specific and highly potent at femtomolar levels in cells with cancer stem cell properties. Journal of controlled release : official journal of the Controlled Release Society. 2013;168(3):317-26.

138. Berstad MB, Weyergang A, Berg K. Photochemical internalization (PCI) of HER2-targeted toxins: synergy is dependent on the treatment sequence. Biochimica et biophysica acta. 2012;1820(12):1849-58.

139. Wang K, Ramji S, Bhathena A, Lee C, Riddick DS. Glutathione S-transferases in wild-type and doxorubicin-resistant MCF-7 human breast cancer cell lines.

Xenobiotica; the fate of foreign compounds in biological systems. 1999;29(2):155-70.

140. Goto S, Ihara Y, Urata Y, Izumi S, Abe K, Koji T, et al. Doxorubicin-induced DNA intercalation and scavenging by nuclear glutathione S-transferase pi. FASEB journal : official publication of the Federation of American Societies for Experimental Biology. 2001;15(14):2702-14.

141. Golab J, Nowis D, Skrzycki M, Czeczot H, Baranczyk-Kuzma A, Wilczynski GM, et al. Antitumor effects of photodynamic therapy are potentiated by 2-methoxyestradiol. A superoxide dismutase inhibitor. The Journal of biological chemistry. 2003;278(1):407-14.

142. Kawamoto T, Ikeda Y, Teramoto A. [Protective effect of L-histidine (singlet oxygen scavenger) on transient forebrain ischemia in the rat]. No to shinkei = Brain and nerve. 1997;49(7):612-8.

143. Luo G, Long J, Zhang B, Liu C, Ji S, Xu J, et al. Quantum dots in cancer therapy. Expert opinion on drug delivery. 2012;9(1):47-58.

144. Beerens AM, Al Hadithy AF, Rots MG, Haisma HJ. Protein transduction domains and their utility in gene therapy. Current gene therapy. 2003;3(5):486-94.

145. Wadia JS, Dowdy SF. Transmembrane delivery of protein and peptide drugs by TAT-mediated transduction in the treatment of cancer. Advanced drug delivery reviews. 2005;57(4):579-96.

146. Joliot A, Prochiantz A. Transduction peptides: from technology to physiology. Nature cell biology. 2004;6(3):189-96.

147. Schwarze SR, Ho A, Vocero-Akbani A, Dowdy SF. In vivo protein transduction: delivery of a biologically active protein into the mouse. Science. 1999;285(5433):1569-72.

148. Li T, Fan Y, Luo Y, Xiao B, Lu C. In vivo delivery of a XIAP (BIR3-RING) fusion protein containing the protein transduction domain protects against neuronal death induced by seizures. Experimental neurology. 2006;197(2):301-8.

149. Choi HS, Lee SH, Kim SY, An JJ, Hwang SI, Kim DW, et al. Transduced Tat-alpha-synuclein protects against oxidative stress in vitro and in vivo. Journal of biochemistry and molecular biology. 2006;39(3):253-62.

150. Wohlschlegel JA, Dwyer BT, Dhar SK, Cvetic C, Walter JC, Dutta A. Inhibition of eukaryotic DNA replication by geminin binding to Cdt1. Science. 2000;290(5500):2309-12.

151. Bonsted A, Engesaeter BO, Hogset A, Maelandsmo GM, Prasmickaite L, Kaalhus O, et al. Transgene expression is increased by photochemically mediated transduction of polycation-complexed adenoviruses. Gene therapy. 2004;11(2):152-60.

152. Dalby B, Cates S, Harris A, Ohki EC, Tilkins ML, Price PJ, et al. Advanced transfection with Lipofectamine 2000 reagent: primary neurons, siRNA, and high-throughput applications. Methods (San Diego, Calif). 2004;33(2):95-103.

153. Sutherland RM. Cell and environment interactions in tumor microregions: the multicell spheroid model. Science. 1988;240(4849):177-84.

154. Hirschhaeuser F, Menne H, Dittfeld C, West J, Mueller-Klieser W, Kunz-Schughart LA. Multicellular tumor spheroids: an underestimated tool is catching up again. Journal of biotechnology. 2010;148(1):3-15.

155. Kenny PA, Lee GY, Myers CA, Neve RM, Semeiks JR, Spellman PT, et al. The morphologies of breast cancer cell lines in three-dimensional assays correlate with their profiles of gene expression. Molecular oncology. 2007;1(1):84-96.

156. Gurski LA, Jha AK, Zhang C, Jia X, Farach-Carson MC. Hyaluronic acid-based hydrogels as 3D matrices for in vitro evaluation of chemotherapeutic drugs using poorly adherent prostate cancer cells. Biomaterials. 2009;30(30):6076-85.

157. Timpl R, Rohde H, Robey PG, Rennard SI, Foidart JM, Martin GR. Laminin--a glycoprotein from basement membranes. The Journal of biological chemistry. 1979;254(19):9933-7.

158. Villanueva I, Weigel CA, Bryant SJ. Cell-matrix interactions and dynamic mechanical loading influence chondrocyte gene expression and bioactivity in PEG-RGD hydrogels. Acta biomaterialia. 2009;5(8):2832-46.

159. Szot CS, Buchanan CF, Gatenholm P, Rylander MN, Freeman JW. Investigation of cancer cell behavior on nanofibrous scaffolds. Materials Science and Engineering: C. 2011;31(1):37-42.

160. Brown RA, Wiseman M, Chuo CB, Cheema U, Nazhat SN. Ultrarapid Engineering of Biomimetic Materials and Tissues: Fabrication of Nano- and Microstructures by Plastic Compression. Advanced Functional Materials. 2005;15(11):1762-70.

161. Huang Z. A review of progress in clinical photodynamic therapy. Technology in cancer research & treatment. 2005;4(3):283-93.

162. Kennedy JC, Pottier RH. Endogenous protoporphyrin IX, a clinically useful photosensitizer for photodynamic therapy. Journal of photochemistry and photobiology B, Biology. 1992;14(4):275-92.

163. Fink-Puches R, Hofer A, Smolle J, Kerl H, Wolf P. Primary clinical response and long-term follow-up of solar keratoses treated with topically applied 5-aminolevulinic acid and irradiation by different wave bands of light. Journal of photochemistry and photobiology B, Biology. 1997;41(1-2):145-51.

164. Ormrod D, Jarvis B. Topical aminolevulinic acid HCl photodynamic therapy. American journal of clinical dermatology. 2000;1(2):133-9; discussion 40-1.

165. Photodynamic Therapy for Barrett's Oesophagus. National Institute of Clinical Excellence. 2010.

166. de Wet JR, Wood KV, DeLuca M, Helinski DR, Subramani S. Firefly luciferase gene: structure and expression in mammalian cells. Molecular and cellular biology. 1987;7(2):725-37.

167. Wood KV, Lam YA, Seliger HH, McElroy WD. Complementary DNA coding click beetle luciferases can elicit bioluminescence of different colors. Science. 1989;244(4905):700-2.

168. Squirrel DJ, Price RL, Murphy MJ. Rapid and specific detection of bacteria using bioluminescence. Anal Chim Acta. 2002;457(1):109-14.

169. Urata M, Iwata R, Noda K, Murakami Y, Kuroda A. Detection of living Salmonella cells using bioluminescence. Biotechnol Lett. 2009;31:737-41.

170. Arai R, Nakagawa H, Kitayama A, Ueda H, Nagamune T. Detection of protein-protein interaction by bioluminescence resonance energy transfer from firefly luciferase to red fluorescent protein. Journal of bioscience and bioengineering. 2002;94(4):362-4.

171. Joly E, Houle B, Dionne P, Taylor S, Ménard L. Bioluminescence Resonance Energy Transfer (BRET2 TM) Principle, Applications and Products http://www2.cbm.uam.es/confocal/manuales/bret.pdf: Packard BioScience Company Inc.; 2001.

172. Lorenz WW, McCann RO, Longiaru M, Cormier MJ. Isolation and expression of a cDNA encoding Renilla reniformis luciferase. Proceedings of the National Academy of Sciences of the United States of America. 1991;88(10):4438-42.

173. Förster T. Zwischenmolekulare Energiewanderung und Fluoreszenz. Annalen der Physik. 1948;437(1-2):55-75.

174. Rehemtulla A, Stegman LD, Cardozo SJ, Gupta S, Hall DE, Contag CH, et al. Rapid and quantitative assessment of cancer treatment response using in vivo bioluminescence imaging. Neoplasia. 2000;2:491-5.

175. Yu YA, Timiryasova T, Zhang Q, Beltz R, Szalay AA. Optical imaging: bacteria, viruses, and mammalian cells encoding light-emitting proteins reveal the locations of primary tumors and metastases in animals. Analytical and bioanalytical chemistry. 2003;377(6):964-72.

176. Sureau F, Miskovsky P, Chinsky L, Turpin PY. Hypericin-Induced Cell Photosensitization Involves an Intracellular pH Decrease. Journal of the American Chemical Society. 1996;118(40):9484-7.

177. Agostinis P, Vantieghem A, Merlevede W, de Witte PA. Hypericin in cancer treatment: more light on the way. The international journal of biochemistry & cell biology. 2002;34(3):221-41.

178. Hadjur C, Richard MJ, Parat MO, Favier A, Jardon P. Photodynamically induced cytotoxicity of hypericin dye on human fibroblast cell line MRC5. Journal of photochemistry and photobiology B, Biology. 1995;27(2):139-46.

179. Yu H, Wolford ST, Kegode R, Zhao W, Osweller GD. Hypericin-induced phototoxicity in cultured fibroblasts and swine erythrocytes. Photochemistry and photobiology. 1996;64(1):168-73.

180. Theodossiou T, Spiro MD, Jacobson J, Hothersall JS, Macrobert AJ. Evidence for intracellular aggregation of hypericin and the impact on its photocytotoxicity in PAM 212 murine keratinocytes. Photochemistry and photobiology. 2004;80(3):438-43.

181. Hadjur C, Richard MJ, Parat MO, Jardon P, Favier A. Photodynamic effects of hypericin on lipid peroxidation and antioxidant status in melanoma cells. Photochemistry and photobiology. 1996;64(2):375-81.

182. Vuong TTK, Vever-Bizet C, Bonneau S, Bourg-Heckly G. Hypericin incorporation and localization in fixed HeLa cells for various conditions of fixation and incubation. Photochemical & Photobiological Sciences. 2011;10(4):561-8.

183. Gandin E, Lion Y, Van de Vorst A. QUANTUM YIELD OF SINGLET OXYGEN PRODUCTION BY XANTHENE DERIVATIVES. Photochemistry and photobiology. 1983;37(3):271-8.

184. Berg K. Photosensitizers in Medicine http://www.photobiology.info/Berg.html. Web based text].

185. http://www.bioscience.co.uk/product~88606. Tetrabromrhodamine 123 data. Cambridge Bioscience Website.

186. Photodynamic Therapy for Cancer. National Cancer Institute.http://www.cancer.gov/cancertopics/factsheet/Therapy/photodynamic - r3.

187. Dougherty TJ, Gomer CJ, Henderson BW, Jori G, Kessel D, Korbelik M, et al. Photodynamic therapy. Journal of the National Cancer Institute. 1998;90(12):889-905.

188. Wilson BC. Photodynamic therapy for cancer: principles. Canadian journal of gastroenterology = Journal canadien de gastroenterologie. 2002;16(6):393-6.

189. Vrouenraets MB, Visser GW, Snow GB, van Dongen GA. Basic principles, applications in oncology and improved selectivity of photodynamic therapy. Anticancer research. 2003;23(1B):505-22.

190. Capella MA, Capella LS. A light in multidrug resistance: photodynamic treatment of multidrug-resistant tumors. Journal of biomedical science. 2003;10(4):361-6.

191. Mesnil M, Piccoli C, Tiraby G, Willecke K, Yamasaki H. Bystander killing of cancer cells by herpes simplex virus thymidine kinase gene is mediated by connexins. Proceedings of the National Academy of Sciences of the United States of America. 1996;93(5):1831-5.

192. Castillo-Rodriguez RA, Arango-Rodriguez ML, Escobedo L, Hernandez-Baltazar D, Gompel A, Forgez P, et al. Suicide HSVtk gene delivery by neurotensin-polyplex nanoparticles via the bloodstream and GCV Treatment specifically inhibit the growth of human MDA-MB-231 triple negative breast cancer tumors xenografted in athymic mice. PloS one. 2014;9(5):e97151.

193. Niers JM, Kerami M, Pike L, Lewandrowski G, Tannous BA. Multimodal in vivo imaging and blood monitoring of intrinsic and extrinsic apoptosis. Molecular therapy : the journal of the American Society of Gene Therapy. 2011;19(6):1090-6.

194. Uzdensky AB, Ma LW, Iani V, Hjortland GO, Steen HB, Moan J. Intracellular localisation of hypericin in human glioblastoma and carcinoma cell lines. Lasers in medical science. 2001;16(4):276-83.

195. Theodossiou T, Hothersall JS, Woods EA, Okkenhaug K, Jacobson J, MacRobert AJ. Firefly luciferin-activated rose bengal: in vitro photodynamic therapy by intracellular chemiluminescence in transgenic NIH 3T3 cells. Cancer research. 2003;63(8):1818-21.

196. Li L, Zhao JF, Won N, Jin H, Kim S, Chen JY. Quantum dot-aluminum phthalocyanine conjugates perform photodynamic reactions to kill cancer cells via fluorescence resonance energy transfer. Nanoscale research letters. 2012;7(1):386.

197. Keller GA, Gould S, Deluca M, Subramani S. Firefly luciferase is targeted to peroxisomes in mammalian cells. Proceedings of the National Academy of Sciences of the United States of America. 1987;84(10):3264-8.

198. Shrestha TB, Seo GM, Basel MT, Kalita M, Wang H, Villanueva D, et al. Stem cell-based photodynamic therapy. Photochemical & photobiological sciences : Official journal of the European Photochemistry Association and the European Society for Photobiology. 2012;11(7):1251-8.

199. McLatchie AP, Burrell-Saward H, Myburgh E, Lewis MD, Ward TH, Mottram JC, et al. Highly sensitive in vivo imaging of Trypanosoma brucei expressing "red-shifted" luciferase. PLoS neglected tropical diseases. 2013;7(11):e2571.

200. Bulina ME, Chudakov DM, Britanova OV, Yanushevich YG, Staroverov DB, Chepurnykh TV, et al. A genetically encoded photosensitizer. Nature biotechnology. 2006;24(1):95-9.

201. Relling MV, Dervieux T. Pharmacogenetics and cancer therapy. Nature reviews Cancer. 2001;1(2):99-108.

202. Sturgess R. A Phase I/II Study Safety and Efficacy Study of PCI of Gemcitabine and Chemotherapy in Patients With Cholangiocarcinomas [Clinical Trial data]. PCI Biotech AS; 2013 [NCT01900158]. Available from: http://clinicaltrials.gov/ct2/show/NCT01900158?term=Photochemical+internalisation&rank=2.

203. Pasparakis G, Manouras T, Vamvakaki M, Argitis P. Harnessing photochemical internalization with dual degradable nanoparticles for combinatorial photo–chemotherapy. Nat Commun. 2014;5.

204. Evanko D. Bioluminescent quantum dots. Nat Meth. 2006;3(4):240-1.

205. Frangioni JV. Self-illuminating quantum dots light the way. Nat Biotech. 2006;24(3):326-8.